MAGNETIC CLUSTERS IN DILUTE ALLOYS OF IRON IN COPPER-NICKEL SOLID SOLUTIONS

BY

SANAK MISHRA

B.Sc.Honours, Utkal University, 1965
B.E., Indian Institute of Science, 1968
M.S., University of Illinois, 1970

THESIS

Submitted in partial fulfillment of the requirements
for the degree of Doctor of Philosophy in Metallurgical Engineering
in the Graduate College of the
University of Illinois at Urbana-Champaign, 1973

Urbana, Illinois

ACKNOWLEDGEMENTS

The author wishes to express sincere appreciation to Professor Paul A. Beck for his encouragement, guidance, and help throughout the course of this work.

Thanks are due to Professor H. Claus of the University of Illinois at Chicago Circle and to Dr. S. Foner of the National Magnet Laboratory, for making high field magnetic measurements on some of the specimens.

The author would also like to thank Dr. R. J. Raudebaugh and the International Nickel Company for the high purity nickel metal used in this investigation.

This research was supported by a grant from the National Science Foundation.

TABLE OF CONTENTS

		Page
I.	INTRODUCTION.	1
II.	SPECIMEN PREPARATION.	4
	A. Materials	4
	B. Melting	4
	C. Homogenizing Treatment.	9
	D. Deformed and Aged Specimens	14
	E. Chemical Analysis	14
	F. Storage of Specimens.	17
III.	EXPERIMENTAL PROCEDURE.	18
	A. Force Measurement	18
	B. Measurement and Control of Temperature.	19
	C. Measurement of the Field.	20
	D. Corrections	21
	E. Additional Measurements	22
IV.	EXPERIMENTAL RESULTS.	27
	A. Data Tables	27
	B. Data Analysis	86
V.	DISCUSSION.	222
	A. Cu-Fe	222
	B. Cu-Ni-Fe.	231
	C. Cu-Ni	261
VI.	SUMMARY	280
	REFERENCES.	282

Page

APPENDIX

A. SIGMA-5 COMPUTER PROGRAM FOR FITTING OF EQ. 9 (OR 11, 13, OR 14) TO MAGNETIZATION DATA. 285

B. SIGMA-5 COMPUTER PROGRAM FOR THE DETERMINATION OF $_{i}S_{k}$. 294

C. SIGMA-5 COMPUTER PROGRAM FOR CALCULATING THE RATIO OF c_2/c_1 ON THE BASIS OF RANDOM ALLOY MODEL,[4] FROM EQ. 30 302

VITA. 306

LIST OF TABLES

Table		Page
1.	Analysis of W.A.W. grade nickel (99.99%).	5
2.	Spectrographic analysis of copper (99.999%) and lot analysis of iron.	6
3.	List of alloys used in the present investigation	11
4.	Results of quantitative analysis for iron by spectrophotometry.	15
5.	Results of mass spectrographic analysis for impurities.	16
6.	Measured values of Δw_g as a function of temperature and field	23
7.	Magnetization data for quenched $Cu_{0.5}Ni_{0.5}$.	28
8.	Magnetization data for quenched $Cu_{0.52}Ni_{0.48}$. . . .	34
9.	Magnetization data for quenched $Cu_{0.54}Ni_{0.46}$. . . .	35
10.	Magnetization data for quenched $Cu_{0.9}Ni_{0.1}$.	37
11.	Magnetization data for quenched $Cu_{0.7}Ni_{0.3}$.	38
12.	Magnetization data for quenched $Cu_{0.6}Ni_{0.4}$.	39
13.	Magnetization data for aged $Cu_{0.6}Ni_{0.4}$.	42
14.	Magnetization data for quenched $Cu_{0.99}Fe_{0.01}$. . . .	45
15.	Magnetization data for quenched $(Cu_{0.9}Ni_{0.1})_{0.99}$ $Fe_{0.01}$.	49
16.	Magnetization data for quenched $(Cu_{0.8}Ni_{0.2})_{0.99}$ $Fe_{0.01}$.	54
17.	Magnetization data for 108 ppm Fe in Cu	59
18.	Magnetization data for 112 ppm Fe in Cu	60

Table Page

19. Magnetization data for 478 ppm Fe in Cu. 63

20. Magnetization data for the quenched $Cu_{0.9}Ni_{0.1}$ alloy containing 100 ppm Fe. 64

21. Magnetization data for the quenched $Cu_{0.9}Ni_{0.1}$ alloy containing 500 ppm Fe. 66

22. Magnetization data for the quenched $Cu_{0.9}Ni_{0.1}$ alloy containing 1000 ppm Fe 68

23. Magnetization data for the quenched $Cu_{0.8}Ni_{0.2}$ alloy containing 100 ppm Fe. 70

24. Magnetization data for the quenched $Cu_{0.8}Ni_{0.2}$ alloy containing 250 ppm Fe. 71

25. Magnetization data for the quenched $Cu_{0.8}Ni_{0.2}$ alloy containing 500 ppm Fe. 72

26. Magnetization data for the quenched $Cu_{0.8}Ni_{0.2}$ alloy containing 1000 ppm Fe 73

27. Magnetization data for the quenched $Cu_{0.7}Ni_{0.3}$ alloy containing 100 ppm Fe. 74

28. Magnetization data for the deformed $Cu_{0.9}Ni_{0.1}$ alloy containing 100 ppm Fe. 75

29. Magnetization data for the deformed $Cu_{0.9}Ni_{0.1}$ alloy containing 500 ppm Fe. 76

30. Magnetization data for the deformed $Cu_{0.9}Ni_{0.1}$ alloy containing 1000 ppm Fe 78

31. Magnetization data for the deformed $Cu_{0.8}Ni_{0.2}$ alloy containing 100 ppm Fe. 80

32. Magnetization data for the deformed $Cu_{0.8}Ni_{0.2}$ alloy containing 500 ppm Fe. 82

33. Magnetization data for the deformed $Cu_{0.8}Ni_{0.2}$ alloy containing 1000 ppm Fe 84

34. Values of the saturation magnetization $\sigma_{\infty,o}$ (emu/g) and of $\bar{\mu}$, the average magnetic moment per alloy atom, in Bohr magnetons. 104

Table — Page

35. Results of analysis of data for quenched, and aged $Cu_{0.6}Ni_{0.4}$ 126

36. Parameters from least squares fitting of Eq. 14 to magnetization data for Cu-Fe alloy, Tholence and Tournier[6] and Hirschkoff et al.[9] 163

37. Parameters from least squares fitting of Eq. 11 or Eq. 13 to magnetization data for quenched $Cu_{0.9}Ni_{0.1}$ alloys containing Fe. 178

38. Parameters from least squares fitting of Eq. 11 or Eq. 13 to magnetization data for quenched $Cu_{0.8}Ni_{0.2}$ alloys containing Fe. 179

39. Parameters from least squares fitting of Eq. 11 to magnetization of the quenched $Cu_{0.7}Ni_{0.3}$ alloy containing 100 ppm Fe minus the magnetization of $Cu_{0.7}Ni_{0.3}$ without the Fe 197

40. Parameters from least squares fitting of Eq. 11 or Eq. 13 to magnetization data for deformed $Cu_{0.9}Ni_{0.1}$ alloys containing Fe. 200

41. Parameters from least squares fitting of Eq. 11 or Eq. 13 to magnetization data for deformed $Cu_{0.8}Ni_{0.2}$ alloys containing Fe. 201

42. Percentage decrease as a result of plastic deformation, of the magnetization of quenched alloys at 4.2°K in an applied field of ~12.6 kOe . . . 218

43. Connection probabilities for random alloy. 238

44. The number ${}_iS_k$ of sites on the k^{th} shell of atom B, which are shared with the 1st through 9th shells of atom A. 238

45. Results for quenched alloys for the effective concentration, x_1, of Ni atoms in the nearest neighbor shells of isolated Fe atoms, and the Fe-Ni short range order parameter ${}_{Fe\text{-}Ni}\alpha_1$. 256

46. Moment assignments, $\mu_{n,m}$ in μ_B, in Cu-Ni alloys for Ni atoms with n nearest and m second nearest neighbor Ni atoms. 276

LIST OF FIGURES

Figure — Page

1. Isothermal magnetization data for quenched $Cu_{0.5}Ni_{0.5}$ between 78.08°K and 10.39°K. 87
2. Isothermal low temperature ($T \leq 4.2$°K) magnetization data for quenched $Cu_{0.5}Ni_{0.5}$. 89
3. Isothermal low temperature ($T \leq 4.2$°K) magnetization data for quenched $Cu_{0.52}Ni_{0.48}$. . . . 91
4. Isothermal low temperature ($T \leq 4.2$°K) magnetization data for quenched $Cu_{0.54}Ni_{0.46}$. . . . 93
5. σ^2 vs. $\frac{H_i}{\sigma}$ graphs, at low fields, for quenched $Cu_{0.5}Ni_{0.5}$. 95
6. χ_i vs. T and $\frac{1}{\chi_i}$ vs. T graphs for quenched $Cu_{0.5}Ni_{0.5}$. 98
7. Logarithmic graph of χ_i vs. $(T-T_c)$ for quenched $Cu_{0.5}Ni_{0.5}$ 100
8. σ^2 vs. $\frac{H_i}{\sigma}$ graph for the quenched $Cu_{0.54}Ni_{0.46}$ alloy for 4.2°K 102
9. σ vs. $\frac{1}{H_i}$ graphs for quenched $Cu_{0.5}Ni_{0.5}$ 105
10. σ vs. $\frac{1}{H_i}$ graphs for quenched $Cu_{0.52}Ni_{0.48}$ 107
11. σ vs. $\frac{1}{H_i}$ graphs for quenched $Cu_{0.54}Ni_{0.46}$ 109
12. $\sigma_{H_i=\infty,T}$ vs. T for quenched $Cu_{0.5}Ni_{0.5}$ (O), $Cu_{0.52}Ni_{0.48}$ (Δ), and $Cu_{0.54}Ni_{0.46}$ ( ) alloys. . . . 111
13. Magnetization data at 4.2°K for quenched $Cu_{0.9}Ni_{0.1}$. 113
14. χ vs. T for quenched $Cu_{0.9}Ni_{0.1}$, $Cu_{0.8}Ni_{0.2}$ (from Refs. 1,2), and $Cu_{0.7}Ni_{0.3}$ (from Ref. 1) alloys. 115
15. χ vs. T (from Ref. 1) and σ vs. H at 4.2°K (see Table 11) for quenched $Cu_{0.7}Ni_{0.3}$. 119

Table

16. $\Delta\sigma(=\sigma_{calculated} - \sigma_{measured})$ vs. H at 2.52°K and 4.2°K and $\Delta\chi(=\chi_{calculated} - \chi_{measured})$ vs. T for quenched $Cu_{0.6}Ni_{0.4}$ 123

17. Magnetization vs. field (Table 12) at temperatures indicated for quenched $Cu_{0.6}Ni_{0.4}$ 127

18. Magnetization vs. field up to 55 kOe at 4.2°K in both the as-quenched and the aged condition for $Cu_{0.6}Ni_{0.4}$ (Tables 12 and 13). 129

19. Susceptibility vs. temperature for $Cu_{0.6}Ni_{0.4}$ in both the as-quenched and the aged condition . . . 131

20. Magnetization vs. field at temperatures indicated, for aged $Cu_{0.6}Ni_{0.4}$ 133

21. Schematic representation of various possible types of cluster distribution. 136

22. $\frac{1}{\chi_i - \chi_o}$ vs. T graphs for quenched and aged $Cu_{0.6}Ni_{0.4}$ 140

23. σ^2 vs. $\frac{H_i}{\sigma}$ graphs for quenched $Cu_{0.99}Fe_{0.01}$ 142

24. σ^2 vs. $\frac{H_i}{\sigma}$ graphs for quenched $(Cu_{0.9}Ni_{0.1})_{0.99}Fe_{0.01}$ 144

25. σ^2 vs. $\frac{H_i}{\sigma}$ graphs for quenched $(Cu_{0.8}Ni_{0.2})_{0.99}Fe_{0.01}$ 146

26. σ vs. H for quenched $Cu_{0.99}Fe_{0.01}$ at temperatures indicated. 149

27. σ vs. H for quenched $(Cu_{0.9}Ni_{0.1})_{0.99}Fe_{0.01}$ at temperatures indicated. 151

28. σ vs. H for quenched $(Cu_{0.8}Ni_{0.2})_{0.99}Fe_{0.01}$ 153

29. σ vs. T at H = 1000 Oe for quenched $Cu_{0.99}Fe_{0.01}$ . . 155

30. σ vs. T at H = 700 Oe for quenched $(Cu_{0.9}Ni_{0.1})_{0.99}Fe_{0.01}$ 157

31. σ vs. T at H = 1000 Oe for quenched $(Cu_{0.8}Ni_{0.2})_{0.99}Fe_{0.01}$ 159

Table Page

32. σ vs. H isotherms for 108 ppm Fe in Cu. 164

33. σ vs. H isotherms for 112 ppm Fe in Cu for temperatures indicated. 167

34. σ vs. T at H = 10 Oe for 112 ppm Fe in Cu 169

35. σ vs. T at H = 10 Oe for 478 ppm Fe alloy 171

36. χ vs. T for quenched $Cu_{0.9}Ni_{0.1}$ alloys containing various amounts of Fe 180

37. Magnetization vs. field for quenched $Cu_{0.9}Ni_{0.1}$ with 100 ppm Fe 182

38. Magnetization vs. field for quenched $Cu_{0.9}Ni_{0.1}$ with 500 ppm Fe 184

39. Magnetization vs. field for quenched $Cu_{0.9}Ni_{0.1}$ with 1000 ppm Fe. 186

40. χ vs. T for quenched $Cu_{0.8}Ni_{0.2}$ alloys containing various amounts of Fe 188

41. Magnetization vs. field for quenched $Cu_{0.8}Ni_{0.2}$ with 100 ppm Fe 190

42. Magnetization vs. field for quenched $Cu_{0.8}Ni_{0.2}$ with 500 ppm Fe 192

43. Magnetization vs. field for quenched $Cu_{0.8}Ni_{0.2}$ with 1000 ppm Fe. 194

44. $\Delta\sigma_{Fe}$ vs. H at 4.2°K and $\Delta\chi_{Fe}$ vs. T for quenched $Cu_{0.7}Ni_{0.3}$ alloy with 100 ppm Fe. 198

45. χ vs. T for deformed $Cu_{0.9}Ni_{0.1}$ alloys containing various amounts of Fe 202

46. Magnetization vs. field for deformed $Cu_{0.9}Ni_{0.1}$ with 100 ppm Fe 204

47. Magnetization vs. field for deformed $Cu_{0.9}Ni_{0.1}$ with 500 ppm Fe 206

48. Magnetization vs. field for deformed $Cu_{0.9}Ni_{0.1}$ with 1000 ppm Fe. 208

49. χ vs. T for deformed $Cu_{0.8}Ni_{0.2}$ alloys containing various amounts of Fe. 210

Table

50. Magnetization vs. field for deformed $Cu_{0.8}Ni_{0.2}$ with 100 ppm Fe. 212

51. Magnetization vs. field for deformed $Cu_{0.8}Ni_{0.2}$ with 500 ppm Fe. 214

52. Magnetization vs. field for deformed $Cu_{0.8}Ni_{0.2}$ with 1000 ppm Fe 216

53. Effect of plastic deformation on the magnetization . . 219

54. χ_i vs. T for Cu-Fe with ∿110 ppm Fe. 225

55. μ_1 and μ_2 for quenched Cu-Ni-Fe alloys as a function of Fe and Ni contents 232

56. Some atomic sites in an f.c.c. structure 236

57. Experimental and calculated (on the basis of random alloy model) values of c_2/c_1. 246

58. c_2/c_1 vs. x_1 249

59. $_{Fe\text{-}Fe}\alpha_1$ and D vs. z. 252

60. $_{Fe\text{-}Ni}\alpha_1$ as a function of Fe and Ni content (see Table 45) for quenched alloys 257

61. χ_o vs. at. fraction Ni 265

62. χ_p and S vs. at. fraction Ni 269

63. $_{Ni\text{-}Ni}\alpha_1$ and $\bar{\mu}$ vs. at. % Cu 273

64. A modified moment assignment scheme for Cu-Ni alloys 277

I. INTRODUCTION

It has been shown[1] that the paramagnetic properties of f.c.c. copper-rich Cu-Ni solid solutions change considerably when small amounts of Fe are added. For virtually Fe-free $Cu_{0.8}Ni_{0.2}$ alloy, the temperature dependent part of the susceptibility is very small, but it increases greatly with Fe addition. A preliminary investigation[2] indicated that in quenched alloys up to a level of 100 ppm Fe most Fe atoms tend to form a magnetic dipole (including the moment of nearest neighbor Ni atoms) with a moment of $\mu = 3.76\ \mu_B$. For a quenched $Cu_{0.8}Ni_{0.2}$ alloy with 1000 ppm Fe the magnetization can be well described,[2] on the assumption of clustering of Fe atoms, in terms of magnetic dipoles associated with one, two, three, and four, or more Fe atoms.

From Mössbauer source experiments Bennett et al.[3] concluded that a small isolated magnetic cluster with $\mu = 4.2\ \mu_B$ is centered on each Fe atom in a rapidly quenched $Cu_{0.79}Ni_{0.21}$ alloy, to which trace amounts of ^{57}Co have been added. Similar, but larger, magnetic clusters were shown to exist[3] in alloys of higher Ni content. From ^{57}Fe Mössbauer absorption data for alloys with higher Fe concentrations (0.25 to 3%) Bennett et al.[4] concluded that in these alloys two distinct moment values are present; the smaller moment was claimed to be identical with that observed in the source experiments[3] and the larger

moment was ascribed to coupled pairs of the smaller clusters. The concentration of the two moment species, derived from the analysis of Mössbauer spectral line intensities, were claimed to be consistent,[4] within a factor of two, with a model, which assumes that the Fe and the Ni atoms are randomly distributed in the alloy and that the larger moment is formed when one small Fe-Ni cluster is the nearest neighbor of another. Under such conditions the two Fe moments may be coupled, even when one is the ninth-nearest neighbor of the other. Thus Bennett et al.[4] have in effect, proposed a long-range interaction between Fe moments via nearest neighbor Ni moments.

In contrast to the views of Bennett et al.[4] Window et al.[5] concluded from the isomer shift and the quadrupole splitting in Mössbauer spectra of dilute alloys of ^{57}Fe in Cu-Ni that both Fe-Fe and Fe-Ni clustering tendencies are present in Cu-Ni-Fe alloys.

As the above discussion points out, previous work has not unequivocally cleared up the question whether Cu-Ni-Fe alloys are random[4] or clustering effects are present.[2,5] In order to resolve this question it was decided to carry out extensive magnetization measurements as a function of the Fe content for $Cu_{0.9}Ni_{0.1}$ and $Cu_{0.8}Ni_{0.2}$ alloys containing 100 to 1000 ppm Fe. The reason for choosing Ni concentrations of 10 and 20 atomic percent is that at these compositions very few, if any, magnetic clusters are formed in the absence of Fe,[1] while at

are formed by Ni moments. For Fe levels up to 1000 ppm, the concentrations of single Fe and Fe pair clusters can be well determined from an analysis of the magnetization in terms of Brillouin functions.[2] These values may then be compared with the concentrations calculated on the basis of complete randomness.[4] If complete randomness is found to be inappropriate, and Fe-Fe clustering has to be postulated, it can be determined how the short range order parameter changes with the composition.

A long-range interaction between Fe moments, assuming randomness of the Fe atoms, has also been suggested for dilute Cu-Fe alloys.[6] However, recent Mössbauer work resolved[7,8] the presence in Cu-Fe alloys of Fe nearest neighbor pairs and larger aggregates in concentrations greater than that expected for random alloys. We therefore set out to make a careful reexamination of available magnetic data,[6,9] in order to ascertain whether or not they indicate the presence of magnetic clusters in dilute Cu-Fe alloys.

Based on observations of hyperfine splitting in Mössbauer spectra, it was suggested that Cu-Fe and Cu-Ni-Fe alloys are magnetically ordered at low temperatures.[5,10,11] It has been decided to check the validity of this suggestion by means of magnetization measurements.

II. SPECIMEN PREPARATION

A. Materials

The copper used for preparing the alloys was obtained in rod form from the American Smelting & Refining Company. It was 99.99% pure and contained less than 0.7 parts per million of Fe and 0.5 parts per million of Cr. High purity nickel (W.A.W. Grade; 99.99%) was supplied in strip form by the International Nickel Company. The major impurities present in the nickel were: Al (0.001%) and Ag (0.001%). All other impurities present were in concentrations of less than 0.0005%. The iron used was 99.98% pure. The major impurity was Ni (0.01%). The impurity content of each of these metals as reported by the suppliers is listed in Tables 1 and 2.

B. Melting

To facilitate weighing out the right amount for melting, the copper rod was cut into short lengths. The cut pieces were pickled in a 30% HNO_3 solution which removed the outer layers of the material. The residual acid was removed by washing repeatedly in distilled water, and finally in alcohol. As soon as the cleaning was finished the metal was placed under vacuum in a bell jar in order to prevent surface contamination and oxidation. The nickel strip was cut into rectangular pieces and then cleaned by etching, using a solution consisting of 1500

Table 1. Analysis of W.A.W. grade nickel (99.99%).

Impurity	% Amount
Al	< 0.001
As	< 0.0001
B	< 0.0001
Ca	< 0.0001
Cu	< 0.0004
Pb	< 0.0005
Mg	< 0.0001
Pd	< 0.0001
Ag	< 0.001
Na	< 0.0001
Sn	< 0.0003
Ti	< 0.0001
Zn	< 0.0001
V	< 0.0001
Zr	< 0.0001

Not found: Sb, Ba, Bi, Cs, Cr, Co, Cd, Ga, Ge, Au, In, Ir, La, Li, Mn, Hg, Mo, Os, Pt, K, Rh, Rb, Ru, Sc, Si, Sr, Ta, Te, Tl, W, Y.

Table 2. Spectrographic analysis of copper (99.999%) and lot analysis of iron.

Impurity	Amount in ppm.
Copper	
Fe	< 0.7
Sb	< 1.0
Pb	< 1
Sn	< 1
Ni	< 1
Bi	< 0.1
Cr	< 0.5
Si	< 0.1
Te	< 2
Ag	< 0.3
As	< 2
Iron	
Ti	20
Mn	10
Ni	100
Al	5
Balance Fe.	

parts concentrated H_2SO_4, 2250 parts concentrated HNO_3, 1000 parts H_2O and 30 grams NaCl. An etching time of about 10 seconds was found to be very satisfactory at room temperature. The residual reagent was removed by rinsing with distilled water and then with absolute alcohol. The iron was in the form of clean, shiny pieces and was cleaned with distilled water and absolute alcohol.

A special technique was developed for the preparation of virtually Fe-free Cu-Ni solid solutions. The technique involved melting the charge in a recrystallized alumina crucible under a slightly oxidizing atmosphere in an induction furnace. It was expected that any iron present would form iron oxide because of its greater affinity for oxygen. The empty alumina crucible was baked for four hours prior to the melting in order to drive out adsorbed moisture. Then the charge (about 20 grams) was placed in it and the crucible lowered into the furnace. The system was pumped down to about 5 microns of mercury and flushed several times with argon. Just before switching on the power, a calculated amount of air was introduced along with 1/2 atmosphere of argon so as to give a melting atmosphere with approximately 0.5% oxygen. Once the charge was completely molten ripples could be observed at the surface of the molten pool through a plexi-glass window at the top of the furnace. The power was kept "on" for 10 more minutes to insure good mixing. The alloy was then left in the furnace for about 3 hours to cool. The weight loss during melting was

The binary $Cu_{0.5}Ni_{0.5}$, $Cu_{0.52}Ni_{0.48}$, $Cu_{0.54}Ni_{0.46}$, $Cu_{0.6}Ni_{0.4}$ and $Cu_{0.9}Ni_{0.1}$ alloys were melted as described above. Two additional binary alloys, i.e, $Cu_{0.7}Ni_{0.3}$ and $Cu_{0.8}Ni_{0.2}$, prepared during the course of an earlier investigation by us, were also used in the present work. The $Cu_{0.7}Ni_{0.3}$ alloy was induction melted in an argon atmosphere and later remelted in an arc furnace; the $Cu_{0.8}Ni_{0.2}$ was melted in the induction furnace in a slightly oxidizing atmosphere, described above.

Small known amounts of Fe additions (up to 1000 atomic ppm) to the binary $Cu_{0.7}Ni_{0.3}$, $Cu_{0.8}Ni_{0.2}$ and $Cu_{0.9}Ni_{0.1}$ alloys were made as follows. First of all a master alloy (No. 1) was prepared by arc melting, using tungsten electrode and a water cooled copper crucible. This alloy was of the composition $Ni_{0.95}Fe_{0.05}$. The melting was carried out under approximately one atmosphere of argon gas and repeated six times, turning the button upside down on the copper crucible after each melting operation. This was expected to give a more uniform distribution of Fe. The arc melted button was rolled to a thickness of 0.007". This was cut into very small pieces and cleaned by etching with the same reagent which was used for cleaning the high purity nickel. A longer etching time was employed to dissolve completely any Fe contamination on the surface. This master alloy (No. 1) was used in turn to prepare another master alloy (No. 2) of the composition $Ni_{0.999}Fe_{0.001}$. The procedure was the same as that just described. Master alloy No. 2 was used to make small additions of Fe, in desired amounts, to the $Cu_{0.7}Ni_{0.3}$ (100 at ppm),

$Cu_{0.8}Ni_{0.2}$ (250 and 500 ppm) and $Cu_{0.9}Ni_{0.1}$ (100, 500 and 1000 ppm) alloys. An appropriate amount of the master alloy was placed underneath a piece of the binary Cu-Ni alloy and then the charge was arc melted, striking the arc on the latter. Melting was repeated three times. A $Cu_{0.8}Ni_{0.2}$ alloy containing 1000 at ppm Fe, melted in this way in our earlier investigation[1,2] was also used for the purposes of the present work. The specimen of a $Cu_{0.8}Ni_{0.2}$ alloy containing 100 ppm Fe, and prepared in the way discussed above during the course of the earlier work, was also available, but its size was found to be too small for accurate magnetization measurements, having been reduced in diameter for the high field measurements of Reference 2. A new alloy of this composition was prepared. The 100 ppm Fe alloy of Reference 2 shall be referred to as the "old $Cu_{0.8}Ni_{0.2}$ alloy with 100 ppm Fe."

Three alloys containing 1% Fe, namely $Cu_{0.99}Fe_{0.01}$, $(Cu_{0.9}Ni_{0.1})_{0.99}Fe_{0.01}$ and $(Cu_{0.8}Ni_{0.2})_{0.99}Fe_{0.01}$, were also prepared by arc melting. But here no master alloy was used; appropriate amounts of the metals were melted together, and the melting was repeated four times, turning the button upside down between successive melting operations.

C. Homogenizing Treatment

The as-cast buttons were first cold worked by compressing in a vise between two clean steel plates in three mutually perpendicular directions. The amount of deformation in each case

was about 20%. During compression the alloy button was kept at a temperature of ∿100° C with the help of a hot air gun. This aided in preventing the formation of cracks. The deformed alloy button, covered by molybdenum foil to act as an oxygen-getter, was enclosed in a fused silica capsule with 1/4 atmosphere of argon, then homogenized at 1050° C (or, 1000° C; see Table 3) for 24 hours and quenched into water (or, iced-brine). A suitable portion was cut out from each homogenized button. This piece was deformed, in the same way as discussed above, and then ground into the desired shape, reannealed for 1 hour and quenched. This double deformation technique ensures good homogenization. This was established in the following manner. The magnetization of a $Cu_{0.6}Ni_{0.4}$ alloy (prepared before the present investigation), deformed only once and quenched from 1050° C, was found to be 0.519 emu/g at 4.2° K in an applied field of 1.26 kOe; after a second deformation and quenching from the high temperature the magnetization was found under the same conditions as before to be 0.544 emu/g (∿4.5% higher). After repeating the deformation and quenching process a third time, measurements were found to yield a magnetization value of 0.539 emu/g. The reproducibility between the second and third measurements was thus better than 1% indicating that the degree of homogenization when the alloy was annealed following the second deformation was adequate.

Table 3. List of alloys used in the present investigation.

.	Alloy	Method of Melting	Quenching Temperature	Quenching Medium	Shape of Specimen
	$Cu_{0.5}Ni_{0.5}$	Induction (oxidizing atmosphere)	1050° C	Water	Spherical
	$Cu_{0.52}Ni_{0.48}$	- do -	- do -	- do -	- do -
	$Cu_{0.54}Ni_{0.46}$	- do -	- do -	- do -	- do -
	$Cu_{0.6}Ni_{0.4}$	- do -	- do -	- do -	Cylindrical
	$Cu_{0.7}Ni_{0.3}$	Induction (remelted in Arc furnace)	- do -	- do -	Rectangular-Parallelepiped
	$Cu_{0.8}Ni_{0.2}$	Induction (oxidizing atmosphere)	- do -		Cylindrical
	$Cu_{0.9}Ni_{0.1}$	- do -	- do -	- do -	Rectangular-Parallelepiped
	$Ni_{0.95}Fe_{0.05}$	Arc			
	$Ni_{0.999}Fe_{0.001}$	- do -			

Table 3 (Continued)

Alloy	Method of Melting	Quenching Temperature	Quenching Medium	Shape of Specimen
100 ppm Fe in $Cu_{0.7}Ni_{0.3}$	Arc	1050° C	Water	Rectangular-Parallelepiped
100 ppm Fe in $Cu_{0.8}Ni_{0.2}$	- do -	- do -	- do -	- do -
250 ppm Fe in $Cu_{0.8}Ni_{0.2}$	- do -	- do -	- do -	- do -
500 ppm Fe in $Cu_{0.8}Ni_{0.2}$	- do -	- do -	- do -	- do -
1000 ppm Fe in $Cu_{0.8}Ni_{0.2}$	- do -	- do -	- do -	Cylindrical
100 ppm Fe in $Cu_{0.9}Ni_{0.1}$	- do -	- do -	- do -	Rectangular-Parallelepiped
500 ppm Fe in $Cu_{0.9}Ni_{0.1}$	- do -	- do -	- do -	- do -

D. Deformed and Aged Specimens

After carrying out magnetization measurements with the as-quenched specimens of the $Cu_{0.8}Ni_{0.2}$ alloys with 100, 500 and 1000 ppm Fe, and $Cu_{0.9}Ni_{0.1}$ alloys with 100, 500 and 1000 ppm Fe, the specimens were deformed by about ∿20% in three mutually perpendicular directions, this time without the use of the hot air gun, and magnetic measurements were made in the deformed state.

In the case of the $Cu_{0.6}Ni_{0.4}$ alloy, after making measurements in the as-quenched condition the specimen was aged at 300° C for 3 days and quenched into water and measurements were made in the aged condition.

E. Chemical Analysis

Some of the iron-containing alloys were analyzed by absorption spectrophotometric methods to determine the actual iron concentrations. The results of such analyses are presented in Table 4. For each alloy two samples were analyzed. Except for the $Cu_{0.8}Ni_{0.2}$ alloy with a nominal concentration of 250 ppm Fe, the results of the analyses agree with the intended composition within experimental accuracy. The $Cu_{0.8}Ni_{0.2}$ alloy with 250 ppm Fe was found to be inhomogeneous. It was not possible to determine the reason for this inhomogeneity. For all ternary Cu-Ni-Fe alloys analyzed, the iron content was found to be slightly greater than the corresponding nominal concentration.

Table 4. Results of quantitative analysis for iron by spectrophotometry.

Alloy	Atomic ppm Fe	Average Atomic ppm Fe
	(a) Cu-Ni-Fe	
100 ppm Fe in $Cu_{0.9}Ni_{0.1}$	108 ± 3	108
	108 ± 3	
500 ppm Fe in $Cu_{0.9}Ni_{0.1}$	524 ± 16	521
	518 ± 16	
1000 ppm Fe in $Cu_{0.9}Ni_{0.1}$	1052 ± 34	1051
	1050 ± 34	
100 ppm Fe in $Cu_{0.8}Ni_{0.2}$	118 ± 3	116
	114 ± 3	
250 ppm Fe in $Cu_{0.8}Ni_{0.2}$	288 ± 8	312
	336 ± 8	
500 ppm Fe in $Cu_{0.8}Ni_{0.2}$	545 ± 14	559
	573 ± 14	
	(b) Cu-Fe	
$Cu_{0.99}Fe_{0.01}$	9110 ± 230	9250
	9390 ± 240	

Table 5. Results of mass spectrographic analysis for impurities. The concentrations are reported in atomic ppm within a factor of 3. Symbols: X--not detected; *--see Table 4.

Alloy	Cr	Mn	Fe	Co	W	Mo
$Cu_{0.6}Ni_{0.4}$	0.8	0.2	4.2	2.5	X	X
$Cu_{0.5}Ni_{0.5}$	4	4	15	X	X	300
$Cu_{0.99}Fe_{0.01}$	0.06	X	*	X	X	X
100 ppm Fe in $Cu_{0.9}Ni_{0.1}$	3	≤0.3	*	3	6	1
500 ppm Fe in $Cu_{0.9}Ni_{0.1}$	1	≤0.2	*	≤0.3	1	<0.1
1000 ppm Fe in $Cu_{0.9}Ni_{0.1}$	1	≤0.1	*	≤0.1	≤0.4	0.3
100 ppm Fe in $Cu_{0.8}Ni_{0.2}$	4	0.5	*	3.5	X	4.8
250 ppm Fe in $Cu_{0.8}Ni_{0.2}$	2.5	0.5	*	2.5	X	70
500 ppm Fe in $Cu_{0.8}Ni_{0.2}$	3	0.6	*	4	X	20

For the sake of convenience, however, we shall continue to refer to the alloys by their nominal concentrations.

Samples from some of the alloys were analyzed for minor impurities. The analyses were carried out by mass-spectrographic methods. The results are listed in Table 5.

Both types of analyses, i.e., absorption spectro-photometric and mass-spectrographic, were performed by the Chemical Analysis Division at the Materials Research Laboratory, University of Illinois.

F. Storage of Specimens

Since it has been reported[6] that Cu-Fe alloys change their magnetic properties when stored at room temperature over long periods of time, the $Cu_{0.99}Fe_{0.01}$, $(Cu_{0.9}Ni_{0.1})_{0.99}Fe_{0.01}$, and $(Cu_{0.8}Ni_{0.2})_{0.99}Fe_{0.01}$ alloys were stored in liquid nitrogen when not in use. All other specimens were stored at room temperature.

III. EXPERIMENTAL PROCEDURE

A. Force Measurement

The magnetization measurements were made by the Faraday method. In the Faraday method the force acting on a specimen in a nonuniform magnetic field is measured. The magnetic field is so arranged that the direction of the field is horizontal (H_X in Oersteds) and the gradient of the field is in the vertical direction (Z). A force F_Z, proportional to the susceptibility χ (defined here as $\frac{\sigma}{H_X}$ where σ is the magnetization) acts in the direction of the field gradient:

$$F_Z = \chi H_X \frac{dH_X}{dZ} \tag{1}$$

The force is measured by means of a balance, as an apparent weight change Δw (in grams). The susceptibility of the specimen in emu/g is calculated from the weight change

$$\chi = \Delta w \ (980.1)/H_X \frac{dH_X}{dZ} \cdot W \tag{2}$$

where 980.1 is the acceleration due to gravity in cm/sec^2 and W is the specimen mass in grams.

The specimen was suspended by means of a gold chain in the field produced by a Varian electromagnet. An aluminium heat shield was mounted near the specimen. (Prior to September 1970, a nylon string was used instead of the gold chain. All our measurements reported earlier[1,2] made use of this practice. It was

later noticed that the nylon string had a tendency to shrink a little when the surrounding medium was evacuated, thus displacing the specimen from the geometric center of the magnet gap. With a gold chain this problem does not arise.) The weight change Δw, in an applied field H (in the following we shall use the notation "H" for "H_x"), was calculated as:

$$\Delta w = {}_{H}W_{specimen} - {}_{H=0}W_{specimen} - \Delta w_g \qquad (3)$$

where the term Δw_g is the apparent weight change upon application of the field in the absence of a specimen. It represents the force acting on the gold chain and the aluminium heat shield in the field of the magnet. An automatic mechanism, located within the bell jar, housing the balance, allows the weights to be added or removed from the tare pan in one milligram increments up to a total of 100 milligrams. Weights smaller than one milligram were read from a strip chart recorder automatically operated by the balance.

B. Measurement and Control of Temperature

1. Cryostat for 300°K to 4.2°K (metal cryostat).

To control the temperature of the specimen in the temperature range 300-4.2°K, a cold finger type of cryostat was used. In this cryostat liquid helium is drawn up through a capillary and a 1/4" copper tube wound around the specimen chamber, thus cooling the specimen in turn. By varying the rate at which the helium is drawn up the tube, the temperature can be continuously

varied from 300° to 4.2°K. The temperature was measured by a Phylatron Model CD-500A GaAs sensor. A detailed description of the cryostat and the temperature measuring circuit can be found in the thesis of E. E. Barton, Jr.[12] Recently (1971) the length of the capillary has been changed to 2", and a filter assembly, using two 0.45 micron pore-filters, has been added between the capillary and the helium supply. These two changes were made for the purpose of reducing thermal oscillations at temperatures near 4.2°K.

2. Cryostat for 4.2°K to 1.3°K (glass cryostat).

Magnetization measurements in the temperature range of 4.2°K to 1.3°K were made in a double glass cryostat. In this case the specimen is suspended in a glass tube which is surrounded by a bath of liquid helium. The temperature can then be controlled by controlling the pressure of the helium vapor over the bath with the help of a vacuum pump. The temperature was determined by measuring the vapor pressure of the helium with a mercury manometer. The procedures for the operation of the cryostat and the measurement of the temperature are described in detail in the thesis of R. D. Shull.[13]

C. Measurement of the Field

In our present work the applied field (0 to 12.6 kOe) was measured by means of a Hall probe (InAs diode, Model FC-34, manufactured by Siemens). Previously (our measurements reported

in 1970; see References 1 and 2) it was the practice to measure the applied field with the help of a rotating coil gaussmeter positioned as close as possible to the specimen at the center of the magnet gap. This method resulted in a small error since the field actually experienced by the specimen was slightly different from that recorded by the gaussmeter; the positions of the gaussmeter and of the specimen were not exactly the same. For the present investigation, the Hall probe readings were calibrated with the rotating coil of the gaussmeter positioned at the center of the gap. In order to calibrate the field gradient, the magnetization of a spherical nickel specimen, prepared from WAW grade Ni, was measured at 293°K as a function of the applied field between 0.2 and 12.7 kOe and compared with corresponding literature values. The details of the calibration of the field and of the field gradient are discussed in detail in a special report.[14]

D. Corrections

(1). It was pointed out that in order to obtain the correct apparent weight change Δw of the specimen in an applied field H (Eq. 3) the weight change Δw_g due to the gold chain and to the shield assembly should be subtracted. The quantity Δw_g was measured as a function of field (up to ∿12.6 kOe) at various fixed temperatures (between ∿300°K and 4.2°K with the metal cryostat and between 4.2° and 1.35°K with the glass cryostat) and as a function of temperature in a constant applied field of ∿12.6 kOe

(Table 6). It was found that the variation of Δw_g (mg) with the field (kOe) and the temperature (°K) can be described by the following equations:

$$\Delta w_g = \begin{cases} (0.0128 - 5.88 \times 10^{-6} T) H^{1.81} & T \geq 80°K \\ (0.0121 + \frac{4.54 \times 10^{-3}}{T}) H^{1.81} & T \leq 80°K \end{cases} \quad (4)$$

(2). Of late (May, 1972) it has been found advantageous to make a small correction to the weight reading given by the Ainsworth microbalance, the balance weights (two 1mg, one 2mg, one 5mg, two 10mg, one 20mg, and one 50mg) apparently not being exact integer multiples of 1mg. The details of this correction may be found in the thesis of R. W. Tustison.[15] It should be noted that apart from this correction, the observed reproducibility of the balance was ±0.01mg.

The accuracy of the force, temperature, and field measurements is discussed in the thesis of R. D. Shull.[13]

E. Additional Measurements

Additional magnetization measurements were made on some of the specimens with a Foner-type vibrating-specimen magnetometer at the University of Illinois in Chicago. These measurements were made at 4.2°K as a function of applied field from 0 to 55 kOe. The 4.2°K isothermal data so obtained by the Foner method were found to be different (lower in all cases but one) from similar data obtained by the Faraday method in fields up to

Table 6. Measured values of Δw_g as a function of temperature and field. The measurements between ~300°K and 4.2°K were made in the metal cryostat; measurements at and below 4.2°K were made in the glass cryostat.

T (°K)	H (Oe)	Δw_g (mg)	T (°K)	H (Oe)	Δw_g (mg)
295.13	12738	1.099	64.78	12640	1.224
	10857	0.830	52.46	12640	1.226
	8900	0.590	34.45	12640	1.223
	7160	0.412	24.39	12640	1.219
	5677	0.284	16.69	12640	1.227
	4618	0.164			
	3690	0.112	11.09	12702	1.239
	2741	0.067		10833	0.921
	1492	0.022		8884	0.651
	411	0.001		7147	0.446
				5667	0.262
242.16	12640	1.134		4611	0.186
188.65	12640	1.151		3684	0.125
132.64	12640	1.183		2734	0.065
99.30	12640	1.193		1487	0.021
				404	0.001
78.08	12738	1.224			
	10857	0.921	6.61	12640	1.239
	8900	0.651			
	7158	0.457	4.2	12604	1.338
	5670	0.311		10847	1.054
	4615	0.185		8905	0.754
	3689	0.125		7160	0.469
	2739	0.075		5679	0.312
	1490	0.028		4626	0.195
	411	0.008		3694	0.134
	209	0.003		2744	0.080

Table 6. (Continued)

T (°K)	H (Oe)	Δwg (mg)	T (°K)	H (Oe)	Δwg (mg)
4.2	1500	0.028	1.35	12560	1.557
	415	0.006		10849	1.148
	275	0.002		8904	0.819
	214	0.001		7162	0.586
				5680	0.334
3.38	12640	1.333		4622	0.240
2.81	12640	1.360		3699	0.150
1.90	12640	1.436		2746	0.083
				1503	0.033
				414	0.003
				274	0.001

12.6 kOe. In some cases where the absolute value of the magnetization was small, e.g., for 100 ppm Fe in $Cu_{0.9}Ni_{0.1}$ the magnetization in a field of 12.6 kOe is $\sim 8.9 \times 10^{-3}$ emu/g at 4.2°K, reproducibility of the vibrating magnetometer data was very poor. For the $Cu_{0.6}Ni_{0.4}$ alloy, where the absolute value of the magnetization is quite large (i.e., of the order of $\sim$0.5 emu/g in 12 kOe field at 4.2°K), the difference in the magnetization values obtained by the vibrating magnetomer and Faraday methods was rather small. Therefore except for $Cu_{0.6}Ni_{0.4}$, the vibrating magnetometer data obtained at Chicago were not utilized.

Magnetization measurements on the quenched $Cu_{0.7}Ni_{0.3}$ alloy (Reference 1) were also performed at 4.2°K and in fields up to 54 kOe with a vibrating magnetometer by Dr. S. Foner at the National Magnet Laboratory at M. I. T., Cambridge. These data were somewhat lower than the corresponding Faraday technique data obtained by us during the course of our earlier investigation[1] of the same alloy. In spite of uncertainties of the Foner data, it was found possible to use these high field data for the analysis.

For the two alloys $Cu_{0.6}Ni_{0.4}$ and $Cu_{0.7}Ni_{0.3}$, the Faraday technique data were assumed to be more accurate in an absolute sense. The higher field magnetometer data were used as relative values and they were normalized to the Faraday method data by using a constant factor determined at fields of 12.6 kOe and less,

$$\sigma = \sigma_F \, R \qquad (5)$$

where,

R is the normalization factor

σ_F is the magnetization in emu/g as measured with the vibrating-specimen magnetometer

σ is the normalized magnetization in emu/g

The normalization factors used are listed in the corresponding data tables.

IV. EXPERIMENTAL RESULTS

A. Data Tables

Table 7. Magnetization data for quenched $Cu_{0.5}Ni_{0.5}$. The measurements between ∿300°K and 4.2°K were made in the metal cryostat; the measurements at and below 4.2° K were made in the glass cryostat. See Figures 1, 2, 5, and 9.

T (°K)	H (Oe)	σ (emu/g)	T (°K)	H (Oe)	σ (emu/g)
299.44	12566	0.092	40.25	7649	3.078
243.20	12538	0.125		7365	3.050
189.81	12538	0.192		6241	2.923
132.57	12538	0.399		5084	2.766
101.12	12535	0.740		4065	2.587
				3298	2.431
78.08	12529	1.308		2102	2.080
	10649	1.155		1016	1.560
	8705	0.976		913	1.501
	6998	0.807		802	1.389
	5548	0.656		669	1.255
	4524	0.542		605	1.194
	3611	0.436		503	1.089
	2640	0.320		442	1.000
	1404	0.172		315	0.820
	369	0.036		308	0.783
				281	0.750
53.31	9646	2.354		258	0.720
	7867	2.147		226	0.672
	6241	1.913		213	0.657
	5079	1.711		193	0.597
	4455	1.502		161	0.524
	3295	1.311		129	0.442
	2099	0.943		97	0.362
	1017	0.509		64	0.269
	407	0.203		32	0.198

Table 7. (Continued)

T (°K)	H (Oe)	σ (emu/g)	T (°K)	H (Oe)	σ (emu/g)
34.80	6882	3.409	29.98	6343	3.710
	6232	3.344		6226	3.694
	5086	3.215		5091	3.592
	4061	3.069		4064	3.474
	3298	2.935		3300	3.371
	2099	2.658		2102	3.147
	1017	2.255		1019	2.848
	929	2.216		866	2.768
	866	2.158		739	2.716
	802	2.102		611	2.664
	738	2.082		483	2.586
	674	2.059		357	2.472
	610	2.004		290	2.458
	546	1.955		226	2.407
	482	1.866		194	2.254
	418	1.795		161	2.278
	354	1.714		129	2.185
	322	1.690		97	2.113
	290	1.654		81	2.044
	258	1.622		64	1.783
	226	1.522		44	1.261
	193	1.459		32	1.087
	161	1.326		16	0.851
	129	1.281			
	97	1.199	25.22	5910	4.007
	64	1.060		5082	3.942
	32	0.993		4061	3.853
				3299	3.767
				2498	3.662

Table 7. (Continued)

T (°K)	H (Oe)	σ (emu/g)	T (°K)	H (Oe)	σ (emu/g)
25.22	2085	3.596	20.08	4236	4.249
	1269	3.451		3866	4.214
	1022	3.393		4040	4.224
	866	3.308		3529	4.188
	738	3.312		3092	4.148
	611	3.280		2563	4.083
	482	3.221		2085	4.025
	418	3.192		1548	3.953
	354	3.156		1015	3.868
	290	3.129		866	3.830
	258	3.094		739	3.805
	226	3.074		611	3.771
	193	3.026		483	3.749
	161	3.002		419	3.742
	145	2.986		354	3.716
	129	2.985		290	3.684
	113	2.776		258	3.652
	97	2.538		226	3.617
	81	2.086		193	3.589
	64	1.836		161	3.563
	48	1.470		145	3.349
	32	1.211		129	3.305
	24	1.135		113	2.950
	16	0.908		97	2.622
	8	0.794		81	2.108
				64	1.915
20.08	5458	4.327		48	1.576
	4747	4.283		32	1.229

Table 7. (Continued)

T (°K)	H (Oe)	σ (emu/g)	T (°K)	H (Oe)	σ (emu/g)
20.08	24	0.996	14.98	64	1.868
	16	0.813		48	1.564
	8	0.680		40	1.392
				32	1.229
14.98	5080	4.632		24	1.021
	4699	4.619		16	0.718
	4061	4.578		8	0.680
	3678	4.562			
	3288	4.531	10.39	4830	4.902
	2602	4.478		4441	4.890
	2030	4.433		4057	4.872
	1605	4.383		3589	4.851
	1214	4.360		3305	4.843
	1006	4.318		2625	4.807
	866	4.316		2084	4.761
	739	4.287		1447	4.740
	611	4.286		1024	4.695
	483	4.263		897	4.676
	354	4.257		739	4.657
	290	4.179		611	4.653
	258	4.227		483	4.689
	226	4.194		418	4.627
	194	4.137		354	4.603
	161	3.790		290	4.578
	145	3.511		258	4.616
	129	3.204		226	4.575
	113	2.878		193	4.372
	97	2.584		161	3.871
	81	2.214		145	3.523

Table 7. (Continued)

T (°K)	H (Oe)	σ (emu/g)	T (°K)	H (Oe)	σ (emu/g)
10.39	129	3.150	3.22	3796	5.211
	113	2.899		3487	5.205
	97	2.590		3176	5.197
	81	2.081		2864	5.184
	64	1.769		2550	5.171
	48	1.469		2236	5.168
	32	1.087		1920	5.150
	24	1.046		1603	5.135
	16	0.718		1282	5.135
	8	0.605		964	5.122
				644	5.102
4.2	4501	5.204		484	5.104
	4087	5.188		323	5.066
	3794	5.180		258	5.014
	3485	5.168		194	4.507
	3174	5.159		129	3.333
	2862	5.144		65	1.875
	2549	5.136			
	2234	5.120	1.95	4508	5.258
	1919	5.095		4105	5.256
	1602	5.086		3796	5.264
	1281	5.072		3487	5.244
	963	5.061		3176	5.235
	644	5.040		2864	5.227
	323	4.691		2550	5.224
				2236	5.208
3.22	4505	5.231		1920	5.191
	4105	5.221		1603	5.183

Table 7. (Continued)

T (°K)	H (Oe)	σ (emu/g)	T (°K)	H (Oe)	σ (emu/g)
1.95	1282	5.190	1.63	2863	5.235
	964	5.175		2550	5.227
	644	5.163		2235	5.213
	484	5.161		1920	5.199
	323	5.150		1603	5.190
	258	5.079		1281	5.186
	194	4.497		964	5.179
	129	3.244		644	5.140
	64	1.830		483	5.173
				323	5.121
1.63	4506	5.260		258	5.073
	4104	5.260		194	4.494
	3796	5.252		129	3.274
	3486	5.242		64	1.687
	3175	5.240			

Table 8. Magnetization data for quenched $Cu_{0.52}Ni_{0.48}$. The measurements were made in the glass cryostat. See Figures 3 and 10.

T (°K)	H (Oe)	σ (emu/g)	T (°K)	H (Oe)	σ (emu/g)
4.2	12499	3.597	2.81	5617	3.512
	11677	3.582		4708	3.493
	10842	3.566		3788	3.465
	9998	3.551		2858	3.417
	9144	3.527		1916	3.351
	8279	3.504		643	3.224
	7403	3.484			
	6516	3.465	1.48	12503	3.666
	5618	3.434		11676	3.655
	4709	3.389		10841	3.644
	3789	3.356		9997	3.631
	2858	3.291		9143	3.620
	1916	3.202		8278	3.606
	962	3.127		7402	3.592
				6515	3.574
2.81	12530	3.635		5617	3.552
	11677	3.622		4708	3.544
	10842	3.607		3788	3.510
	9997	3.594		2858	3.454
	9143	3.579		1916	3.428
	8278	3.566		1279	3.374
	7402	3.548		643	3.327
	6515	3.526		322	3.311

Table 9. Magnetization data for quenched $Cu_{0.54}Ni_{0.46}$. The measurements were made in the glass cryostat. See Figures 4 and 11.

T (°K)	H (Oe)	σ (emu/g)	T (°K)	H (Oe)	σ (emu/g)
4.2	12536	2.409	4.2	32	1.090
	11689	2.388		16	0.844
	10853	2.370		8	0.633
	10007	2.350			
	9153	2.325	2.89	12574	2.468
	8287	2.298		11686	2.451
	7410	2.264		10850	2.430
	6522	2.233		10005	2.410
	5623	2.196		9150	2.389
	4714	2.149		8285	2.368
	3793	2.086		7408	2.341
	2861	2.001		6521	2.314
	1918	1.935		5622	2.277
	1280	1.803		4712	2.244
	963	1.713		3792	2.194
	643	1.611		2860	2.127
	483	1.540		1917	2.032
	387	1.500		1280	1.935
	322	1.470		962	1.864
	260	1.404		643	1.762
	196	1.310		322	1.645
	161	1.330		56	1.298
	129	1.284			
	97	1.254	1.45	12618	2.518
	64	1.266		11681	2.508
	48	1.172		10846	2.490

Table 9. (Continued)

T (°K)	H (Oe)	σ (emu/g)	T (°K)	H (Oe)	σ (emu/g)
1.45	10001	2.479	1.45	2859	2.265
	9147	2.462		1917	2.189
	8281	2.445		1279	2.122
	7405	2.427		962	2.047
	6518	2.404		643	2.001
	5620	2.381		322	1.859
	4710	2.352		206	1.781
	3790	2.315		58	1.447

Table 10. Magnetization data for quenched $Cu_{0.9}Ni_{0.1}$. The measurements were made in the metal cryostat. See Figures 13, 14, and 36.

T (°K)	H (Oe)	σ (10^{-3} emu/g)	(°K)	(Oe)	σ (10^{-3} emu/g)
300.38	12554	1.806	14.84	12570	1.987
242.44	12549	1.762	10.92	12570	1.974
190.69	12560	1.843	8.89	12568	2.012
130.37	12562	1.766			
99.17	12560	1.736	4.2	12638	2.521
76.64	12564	1.771		10770	2.101
60.44	12560	1.776		8838	1.701
44.88	12560	1.818		7101	1.432
34.63	12565	1.868		5639	1.040
33.18	12570	1.831		4591	0.883
25.33	12572	1.895		3662	0.743
20.84	12570	1.978			

Table 11. Magnetization data for quenched $Cu_{0.7}Ni_{0.3}$.

T (°K)	H (Oe)	σ (10^{-3}emu/g)	T (°K)	H (Oe)	σ (10^{-3}emu/g)

(a) Faraday method data. These measurements were made in the metal cryostat. See Figures 14 and 15.

299.27	12638	13.00	7.84	12638	16.83
215.11	12638	13.05	6.1	12638	17.39
131.15	12638	13.30			
76.45	12638	13.77	4.2	12608	18.84
60.91	12638	13.96		10674	16.17
40.54	12638	14.39		8784	13.07
24.85	12638	14.97		5601	8.10
11.09	12638	16.25		3637	5.24

(b) Normalized magnetometer data. Normalization factor R = 1.068. See Figure 15.

4.2	54300	76.04	4.2	23160	34.30
	50407	71.00		19267	28.56
	46514	66.31		15375	21.93
	42622	61.10		12608	18.66
	38729	55.79		10674	15.83
	34837	50.48		8784	12.99
	30944	45.09		5601	8.31
	27052	39.78		3637	5.31

Table 12. Magnetization data for quenched $Cu_{0.6}Ni_{0.4}$.

T (°K)	H (Oe)	σ (10^{-2}emu/g)	T (°K)	H (Oe)	σ (10^{-2}emu/g)

(a) Faraday method data. The measurements between ∿300°K and 4.2°K were made in the metal cryostat; the measurements at and below 4.2°K were made in the glass cryostat. See Figures 16 through 19.

298.41	12567	3.32	29.47	2644	3.08
243.49	12570	3.62		1406	1.48
190.77	12566	4.03			
131.15	12571	5.09	20.58	12552	18.50
95.04	12569	6.25		10669	15.99
74.75	12558	7.29		8688	13.11
61.49	12558	8.43		7010	10.70
				5556	8.49
40.84	12541	11.48		4521	6.86
	10666	9.78		3613	5.57
	8714	8.04		2643	4.09
	7004	6.42		1409	1.94
	5554	5.07			
	4524	4.04	14.84	12566	23.74
	3612	3.36		10680	20.48
	2642	2.36		8711	16.99
	1406	1.21		7015	13.97
				5563	11.10
29.47	12552	14.57		4528	9.21
	10670	12.42		3617	7.45
	8718	10.22		2641	5.34
	7016	8.25		1409	2.84
	5557	6.53			
	4522	5.30	10.39	12554	29.77
	3613	4.27		10673	26.17

Table 12. (Continued)

T (°K)	H (Oe)	σ (10^{-2}emu/g)	T (°K)	H (Oe)	σ (10^{-2}emu/g)
10.39	8720	22.21	2.52	4060	30.32
	7014	18.40		3297	26.74
	5561	15.01		2101	19.77
	4520	12.47		1019	11.26
	3616	10.03		642	7.66
	2646	7.56		467	4.44
	1407	3.92		374	3.80
				292	3.27
4.20	12694	45.49		245	2.65
	11556	43.45		212	2.00
	9743	39.90			
	7881	35.49	1.49	12675	54.17
	6255	30.93		11540	52.60
	5091	27.18		9733	50.01
	4066	22.96		7868	46.73
	3301	19.74		6244	43.19
	2104	13.15		5081	40.03
	1018	7.01		4057	36.32
	538	3.04		3295	33.01
	340	1.87		2097	26.03
	257	1.55		1014	16.48
	205	1.16		636	11.73
				534	10.11
2.52	12678	50.84		443	6.66
	11540	49.11		338	5.46
	9730	46.03		289	4.74
	7869	41.91		254	4.35
	6246	38.00		229	3.94

Table 12. (Continued)

T (°K)	H (Oe)	σ (10^{-2}emu/g)	T (°K)	H (Oe)	σ (10^{-2}emu/g)

(b) Normalized magnetometer data.
Normalization factor R = 1.046.
See Figures 16 and 18.

4.2	55000	82.80	4.2	15000	49.20
	50000	79.82		12000	44.30
	45000	76.61		10000	40.42
	40000	73.22		8000	35.80
	35000	69.56		6000	30.13
	30000	65.58		4000	22.85
	25000	61.00		2000	13.14
	20000	55.68			

Table 13. Magnetization data for aged $Cu_{0.6}Ni_{0.4}$.

T (°K)	H (Oe)	σ (10^{-2}emu/g)	T (°K)	H (Oe)	σ (10^{-2}emu/g)

(a) Faraday method data. The measurements between ∿300°K and 4.2°K were made in the metal cryostat; the measurements at and below 4.2°K were made in the glass cryostat. See Figures 18, 19, and 20.

297.33	12559	3.27	40.84	12566	14.77
	10670	2.71		10660	12.54
	8716	2.25		8665	9.99
	7007	1.81		6993	8.04
	4517	1.14		5534	6.89
	5551	1.47		4503	5.61
	3609	1.01		3598	3.83
	2645	0.82		2634	2.89
244.19	12583	3.52	34.63	3573	4.77
189.75	12578	4.10			
132.64	12581	5.40	20.58	12560	26.11
101.14	12581	6.72		10645	22.47
				8683	18.60
77.67	12578	8.31		6981	15.14
	10682	6.91		5531	12.42
	8722	5.70		4503	10.27
	7013	4.65		3592	7.62
	5560	3.63		2651	5.10
	4523	2.97		1401	3.21
	3612	2.42			
	2642	1.86	15.27	3573	10.71
	1406	0.90		2626	7.53
60.60	12578	10.13	10.39	12594	42.03
52.55	12578	11.66		10702	37.88

Table 13. (Continued)

T (°K)	H (Oe)	σ (10^{-2}emu/g)	T (°K)	H (Oe)	σ (10^{-2}emu/g)
10.39	8741	32.54	2.52	12615	68.97
	6976	27.79		10718	65.96
	5574	23.12		8725	61.10
	4540	19.51		6896	56.71
	3624	15.96		5579	51.98
	2651	12.25		4539	47.72
	1409	6.30		3629	42.79
				2656	36.35
7.06	12525	50.60		1409	25.11
	10631	46.12		1056	20.32
	8673	40.83		373	8.55
	6974	35.50		241	5.69
	5531	30.54			
	4500	26.21	1.49	12602	72.93
	3597	21.30		10713	70.23
	2631	16.66		8759	66.79
	1399	9.66		7037	63.10
				5579	58.77
4.2	12602	62.41		4540	55.01
	10719	58.30		3627	50.55
	8754	53.40		2652	44.20
	7039	48.07		1411	33.06
	5579	42.60		1214	30.93
	4544	38.00		1067	28.82
	3626	32.11		953	26.86
	2656	26.12		804	24.52
	1411	16.31		644	21.12
	372	5.08		484	18.40
				323	15.54
				216	11.61

Table 13. (Continued)

T (°K)	H (Oe)	σ (10^{-2}emu/g)	T (°K)	H (Oe)	σ (10^{-2}emu/g)

(b) Normalized magnetometer data.
Normalization factor R = 0.989.
See Figure 18.

4.2	55000	99.42	4.2	15000	65.75
	50000	96.55		12000	60.50
	45000	93.51		10000	56.17
	40000	90.23		8000	50.88
	35000	86.73		6000	44.18
	30000	82.76		4000	35.04
	25000	78.00		2000	21.52
	20000	72.80			

Table 14. Magnetization data for quenched $Cu_{0.99}Fe_{0.01}$. The measurements between ∿300°K and 4.2°K were made in the metal cryostat; the measurements at and below 4.2°K were made in the glass cryostat. The data are listed in the order in which they were taken.

T (°K)	H (Oe)	σ (emu/g)	T (°K)	H (Oe)	σ (emu/g)

(a) Specimen cooled in an applied field of ∿12.65 kOe. See Figure 26.

295.57	12648	0.0298	35.08	5636	0.1561
245.53	12648	0.0383		4585	0.1281
189.10	12648	0.0543		3664	0.1063
159.30	12647	0.0725		2716	0.0681
99.95	12646	0.1169		1477	0.0459
				402	0.0155
77.84	12644	0.1491			
	10794	0.1258	24.86	12633	0.3764
	8849	0.1025		10785	0.3369
	7117	0.0817		8840	0.2904
	5645	0.0689		7110	0.2456
	4590	0.0543		5639	0.2026
	3668	0.0350		4587	0.1654
	2719	0.0356		3662	0.1404
	1475	0.0206		2716	0.1041
	402	0.0079		1478	0.0567
				402	0.0195
61.90	12643	0.1860			
			11.27	12630	0.5493
35.08	12638	0.3029		10777	0.5044
	10774	0.2696		8833	0.4522
	8838	0.2294		7103	0.3988
	7108	0.1907		5633	0.3438

Table 14. (Continued)

T (°K)	H (Oe)	σ (emu/g)	T (°K)	H (Oe)	σ (emu/g)
11.27	4578	0.2987	4.2	8831	0.5558
	3657	0.2561		7104	0.4964
	2711	0.2048		5635	0.4364
	1473	0.1246		4582	0.3905
	401	0.0457		3657	0.3417
				2711	0.2824
6.61	12643	0.6231		1476	0.1782
	10783	0.5820		400	0.0616
	8834	0.5283			
	7094	0.4737	1.4	12645	0.6743
	5635	0.4176		10771	0.6289
	4582	0.3703		8831	0.5095
	3658	0.3268		7099	0.5096
	2710	0.2684		5629	0.4499
	1475	0.1740		4579	0.4010
	379	0.0615		3656	0.3520
				2710	0.2856
4.2	12643	0.6537		1475	0.1869
	10782	0.6085		400	0.0822

(b) Specimen cooled in a field of 1000 Oe. See Figure 29.

15.27	1000	0.0552	6.50	1000	0.1155
12.81	1000	0.0669	5.67	1000	0.1252
11.09	1000	0.0762	4.80	1000	0.1287
10.05	1000	0.0815	4.23	1000	0.1306
7.71	1000	0.1025	4.20	1000	0.1276
7.19	1000	0.1078	3.80	1000	0.1284

Table 14. (Continued)

T (°K)	H (Oe)	σ (emu/g)	T (°K)	H (Oe)	σ (emu/g)
3.50	1000	0.1266	1.71	1000	0.1217
2.93	1000	0.1272	1.63	1000	0.1218
2.63	1000	0.1238	1.52	1000	0.1159
2.28	1000	0.1232	1.35	1000	0.1182
1.86	1000	0.1238			

(c) Specimen cooled in zero field. See Figure 29.

1.40	1000	0.0965	4.23	1000	0.1296
1.48	1000	0.1042	4.49	1000	0.1296
1.59	1000	0.1085	4.98	1000	0.1286
1.72	1000	0.1105	5.59	1000	0.1257
1.85	1000	0.1136	6.61	1000	0.1140
2.05	1000	0.1202	8.58	1000	0.0932
2.17	1000	0.1233	10.92	1000	0.0771
2.47	1000	0.1242	14.11	1000	0.0628
2.84	1000	0.1251	16.69	1000	0.0545
2.99	1000	0.1254	24.86	1000	0.0405
3.13	1000	0.1254	35.84	1000	0.0243
3.33	1000	0.1271	39.81	1000	0.0236
3.64	1000	0.1259	48.05	1000	0.0200
3.90	1000	0.1290	55.02	1000	0.0162
4.20	1000	0.1296			

(d) Low-field data for remanence-temperature determination. See Figure 23.

4.2	388	0.0539	4.2	322	0.0466
	355	0.0497		290	0.0418

Table 14. (Continued)

T (°K)	H (Oe)	σ (emu/g)	T (°K)	H (Oe)	σ (emu/g)
4.2	258	0.0381	1.43	322	0.0738
	226	0.0335		290	0.0742
	194	0.0283		258	0.0730
	161	0.0231		226	0.0724
	129	0.0184		194	0.0683
	97	0.0160		161	0.0626
	65	0.0144		129	0.0613
	48	0.0107		97	0.0635
	32	0.0096		65	0.0598
	16	0.0064		48	0.0603
				32	0.0614
1.43	381	0.0739		16	0.0582
	355	0.0738			

Table 15. Magnetization data for quenched $(Cu_{0.9}Ni_{0.1})_{0.99}Fe_{0.01}$. The measurements between ∿300°K and 4.2°K were made in the metal cryostat; the measurements at and below 4.2°K were made in the glass cryostat. The data are listed in the order in which they were taken.

T (°K)	H (Oe)	σ (emu/g)	T (°K)	H (Oe)	σ (emu/g)
(a) Specimen cooled in an applied field of ∿12.65 kOe. See Figure 27.					
300.63	12625	0.0492	32.90	12560	0.5969
242.91	12599	0.0659		11460	0.5546
217.74	12583	0.0757		9648	0.4821
189.72	12577	0.0907		7773	0.4001
159.62	12575	0.1123		6179	0.3258
134.23	12567	0.1387		5029	0.2695
104.09	12565	0.1862		4019	0.2179
				3229	0.1763
69.46	12559	0.2900		2019	0.1010
	11539	0.2679		1742	0.0952
	9733	0.2289		1424	0.0791
	7867	0.1865		1214	0.0675
	6243	0.1485		1092	0.0605
	5082	0.1208		956	0.0532
	4065	0.0966		215	0.0146
	3303	0.0785			
	2101	0.0504	23.81	12543	0.7600
	1591	0.0378		11538	0.7179
	1238	0.0296		9729	0.6289
	1068	0.0257		7862	0.5290
	954	0.0228		6239	0.4392
	213	0.0048		5077	0.3658
				4055	0.2994
56.23	12553	0.3620		3295	0.2468
42.43	12548	0.4826		2099	0.1598

Table 15. (Continued)

T (°K)	H (Oe)	σ (emu/g)	T (°K)	H (Oe)	σ (emu/g)
23.81	1747	0.1316	12.14	4053	0.5265
	1491	0.1143		3292	0.4470
	1273	0.0983		2098	0.3089
	1065	0.0828		1710	0.2586
	242	0.0169		1489	0.2306
	211	0.0162		1287	0.2002
				1114	0.1725
16.69	12540	0.9449		952	0.1459
	11524	0.8967		213	0.0298
	9716	0.8000			
	7861	0.6905	7.57	9721	1.0682
	6236	0.5835		7851	0.9527
	5075	0.4982		6205	0.8392
	4054	0.4117		5077	0.7373
	3291	0.3475		4055	0.6376
	2098	0.2278		3296	0.5524
	1826	0.2013		2099	0.3979
	1588	0.1767		1707	0.3396
	1336	0.1509		1491	0.3070
	1159	0.1332		1281	0.2682
	1034	0.1202		1145	0.2452
	953	0.1114		1022	0.2502
	213	0.0298		949	0.2093
				202	0.0564
12.14	11431	1.0336			
	9690	0.9431	5.44	9723	1.1089
	7851	0.8279		7875	0.9842
	6235	0.7128		6238	0.8674
	5075	0.6189		5059	0.7670

Table 15. (Continued)

T (°K)	H (Oe)	σ (emu/g)	T (°K)	H (Oe)	σ (emu/g)
5.44	3292	0.5823	4.2	6237	0.8830
	2090	0.4218		5081	0.7826
	1778	0.3732		4055	0.6768
	1571	0.3385		3297	0.5910
	1411	0.3128		2099	0.4293
	1240	0.2808		1752	0.3712
	1112	0.2591		1510	0.3282
	949	0.2268		1335	0.2983
	211	0.0492		1206	0.2737
				1083	0.2454
4.2	9724	1.1279		953	0.2250
	7861	1.0071		214	0.0453

(b) Specimen cooled in a field of ∿700 Oe. See Figure 30.

4.2	700	0.1732	2.12	700	0.1658
3.68	700	0.1709	1.98	700	0.1614
3.34	700	0.1691	1.82	700	0.1642
2.61	700	0.1741	1.68	700	0.1573
2.20	700	0.1712	1.61	700	0.1648
2.17	700	0.1734	1.45	700	0.1590

(c) Specimen cooled in zero field. See Figure 30.

1.45	700	0.1271	1.65	700	0.1408
1.57	700	0.1484	1.70	700	0.1397
1.61	700	0.1456	1.78	700	0.1441

Table 15. (Continued)

T (°K)	H (Oe)	σ (emu/g)	T (°K)	H (Oe)	σ (emu/g)
1.85	700	0.1510	3.35	700	0.1557
2.03	700	0.1550	3.57	700	0.1574
2.13	700	0.1513	3.64	700	0.1539
2.46	700	0.1539	3.72	700	0.1554
2.72	700	0.1550	3.84	700	0.1656
3.04	700	0.1528	4.00	700	0.1626
3.15	700	0.1554	4.2	700	0.1640

(d) Low-field data for remanence-temperature determination. See Figure 24.

4.2	643	0.1599	2.12	644	0.1579
	579	0.1464		580	0.1504
	515	0.1344		516	0.1375
	451	0.1184		451	0.1230
	419	0.1095		419	0.1119
	387	0.1022		387	0.1075
	355	0.0969		355	0.1003
	322	0.0922		323	0.0949
	290	0.0842		290	0.0888
	258	0.0765		258	0.0835
	226	0.0701		226	0.0788
	194	0.0592		194	0.0740
	161	0.0523		161	0.0654
	129	0.0444		129	0.0596
	97	0.0374		97	0.0561
	65	0.0304		65	0.0515
	32	0.0187		32	0.0468

Table 15. (Continued)

T (°K)	H (Oe)	σ (emu/g)	T (°K)	H (Oe)	σ (emu/g)
1.61	644	0.1657	1.61	258	0.0947
	580	0.1606		226	0.0948
	515	0.1549		194	0.0834
	451	0.1462		161	0.0739
	419	0.1329		129	0.0725
	287	0.1287		97	0.0624
	355	0.1208		65	0.0585
	323	0.1109		32	0.0422
	290	0.1024			

Table 16. Magnetization data for quenched $(Cu_{0.8}Ni_{0.2})_{0.99}Fe_{0.01}$. The measurements between ∿300°K and 4.2°K were made in the metal cryostat; the measurements at and below 4.2°K were made in the glass cryostat. The data are listed in the order in which they were taken.

T (°K)	H (Oe)	σ (emu/g)	T (°K)	H (Oe)	σ (emu/g)
(a) Specimen cooled in an applied field of ∿12.55 kOe. See Figure 28.					
297.86	12575	0.0494	42.50	8871	0.3923
266.93	12561	0.0562		7131	0.3195
245.76	12560	0.0631		5656	0.2545
216.38	12556	0.0741		4608	0.2091
191.24	12553	0.0863		3679	0.1678
163.64	12553	0.1049		2738	0.1249
131.10	12555	0.1382		1491	0.0683
102.65	12552	0.1873		412	0.0180
				273	0.0113
70.06	12548	0.2979		212	0.0088
	10804	0.2582			
	8874	0.2134	33.37	12541	0.6864
	7133	0.1722			
	5657	0.1370	24.28	12540	0.9082
	4607	0.1115		10795	0.8106
	3684	0.0897		8872	0.6927
	2739	0.0676		7129	0.5773
	1490	0.0363		5655	0.4668
	412	0.0095		4604	0.3852
	273	0.0067		3679	0.3115
	213	0.0035		2734	0.2347
				1490	0.1230
56.39	12541	0.3853		412	0.0355
				273	0.0236
42.50	12541	0.5373		212	0.0175
	10780	0.4706			

Table 16. (Continued)

T (°K)	H (Oe)	σ (emu/g)	T (°K)	H (Oe)	σ (emu/g)
15.70	10067	1.0785	7.99	1497	0.3838
	8829	0.9919		1276	0.3353
	7134	0.8545		1163	0.3082
	5657	0.7139		1053	0.2855
	2611	0.6082		957	0.2591
	3682	0.4991		215	0.0466
	2735	0.3836		60	0.0045
	1492	0.2162			
	412	0.0599	5.59	8126	1.3725
	272	0.0408		7139	1.2819
	56	0.0123		5658	1.1235
				4598	0.9959
10.92	8821	1.2110		3682	0.8691
	7138	1.0673		2736	0.7149
	5657	0.9124		1490	0.4626
	4605	0.7934		412	0.1594
	3680	0.6740		315	0.1110
	2735	0.5334		258	0.0975
	2334	0.4620		213	0.0853
	2040	0.4132		56	0.0248
	998	0.2124			
	941	0.2023	4.2	8080	1.4131
	209	0.0346		7145	1.3265
				5662	1.1673
7.99	8896	1.3291		4612	1.0364
	7151	1.1763		3688	0.9015
	5670	1.0235		2742	0.7420
	4617	0.8985		1496	0.4778
	3687	0.7725		1276	0.4174
	2745	0.5234		1115	0.3798

Table 16. (Continued)

T (°K)	H (Oe)	σ (emu/g)	T (°K)	H (Oe)	σ (emu/g)
4.2	958	0.3295	4.2	55	0.0253
	216	0.0676			

(b) Specimen cooled in a field of ∿1000 Oe. See Figure 31.

303.20	1000	0.0049	5.44	1000	0.3344
241.79	1000	0.0046	4.92	1000	0.3463
189.31	1000	0.0064	4.2	1000	0.3526
136.47	1000	0.0099	4.2	1000	0.3469
71.88	1000	0.0193	3.74	1000	0.3563
60.16	1000	0.0269	3.15	1000	0.3555
43.61	1000	0.0413	2.28	1000	0.3501
34.98	1000	0.0536	2.11	1000	0.3524
26.47	1000	0.0736	1.89	1000	0.3428
19.80	1000	0.1043	1.72	1000	0.3439
13.14	1000	0.1645	1.64	1000	0.3485
8.73	1000	0.2485	1.61	1000	0.3526
7.31	1000	0.2783	1.45	1000	0.3432
6.50	1000	0.3031			

(c) Specimen cooled in zero field. See Figure 31.

1.50	1000	0.3438	2.00	1000	0.3522
1.60	1000	0.3408	2.09	1000	0.3512
1.64	1000	0.3457	2.53	1000	0.3500
1.67	1000	0.3480	2.75	1000	0.3470
1.76	1000	0.3463	3.01	1000	0.3539
1.81	1000	0.3481	3.16	1000	0.3492
1.86	1000	0.3490	3.34	1000	0.3506

Table 16. (Continued)

T (°K)	H (Oe)	σ (emu/g)	T (°K)	H (Oe)	σ (emu/g)
3.42	1000	0.3486	7.19	1000	0.2962
3.58	1000	0.3494	8.43	1000	0.2613
3.70	1000	0.3470	9.54	1000	0.2334
3.80	1000	0.3553	10.92	1000	0.2062
3.95	1000	0.3478	12.14	1000	0.1864
4.10	1000	0.3493	14.84	1000	0.1493
4.2	1000	0.3484	19.80	1000	0.1102
4.2	1000	0.3573	23.68	1000	0.0866
4.08	1000	0.3531	26.47	1000	0.0757
5.37	1000	0.3440	35.84	1000	0.0537
6.20	1000	0.3245			

(d) Low-field data for remanence-temperature determination. See Figure 25.

4.2	451	0.1742	4.2	43	0.0357
	421	0.1691		31	0.0245
	390	0.1610			
	355	0.1488	2.42	451	0.1694
	322	0.1369		419	0.1627
	291	0.1245		388	0.1554
	259	0.1139		358	0.1244
	226	0.0979		322	0.1330
	195	0.0884		291	0.1241
	162	0.0731		259	0.1170
	129	0.0641		227	0.1081
	109	0.0590		196	0.0972
	97	0.0508		164	0.0797
	81	0.0457		130	0.0672
	65	0.0405		97	0.0538

Table 16. (Continued)

T (°K)	H (Oe)	σ (emu/g)	T (°K)	H (Oe)	σ (emu/g)
2.42	65	0.0447	1.57	227	0.0965
	46	0.0335		196	0.0884
	29	0.0212		164	0.0807
				130	0.0721
1.57	451	0.1570		97	0.0602
	420	0.1485		65	0.0496
	388	0.1418		42	0.0401
	356	0.1329		26	0.0298
	290	0.1127			

Table 17. Magnetization data for 108 ppm Fe in Cu. These values were read off from σ vs. H plots at various temperatures supplied to us by Dr. J. L. Tholence and Dr. R. Tournier (Reference 6). See Figure 32.

T (°K)	H (Oe)	σ (10^{-3} emu/g)	T (°K)	H (Oe)	σ (10^{-3} emu/g)
1.3	10000	1.242	10	40000	3.175
	20000	2.354		50000	3.866
	30000	3.369		60000	4.579
	40000	4.352			
	50000	5.238	20	10000	0.616
	60000	6.026		20000	1.242
				30000	1.857
4.2	10000	1.058		40000	2.430
	20000	2.095		50000	2.948
	30000	3.067		60000	3.488
	40000	3.942			
	50000	4.827	32.5	10000	0.497
	60000	5.616		20000	0.983
				30000	1.470
10	10000	8.210		40000	1.944
	20000	1.631		50000	2.354
	30000	2.430		60000	2.786

Table 18. Magnetization data for 112 ppm Fe in Cu. These data were supplied to us by Dr. E. C. Hirschkoff and Prof. J. C. Wheatley. (Reference 9) See Figures 33 and 34.

T (°K)	H (Oe)	σ (10^{-5}emu/g)	T (°K)	H (Oe)	σ (10^{-5}emu/g)
0.0126	0.977	0.2644	0.0135	0.977	0.2484
0.0206	0.977	0.1836	0.0116	0.977	0.2731
0.0346	0.977	0.1326	0.0092	0.977	0.3147
0.0935	0.977	0.0679			
0.1131	0.977	0.0590	0.0123	10.000	2.7056
0.0516	0.977	0.1012	0.0291	10.000	1.5409
0.1715	0.977	0.0437	0.0194	10.000	2.0149
0.1285	0.977	0.0555	0.0360	10.000	1.3299
0.0253	0.977	0.1663	0.1000	10.000	0.6732
0.0170	0.977	0.2159	0.1795	10.000	0.4558
0.0135	0.977	0.2513	0.1451	10.000	0.5268
0.0796	0.977	0.0765	0.2967	10.000	0.3097
0.2092	0.977	0.0410	0.4065	10.000	0.2445
0.3521	0.977	0.0278	0.2118	10.000	0.3810
0.4098	0.977	0.0243	0.1187	10.000	0.5897
0.2404	0.977	0.0373	0.0792	10.000	0.7704
0.1053	0.977	0.0633	0.0247	10.000	1.7277
0.1524	0.977	0.0495	0.0148	10.000	2.3938
0.0876	0.977	0.0713	0.0411	10.000	1.2185
0.0705	0.977	0.0824	0.0134	10.000	2.5274
0.0603	0.977	0.0909	0.0633	10.000	0.9096
0.0443	0.977	0.1119	0.1314	10.000	0.5656
0.0297	0.977	0.1476	0.2421	10.000	0.3821
0.0394	0.977	0.1216	0.0904	10.000	0.7223
0.0519	0.977	0.1027	0.0216	10.000	1.8693
0.0189	0.977	0.2004	0.0501	10.000	1.0672
0.0148	0.977	0.2337	0.0710	10.000	0.8470

Table 18. (Continued)

T (°K)	H (Oe)	σ (10^{-5}emu/g)	T (°K)	H (Oe)	σ (10^{-5}emu/g)
0.1092	10.000	0.6351	0.0288	60.830	8.5894
0.3401	10.000	0.3075	0.0222	60.830	9.7470
0.1608	10.000	0.4907	0.0141	60.830	11.5402
0.0819	10.000	0.7679	0.0115	60.830	12.2083
0.0579	10.000	0.9755	0.0096	60.830	12.6934
0.0174	10.000	2.1634			
0.0115	10.000	2.7699	0.0124	96.380	15.3762
			0.0263	96.380	12.5616
0.0192	60.830	10.4108	0.0933	96.380	6.7219
0.0166	60.830	10.9108	0.1497	96.380	5.0696
0.0383	60.830	7.4624	0.0413	96.380	10.6342
0.0606	60.830	5.6736	0.0211	96.380	13.6435
0.1049	60.830	3.9735	0.0344	96.380	11.4576
0.1309	60.830	3.4251	0.0171	96.380	14.2972
0.1587	60.830	3.0402	0.0148	96.380	14.7061
0.1912	60.830	2.6620	0.0189	96.380	13.8442
0.2512	60.830	2.2220	0.0594	96.380	8.6292
0.3030	60.830	1.9143	0.0298	96.380	12.0305
0.3937	60.830	1.6391	0.1453	96.380	4.9850
0.2174	60.830	2.4190	0.2695	96.380	3.2640
0.3436	60.830	1.7772	0.3086	96.380	3.0416
0.1132	60.830	3.7458	0.3472	96.380	2.8225
0.0124	60.830	12.0478	0.0788	96.380	7.4572
0.0257	60.830	9.1028	0.1130	96.380	5.9324
0.0333	60.830	7.9826	0.1842	96.380	4.3253
0.0436	60.830	6.8734	0.2247	96.380	3.7946
0.0508	60.830	6.2786	0.1326	96.380	5.3898
0.0866	60.830	4.4797	0.1026	96.380	6.3111
0.0711	60.830	5.1047	0.0915	96.380	6.7924

Table 18. (Continued)

T (°K)	H (Oe)	σ (10^{-5}emu/g)	T (°K)	H (Oe)	σ (10^{-5}emu/g)
0.0711	96.380	7.9135	0.0132	217.110	26.9653
0.0519	96.380	9.4417	0.0198	217.110	25.1694
0.0240	96.380	13.0452	0.0391	217.110	21.0806
0.0135	96.380	15.0311	0.1085	217.110	13.1701
0.0117	96.380	15.4190	0.2584	217.110	7.7274
			0.1567	217.110	10.7818
0.0133	160.200	21.5650	0.0680	217.110	17.0691
0.0196	160.200	19.9037	0.1916	217.110	9.4598
0.0278	160.200	18.0702	0.2392	217.110	8.1838
0.0394	160.200	16.0681	0.3174	217.110	6.7300
0.0621	160.200	13.1921	0.4424	217.110	5.2412
0.0828	160.200	11.4262	0.3831	217.110	5.9578
0.1073	160.200	9.7970	0.0830	217.110	15.4190
0.1316	160.200	8.7678	0.1381	217.110	11.5785
0.1543	160.200	7.9118	0.2207	217.110	8.6325
0.1658	160.200	7.6572	0.1745	217.110	10.0580
0.2169	160.200	6.4306	0.0526	217.110	19.1162
0.3164	160.200	4.9955	0.0296	217.110	23.1899
0.4048	160.200	4.2175	0.0148	217.110	26.4578
0.1174	160.200	9.4418	0.0239	217.110	24.0937
0.1828	160.200	7.2019	0.0344	217.110	21.9296
0.2532	160.200	5.7883	0.0118	217.110	27.1538
0.0512	160.200	14.6311	0.0095	217.110	27.7238
0.0166	160.200	20.7914			
0.0126	160.200	21.7845			
0.0094	160.200	22.4364			

Table 19. Magnetization data for 478 ppm Fe in Cu. These data were supplied to us by Dr. E. C. Hirschkoff and Prof. J. C. Wheatley (Reference 9). See Figure 35.

T (°K)	H (Oe)	σ (10^{-5}emu/g)	T (°K)	H (Oe)	σ (10^{-5}emu/g)
0.0145	10.000	12.6179	0.2487	10.000	5.8180
0.0197	10.000	12.5495	0.3185	10.000	4.9416
0.0377	10.000	12.2604	0.4098	10.000	4.2110
0.0632	10.000	11.5726	0.2932	10.000	5.2708
0.0111	10.000	9.6524	0.2212	10.000	6.4294
0.1595	10.000	7.8626	0.3745	10.000	4.4124
0.0808	10.000	10.9528	0.2053	10.000	6.6182
0.0229	10.000	12.5591	0.1802	10.000	7.2198
0.0298	10.000	12.4704	0.1456	10.000	8.3170
0.0131	10.000	12.5403	0.0464	10.000	12.1152
0.0164	10.000	12.5543	0.0114	10.000	12.5200
0.0964	10.000	10.3105	0.0094	10.000	12.4793
0.1330	10.000	8.8045	0.0090	10.000	12.4517

Table 20. Magnetization data for the quenched $Cu_{0.9}Ni_{0.1}$ alloy containing 100 ppm Fe. The measurements between ∿300°K and 4.2°K were made in the metal cryostat; the measurements at and below 4.2°K were made in the glass cryostat. See Figures 36 and 37.

T (°K)	H (Oe)	σ (10^{-3}emu/g)	T (°K)	H (Oe)	σ (10^{-3}emu/g)
299.44	12565	2.09	4.2	8866	6.20
244.22	12565	2.14		7137	4.93
190.55	12557	2.16		5661	4.03
132.24	12553	2.23		4600	3.30
102.56	12550	2.31		3682	2.38
78.08	12545	2.47		2737	1.65
63.23	12544	2.60		2690	1.71
42.96	12567	2.84		1453	1.10
39.44	12551	2.97		395	0.24
34.09	12556	3.13			
28.21	12555	3.29	3.15	12597	10.52
21.6	12553	3.74		10828	9.07
14.80	12593	4.45		8862	7.59
9.80	12560	5.31		7149	6.13
				5668	4.81
6.00	12566	6.94		4601	4.00
	10676	5.89		3684	3.27
	8720	4.80		2738	2.30
	7009	3.78		412	0.38
	5557	3.07			
	4610	2.40	2.42	12572	12.10
	3685	1.84		10825	10.53
	2690	1.47		8893	8.81
	1454	1.00		7147	7.29
				5666	5.81
4.2	12550	8.85		4617	4.89
	10663	7.56		3685	4.09

Table 20. (Continued)

T (°K)	H (Oe)	σ (10^{-3}emu/g)	T (°K)	H (Oe)	σ (10^{-3}emu/g)
2.42	2740	2.58	1.34	12572	15.40
	1491	1.49		10826	14.10
				8896	12.00
1.97	12569	13.32		7147	10.43
	10824	11.83		5666	8.67
	8895	10.00		4614	7.37
	7147	8.08		3687	6.10
	5667	6.62		2740	4.62
	4611	5.36		1491	2.70
	3685	4.49			
	2738	2.89			
	411	0.45			

Table 21. Magnetization data for the quenched $Cu_{0.9}Ni_{0.1}$ alloy containing 500 ppm Fe. The measurements between ∿300°K and 4.2°K were made in the metal cryostat; measurements at and below 4.2°K were made in the glass cryostat. See Figures 36 and 38.

T (°K)	H (Oe)	σ (10^{-2}emu/g)
300.50	12568	0.278
243.28	12564	0.291
189.78	12555	0.315
132.54	12546	0.360
101.54	12545	0.407
78.54	12545	0.476
61.74	12543	0.544
41.95	12542	0.711
33.09	12547	0.830
25.90	12547	0.986
18.34	12547	1.264
12.48	12520	1.741
7.77	12520	2.461
	10639	2.124
	8689	1.748
	6986	1.414
	5537	1.109
	4505	0.915
	3600	0.733
	2623	0.525
	1401	0.319
	368	0.089
5.59	12523	3.163
4.2	12557	3.795
	10671	3.286
	8715	2.723
	7006	2.238
	5554	1.784
	4520	1.476
	3612	1.161
	2646	0.873
	1403	0.479
	366	0.185
3.34	12538	4.361
	10657	3.784
	8715	3.186
	6996	2.597
	5546	2.093
	4513	1.690
	3606	1.355
	2650	1.013
	1402	0.533
	366	0.129
2.05	12507	5.640
	10655	5.010
	8702	4.295

Table 21. (Continued)

T (°K)	H (Oe)	σ (10^{-2}emu/g)	T (°K)	H (Oe)	σ (10^{-2}emu/g)
2.05	6995	3.602	1.51	12542	6.275
	5546	2.945		10655	5.661
	4515	2.428		8680	4.911
	3598	1.968		6998	4.201
	2642	1.438		5547	3.494
	1403	0.783		4507	2.927
	367	0.152		3607	2.394
				2639	1.817
				1404	0.985
				367	0.303

Table 22. Magnetization data for the quenched $Cu_{0.9}Ni_{0.1}$ alloy containing 1000 ppm Fe. The measurements between ~300°K and 4.2°K were made in the metal cryostat; the measurements at and below 4.2°K were made in the glass cryostat. See Figures 36 and 39.

T (°K)	H (Oe)	σ (10^{-2}emu/g)	T (°K)	H (Oe)	σ (10^{-2}emu/g)
301.34	12569	0.377	9.71	12564	4.121
243.93	12563	0.406			
189.75	12564	0.455	7.06	12545	5.172
135.60	12556	0.556		10657	4.474
103.01	12566	0.655		8703	3.704
82.74	12564	0.771		6997	3.022
64.66	12564	0.921		5548	2.430
48.47	12566	1.155		4515	1.985
39.22	12566	1.365		3608	1.566
30.79	12566	1.636		2644	1.128
24.16	12563	1.965		1413	0.598
22.96	12561	2.074		373	0.121
19.93	12559	2.288			
16.55	12541	2.653	6.20	12563	5.788
13.63	12563	3.176	5.75	12563	6.295
11.09	12549	3.665	4.2	12565	7.606
	10658	3.157		10679	6.653
	8695	2.604		8728	5.575
	6998	2.093		7010	4.573
	5549	1.673		5559	3.677
	4520	1.378		4523	3.022
	3609	1.079		3616	2.433
	2645	0.794		2645	1.778
	1409	0.426		1411	0.954
	375	0.274		373	0.242

Table 22. (Continued)

T (°K)	H (Oe)	σ (10^{-2}emu/g)	T (°K)	H (Oe)	σ (10^{-2}emu/g)
3.28	12569	8.706	2.02	4523	4.984
	10681	7.678		3614	4.099
	8727	6.517		2648	3.100
	7013	5.397		1409	1.703
	5559	4.398		369	0.440
	4523	3.630			
	3615	2.925	1.42	12563	11.582
	2650	2.149		10666	10.538
	1409	1.134		8687	9.263
	371	0.318		7000	8.033
				5548	6.823
2.02	12567	10.594		4514	5.845
	10678	9.539		3607	4.893
	8701	8.272		2637	3.751
	7010	7.081		1400	2.146
	5557	5.902		362	0.524

Table 23. Magnetization data for the quenched $Cu_{0.8}Ni_{0.2}$ alloy containing 100 ppm Fe. The measurements between ∿300°K and 4.2°K were made in the metal cryostat; the measurements at and below 4.2°K were made in the glass cryostat. See Figures 40 and 41.

T (°K)	H (Oe)	σ (10^{-3}emu/g)	T (°K)	H (Oe)	σ (10^{-3}emu/g)
299.09	12688	6.50	4.2	8840	13.43
244.22	12687	6.53		7109	10.67
188.87	12677	6.56		5637	8.28
124.15	12670	6.66		4586	6.95
98.80	12668	6.91		3664	5.88
74.75	12666	6.96		2715	4.06
59.67	12662	7.14		1463	2.25
43.67	12660	7.25			
31.38	12650	8.04	2.84	12602	22.40
27.89	12650	8.28		10616	19.56
				8683	16.49
20.20	12649	8.89		7017	13.55
				5538	10.90
9.70	12649	11.72		4519	8.71
	10784	10.13		3586	7.10
	8839	8.48		2600	5.01
	7109	6.55		1406	2.75
	5636	5.12			
	4586	3.87	1.58	12606	25.54
	3664	2.92		10625	22.81
	2614	2.45		8739	20.01
	1417	1.77		6983	16.72
				5568	13.90
6.50	12650	14.56		4482	11.72
				3583	9.51
4.2	12650	18.64		2613	7.05
	10785	16.16		1379	4.80

Table 24. Magnetization data for the quenched $Cu_{0.8}Ni_{0.2}$ alloy containing 250 ppm Fe. The measurements between ∿300°K and 4.2°K were made in the metal cryostat; the measurements at and below 4.2°K were made in the glass cryostat.

T (°K)	H (Oe)	σ (10^{-3}emu/g)	T (°K)	H (Oe)	σ (10^{-3}emu/g)
296.06	12650	6.93	4.2	8725	24.97
243.59	12650	6.97		6981	20.38
189.78	12650	7.12		5550	16.20
122.42	12650	7.43		4487	12.97
100.68	12650	7.81		3578	10.33
78.05	12650	8.02		2628	7.71
64.70	12650	8.67		1375	3.77
55.88	12650	9.06			
47.44	12650	9.41	2.73	12578	46.57
41.54	12650	9.61		10605	41.00
33.64	12650	11.09		8722	35.00
30.99	12650	11.01		6956	28.22
				5551	22.61
20.06	12684	13.59		4493	18.25
	10811	11.53		3600	14.50
	8859	9.50		2608	10.61
	7125	7.87		1395	5.35
	5649	6.01			
	4595	5.17	1.49	12581	58.25
	3671	4.22		10617	52.51
	2724	2.66		8740	46.05
	1484	1.61		6979	39.10
				5552	32.51
16.69	12650	14.86		4493	27.25
11.09	12650	18.80		3579	22.48
6.3	12650	27.71		2629	17.58
				1401	9.25
4.2	12567	34.25			
	10687	29.88			

Table 25. Magnetization data for the quenched $Cu_{0.8}Ni_{0.2}$ alloy containing 500 ppm Fe. The measurements between ~300°K and 4.2°K were made in the metal cryostat; the measurements at and below 4.2°K were made in the glass cryostat. See Figures 40 and 42.

T (°K)	H (Oe)	σ (10^{-2}emu/g)	T (°K)	H (Oe)	σ (10^{-2}emu/g)
297.70	12650	0.742	9.90	7117	2.051
270.00	12650	0.755		5642	1.650
217.30	12650	0.779		4590	1.336
159.70	12650	0.824		3667	1.070
99.90	12650	0.970		2721	0.823
78.00	12650	1.036		1468	0.394
76.05	12650	1.045			
62.02	12650	1.150	7.19	12650	4.618
46.24	12650	1.331			
44.45	12650	1.336	4.2	12664	6.865
38.68	12650	1.455		10796	5.971
33.64	12650	1.585		8848	5.012
				7117	4.092
25.15	12668	1.861		5642	3.311
	10802	1.591		4590	2.705
	8853	1.299		3667	2.176
	7120	1.028		2718	1.658
	5643	0.831		1474	0.925
	4591	0.687			
	3667	0.532	2.66	12583	9.338
	2735	0.413		10695	8.291
	1468	0.228		8690	7.016
				7025	5.799
17.39	12650	0.242		5568	4.647
				4532	3.815
9.90	12654	3.627		3622	3.100
	10796	3.104		2650	2.250
	8848	2.550		1415	1.225

Table 26. Magnetization data for the quenched $Cu_{0.8}Ni_{0.2}$ alloy containing 1000 ppm Fe. The measurements between ∿300°K and 4.2°K were made in the metal cryostat; the measurements at and below 4.2°K were made in the glass cryostat. See Figures 40 and 43.

T (°K)	H (Oe)	σ (10^{-2}emu/g)	T (°K)	H (Oe)	σ (10^{-2}emu/g)
297.58	12640	0.81	4.2	1407	1.60
242.97	12640	0.85		756	0.74
161.64	12640	0.99			
62.66	12640	1.66	3.03	12572	15.36
42.69	12640	2.20		10690	13.69
27.68	12640	3.03		8734	11.84
24.68	12640	3.30		7023	9.86
19.42	12640	3.98		5570	8.10
10.71	12640	6.44		4516	6.84
				3620	5.36
9.83	12640	6.88		2648	4.23
	10770	5.95		1411	2.22
	8820	4.88		1000	1.45
	5620	3.16			
	3650	2.10	1.50	12580	19.93
	1460	0.93		10690	18.34
				8734	16.28
4.2	12574	12.98		7021	14.22
	10688	11.37		5568	12.18
	8707	9.63		4532	10.67
	6985	7.78		3621	9.03
	5561	6.46		2643	7.06
	4526	5.24		1409	4.00
	3617	4.25		1000	2.93
	2646	3.05			

Table 27. Magnetization data for the quenched $Cu_{0.7}Ni_{0.3}$ alloy containing 100 ppm Fe. The measurements were made in the metal cryostat. See Figure 44.

T (°K)	H (Oe)	σ (10^{-3}emu/g)	T (°K)	H (Oe)	σ (10^{-3}emu/g)
296.16	12640	13.21	5.84	12640	33.16
243.10	12640	13.30			
189.86	12640	13.46	4.2	12640	38.44
131.93	12640	13.88		10770	33.75
101.04	12640	14.31		8824	28.18
77.03	12640	14.85		7100	23.11
60.56	12640	15.45		5630	18.45
39.51	12640	16.90		4585	15.09
31.89	12640	17.69		3660	12.19
24.84	12640	18.82		1470	4.72
16.96	12640	21.11			

Table 28. Magnetization data for the deformed $Cu_{0.9}Ni_{0.1}$ alloy containing 100 ppm Fe. The measurements between ~300°K and 4.2°K were made in the metal cryostat; measurements at and below 4.2°K were made in the glass cryostat. See Figures 45 and 46.

T (°K)	H (Oe)	σ (10^{-3}emu/g)	T (°K)	H (Oe)	σ (10^{-3}emu/g)
297.10	12569	2.17	2.99	12571	9.78
242.99	12569	2.22		10682	8.48
189.72	12569	2.26		8688	6.80
132.48	12560	2.32		7018	5.71
99.76	12560	2.40		5561	4.65
74.86	12560	2.56		4525	3.87
61.30	12560	2.66		3615	3.28
43.29	12550	2.88		2646	2.25
34.45	12550	3.04		1407	1.02
26.25	12550	3.30			
20.71	12550	3.70	2.08	12575	11.04
16.41	12550	3.96		10686	9.55
12.81	12550	4.11		8729	7.96
10.05	12550	4.68		7017	6.67
7.84	12550	5.29		5563	5.11
				4526	4.31
4.2	12554	7.78		3616	3.57
	10672	6.62		2647	2.36
	8718	5.36		1410	1.30
	7009	4.15			
	5556	3.45	1.44	12579	12.93
	4524	2.79		10689	11.55
	3612	2.24		8732	9.67
	2647	1.61		7019	7.90
	1406	0.82		5564	6.54
				4527	5.48
				3617	4.43
				2646	3.35

Table 29. Magnetization data for the deformed $Cu_{0.9}Ni_{0.1}$ alloy containing 500 ppm Fe. The measurements between ∿300°K and 4.2°K were made in the metal cryostat; measurements at and below 4.2°K were made in the glass cryostat. See Figures 45 and 47.

T (°K)	H (Oe)	σ (10^{-2}emu/g)	T (°K)	H (Oe)	σ (10^{-2}emu/g)
297.15	12573	0.272	4.2	8727	2.347
243.02	12559	0.286		7017	1.897
162.55	12563	0.304		5565	1.512
131.78	12559	0.349		4527	1.241
100.48	12559	0.392		2649	0.704
77.63	12559	0.451		1410	0.384
59.42	12559	0.521			
43.74	12557	0.639	3.02	12573	3.952
34.98	12556	0.728		10686	3.446
26.01	12556	0.887		8730	2.886
20.15	12550	0.105		7010	2.362
16.13	12549	1.230		5565	1.902
12.48	12551	1.529		4528	1.572
7.77	12548	2.069		3618	1.267
				2648	0.901
5.60	12543	2.678		1407	0.476
	10667	2.306			
	8716	1.923	2.15	12582	4.721
	7010	1.562		10691	4.175
	5556	1.231		8732	3.459
	4522	1.006		7018	2.968
	3614	0.797		5567	2.415
	2646	0.615		4529	1.999
	1410	0.325		3620	1.613
				2648	1.200
4.2	12570	3.284		1408	0.616
	10683	2.830			

Table 29. (Continued)

T (°K)	H (Oe)	σ (10^{-2}emu/g)	T (°K)	H (Oe)	σ (10^{-2}emu/g)
1.36	12564	5.573	1.36	4530	2.593
	10690	5.046		3621	2.146
	8735	4.348		2647	1.632
	7022	3.699		1413	0.915
	5567	3.067		369	0.235

Table 30. Magnetization data for the deformed $Cu_{0.9}Ni_{0.1}$ alloy containing 1000 ppm Fe. The measurements between ~300°K and 4.2°K were made in the metal cryostat; the measurements at and below 4.2°K were made in the glass cryostat. See Figures 45 and 48.

T (°K)	H (Oe)	σ (10^{-2}emu/g)	T (°K)	H (Oe)	σ (10^{-2}emu/g)
297.53	12589	0.364	4.2	7018	3.881
243.02	12589	0.391		5563	3.116
188.23	12589	0.456		4528	2.556
132.60	12584	0.538		3618	2.058
79.47	12584	0.744		2647	1.505
60.60	12584	0.901		1408	0.796
44.56	12584	1.139			
35.93	12576	1.336	3.14	12573	7.876
26.57	12578	1.679		10687	6.950
20.19	12577	2.040		8732	5.880
14.69	12577	2.648		7020	4.871
11.09	12574	3.246		5565	3.934
				4529	3.285
7.06	12562	4.523		3622	2.650
	10678	3.914		2648	1.962
	8725	3.182		1407	0.998
	7010	2.579			
	5564	2.064	2.30	12591	9.154
	4527	1.683		10694	8.232
	3619	1.327		8737	7.125
	2647	0.980		7025	6.055
	1407	0.526		4531	4.233
				3620	3.516
4.2	12568	6.539		2650	2.663
	10687	5.696		1411	1.498
	8729	4.757		5406	4.950

Table 30. (Continued)

T (°K)	H (Oe)	σ (10^{-2}emu/g)	T (°K)	H (Oe)	σ (10^{-2}emu/g)
1.47	12580	9.977	1.47	4534	4.924
	10694	8.756		3622	4.091
	8748	7.931		2649	3.152
	7022	6.834		1411	1.803
	5571	5.788		369	0.398

Table 31. Magnetization data for the deformed $Cu_{0.8}Ni_{0.2}$ alloy containing 100 ppm Fe. The measurements between ∿300°K and 4.2°K were made in the metal cryostat; the measurements at and below 4.2°K were made in the glass cryostat. See Figures 49 and 50.

T (°K)	H (Oe)	σ (10^{-3}emu/g)	T (°K)	H (Oe)	σ (10^{-3}emu/g)
294.87	12640	6.33	9.71	2729	3.20
246.83	12640	6.34		1486	1.45
132.11	12640	6.39			
68.15	12640	6.75	4.2	12601	16.47
53.92	12640	6.98		10846	14.45
				8904	11.72
20.06	12702	8.62		7162	9.38
	10829	7.30		5679	7.33
	8873	5.98		4622	6.29
	7139	4.76		3695	4.97
	5661	3.78		2747	3.62
	4604	3.14		1497	1.87
	3679	2.49			
	2729	1.78	2.88	12596	20.27
	1484	0.70		10865	17.71
				8917	14.76
10.74	12640	11.11		7163	12.14
				5671	9.74
9.71	12709	11.85		4613	7.76
	10835	10.24		3695	6.25
	8870	8.46		2745	4.60
	7141	6.93		1495	2.52
	5663	5.66			
	4603	4.75	2.26	12604	22.29
	3679	3.42		10846	19.60

Table 31. (Continued)

T (°K)	H (Oe)	σ (10^{-3}emu/g)	T (°K)	H (Oe)	σ (10^{-3}emu/g)
2.26	8909	16.45	1.44	12599	25.68
	7165	13.67		10843	23.13
	5681	10.99		8905	20.00
	4623	8.77		7161	17.11
	3696	7.05		5678	14.19
	2746	5.03		4622	11.64
	1499	2.78		3695	9.17
				2744	6.85
				1495	3.69
				415	1.14

Table 32. Magnetization data for the deformed $Cu_{0.8}Ni_{0.2}$ alloy containing 500 ppm Fe. The measurements between ∿300°K and 4.2°K were made in the metal cryostat; the measurements at and below 4.2°K were made in the glass cryostat. See Figures 49 and 51.

T (°K)	H (Oe)	σ (10^{-2}emu/g)	T (°K)	H (Oe)	σ (10^{-2}emu/g)
292.36	12742	0.733	8.43	1467	0.459
243.65	12733	0.743		406	0.136
183.54	12724	0.775			
128.45	12720	0.841	4.2	12682	6.290
93.63	12714	0.934		10817	5.474
75.88	12710	1.011		8871	4.563
62.15	12720	1.086		7134	3.723
48.05	12716	1.241		5657	2.969
41.60	12713	1.337		4603	2.438
33.37	12712	1.509		3677	1.959
29.72	12712	1.608		2729	1.436
22.35	12716	1.913		1484	0.781
19.40	12707	2.087		407	0.181
16.27	12721	2.378			
14.70	12712	2.598	3.05	12681	7.675
12.14	12710	2.966		10813	6.773
				8866	5.735
8.43	12716	3.871		7132	4.724
	10840	3.322		5654	3.839
	8885	2.731		4604	3.159
	7145	2.217		3677	2.547
	5666	1.745		2729	1.915
	4611	1.440		1484	1.051
	3685	1.129		406	0.237
	2734	0.875			

Table 32. (Continued)

T (°K)	H (Oe)	σ (10^{-2}emu/g)	T (°K)	H (Oe)	σ (10^{-2}emu/g)
1.37	12677	10.469	1.37	4600	5.266
	10812	9.566		3675	4.368
	8866	8.463		2728	3.370
	7131	7.310		1484	1.879
	5655	6.184		407	0.492

Table 33. Magnetization data for the deformed $Cu_{0.8}Ni_{0.2}$ alloy containing 1000 ppm Fe. The measurements between ~300°K and 4.2°K were made in the metal cryostat; the measurements at and below 4.2°K were made in the glass cryostat. See Figures 49 and 52.

T (°K)	H (Oe)	σ (10^{-2} emu/g)	T (°K)	H (Oe)	σ (10^{-2} emu/g)
298.13	12640	0.77	4.2	2710	2.69
243.15	12640	0.81		1470	1.49
189.95	12640	0.87			
132.02	12640	1.00	3.05	12589	13.64
100.88	12640	1.15		10695	12.07
74.93	12640	1.36		8736	10.23
59.30	12640	1.57		7024	8.49
40.99	12640	2.05		5567	7.01
31.16	12640	2.45		4529	5.82
				3621	4.67
20.50	12636	3.30		2649	3.46
	8827	2.29		1407	1.62
	5624	1.49		369	0.45
	3650	0.99			
	1460	0.40	2.00	12593	16.09
				10660	14.61
9.88	12640	5.81		8741	12.84
				7028	11.01
4.2	12640	11.27		5571	9.34
	10780	9.94		4532	8.04
	8833	8.39		3620	6.65
	7100	6.87		2649	5.03
	5629	5.56		1408	2.32
	4568	4.56		369	0.56
	3658	3.69			

Table 33. (Continued)

T (°K)	H (Oe)	σ (10^{-2}emu/g)	T (°K)	H (Oe)	σ (10^{-2}emu/g)
1.47	12582	17.83	1.47	4533	9.41
	10692	16.39		3622	8.19
	8735	14.64		2648	6.45
	7021	12.82		1409	3.56
	5568	11.05		369	0.94

B. Data Analysis

1. Cu-Ni.

a. Weakly ferromagnetic alloys.

The magnetization results for quenched, weakly ferromagnetic Cu-Ni alloys containing 50, 48, and 46 at % nickel are given in Tables 7, 8 and 9 respectively. For the quenched $Cu_{0.5}Ni_{0.5}$ alloy isothermal magnetization measurements were made at 78°K and lower temperatures (Figs. 1, 2); for the $Cu_{0.52}Ni_{0.48}$ and $Cu_{0.54}Ni_{0.46}$ alloys, measurements were made only at 4.2°K and lower temperatures, as shown in Figs. 3 and 4. The Curie temperature T_c for $Cu_{0.5}Ni_{0.5}$ was estimated from σ^2 vs. $\frac{H_i}{\sigma}$ graphs (Fig. 5) to be ~37°K, at which $\sigma^2 = 0$ extrapolates to $\frac{H_i}{\sigma} = 0$. Here H_i (Oe) is the internal field, as calculated from the applied field H(Oe) and the demagnetization correction for a spherical specimen: $H_i = H - \frac{4\pi}{3}\sigma\rho$. Here ρ is the density of the alloy, which was assumed to be 8.95 g/cc. taking the weighted average of the density values of copper and nickel. The Curie temperature so obtained for $Cu_{0.5}Ni_{0.5}$ is in good agreement with the value obtained (36 ± 1°K), for an alloy of the same composition by Robbins et al.[16] Referring now to Fig. 1, one may also note that the isothermal σ vs. H graphs for the $Cu_{0.5}Ni_{0.5}$ alloy at ~40°K and ~53°K show pronounced curvature, indicating that giant magnetic

Figure 1. Isothermal magnetization data for quenched $Cu_{0.5}Ni_{0.5}$ between 78.08°K and 10.39°K. See Table 7.

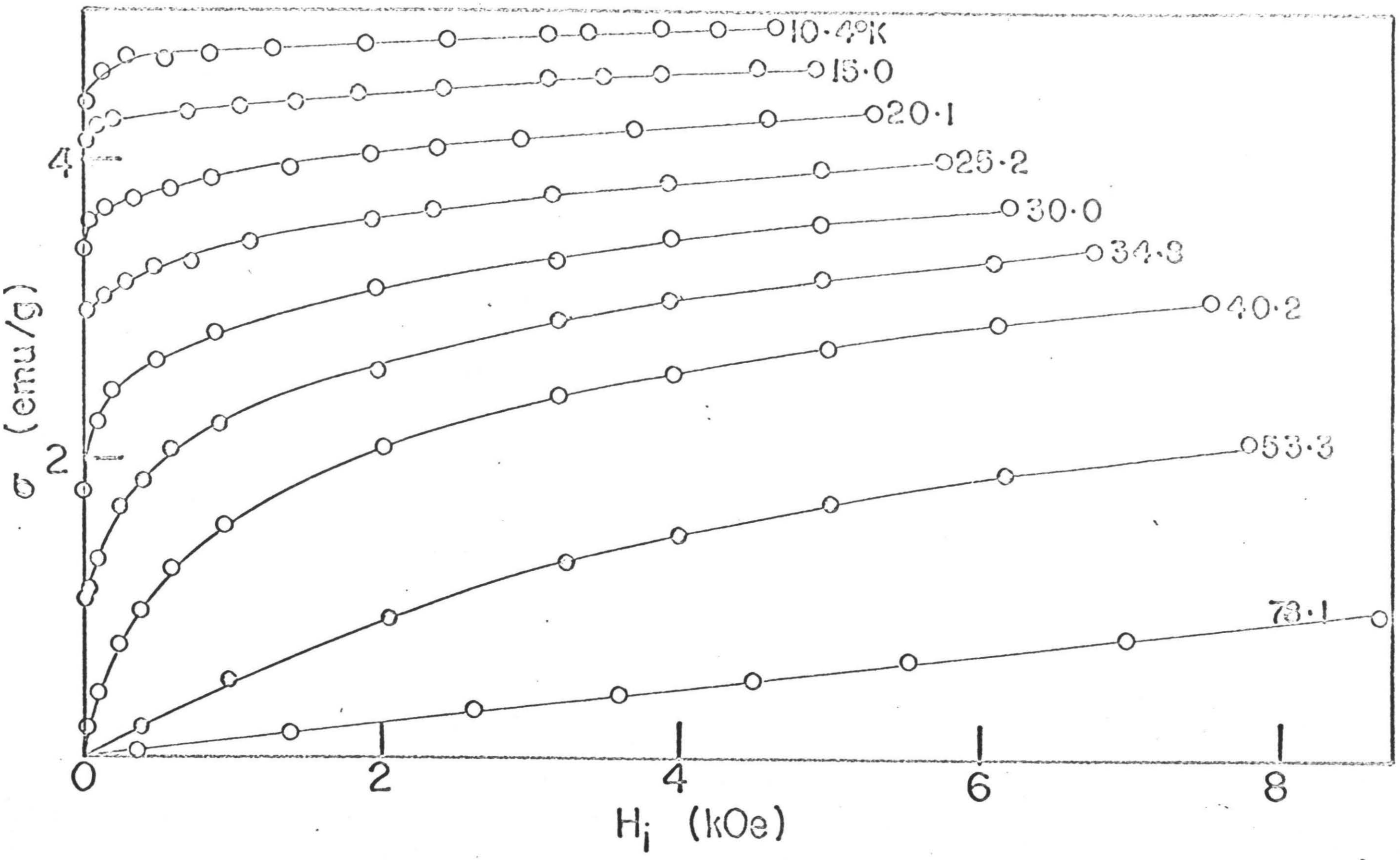
10·4°K
15·0
20·1
25·2
30·0
34·3
40·2
53·3
73·1
σ (emu/g)
4
2
0
2
4
6
8
H_i (kOe)

Figure 2. Isothermal low temperature ($T \leq 4.2°K$) magnetization data for quenched $Cu_{0.5}Ni_{0.5}$. See Table 7.

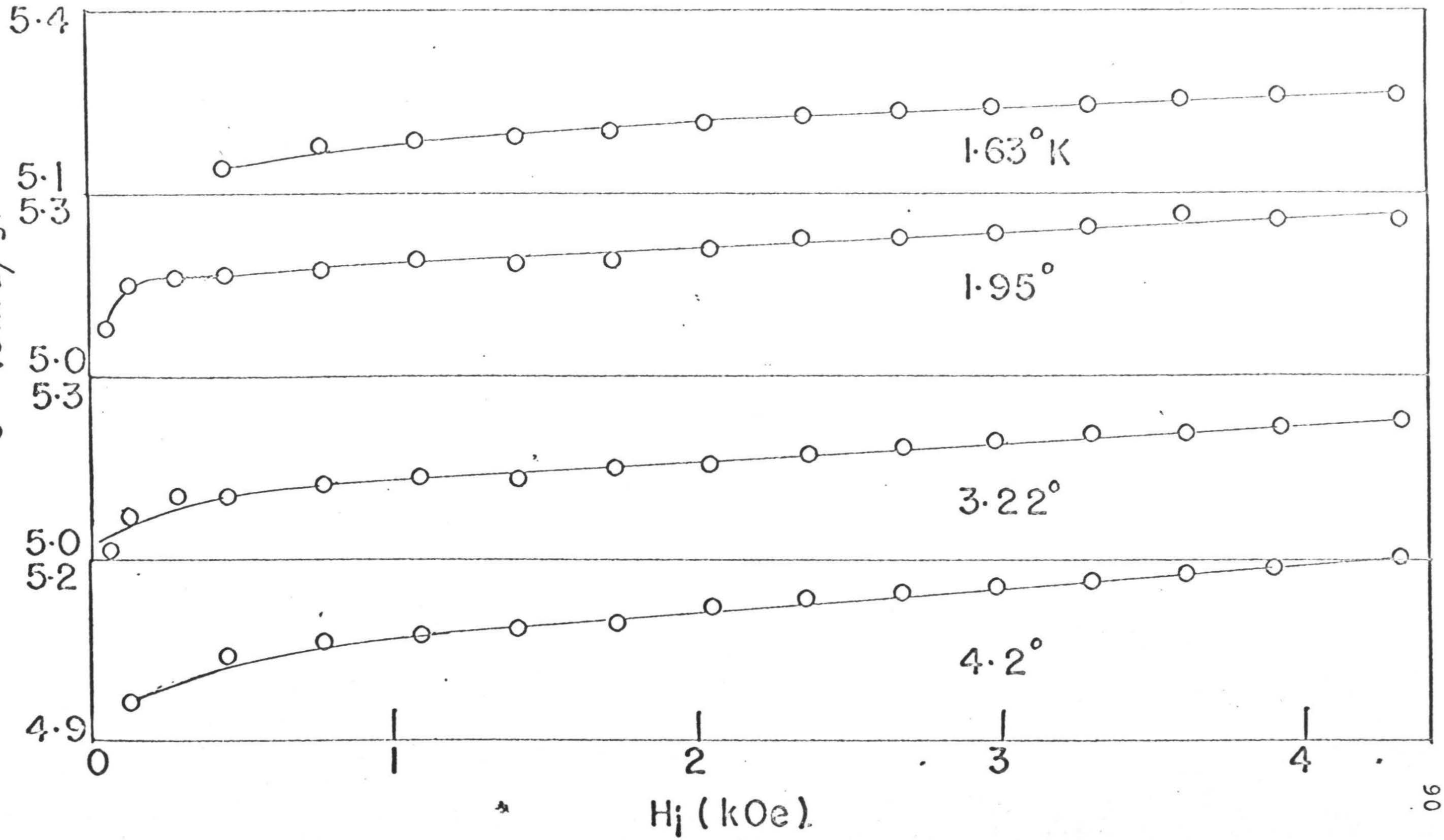
5·4
5·1
5·3
5·0
5·3
5·0
5·2
4·9
σ (emu/g)
1·63°K
1·95°
3·22°
4·2°
0
1
2
3
4
Hj (kOe)

Figure 3. Isothermal low temperature ($T \leq 4.2°K$) magnetization data for quenched $Cu_{0.52}Ni_{0.48}$. See Table 8.

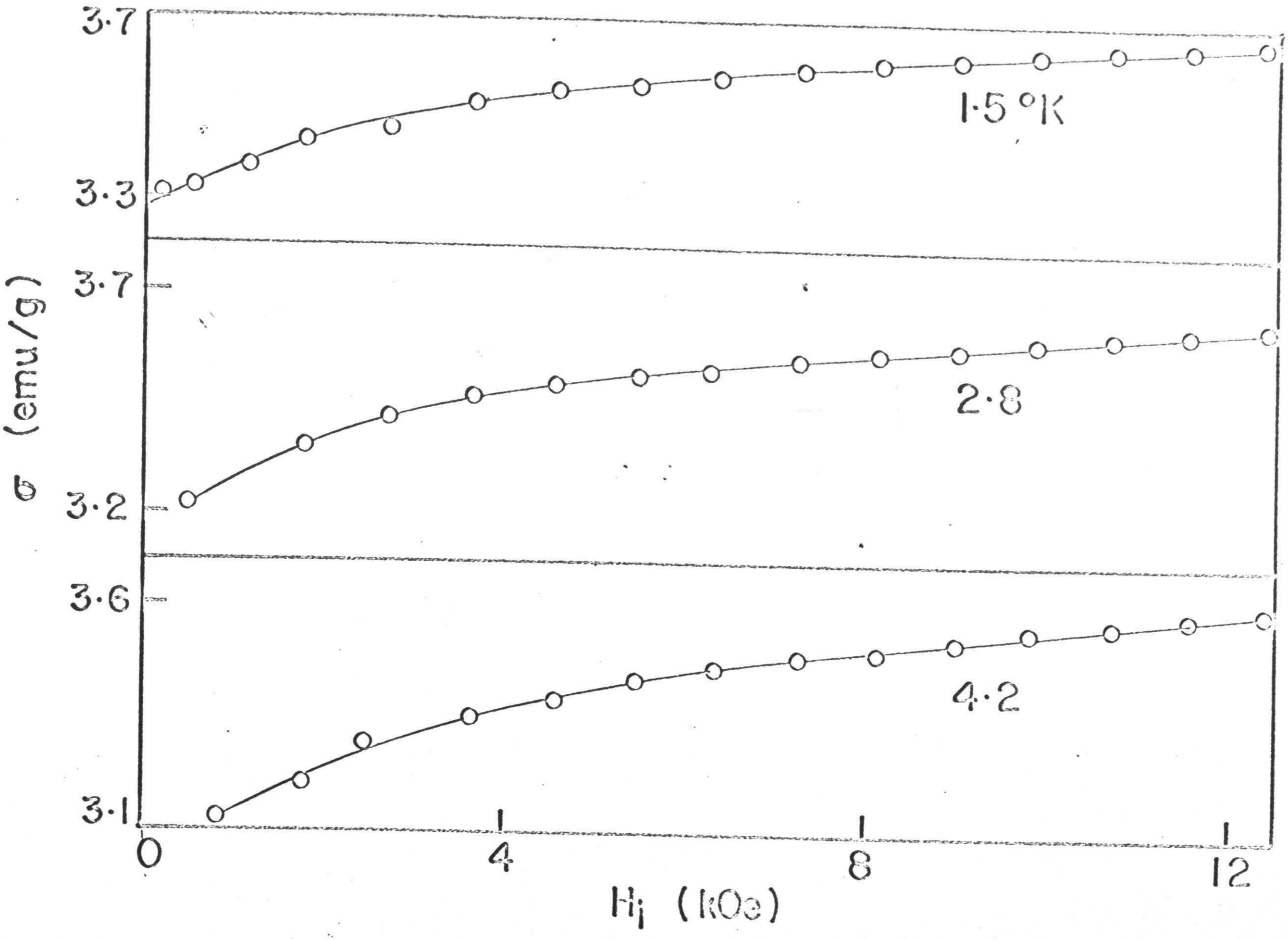
3.7
3.3
1.5 °K
3.7
3.2
2.8
3.6
4.2
3.1
0
4
8
12
σ (emu/g)
Hi (kOe)

Figure 4. Isothermal low temperature ($T \leq 4.2°K$) magnetization data for quenched $Cu_{0.54}Ni_{0.46}$. See Table 9.

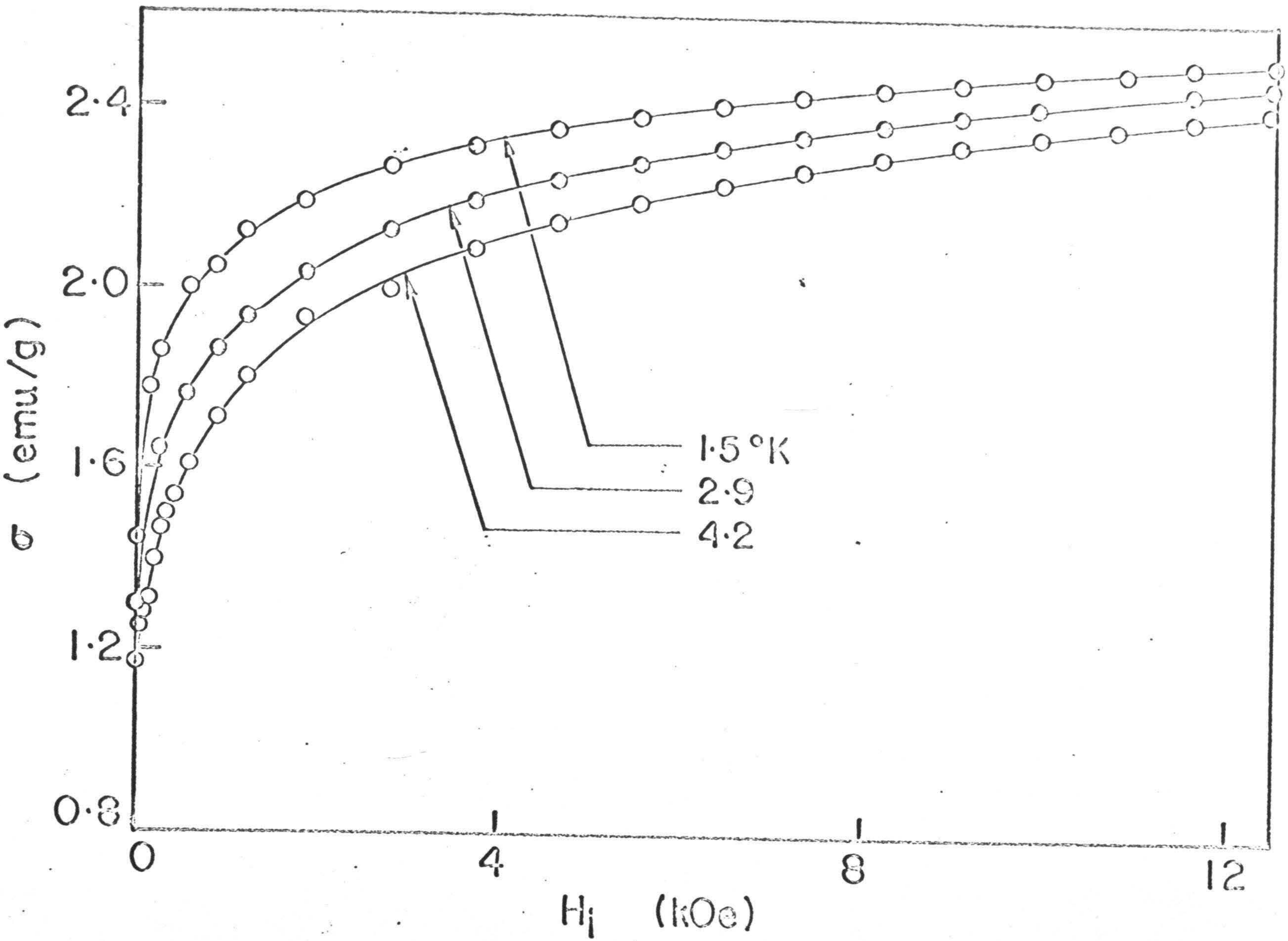
2·4
2·0
1·6
1·2
0·8
σ (emu/g)
0
4
8
12
H_i (kOe)
1·5 °K
2·9
4·2

Figure 5. σ^2 vs. $\frac{H_i}{\sigma}$ graphs at low fields, for quenched $Cu_{0.5}Ni_{0.5}$. The Curie temperature T_c is estimated to be $\simeq$ 37°K.

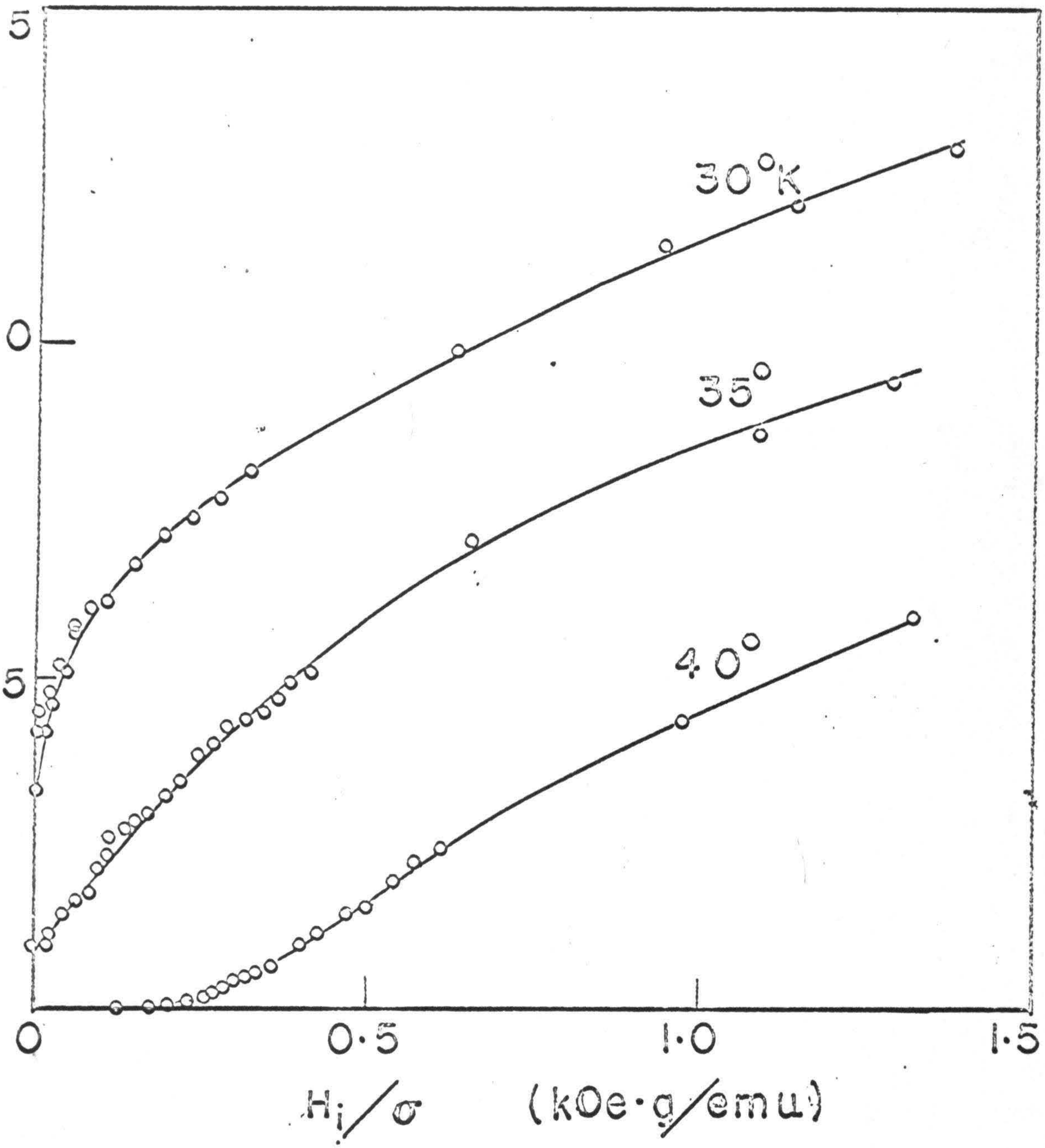
15
10
5
0
σ^2 (emu/g)^2
30°K
35°
40°
0
0·5
1·0
1·5
H_i/σ (kOe·g/emu)

moments are present well above the Curie temperature. The $1/\chi_i$ (the inverse initial susceptibility) versus T graph at temperatures above T_c, shows considerable deviation from normal Curie-Weiss type behavior (Fig. 6). Above ∿160°K the graph is linear, with a paramagnetic Curie temperature ${}_pT_c$ of ∿90°K. Below ∿160°K the graph is curved, indicating a continuous increase in the "differential Curie constant" and a continuous decrease in the "differential Weiss temperature" as the Curie temperature $T_c \simeq 37$°K is approached. These results may be interpreted in terms of giant magnetic moments just above T_c and their gradual breakup into smaller clusters as the temperature is raised.

Recently[17] the initial susceptibility for a $Cu_{0.47}Ni_{0.53}$ alloy was represented by an equation of the form

$$\chi_i(T) = \frac{A}{(T-T_c)^{\nu}} \quad \text{for } T > T_c \tag{6}$$

We found that the susceptibility data for the $Cu_{0.5}Ni_{0.5}$ alloy can also be represented by the above equation with parameter values of $A = 0.0136$ and $\nu = 1.133$, as shown in a $\ln \chi_i$ $\ln(T-T_c)$ graph (Fig. 7). However, the physical significance of Eq. 6 is not entirely clear.

The Curie temperature of the ferromagnetically weakest alloy, i.e., $Cu_{0.54}Ni_{0.46}$, was estimated to be >4.2°K from Fig. 8 where one finds remanence in the σ^2 vs. H_i/σ graphs at 4.2°K.

The saturation magnetization values for all three alloys, i.e., $Cu_{0.5}Ni_{0.5}$, $Cu_{0.52}Ni_{0.48}$ and $Cu_{0.54}Ni_{0.46}$, were determined

Figure 6. χ_i vs. T and $\frac{1}{\chi_i}$ vs. T graphs for quenched $Cu_{0.5}Ni_{0.5}$.

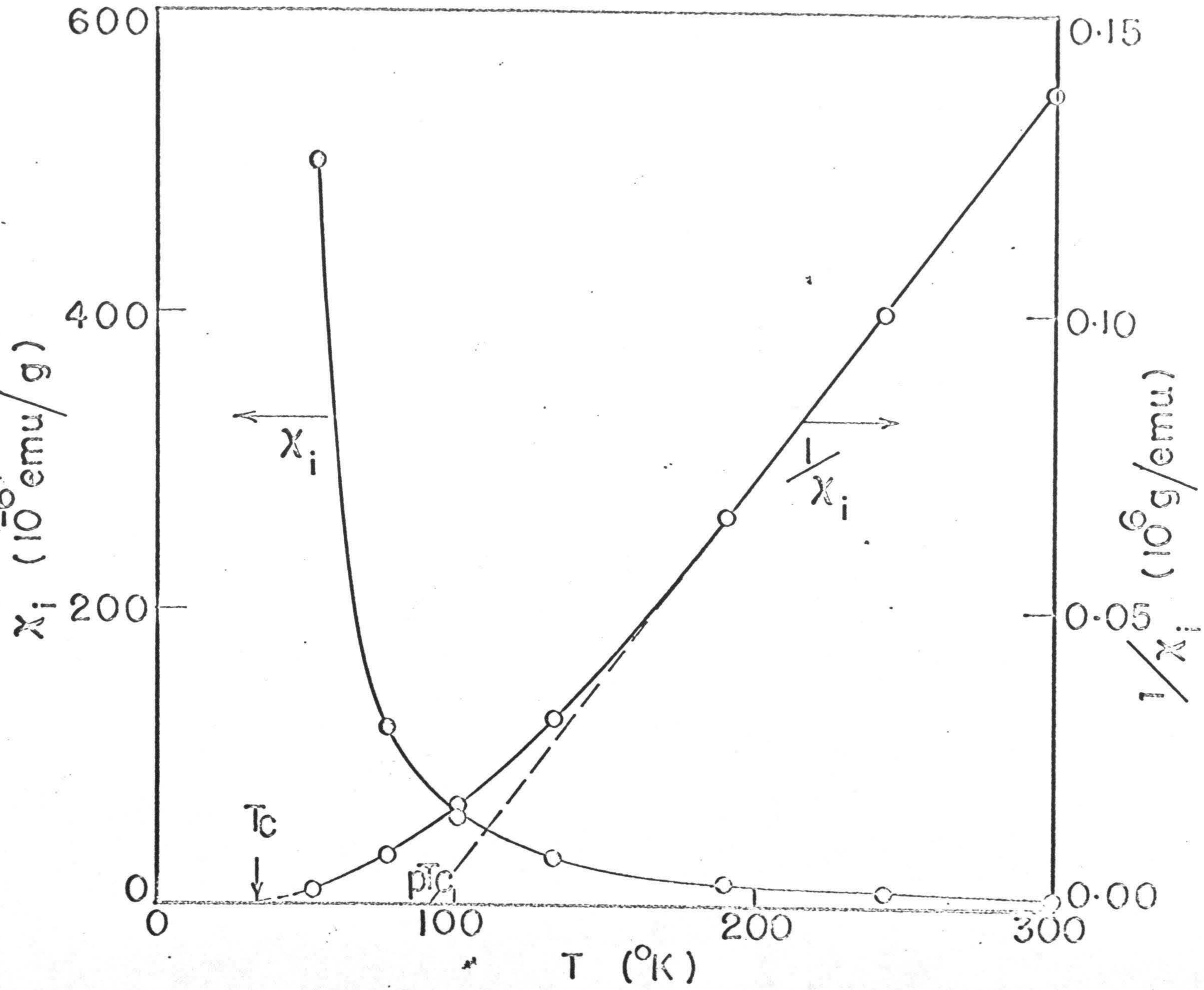
600
400
200
0
0·15
0·10
0·05
0·00
χ_i (10^{-6} emu/gm)
$1/\chi_i$ (10^6 gm/emu)
χ_i
$1/\chi_i$
T_C
pT_C
0
100
200
300
T (°K)

Figure 7. Logarithmic graph of χ_i vs. $(T-T_c)$ for quenched $Cu_{0.5}Ni_{0.5}$.

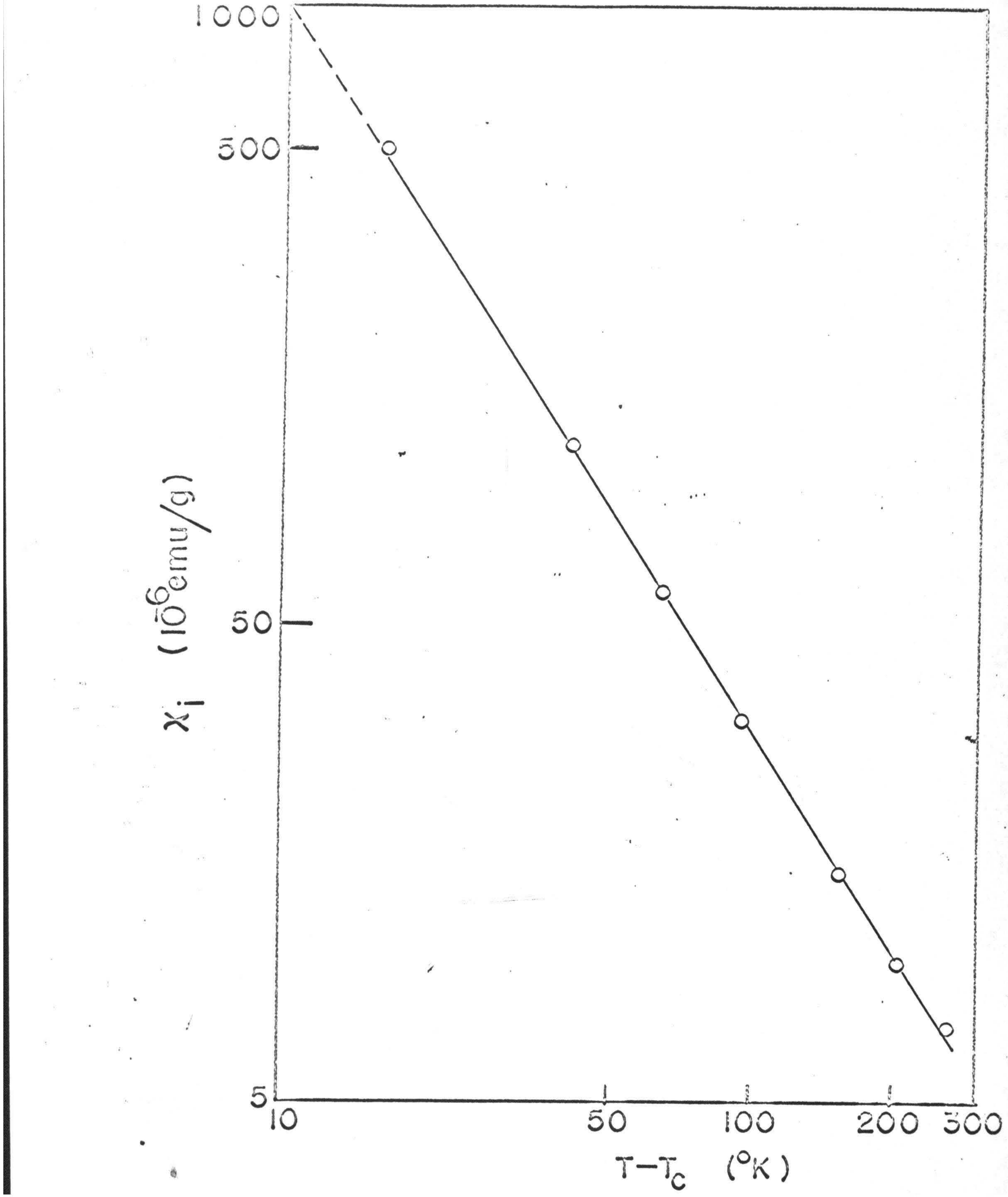
1000
500
50
χ_i (10^{-6} emu/g)
5
10
50
100
200
300
$T-T_c$ (°K)

Figure 8. σ^2 vs. $\frac{H_i}{\sigma}$ graphs for the quenched $Cu_{0.54}Ni_{0.46}$ alloy for 4.2°K. The Curie temperature is somewhat higher than 4.2°K.

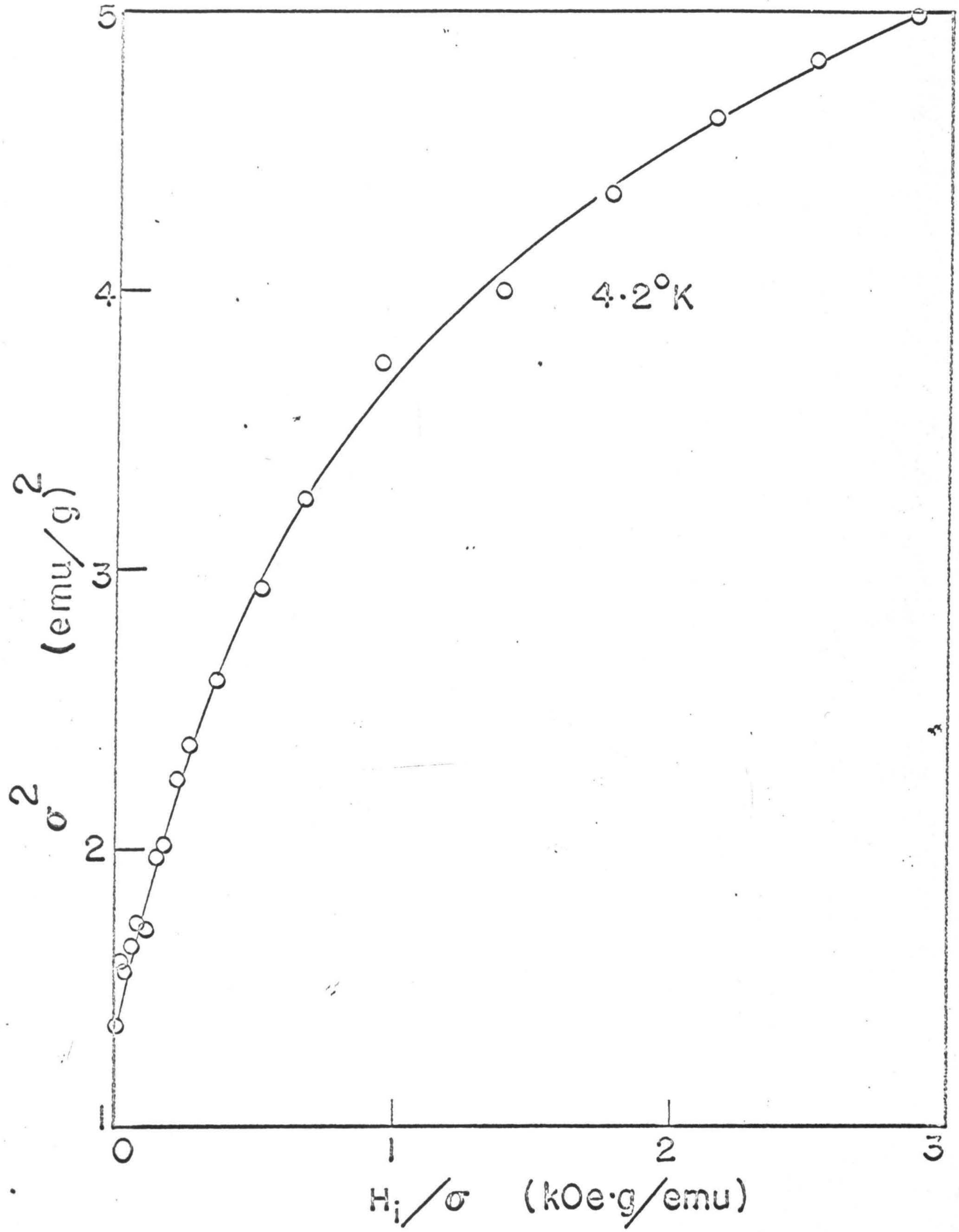
4.2°K
σ^2 (emu/g)^2
H_i/σ (kOe·g/emu)
0
1
2
3
1
2
3
4
5

from the low temperature data ($T \leq 4.2°K$) as follows. For each alloy σ vs. $1/H_i$ isotherms were drawn to obtain the values of $\sigma_{H_i=\infty,T}$ by extrapolation to $1/H_i = 0$ (Figs. 9, 10, 11). A $\sigma_{H_i=\infty,T}$ vs. T graph was then extrapolated to T = 0 (Fig. 12) to give $\sigma_{H_i=\infty,T=0}$, the saturation magnetization at absolute zero (Table 34). From the value of $\sigma_{H_i=\infty,T=0}$, the values of $\bar{\mu}$, the average magnetic moment per alloy atom, were calculated (Table 34).

Table 34. Values of the saturation magnetization $\sigma_{\infty,o}$ (emu/g) and of $\bar{\mu}$, the average magnetic moment per alloy atom, in Bohr magnetons.

Alloy	$\sigma_{\infty,o}$	$\bar{\mu}$
$Cu_{0.5}Ni_{0.5}$	5.30	0.058
$Cu_{0.52}Ni_{0.48}$	3.75	0.041
$Cu_{0.54}Ni_{0.46}$	2.65	0.029

b. Paramagnetic alloys.

The magnetic data for the quenched $Cu_{0.9}Ni_{0.1}$ and $Cu_{0.7}Ni_{0.3}$ alloys, and for the $Cu_{0.6}Ni_{0.4}$ alloy in the as-quenched and aged conditions, are listed in Tables 10 to 20.

$Cu_{0.9}Ni_{0.1}$: The magnetization at 4.2°K for the quenched $Cu_{0.9}Ni_{0.1}$ alloy is found to be linear with H up to 12.6 kOe, as seen in Fig. 13. The susceptibility (Fig. 14) may be thought of[2] as comprising the band susceptibility, χ_b, of the solid solution,

Figure 9. σ vs. $\frac{1}{H_i}$ graphs for quenched $Cu_{0.5}Ni_{0.5}$. By extrapolating to $\frac{1}{H_i} = 0$ values of $\sigma_{H_i=\infty,T}$ were determined for the different temperatures.

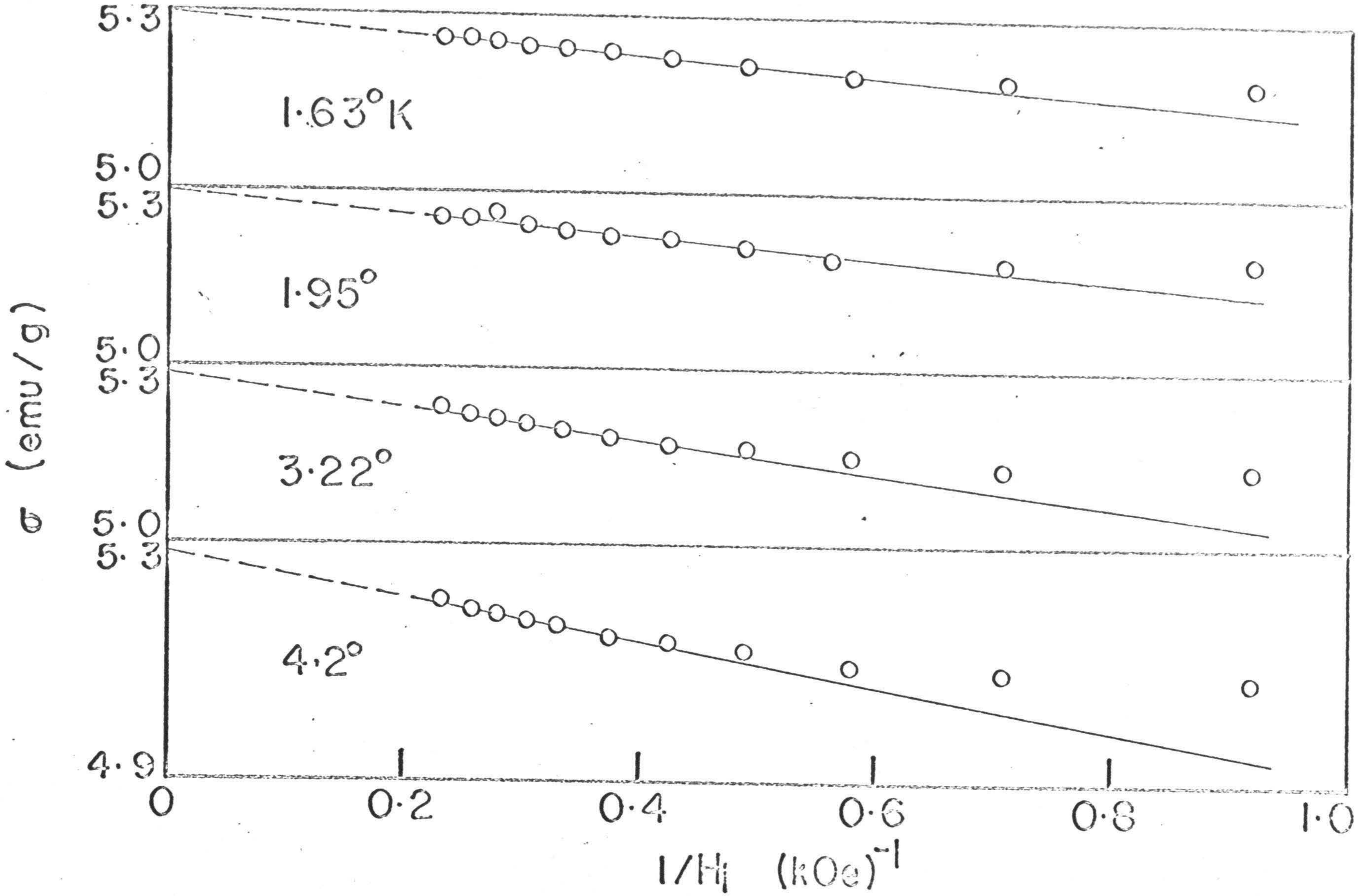
5·3
5·0
1·63°K
5·3
5·0
1·95°
5·3
5·0
3·22°
5·3
4·9
4·2°
σ (emu/g)
0
0·2
0·4
0·6
0·8
1·0
1/H (kOe)⁻¹

Figure 10. σ vs. $\frac{1}{H_i}$ graphs for quenched $Cu_{0.52}Ni_{0.48}$. By extrapolating to $\frac{1}{H_i} = 0$ values of $\sigma_{H_i=\infty,T}$, were determined for the different temperatures.

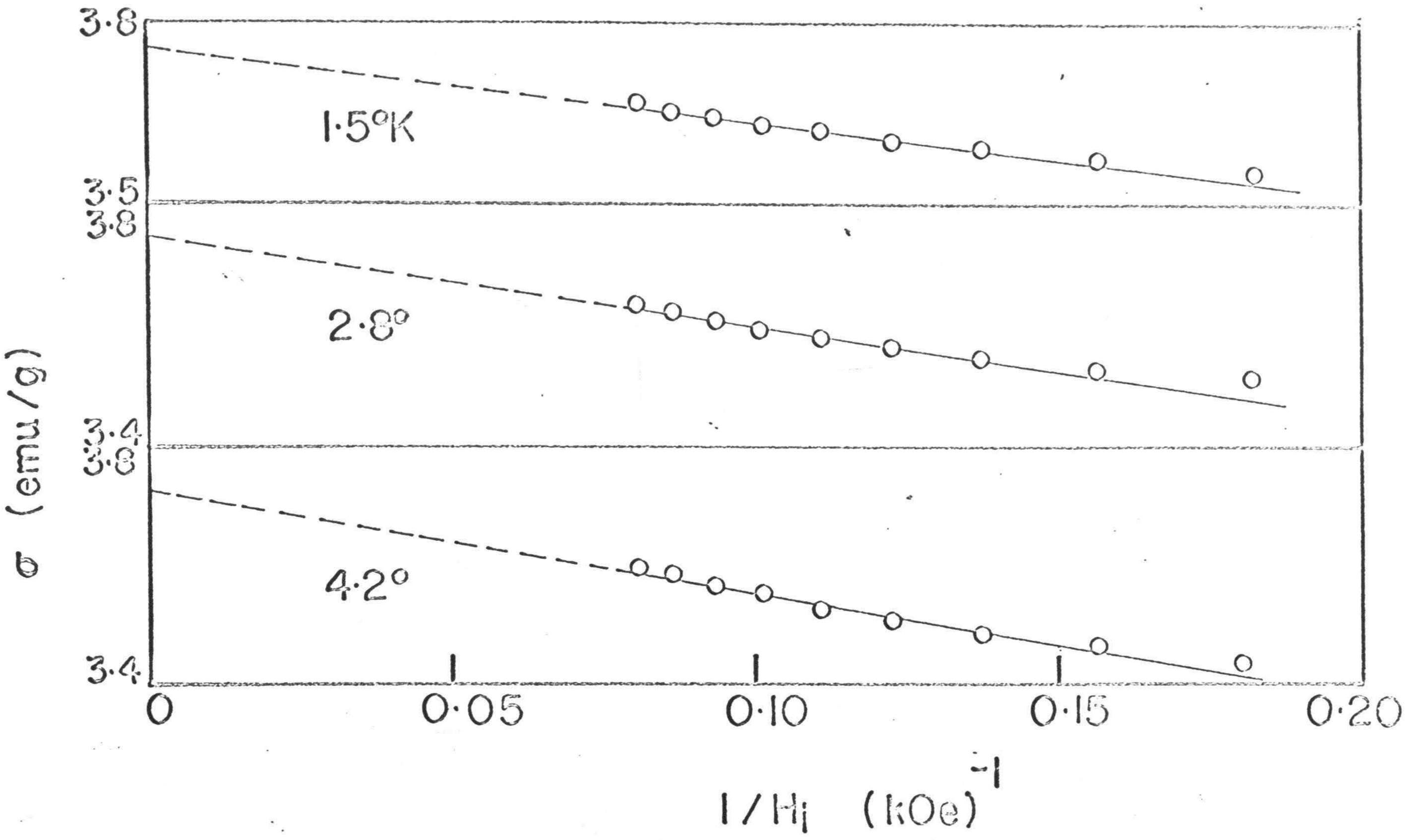
3·8
1·5°K
3·5
3·8
2·8°
3·4
4·2°
3·4
0
0·05
0·10
0·15
0·20
σ (emu/g)
1/Hi (kOe)⁻¹

Figure 11. σ vs. $\frac{1}{H_i}$ graphs for quenched $Cu_{0.54}Ni_{0.46}$. By extrapolating to $\frac{1}{H_i} = 0$ values of $\sigma_{H_i=\infty,T}$ were determined for the different temperatures.

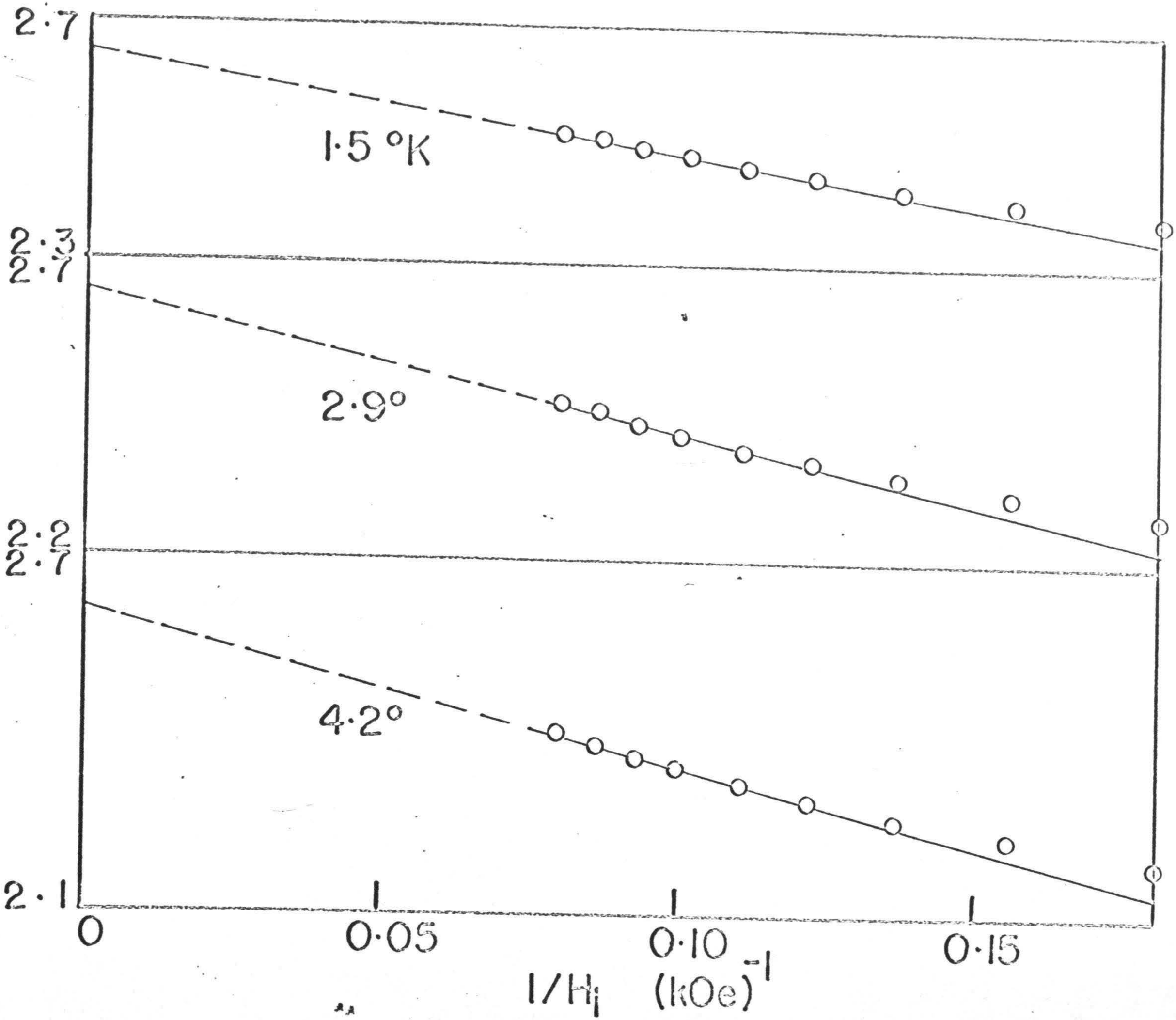
2·7
1·5 °K
2·73
2·7
2·9°
2·72
2·7
4·2°
2·1
0
0·05
0·10
0·15
σ (emu/g)
1/H_i (kOe)^-1

Figure 12. $\sigma_{H_i=\infty,T}$ vs. T for quenched $Cu_{0.5}Ni_{0.5}$ (O), $Cu_{0.52}Ni_{0.48}$ (Δ) and $Cu_{0.54}Ni_{0.46}$ (□) alloys. By extrapolating $\sigma_{H_i=\infty,T}$ to T = 0, the saturation magnetization value $\sigma_{H_i=\infty,T=0}$ was determined for each alloy.

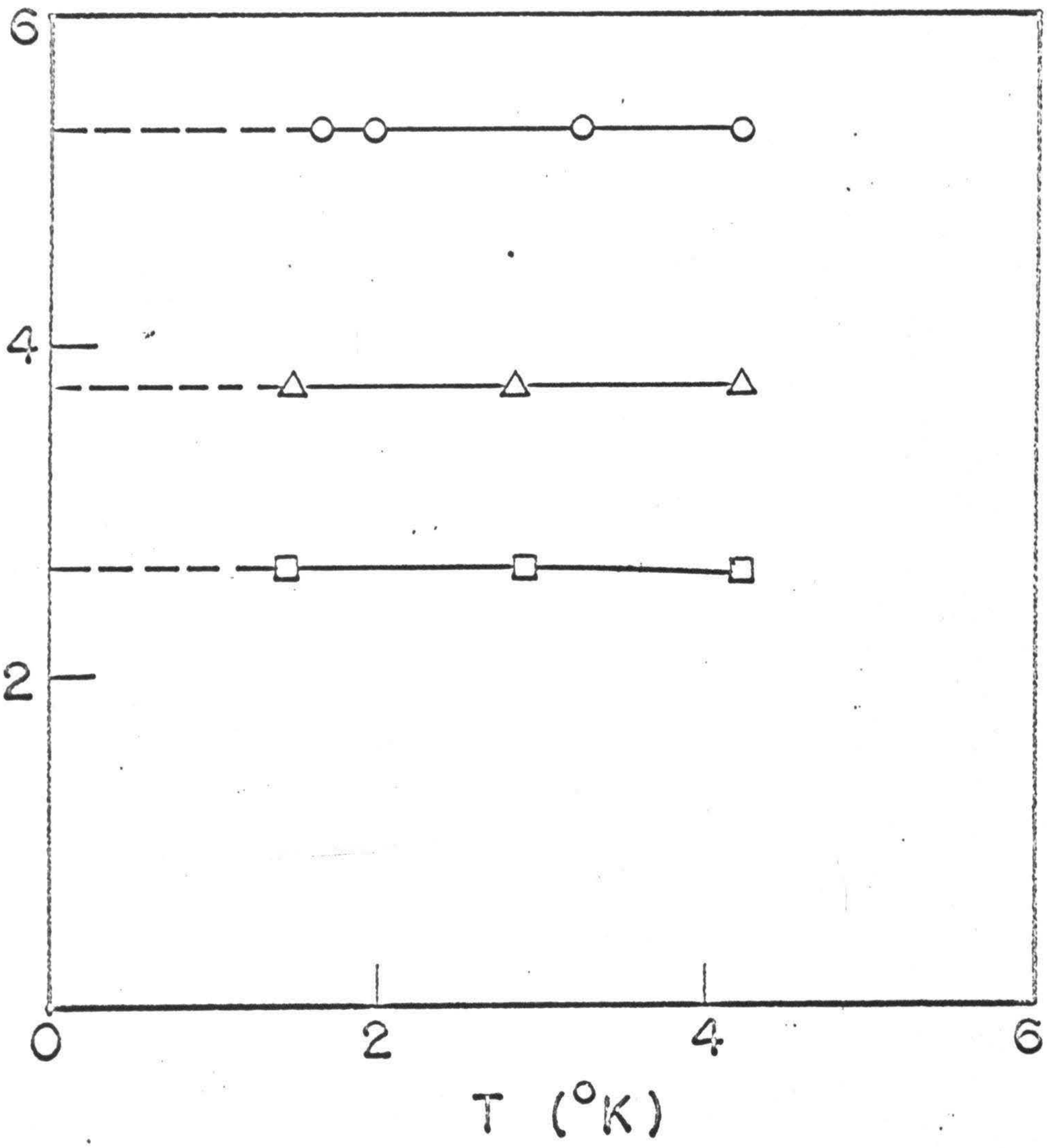
6
4
2
0
2
4
6
$\sigma_{H=\infty}$, T (emu/g)
T (°K)

Figure 13. Magnetization data at 4.2°K for quenched $Cu_{0.9}Ni_{0.1}$. See Table 10.

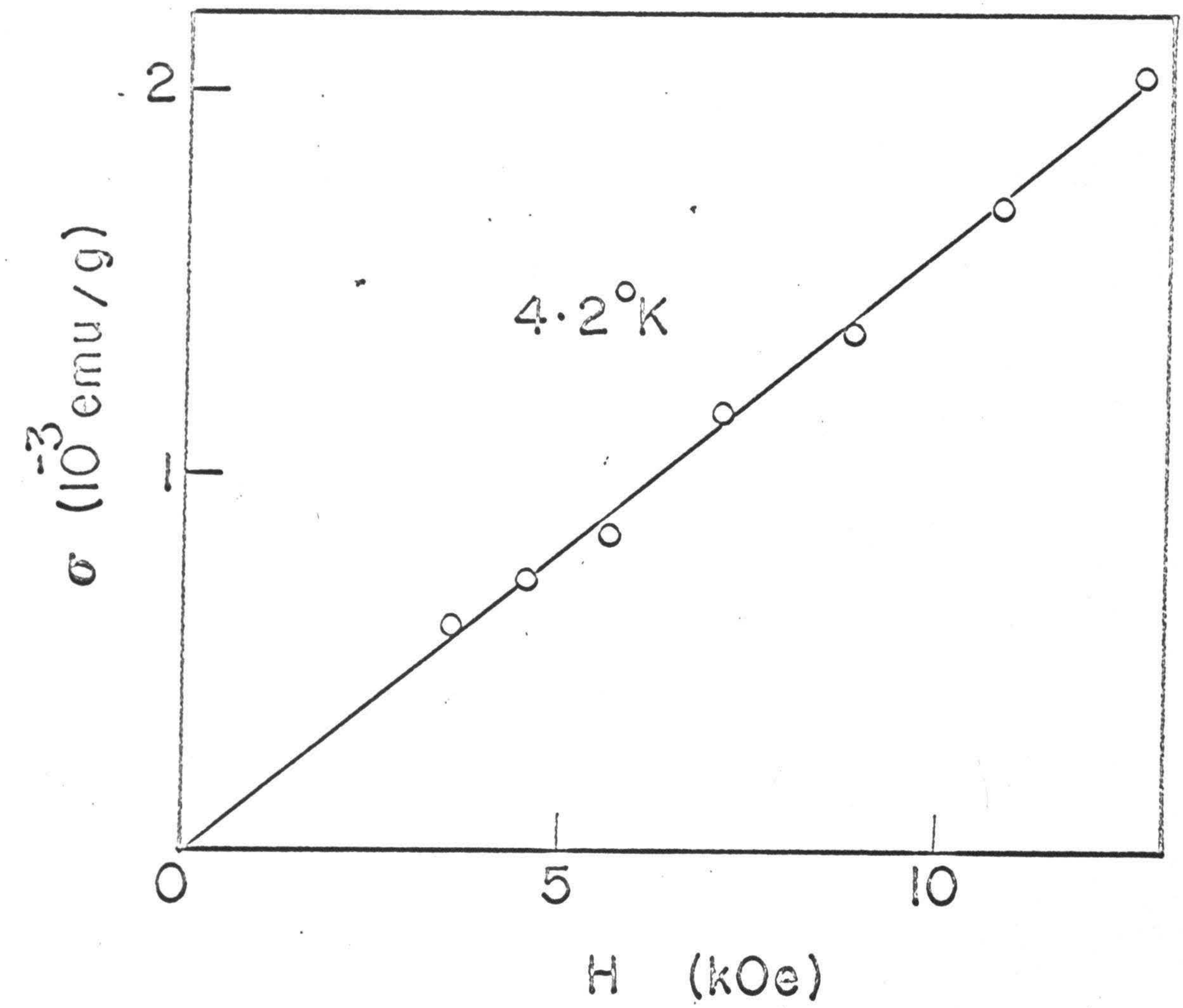
2
1
σ (10^-3 emu/g)
4.2°K
0
5
10
H (kOe)

Figure 14. χ vs. T for quenched $Cu_{0.9}Ni_{0.1}$, $Cu_{0.8}Ni_{0.2}$ (from Refs. 1,2), and $Cu_{0.7}Ni_{0.3}$ (from Ref. 1) alloys.

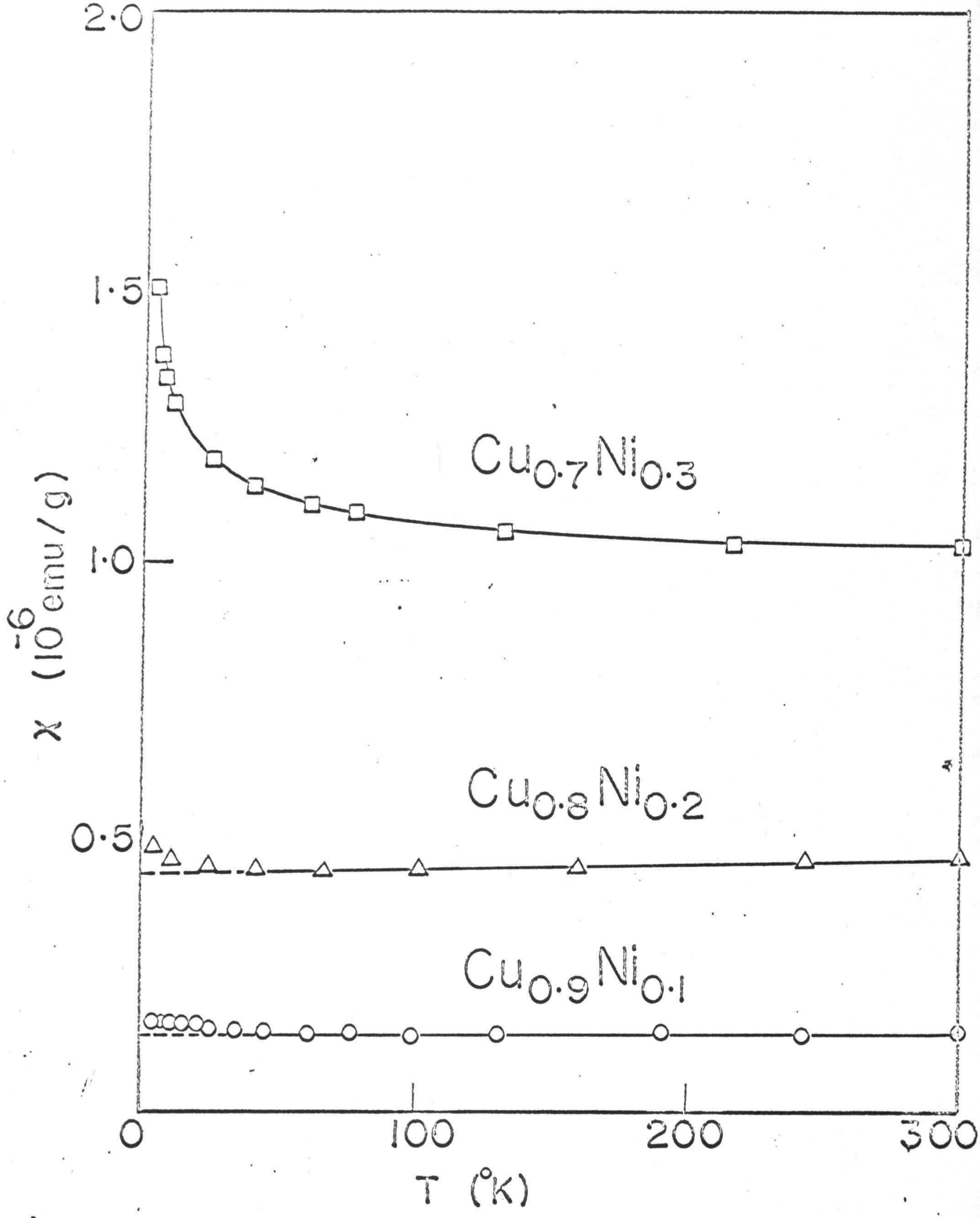
2·0
1·5
1·0
0·5
χ (10⁻⁶ emu/g)
Cu0·7Ni0·3
Cu0·8Ni0·2
Cu0·9Ni0·1
0
100
200
300
T (°K)

which rises slightly with increasing temperature, and a Curie-Weiss component prominent at the lowest temperatures of measurement, but practically disappearing above about 60°K. The band susceptibility χ_b follows the expression: $\chi_b = (\chi_o + bT)$ with $\chi_o = 0.14 \times 10^{-6}$ emu/g and $b = 10^{-11}$ emu/g degree. Due to the scatter in the Curie-Weiss component of the susceptibility, it was not possible to determine the Curie-constant. However, from the absolute value of the susceptibility at 4.2°K one may estimate an Fe-impurity content of about ∿4 ppm in the alloy. Alternatively, the Curie-Weiss component of the susceptibility may also be interpreted as due to small magnetic Ni-rich clusters, as has been done for a $Cu_{0.8}Ni_{0.2}$ alloy.[2]

$\underline{Cu_{0.7}Ni_{0.3}}$: In an earlier report[1] the susceptibility data for the quenched $Cu_{0.7}Ni_{0.3}$ alloy, as a function of temperature between 4.2°K and ∿80°K, and the magnetization data at 4.2°K in fields up to 12.6 kOe were interpreted in terms of small Ni-rich clusters with the average magnetic moment per cluster $\mu < 3\mu_B$. The susceptibility data in the earlier report[1] were graphically represented by the following Curie-Weiss type of expression:

$$\chi \text{ (emu/g)} = \chi_o + \frac{N_o\, cp^2\, (\mu_B)^2}{3\, Mk\, (T-\theta)} \qquad (7)$$

where χ_o is the field- and temperature-independent susceptibility in emu/g, N_o (= 6.02×10^{23}/mole) is Avogadro's number, c is the concentration of magnetic dipoles in atom fraction, i.e., per alloy, atom, p is the effective magnetic moment per dipole in Bohr magnetons, M is the average gram atomic weight of the alloy,

k (= 1.38 x 10^{-16} ergs/^{o}K) is Boltzmann's constant, and θ is the Weiss interaction temperature in ^{o}K. Note that,

$$p^2 = \mu\ (\mu + g) \tag{8}$$

where $\mu = gJ$ is the permanent moment/dipole in Bohr magnetons, g being the Lande splitting factor. J is the total angular momentum quantum number, i.e., the sum of the spin quantum number S and of the orbital angular momentum quantum number L. We assume L << S, i.e., J ≃ S; in such a case g ≃ 2.

Equation 7 was found to fit the susceptibility data between 4.2°K and ∿80°K with cp^2 = 2.62 x 10^{-3}/atom, χ_o = 1.03 x 10^{-6} emu/g and θ ≃ -9°K.

During the course of the present investigation high field magnetization measurements at 4.2°K (Table 11) were made for the same alloy, i.e., quenched $Cu_{0.7}Ni_{0.3}$. Here the σ vs. H graph showed a slight curvature (Fig. 15). The 4.2°K isothermal data were analyzed together with the susceptibility data in the entire temperature range of 4.2°K to 300°K, by least squares fitting of the following equation with the help of a computer program (Appendix A).

$$\sigma\ (\text{emu/g}) = \chi_o H + \frac{N_o}{M}\ c\,\mu\,\mu_B\,B\ (\mu, \frac{H}{T-\theta}) \tag{9}$$

where H is the applied field in Oe and B (μ, $\frac{H}{T-\theta}$) is the Brillouin function, which for g = 2 is given by,

Figure 15. χ vs. T (from Ref. 1) and σ vs. H at 4.2°K (see Table 11) for quenched $Cu_{0.7}Ni_{0.3}$. The empty and filled circles represent measured data points; the solid curves were calculated by using parameter values ($\mu = 2.76\ \mu_B$, $c = 1.297 \times 10^{-4}$ clusters/alloy atom, $\theta = -3.5$°K, $\chi_o = 1.038 \times 10^{-6}$ emu/g) obtained by least squares fitting of Eq. 9.

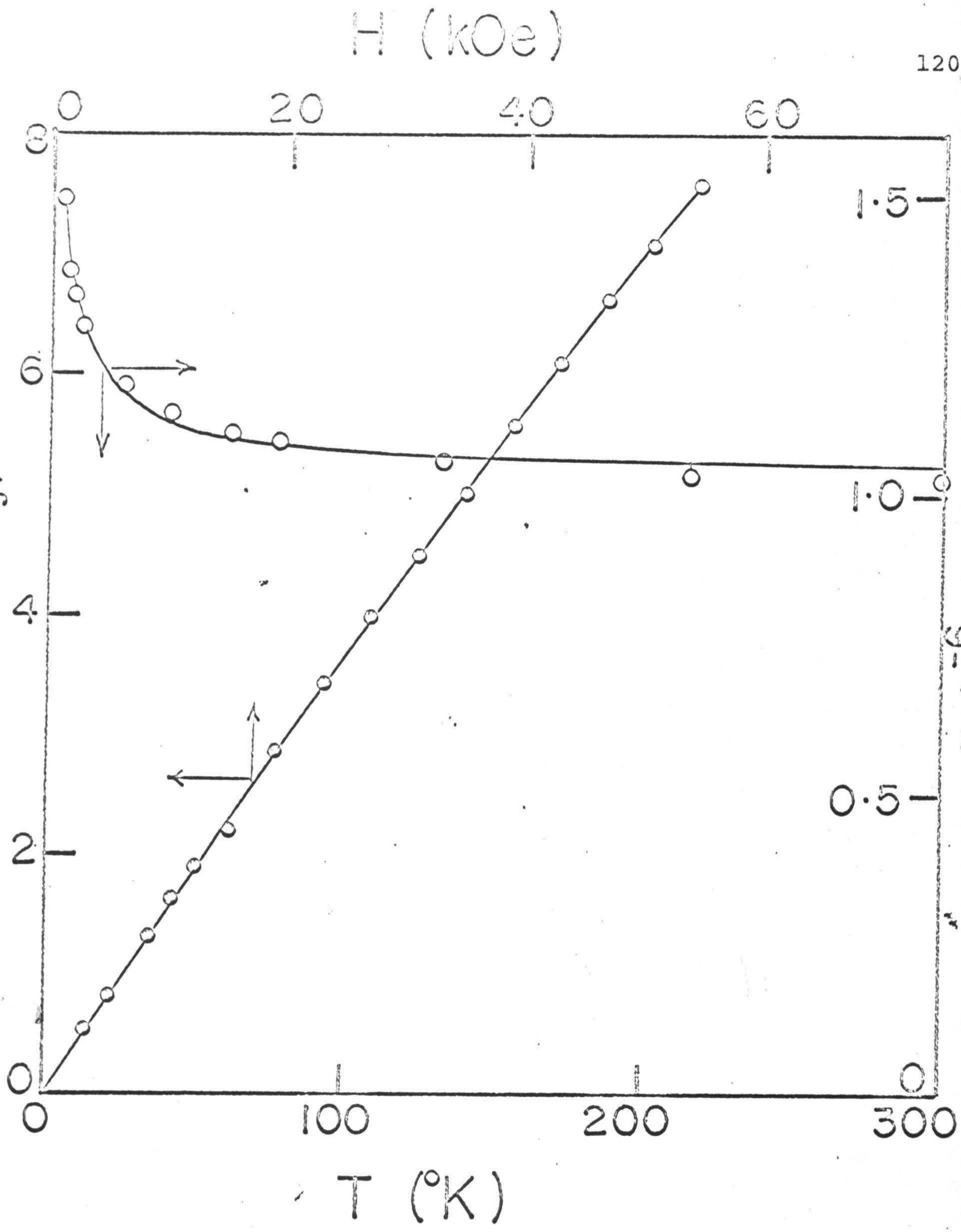
H (kOe)
0
20
40
60
σ (10^-2 emu/g)
6
4
2
0
χ (10^-6 emu/g)
1.5
1.0
0.5
0
0
100
200
300
T (°K)

$$B\ (\mu,\ \frac{H}{T-\theta}) = \frac{\mu+1}{\mu}\ \text{ctnh}\left[(\mu+1)\frac{\mu_B H}{k(T-\theta)}\right] - \frac{1}{\mu}\ \text{ctnh}\left[\frac{\mu_B H}{k(T-\theta)}\right] \quad (10)$$

and all other quantities were defined in connection with Eq. 9.

The practice of using θ, in the argument of the Brillouin function, to represent an interaction temperature has been followed by several investigators.[2,3,18,19,20,21] In a very simple picture $k\theta$ would represent the energy, i.e., strength of interaction of the magnetic dipole with its magnetic environment. In the region where the σ vs. T plot is linear, i.e., at low fields and/or at high temperatures, the Brillouin equation of the type used here then reduces to the familiar Curie-Weiss expression (Eq. 7). At higher fields or at lower temperatures, where the σ vs. H graph is curved, θ is proportional to $\frac{\sigma T}{H}$; and it falls off with decreasing temperature or with increasing field. However, the use of a constant θ value, in the sense of an average quantity over a range of fields and temperatures, has been found to be very suitable for describing magnetization data in a number of alloy systems.[2.18,19]

The parameter values obtained for the quenched $Cu_{0.7}Ni_{0.3}$ alloy are: $\mu = 2.76\ \mu_B$, $c = 1.297 \times 10^{-4}$ clusters/alloy atom, $\theta = -3.50°K$ and $\chi_o = 1.038 \times 10^{-6}$ emu/g. The rmsd was 0.026×10^{-2} emu/g and the degree of fit (the rmsd as expressed as a percentage of the highest magnetization value used in the fitting) was $\sim$0.34%. The resultant fit is illustrated in Fig. 15.

The permanent average moment $\bar{\mu}$ per alloy atom is estimated to be $\simeq 0.00036\ \mu_B$. Also the value of cp^2, calculated from the values of μ and c is $\sim 1.71 \times 10^{-3}\ (\mu_B)^2$/alloy atom. The differences in the cp^2 and θ values obtained by fitting of Eq. 9, from the corresponding values obtained earlier[1] by fitting of Eq. 7 arise from the fact that in the earlier analysis only the susceptibility data in a narrow temperature range, i.e., 4.2°K to ~80°K were used.

$\underline{Cu_{0.6}Ni_{0.4}}$: On fitting Eq. 9 to the data for quenched $Cu_{0.6}Ni_{0.4}$ the following parameter values were obtained: $\mu = 17.1\ \mu_B$, $c = 3.68 \times 10^{-4}$ clusters/alloy atom, $\theta = -0.51$°K, $\chi_o = 4.25 \times 10^{-6}$ emu/g. The rmsd was, however, very high (1.96×10^{-2} emu/g) and the degree of fit very poor (= 2.4%). Large systematic deviations ($\Delta\sigma = \sigma_{calculated} - \sigma_{measured}$; $\Delta\chi = \chi_{calculated} - \chi_{measured}$) were found between the calculated and the measured values of σ and χ (at high temperatures, i.e., T > 30°K, σ is proportional to H and $\chi = \frac{\sigma}{H}$) at all temperatures between 1.49°K and ~300°K. The deviations in σ at 2.52°K and 4.2°K as a function of field and the deviations in χ as a function of temperature are illustrated in Fig. 16. A much better fit was obtained by least squares fitting of the following equation

$$\sigma = \chi_o H + \frac{N_o}{M} c_1 \mu_1 \mu_B B\left(\mu_1, \frac{H}{T-\theta_1}\right) + \frac{N_o}{M} c_2 \mu_2 \mu_B B\left(\mu_2, \frac{H}{T-\theta_2}\right) \qquad (11)$$

Figure 16. $\Delta\sigma$ ($= \sigma_{calculated} - \sigma_{measured}$) vs. H at 2.52°K and 4.2°K, and $\Delta\chi$ ($= \chi_{calculated} - \chi_{measured}$) vs. T for quenched $Cu_{0.6}Ni_{0.4}$. Filled circle: deviations obtained from least squares fitting of Eq. 9; empty circle: deviations obtained from least squares fitting of Eq. 11.

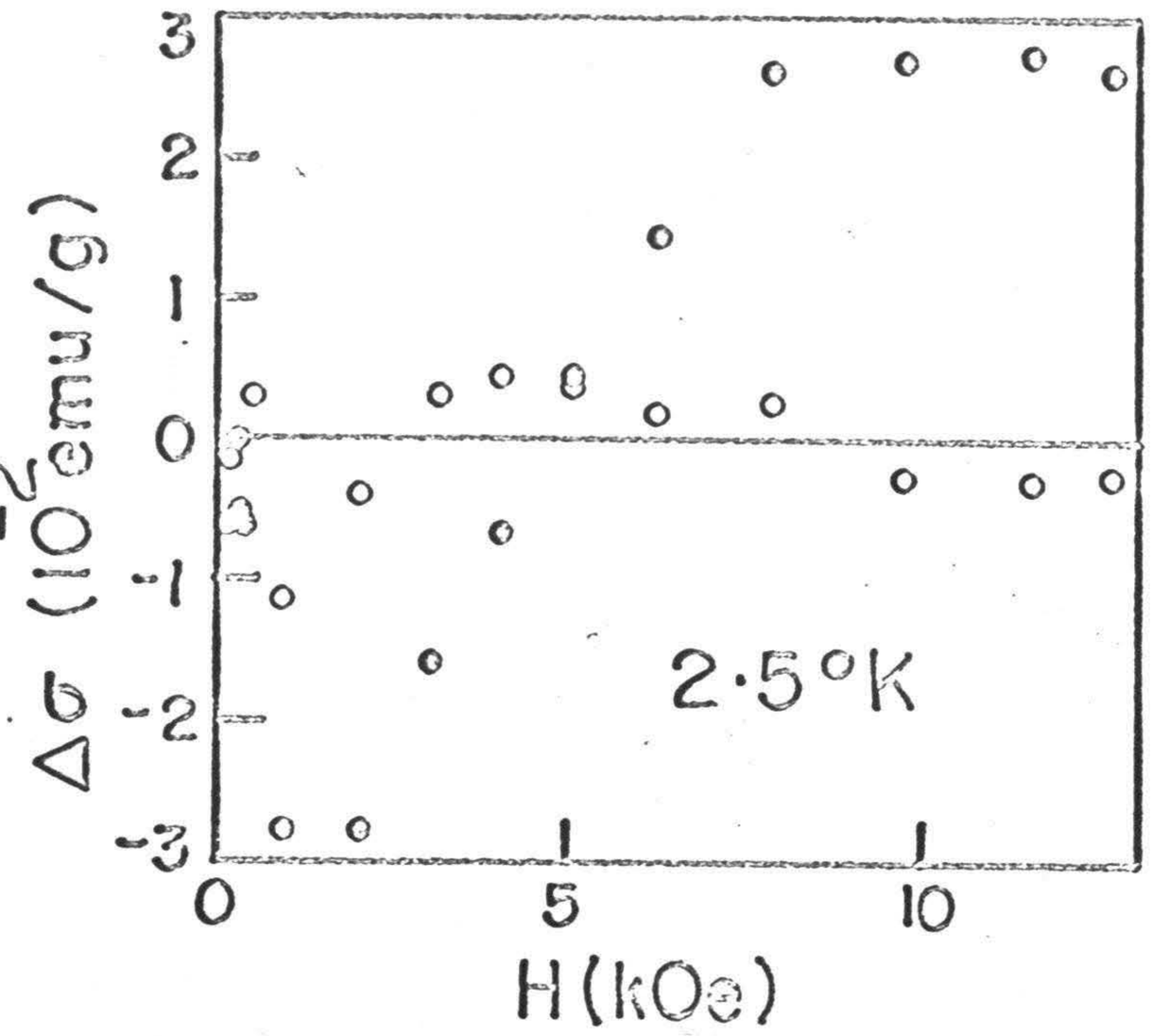
3
2
1
0
-1
-2
-3
$\Delta\sigma$ (10^{-2}emu/g)
2.5°K
0
5
10
H(kOe)

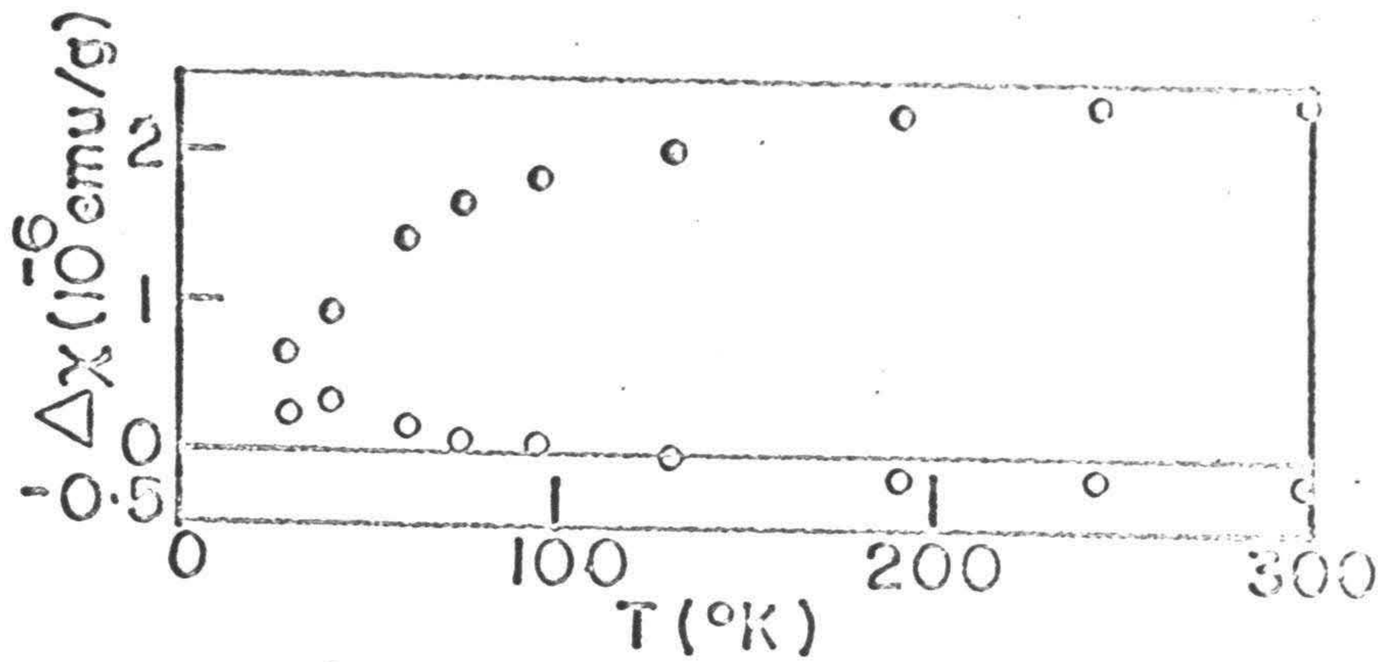
2
1
0
-0.5
$\Delta\chi$ (10^{-6}emu/g)
0
100
200
300
T(°K)

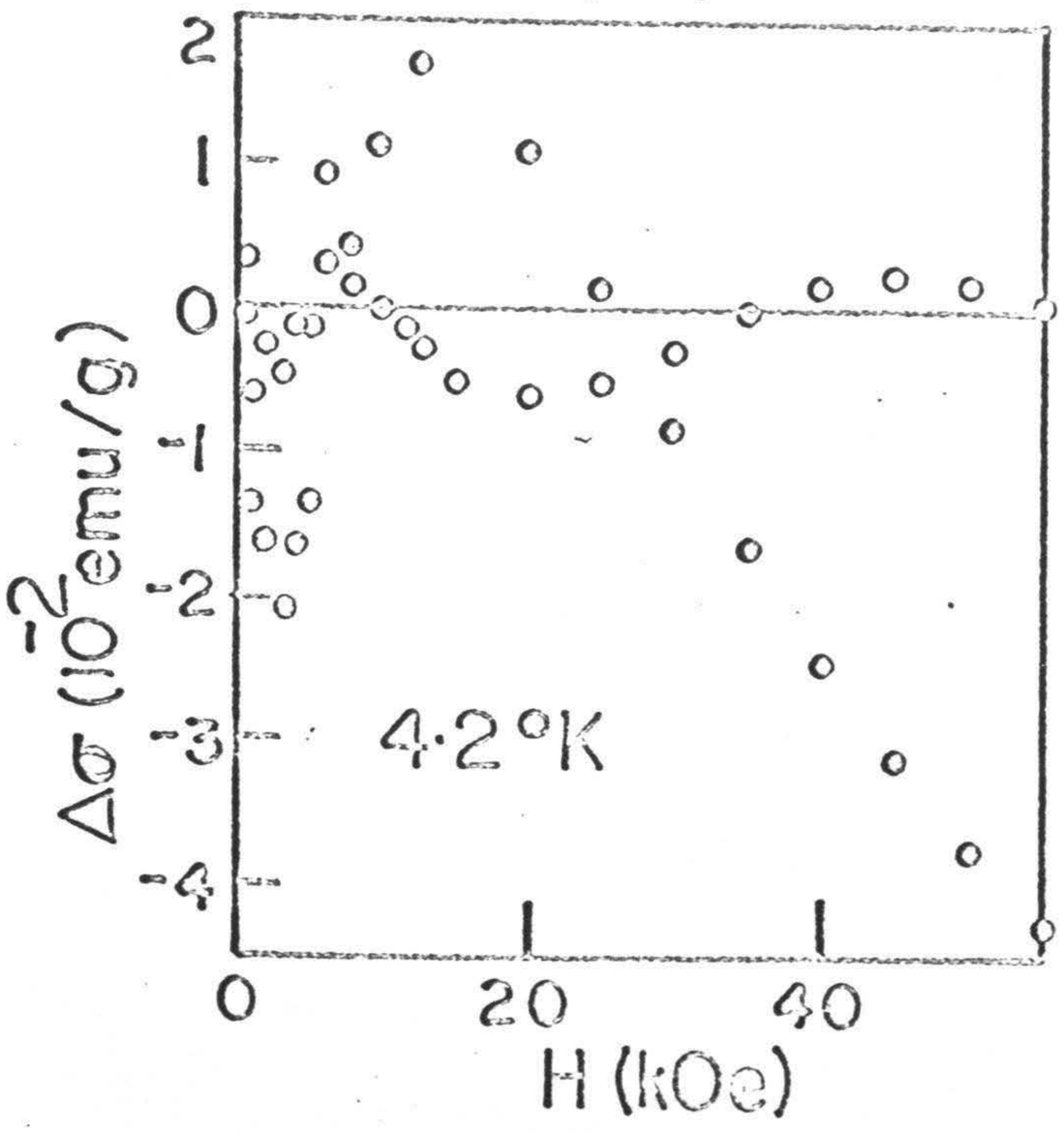
2
1
0
-1
-2
-3
-4
$\Delta\sigma$ (10^{-2}emu/g)
4.2°K
0
20
40
H(kOe)

where μ_1 and μ_2, c_1 and c_2, θ_1 and θ_2 represent two average moments in μ_B, the concentrations of the two moments in atom fractions and the corresponding Weiss temperatures in ^{o}K. The resulting parameter values are listed in Table 35. The accuracy of μ_1 and μ_2 is estimated to be roughly ±2% and ±5% respectively; similar uncertainties are involved in the values of c_1 and c_2. The value of χ_o is within about ±10%. As seen in Fig. 16 the systematic deviations in σ and χ are reduced considerably by using Eq. 11 instead of Eq. 9. The measured and calculated results for this alloy (i.e., quenched $Cu_{0.6}Ni_{0.4}$) are shown in Fig. 17 up to 12.6 kOe and up to 55 kOe in Fig. 18. Above about 30°K the σ vs. H isotherms are linear and the corresponding susceptibility values are given in Fig. 19 as a function of temperature. It is seen in Figs. 17, 18, and 19 that in the temperature range between ∿2.5°K and ∿130°K the calculated values fit the experimental data points well. The systematic deviations at 1.49°K may be interpreted as due to dipole-dipole interaction effects.

Equation 11 was also fitted to the data for the aged $Cu_{0.6}Ni_{0.4}$ alloy. The parameter values are listed in Table 35, and the results shown in Figs. 18, 19, and 20. Here again a similarly good fit was obtained for a wide range of temperatures, i.e., 4.2°K to ∿300°K (for the aged alloy the deviations were so large at 1.49°K that the data for 1.49°K were eliminated from the final stages of the least squares fitting operation).

Table 35. Results of analysis of data for quenched, and aged $Cu_{0.6}Ni_{0.4}$

Parameter	As-quenched Condition	Aged Condition
(a) Brillouin Analysis (Eq. 11)		
Temperature range (°K)	1.49 to ∿300	2.52 to ∿300
μ_1 (μ_B)	5.3	5.3
μ_2 (μ_B)	23.2	29.0
c_1 (atom fraction)	1.04×10^{-3}	$1{\cdot}11 \times 10^{-3}$
c_2 (atom fraction)	1.83×10^{-4}	$1{\cdot}93 \times 10^{-4}$
θ_1 (°K)	- 5.2	- 2.8
θ_2 (°K)	+ 0.1	+ 0.5
χ_o (emu/g)	1.80×10^{-6}	$1{\cdot}00 \times 10^{-6}$
rmsd (emu/g)	4.519×10^{-3}	5.634×10^{-3}
rmsd (%)*	0.55%	0.56%
(b) Curie-Weiss Analysis (Eq. 7)		
cp^2 in (Bohr magneton)^2 per alloy atom	0.157	0.204
θ (°K)	- 0.27	+ 0.71
χ_o (emu/g)	1.612×10^{-6}	1.154×10^{-6}
rmsd (emu/g)	2.669×10^{-6}	1.558×10^{-6}
rmsd (%)*	1.48%	0.29%

*The rmsd as expressed in percents of the highest magnetization (or, susceptibility) value used in the fitting.

Figure 17. Magnetization vs. field (Table 12) at temperatures indicated for quenched $Cu_{0.6}Ni_{0.4}$. Empty circles: measured data; lines were calculated with parameters values from least squares fitting and listed in Table 35a.

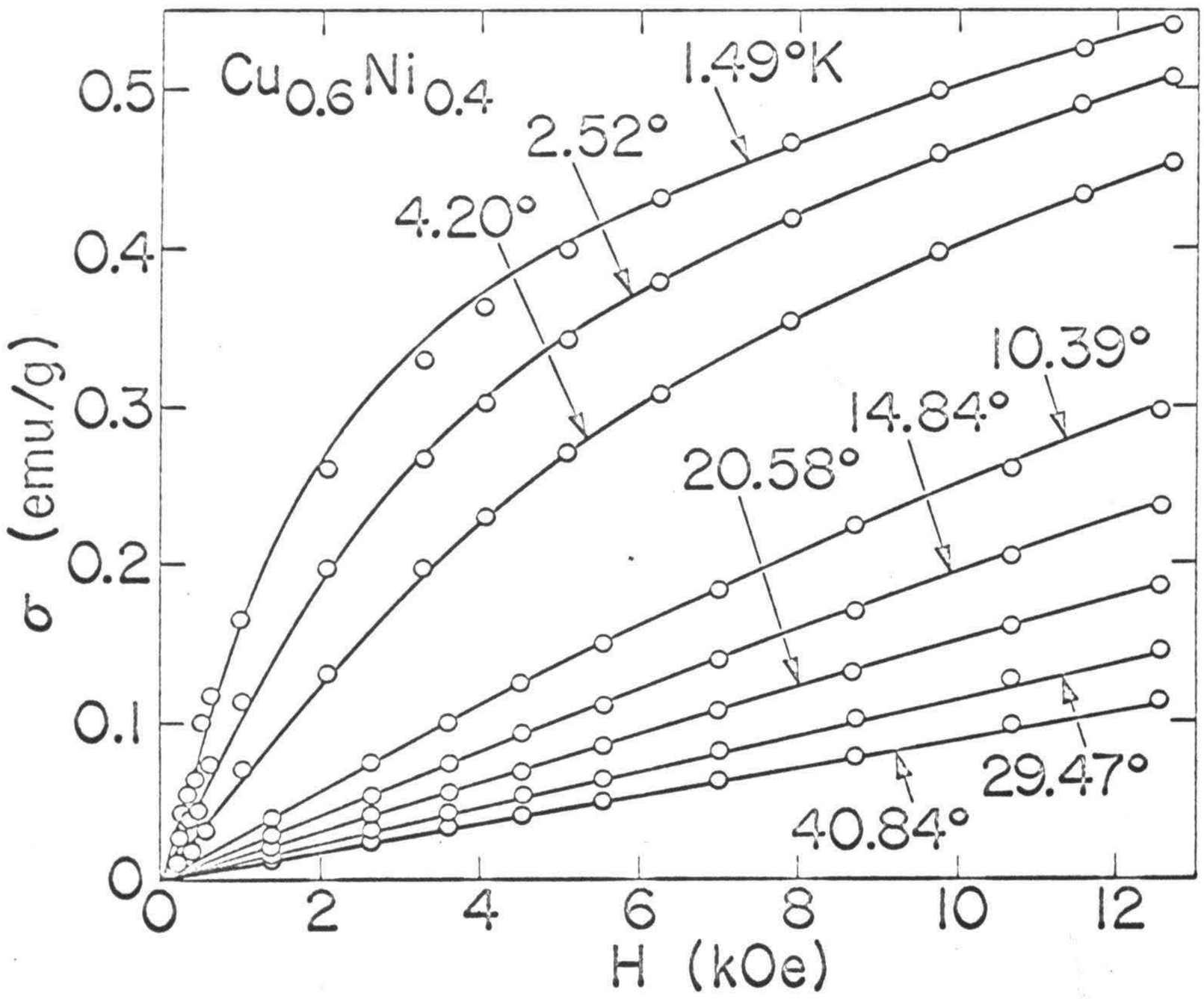
$Cu_{0.6}Ni_{0.4}$
1.49°K
2.52°
4.20°
10.39°
14.84°
20.58°
29.47°
40.84°
σ (emu/g)
H (kOe)
0
0.1
0.2
0.3
0.4
0.5
2
4
6
8
10
12

Figure 18. Magnetization vs. field up to 55 kOe at 4.2°K in both the as-quenched and the aged condition for $Cu_{0.6}Ni_{0.4}$ (Tables 12 and 13). Open circles show measured data points in the as-quenched condition, filled circles in the aged condition. Lines were calculated with parameter values (Table 35[a]) from least squares fitting of Eq. 11.

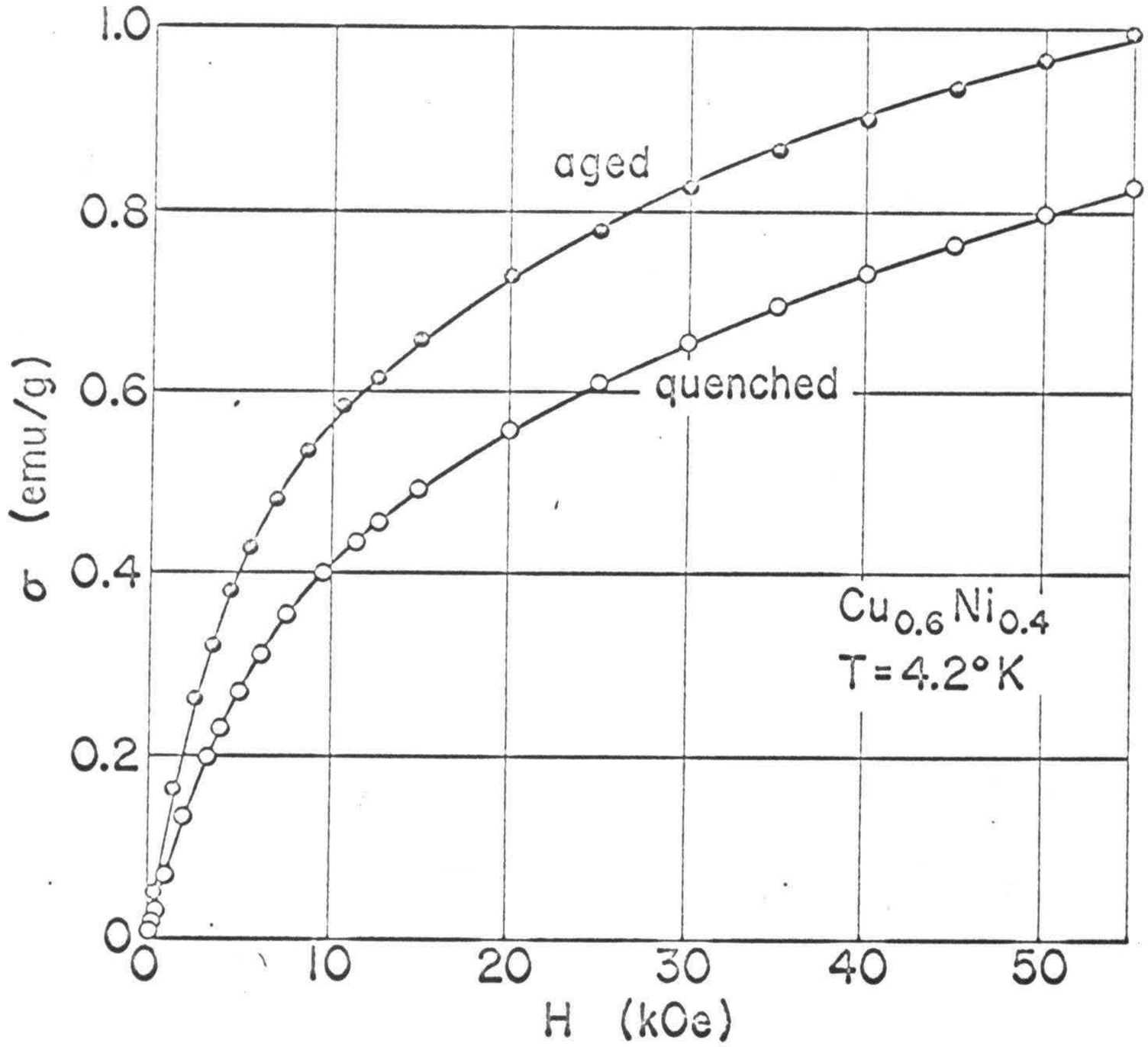
1.0
0.8
0.6
0.4
0.2
0
σ (emu/g)
aged
quenched
$Cu_{0.6}Ni_{0.4}$
T = 4.2°K
0
10
20
30
40
50
H (kOe)

Figure 19. Susceptibility vs. temperature for $Cu_{0.6}Ni_{0.4}$ in both the as-quenched and aged condition. Filled and empty circles show measured values, lines were calculated with parameter values (Table 35[a]) from least squares fitting of Eq. 11.

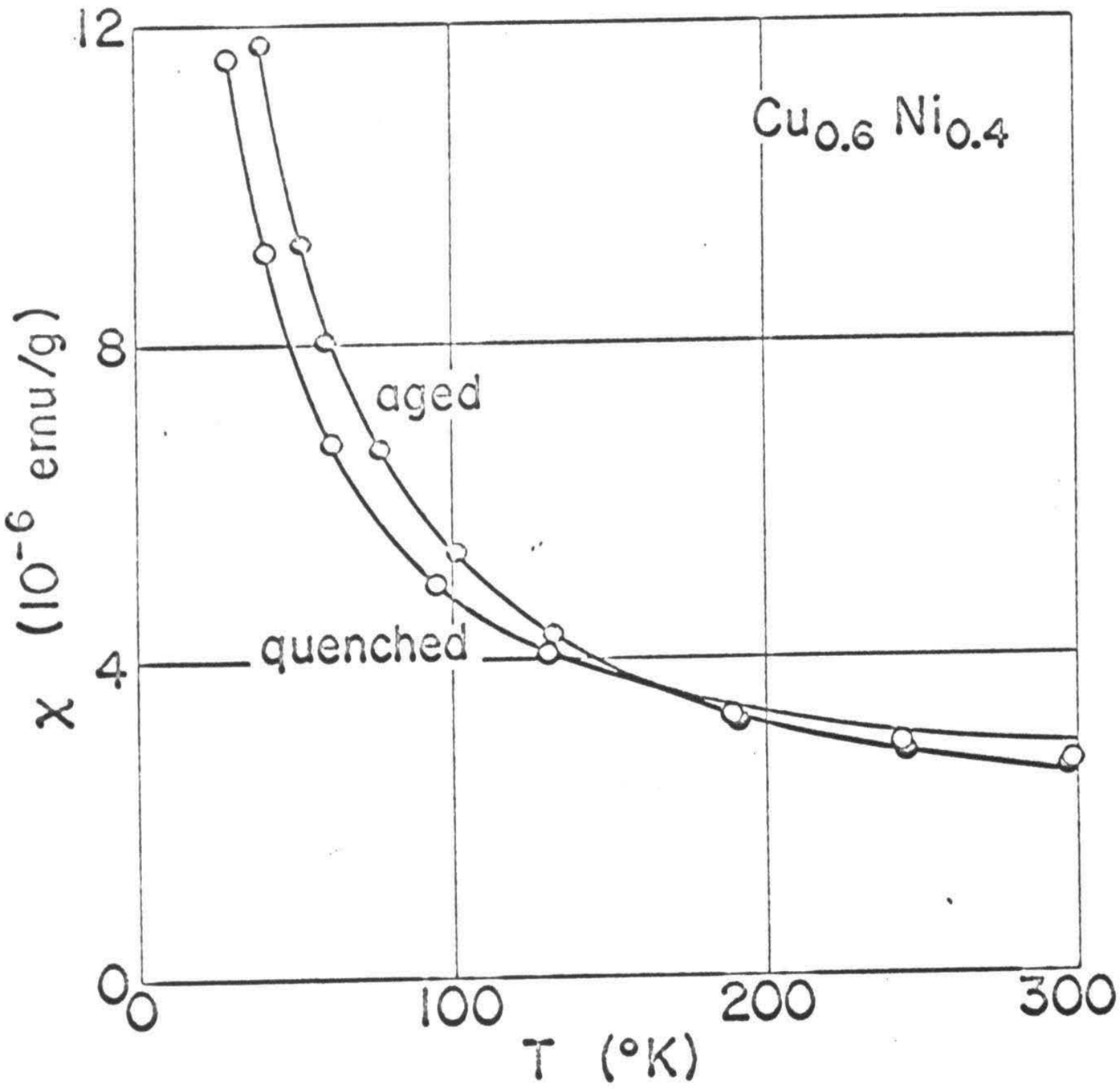
12
$Cu_{0.6}$ $Ni_{0.4}$
8
4
0
aged
quenched
χ (10⁻⁶ emu/g)
0
100
200
300
T (°K)

Figure 20. Magnetization vs. field at temperatures indicated, for aged $Cu_{0.6}Ni_{0.4}$. Filled circles show experimental data (Table 13), lines calculated with parameter values (Table 35[a]) from least squares fitting of Eq. 11.

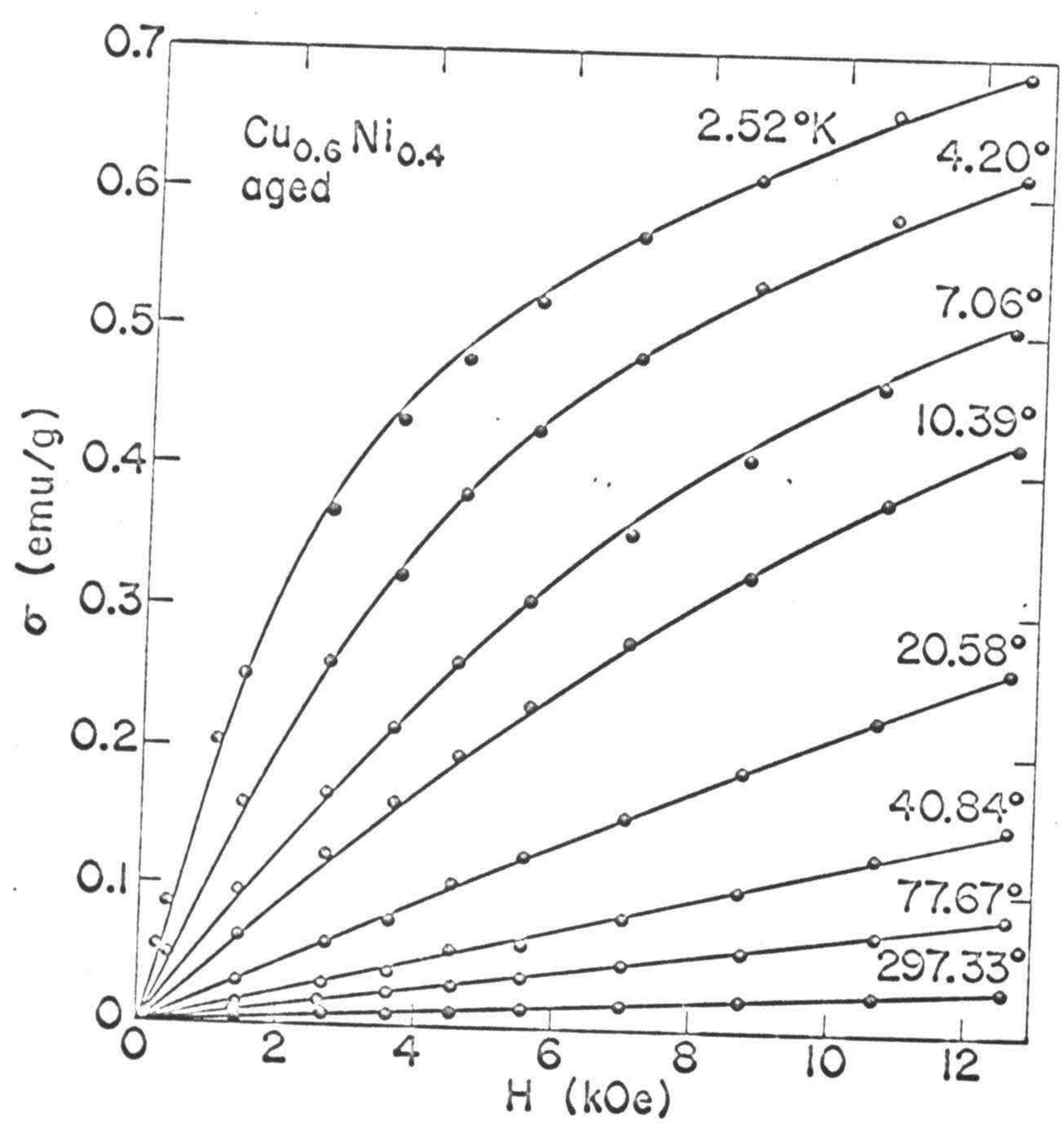
$Cu_{0.6}Ni_{0.4}$
aged
2.52°K
4.20°
7.06°
10.39°
20.58°
40.84°
77.67°
297.33°
σ (emu/g)
H (kOe)
0.7
0.6
0.5
0.4
0.3
0.2
0.1
0
0
2
4
6
8
10
12

An important question that arises now is whether the results from the fitting of Eq. 11 to the data for $Cu_{0.6}Ni_{0.4}$ represent a true bimodal cluster distribution as shown in Fig. 21(a). One may argue that a better rmsd and less systematic deviations were obtained in this case, than when Eq. 10 was fitted, simply because more parameters were used, even though the cluster distribution for $Cu_{0.6}Ni_{0.4}$ is actually symmetrical, e.g., Gaussian, as shown in Fig. 21(b). To examine this possibility, a Gaussian distribution of the type sketched in Fig. 21(b) was assumed. The normalized Gaussian function has the form:

$$c = f(\mu) = \frac{1}{b\sqrt{2\pi}} \exp\left[-\frac{1}{2}\frac{(\mu-a)^2}{b^2}\right] \qquad (12)$$

where b is the standard deviation and a is the distance of the center of symmetry from the origin. The Gaussian, for the present purpose, was taken to be symmetrical about $\mu = 10\ \mu_B$ (Giant moments of this size have been reported by Kouvel et al.[22] for paramagnetic Cu-Ni alloys for Ni concentrations between 44 and 32 at%). The standard deviation b was chosen to be 2.5, so that the value of the Gaussian (i.e., the concentration) is nearly equal to zero for $\mu = 0$ and $\mu = 20$. Magnetization curves at T = 1°K, 10°K and 100°K were synthesized for fields up to 50 kOe. First Eq. 9 (single moment) and then Eq. 11 (two moments) were fitted to these synthesized magnetization curves. The rmsd and the systematic deviations were found to be considerably lower in the second case. Clearly, a better rmsd value,

Figure 21. Schematic representation of various possible types of cluster distribution. (a) bimodal; (b) Gaussian (standard deviation, b = 2.5); (c) Gaussian, (b = 8.5); (d) Gaussian in the limit, b = ∞; (e) Gaussian in the limit, b = 0; (f) suggested cluster distribution in quenched $Cu_{0.6}Ni_{0.4}$.

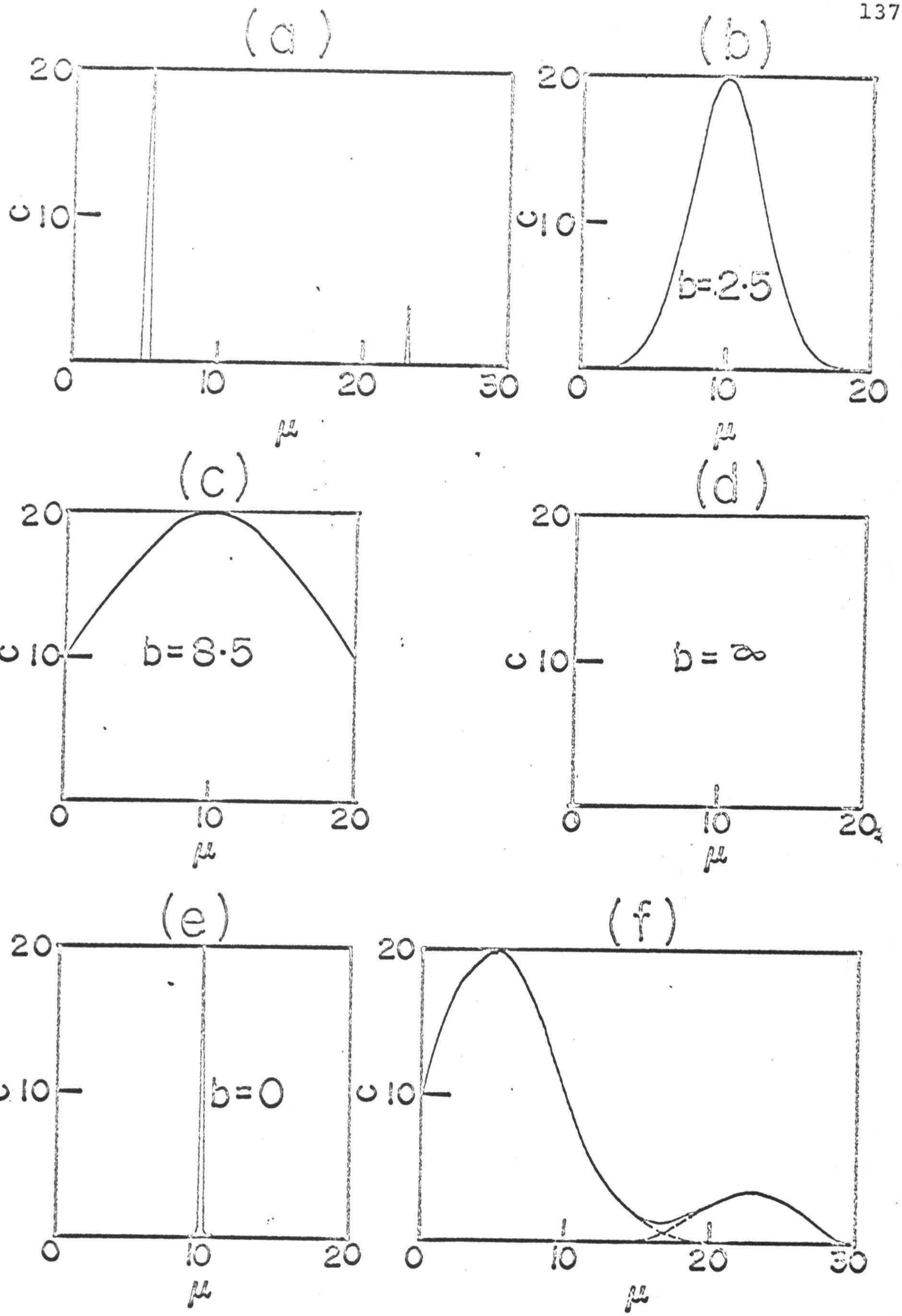
(a)
20
υ 10
0
10
20
30
μ
(b)
20
υ 10
b=2·5
0
10
20
μ
(C)
20
υ 10
b=8·5
0
10
20
μ
(d)
20
υ 10
b=∞
0
10
20
μ
(e)
20
υ 10
b=0
0
10
20
μ
(f)
20
υ 10
0
10
20
30
μ

obtained with the use of Eq. 11 instead of Eq. 9, does not in itself necessarily imply a bimodal distribution. The ratio of $\mu_2 : \mu_1$ was found in the above analysis with Eq. 11 to be ∿1.7. This value is significantly smaller than the corresponding value of ∿4.4 for the as-quenched $Cu_{0.6}Ni_{0.4}$ alloy. To examine whether a larger $\mu_2 : \mu_1$ ratio can be obtained by changing the standard deviation b, a cluster distribution of the type shown in Fig. 21(c) (b = 8.5) was assumed. For this case the ratio of $\mu_2 : \mu_1$ was found to be ∿1.6. In one limiting case, when b ≃ ∞ (Fig. 21(d), a very interesting result was obtained; the values of μ_1 and μ_2 obtained from the fitting of Eq. 11 approached each other and the value of μ obtained from the fitting of Eq. 9, i.e., $\mu_1 = \mu_2 = \mu$. The other limiting case of the Gaussian, when b ≃ 0, is illustrated in Fig. 21(e) and this corresponds again to the condition $\mu_1 = \mu_2 = \mu$. From the above examples, it does not seem likely that in the case of $Cu_{0.6}Ni_{0.4}$, where a large μ_2/μ_1 ratio was obtained by least squares fitting, a single Gaussian can suitably describe the cluster distribution. It is more plausible that μ_1 and μ_2 represent average moments for two symmetrical distributions. In Fig. 21(f) the ratio of the areas under the two symmetrical distributions shown roughly corresponds to the ratio of c_1 and c_2 in Table 35(a) and the values μ_1 and μ_2 also correspond to those obtained for $Cu_{0.6}Ni_{0.4}$. Whether or not the actual moment distribution in the alloy has two maxima, as in Fig. 21(f) can not be decided on the basis of the fitting, since the widths of the two symmetrical distributions are not known.

The average moment per alloy atom $\bar{\mu} = c_1\mu_1 + c_2\mu_2$. With the parameter values in Table 35(a) for the as-quenched state one obtains $\bar{\mu} = 0.0097\ \mu_B$. The corresponding value for the aged condition is $0.0115\ \mu_B$.

As noted earlier, fitting of Eq. 11 to the data gives a value of χ_o, the temperature and field independent susceptibility. This term χ_o, because of the fact that it contributes only a small amount to the total magnetization at low temperatures, is not very accurately determined from a fitting (of Eq. 11) in which a large number of data points taken at low temperatures is used. The value of χ_o was determined much more accurately by fitting of Eq. 7 to the susceptibility vs. temperature data (Fig. 22). The corresponding parameter values are listed in Table 35(b). The χ_o values so obtained are slightly different from those obtained by fitting Eq. 11 (Table 35[a]).

2. Cu-Ni-Fe (∿1 at % Fe; 0, 10, 20 at % Ni).

The results of magnetization measurements for the quenched $Cu_{0.99}Fe_{0.01}$, $(Cu_{0.9}Ni_{0.1})_{0.99}Fe_{0.01}$, and $(Cu_{0.8}Ni_{0.2})Fe_{0.01}$ alloys are given in Tables 14, 15, and 16. σ^2 vs. $\frac{Hi}{\sigma}$ graphs at low applied fields (down to ∿16 Oe) indicate for the $Cu_{0.99}Fe_{0.01}$ alloy a remanence temperature $T_r \simeq 2.8 \pm 1.4°K$ as seen in Fig. 23. In the case of the $(Cu_{0.9}Ni_{0.1})_{0.99}Fe_{0.01}$ alloy, measurements were made at applied fields as low as 32 Oe and the remanence temperature is estimated to be $3.1 \pm 1.1°K$ (Fig. 24). For the $(Cu_{0.8}Ni_{0.2})_{0.99}Fe_{0.01}$ alloy (Fig. 25) no remanence is observable, down to 1.57°K.

Figure 22. $\frac{1}{\chi_i - \chi_o}$ vs. T graphs for quenched and aged $Cu_{0.6}Ni_{0.4}$. The straight line represents values calculated by using the parameters listed in Table 35b. These parameters were obtained from least squares fitting to Eq. 7. The value of χ_o was so adjusted in each case as to give a linear $\frac{1}{\chi_i - \chi_o}$ vs. T plot.

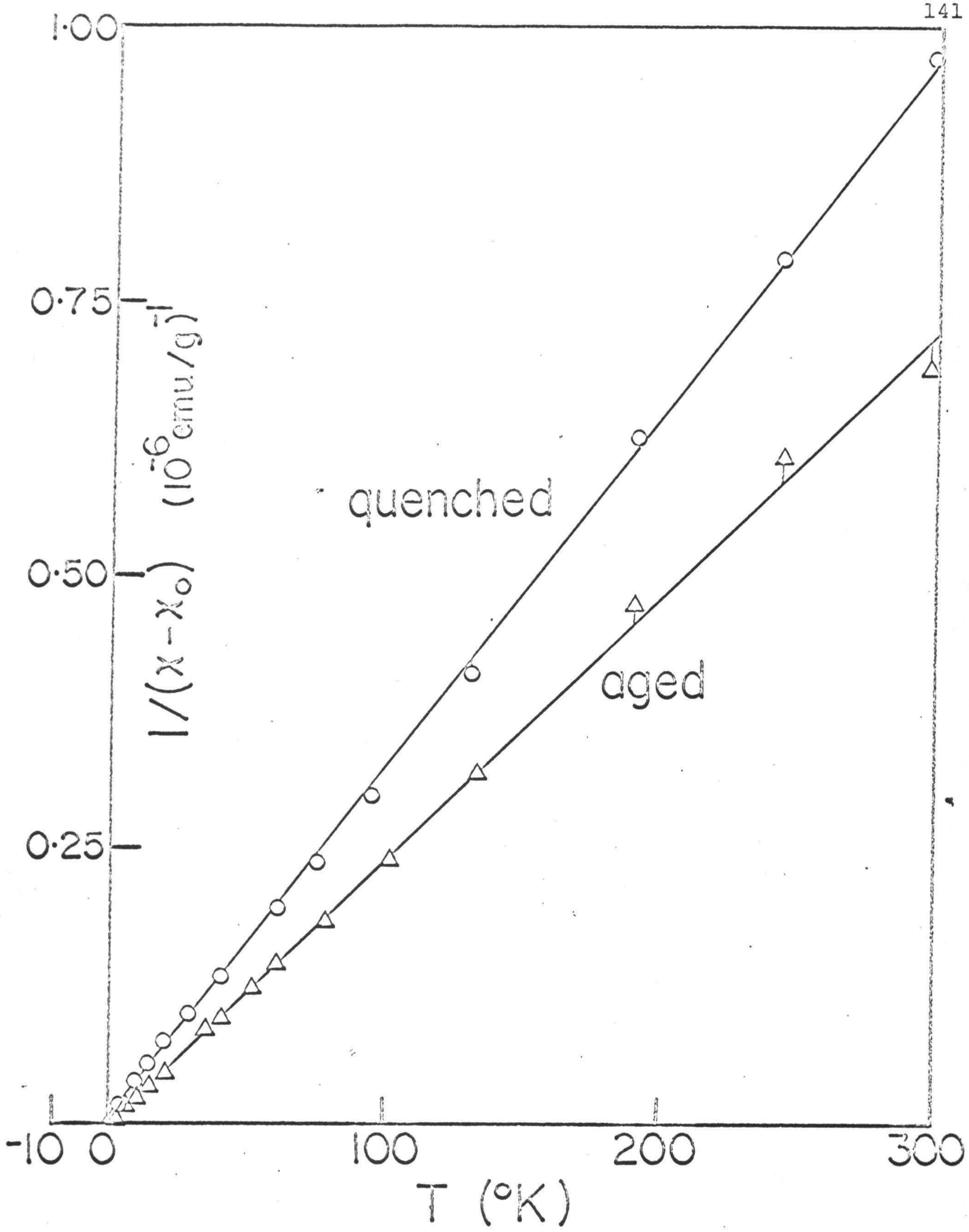
1·00
0·75
0·50
0·25
$1/(\chi - \chi_o)$ $(10^{-6}$ emu/g$)^{-1}$
quenched
aged
-10
0
100
200
300
T (°K)

Figure 23. σ^2 vs. $\frac{H_i}{\sigma}$ graphs for $Cu_{0.99}Fe_{0.01}$. The remanence temperature T_r is estimated to be 2.8 ± 1.4°K.

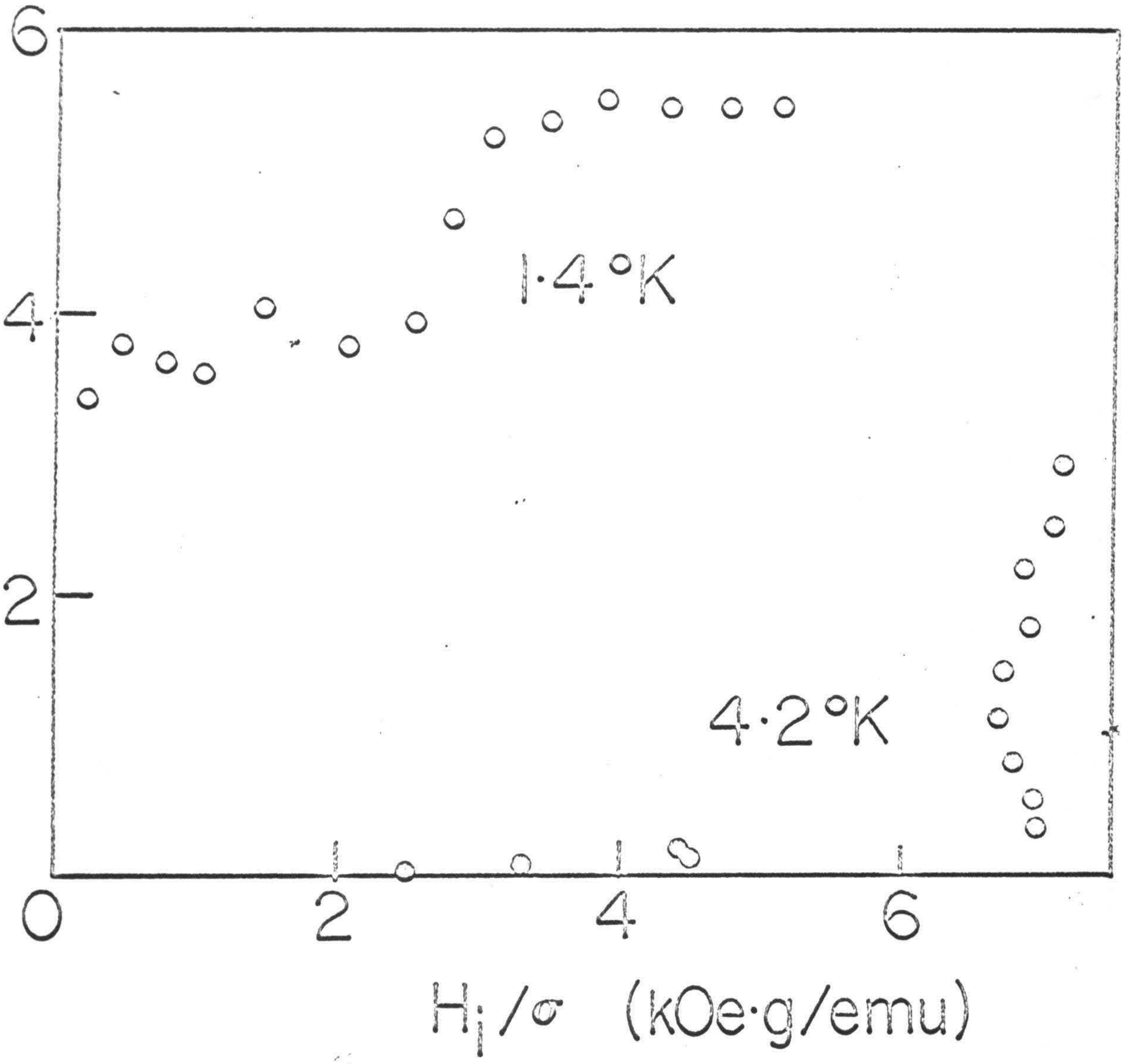
6
4
2
0
2
4
6
σ^2 (10^{-3} emu^2/g^2)
H_i/σ (kOe·g/emu)
1.4°K
4.2°K

Figure 24. σ^2 vs. $\frac{H_i}{\sigma}$ graphs for quenched $(Cu_{0.9}Ni_{0.1})_{0.99}Fe_{0.01}$. The remanence temperature is estimated to be $3.1 \pm 1.1°K$.

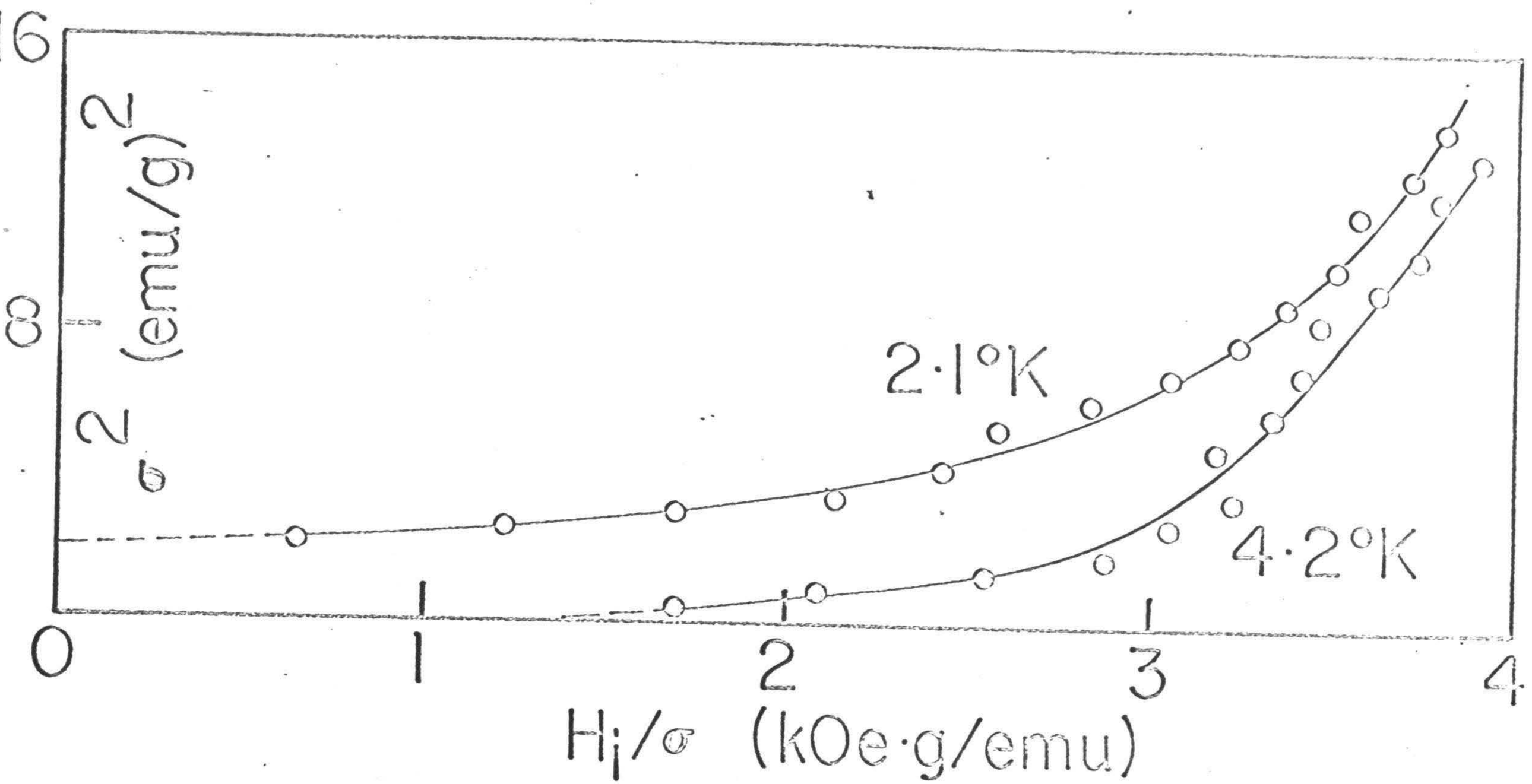
0·016
0·008
σ^2 (emu/g)^2
2·1°K
4·2°K
0
1
2
3
4
H_i/σ (kOe·g/emu)

Figure 25. σ^2 vs. $\frac{Hi}{\sigma}$ graphs for quenched $(Cu_{0.8}Ni_{0.2})_{0.99}Fe_{0.01}$. No remanence is observed, in fields as low as 26 Oe, even at 1.57°K.

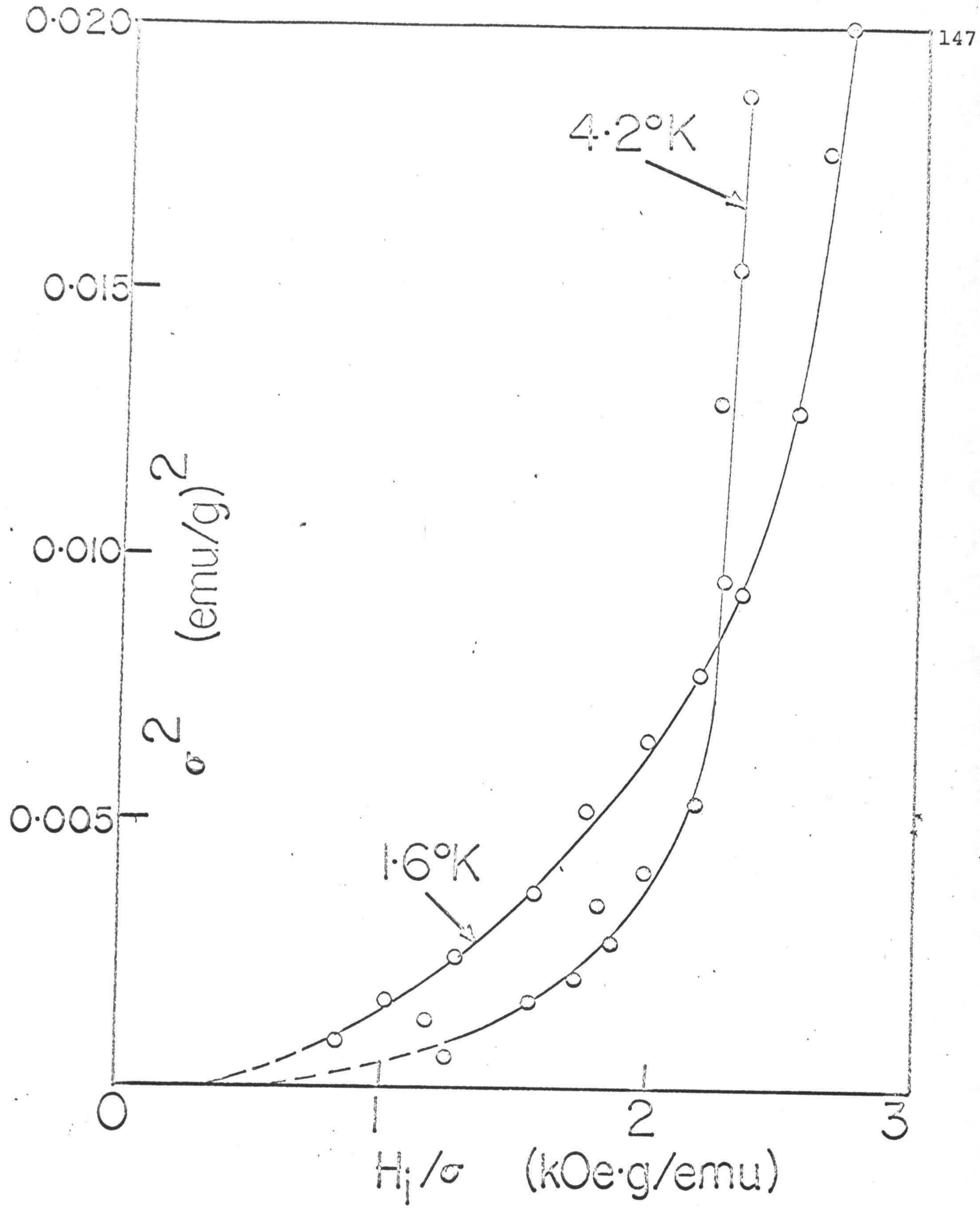
0·020
0·015
0·010
0·005
σ^2 (emu/g)^2
147
4·2°K
1·6°K
0
1
2
3
H_i/σ (kOe·g/emu)

For all three alloys, the σ vs. H graphs show curvature at low temperatures (T < 30°K; Figs. 26, 27, 28) indicating the presence of magnetic clusters.

A maximum in the magnetization of the $Cu_{0.99}Fe_{0.01}$ alloy (Fig. 29) is found around 4.3°K when measured in an applied field of 1000 Oe. At lower temperatures the magnetization values measured after cooling in a magnetic field are characteristically higher than those obtained after the specimen was cooled in zero field. For the $(Cu_{0.9}Ni_{0.1})_{0.99}Fe_{0.01}$ alloy, the magnetization data between 4.2 and 1.45°K in an applied field of 700 Oe are also systematically higher (Fig. 30) when measured after cooling the specimen in the field than after cooling it in zero applied field. A flat maximum is found in the magnetization for the $(Cu_{0.8}Ni_{0.2})_{0.99}Fe_{0.01}$ alloy around 3°K (Fig. 31) in an applied field of 1000 Oe. However, the measurements do not show any difference, within the experimental accuracy, between the magnetization values obtained after cooling the specimen in a magnetic field and those obtained after cooling in zero field.

3. Cu-Fe (∿100 to ∿500 ppm).

The magnetization data for a Cu-Fe alloy with 108 ppm Fe, in the temperature range of 1.3° to 32.5°K and in fields up to H = 70 kOe, were supplied to us by Dr. R. Tournier[6] in graphical form. Thirty points were taken from the graphs, at various temperatures and fields, to construct five isotherms. These data

Figure 26. σ vs. H for quenched $Cu_{0.99}Fe_{0.01}$ at temperatures indicated. The data, at a given temperature, were obtained by cooling the specimen in an applied field of 12.6 kOe and then going down in field. See Table 14(a).

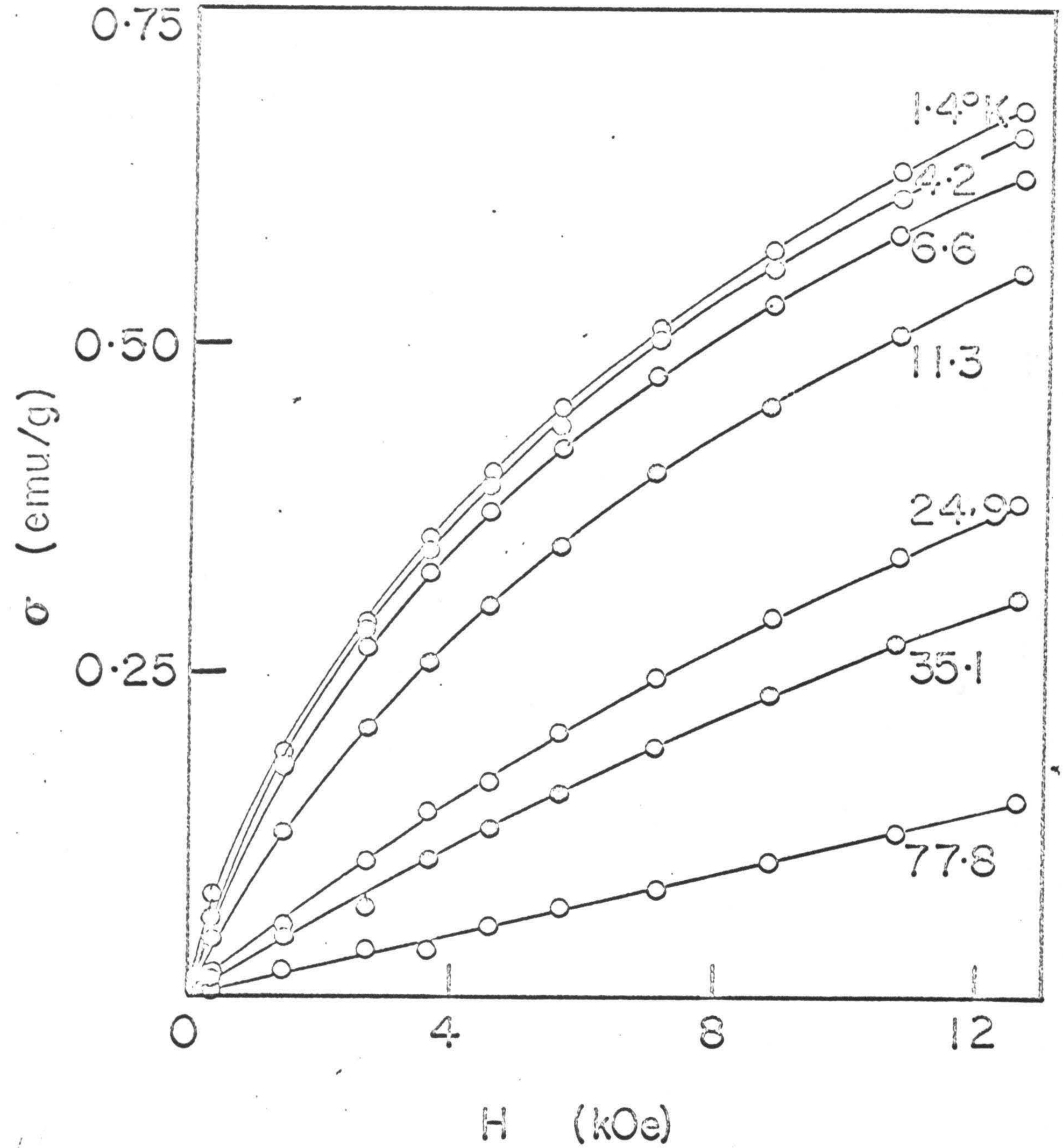
0·75
0·50
0·25
σ (emu/g)
1·4°K
4·2
6·6
11·3
24·9
35·1
77·8
0
4
8
12
H (kOe)

Figure 27. σ vs. H for quenched $(Cu_{0.9}Ni_{0.1})_{0.99}Fe_{0.01}$ at temperatures indicated. The data, at a given temperature, were obtained by cooling the specimen in an applied field of 12.6 kOe and then going down in field. See Table 15(a).

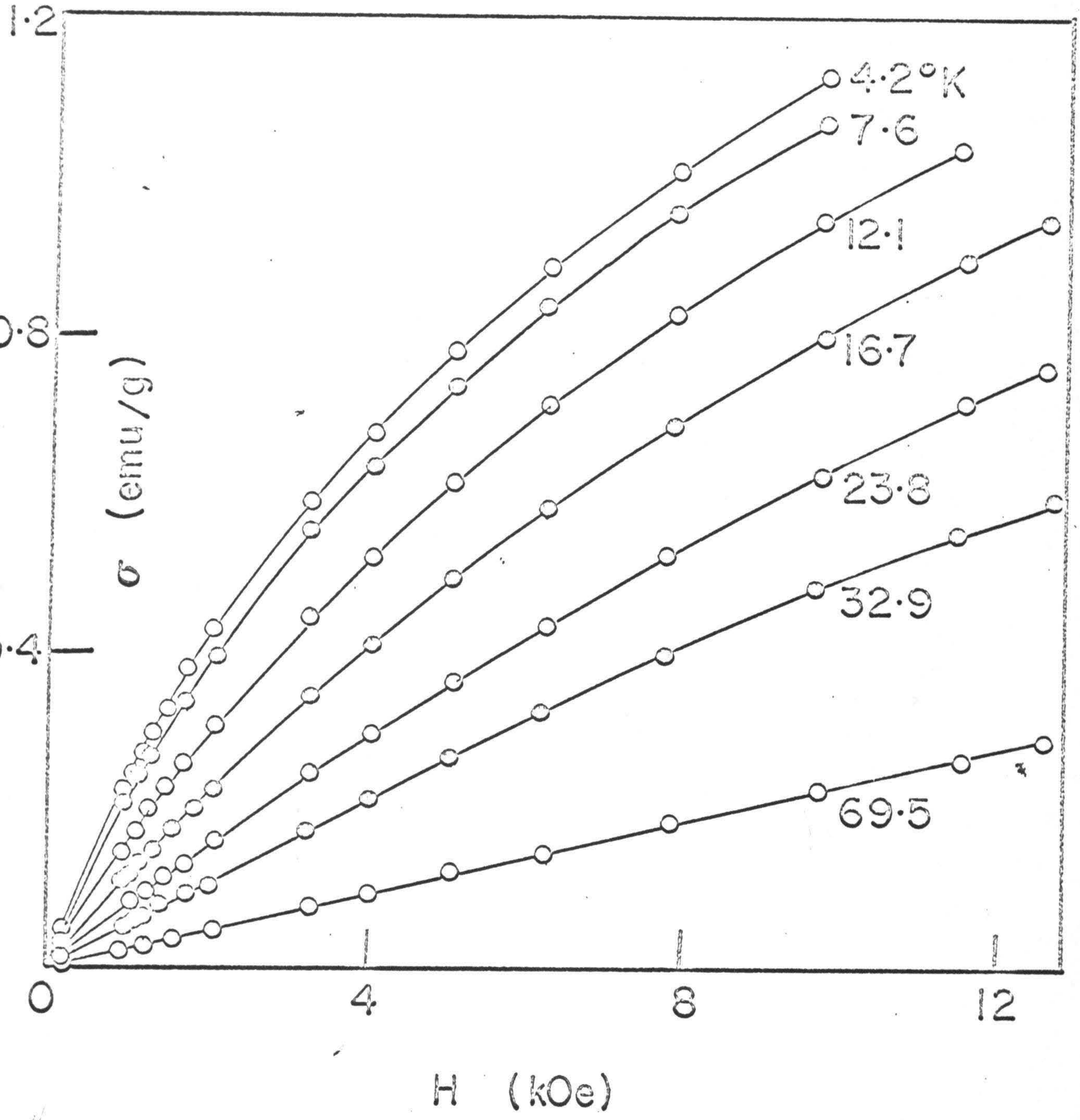
1·2
0·8
0·4
σ (emu/g)
4·2°K
7·6
12·1
16·7
23·8
32·9
69·5
0
4
8
12
H (kOe)

Figure 28. σ vs. H for quenched $(Cu_{0.8}Ni_{0.2})_{0.99}Fe_{0.01}$ at temperatures indicated. The data, at a given temperature, were obtained by cooling the specimen in an applied field of 12.6 kOe and then going down in field. See Table 16(a).

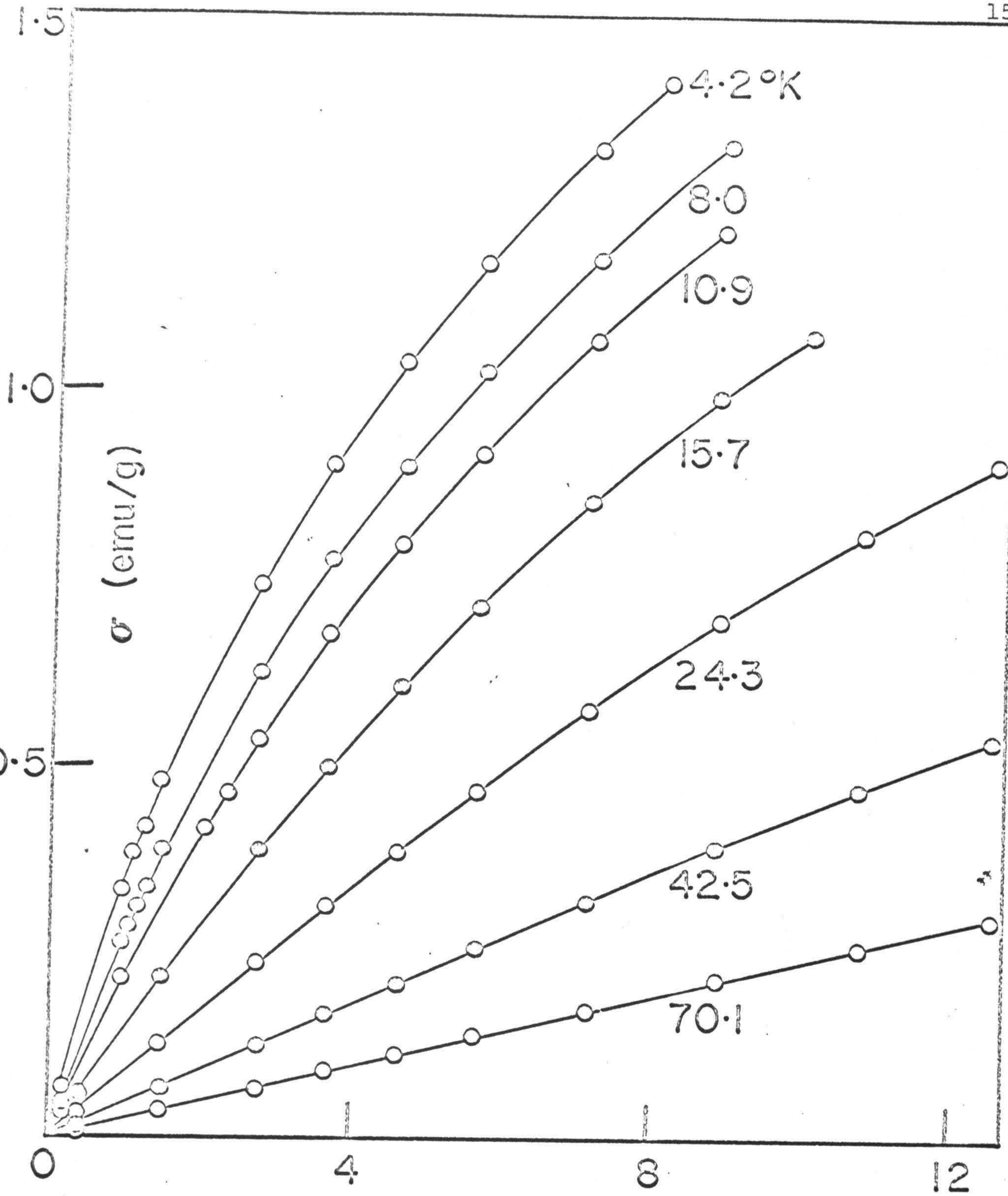
1·5
1·0
0·5
σ (emu/g)
4·2°K
8·0
10·9
15·7
24·3
42·5
70·1
0
4
8
12
H (kOe)

Figure 29. σ vs. T at H = 1000 Oe for quenched $Cu_{0.99}Fe_{0.01}$. Measured after cooling in 1000 Oe field: empty circle; measured after cooling to 1.3°K in zero field: filled circle. See Tables 14(b) and 14(c).

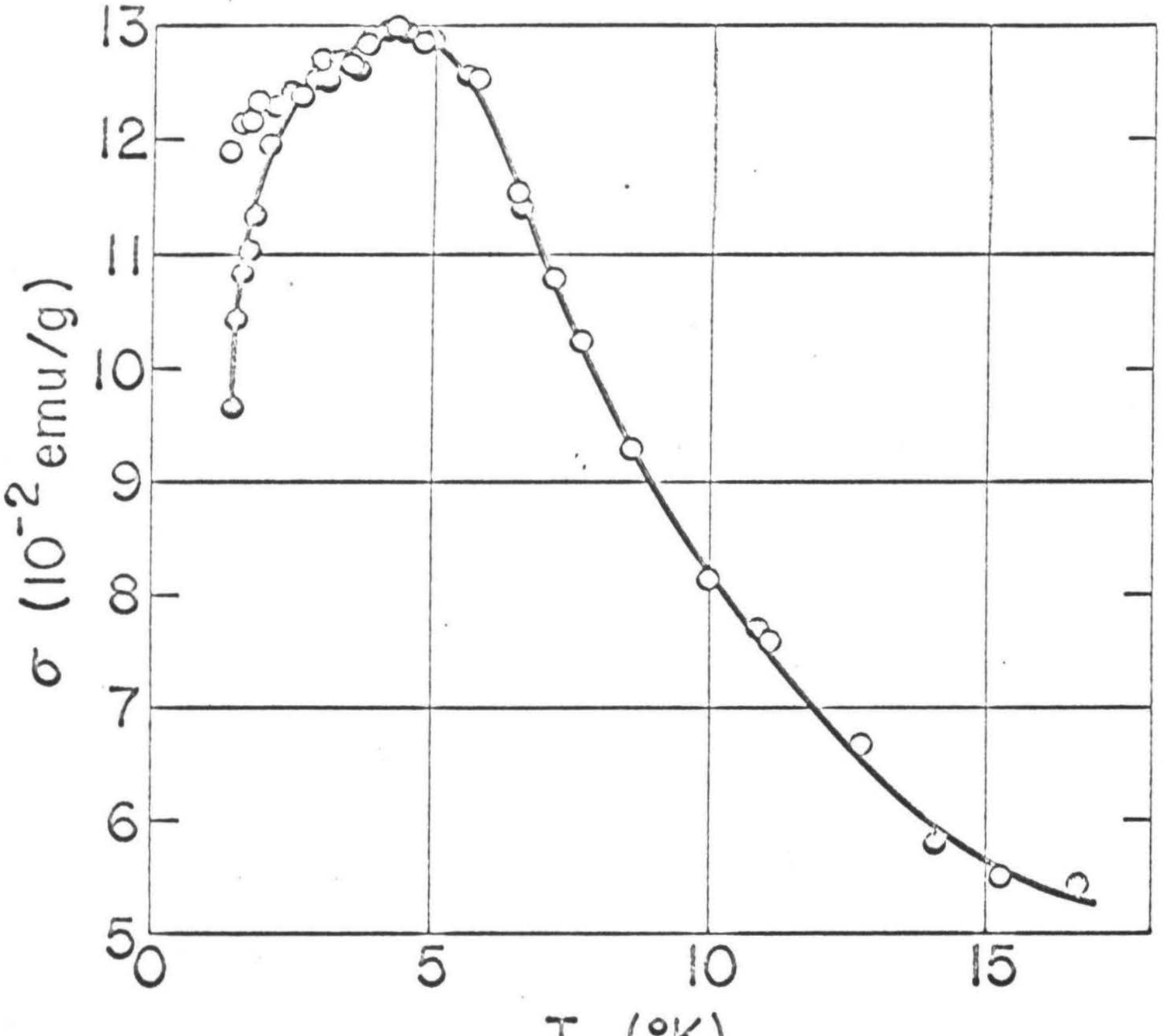
σ (10⁻² emu/g)
13
12
11
10
9
8
7
6
5
0
5
10
15
T (°K)

Figure 30. σ vs. T at H = 700 Oe for quenched $(Cu_{0.9}Ni_{0.1})_{0.99}Fe_{0.01}$. Measured after cooling in 700 Oe field: empty circle; measured after cooling to 1.3°K in zero field: filled circle. See Tables 15(b) and 15(c).

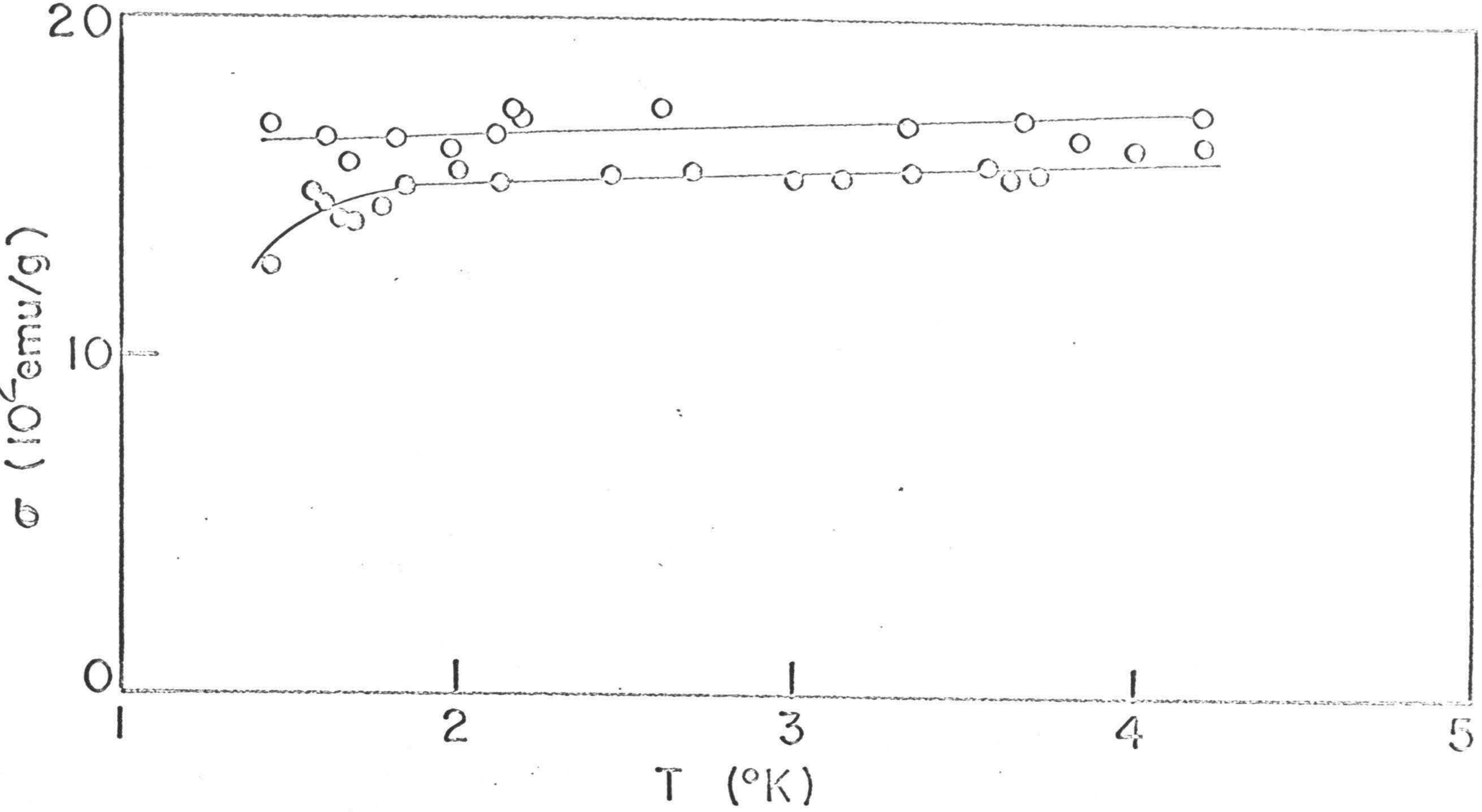
20
10
0
σ (10⁻² emu/g)
1
2
3
4
5
T (°K)

Figure 31. σ vs. T at H = 1000 Oe for quenched $(Cu_{0.8}Ni_{0.2})_{0.99}Fe_{0.01}$. Measured after cooling in 1000 Oe field: empty circle; measured after cooling to 1.3°K in zero field: filled circle. See Tables 16(b) and 16(c).

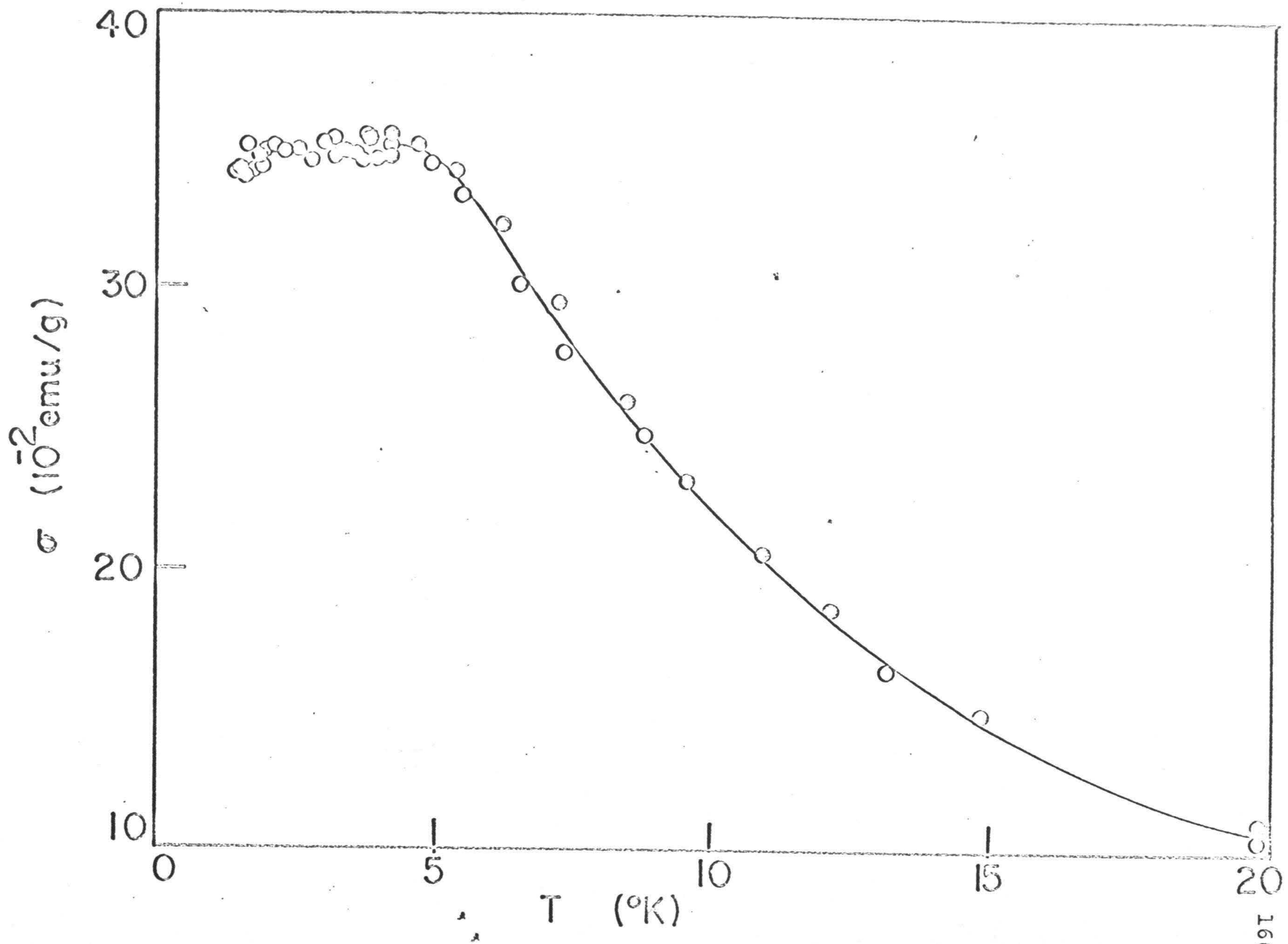
40
30
20
10
σ (10⁻² emu/g)
0
5
10
15
20
T (°K)

a reanalysis of the data was carried out by fitting with an equation containing four Brillouin terms:

$$\sigma = \chi_o H + \frac{N_o}{M} c_1 \mu_1 \mu_B B(\mu_1, \frac{H}{T-\theta_1}) + \frac{N_o}{M} c_2 \mu_2 \mu_B B(\mu_2, \frac{H}{T-\theta_2})$$

$$+ \frac{N_o}{M} c_3 \mu_3 \mu_B B(\mu_3, \frac{H}{T-\theta_3}) + \frac{N_o}{M} c_4 \mu_4 \mu_B B(\mu_4, \frac{H}{T-\theta_4}) \quad (14)$$

and by assuming that μ_1, c_1 and θ_1 have the same values as obtained from the above three-moment analysis, but not placing any restrictions on the other parameters. A slightly better rmsd was obtained with this analysis. The resulting parameter values are listed in Table 36. The values of μ_1, μ_2, μ_3 and μ_4 are now found to be fairly close to the ratio 1 : 2 : 3 : 4. The total concentration of Fe atoms $Z = c_1 + 2c_2 + 3c_3 + 4c_4$ is ~78 ppm. The magnetization values interpolated from experimental data, and the calculated magnetization values are compared in Fig. 32.

Magnetization data for Cu-Fe alloys containing 102 to 478 ppm Fe, at temperatures between 0.01°K and 0.4°K and in fields of 0.97 Oe to 217 Oe, were supplied to us by Dr. E. C. Hirschkoff and Prof. J. C. Wheatley.[9] The magnetization values in their tables were expressed in Gauss but they were converted for the sake of convenience to emu/g units using the relation σ (emu/g) = M(Gauss)ρ (g/cc). ρ is the density of the alloy, and was assumed to be that of copper, i.e., 8.95 g/cc. It was decided to analyze the data for a Cu-Fe alloy containing 112 ppm

Table 36. Parameters from least squares fitting of Eq. 14 to magnetization data for Cu-Fe alloy, Tholence and Tournier[6] and Hirschkoff et al.[9]

Alloy	108 ppm Fe in Cu [6]	112 ppm Fe in Cu [9]
Temp. range (°K)	1.3 to 32.5	0.01 to 0.4
Moments (μ_B)	$\mu_1 = 2.44$, $\mu_2 = 4.86$, $\mu_3 = 7.22$, $\mu_4 = 10.17$	$\mu_1 = 7.0$, $\mu_2 = 9.8$, $\mu_3 = 29.5$
Concentrations (ppm)	$c_1 = 56.7$, $c_2 = 5.29$, $c_3 = 1.49$, $c_4 = 1.56$	$c_1 = 0.55$, $c_2 = 0.022$, $c_3 = 0.003$
Characteristic Temp. (°K)	$\theta_1 = -21.5$, $\theta_2 = -17.9$, $\theta_3 = -17.9$, $\theta_4 = -8.9$	$\theta_1 = -0.039$, $\theta_2 = +0.008$, $\theta_3 = 0$
χ_o (emu/g)	0.48×10^{-8}	8.7×10^{-8}
rmsd (emu/g)	0.044×10^{-3}	0.028×10^{-4}
rmsd (%)*	0.78	1.03

*The rmsd as expressed in percents of the highest magnetization value used in the fitting.

Note: The accuracy with which μ_1, μ_2, μ_3 and μ_4 have been determined is estimated to be roughly ±5%, ±10%, ±20%, and ±20% respectively. Similar uncertainties are involved in the values of c_1, c_2, c_3, c_4 and θ_1, θ_2, θ_3, θ_4; the value of χ_o is within ±5%.

Figure 32. σ vs. H isotherms for 108 ppm Fe in Cu · Points O, interpolated from experimental data by Tholence and Tournier[6] (Table 17); curves calculated from Eq. 14 with parameter values from Table 36. Dashed curve was calculated for 1.3°K according to Ref. 6.

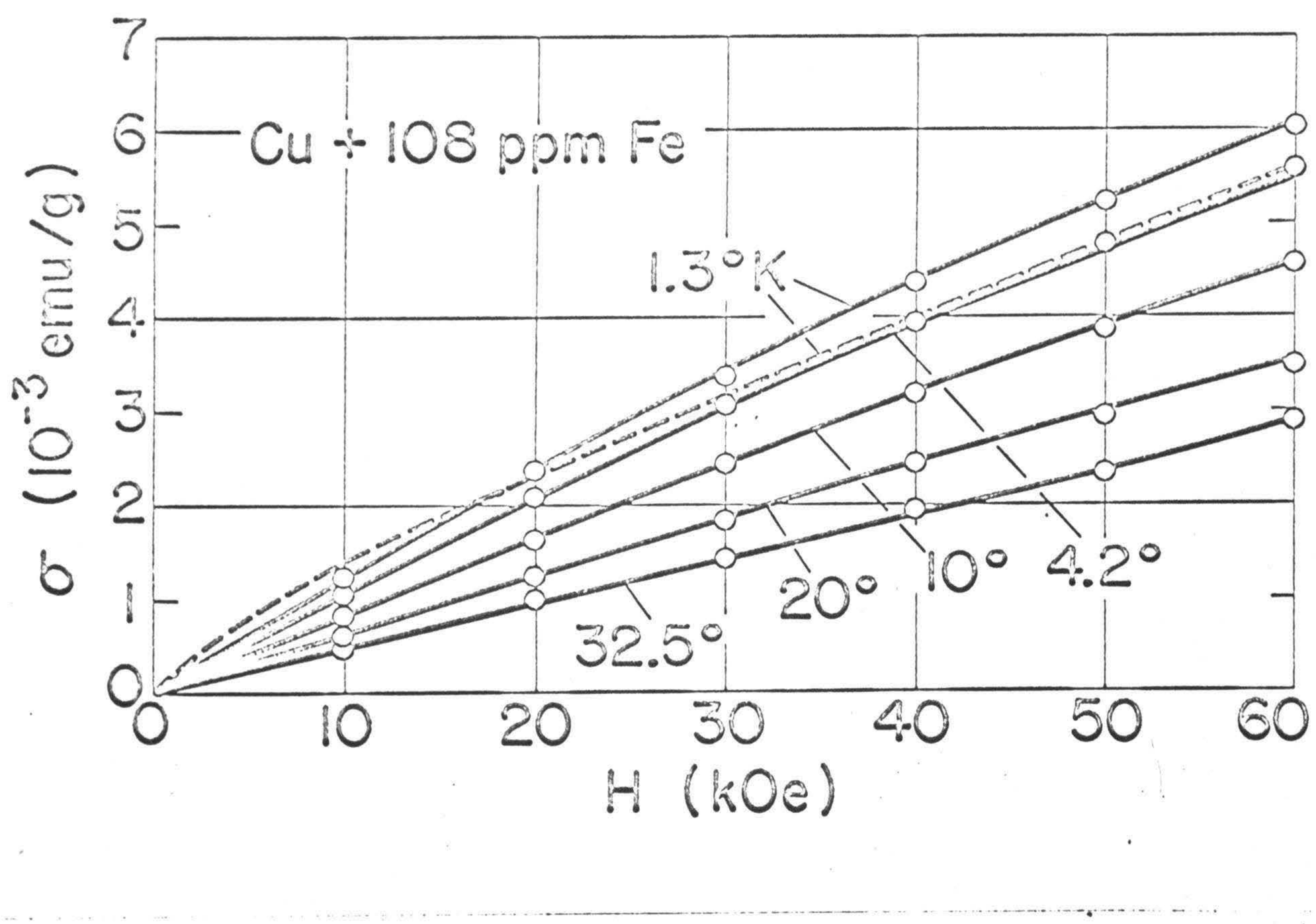
Cu + 108 ppm Fe
1.3°K
4.2°
10°
20°
32.5°
σ (10⁻³ emu/g)
H (kOe)
0
1
2
3
4
5
6
7
10
20
30
40
50
60

Fe; the selection was based on the relative completeness of the data for this alloy as a function of temperature and field and the similarity in composition to the Cu-Fe alloy of Tholence and Tournier[6] containing 108 ppm Fe which was analyzed in a similar fashion. For the purpose of the fitting thirty-six points (Fig. 33) were obtained by interpolation, at various temperatures and fields to construct six isotherms between 0.012° to 0.2°K. A sufficiently good fit was obtained by least squares fitting of Eq. 13; the parameter values obtained are listed in Table 36. Figure 33 shows the isotherms calculated from these parameter values and the magnetization data used. In Fig. 34 one finds that for H = 10 Oe the σ vs. T curves calculated from the same parameter values for temperatures from ∿0.01 to ∿0.4°K represent the actual data points reasonably well. This is also found to be true at all other field values between 0.977 Oe and 217.11 Oe. The fit is very satisfactory in the entire range of fields and temperatures.

At the lowest temperatures the data of Hirschkoff et al.[9] for a Cu-Fe alloy with 478 ppm Fe (Table 19) show appreciable deviations from the Curie-Weiss type behavior. This is shown in Fig. 35, where the dashed line gives the extrapolation below 0.08°K from the data points above that temperature by means of least squares fitting of:

$$\sigma = \chi_o H + \frac{N_o\, cp^2\, \mu_B^2}{3Mk(T-\theta)} H \qquad (15)$$

Figure 33. σ vs. H isotherms for 112 ppm Fe in Cu for temperatures indicated. Points O, interpolated from experimental data by Hirschkoff et al.[9] (Table 18); curves calculated from Eq. 14 with parameter values from Table 36.

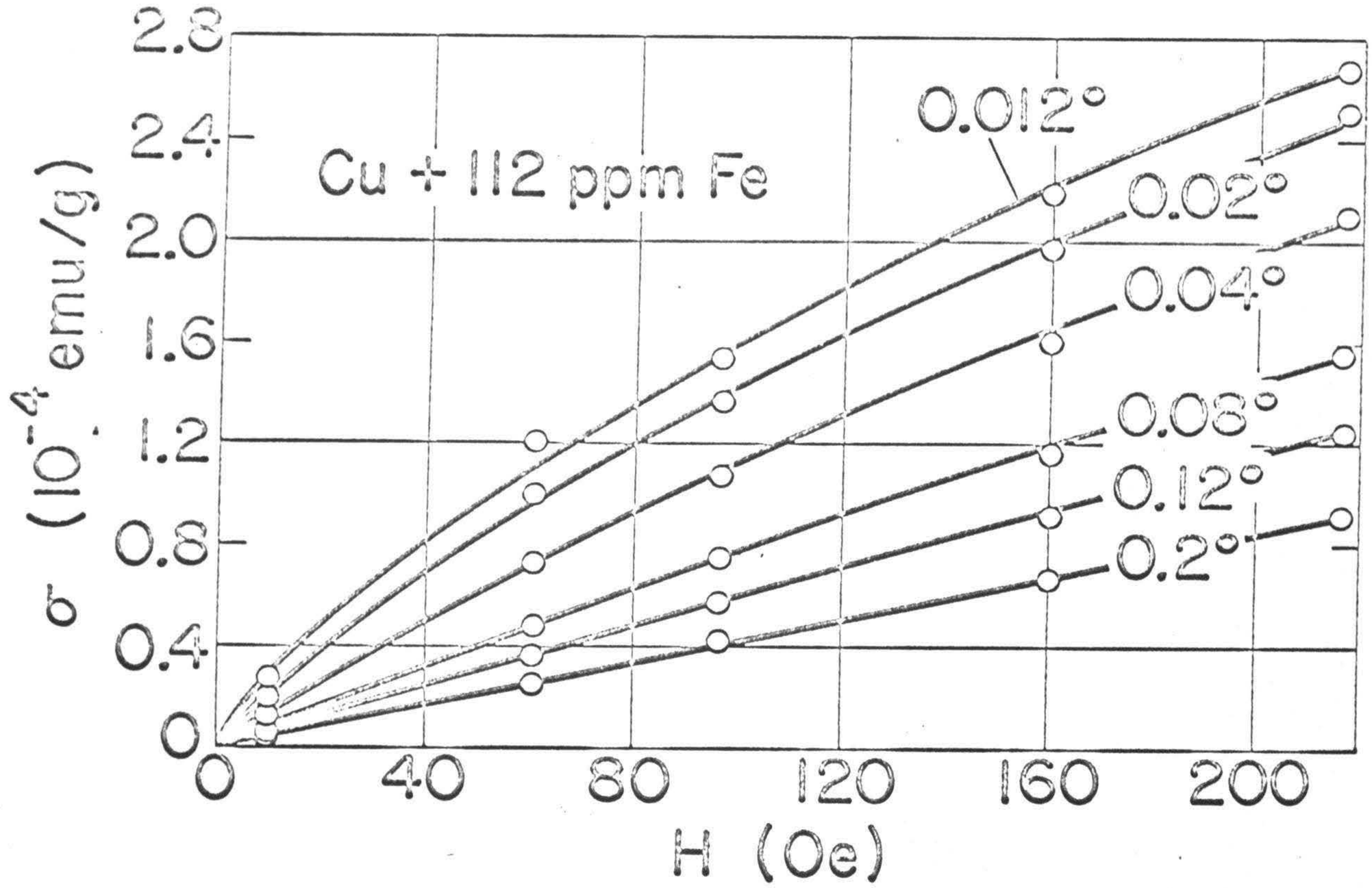
Cu + 112 ppm Fe
0.012°
0.02°
0.04°
0.08°
0.12°
0.2°
σ (10⁻⁴ emu/g)
H (Oe)
0
0.4
0.8
1.2
1.6
2.0
2.4
2.8
40
80
120
160
200

Figure 34. σ vs. T at H = 10 Oe for 112 ppm Fe in Cu. Experimental data by Hirschkoff et al.[9] (Table 18): O; solid curve was calculated with parameter values from Table 36, using Eq. 14.

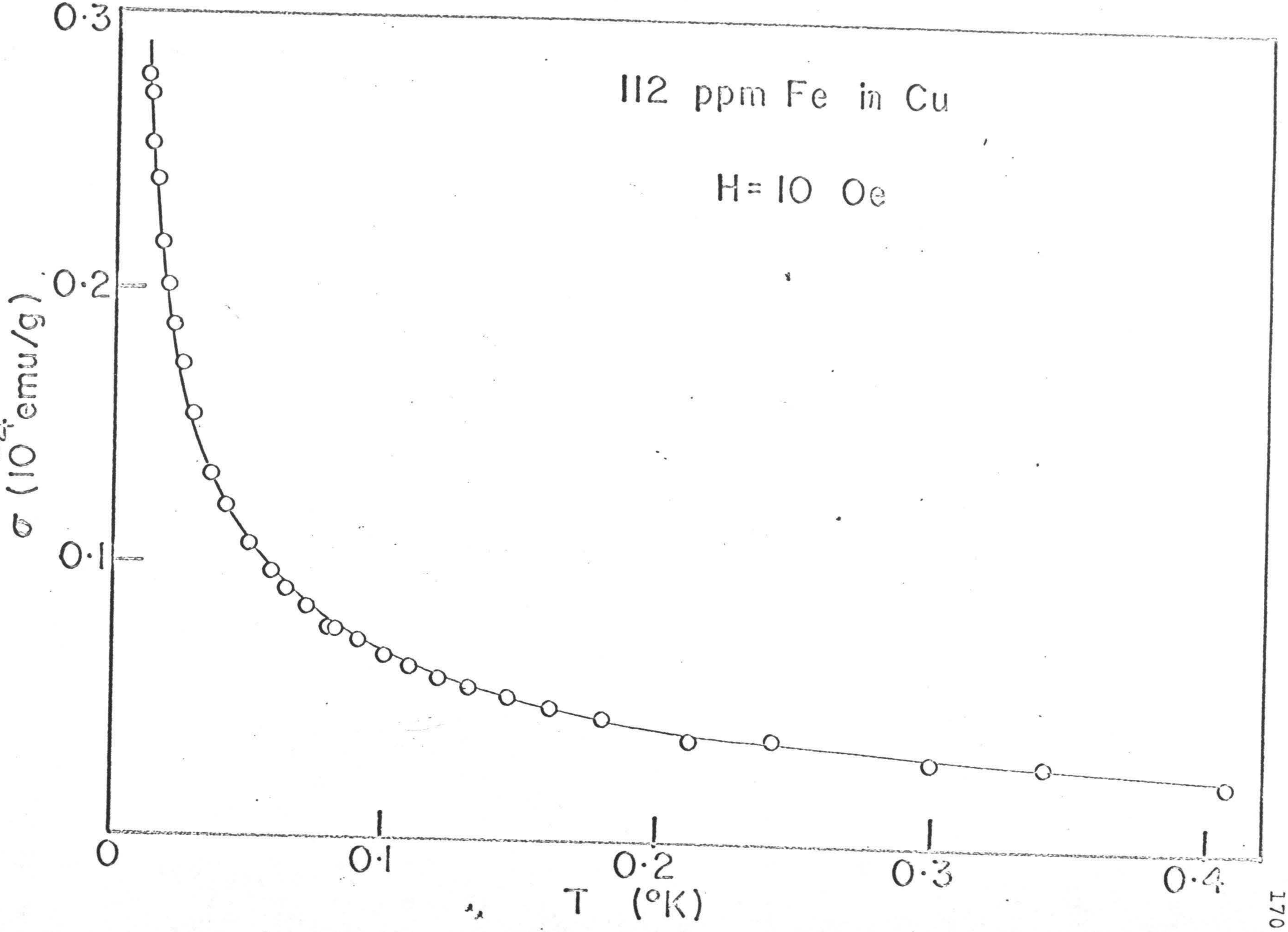
112 ppm Fe in Cu
H = 10 Oe
σ (10⁻⁴ emu/g)
0·3
0·2
0·1
0
0·1
0·2
0·3
0·4
T (°K)

Figure 35. σ vs. T at H = 10 Oe for 478 ppm Fe alloy. Experimental data: O, by Hirschkoff et al.[9] (Table 19); solid curve and dashed line by least squares fitting of Eq. 15 to data at T > 0.08°K.

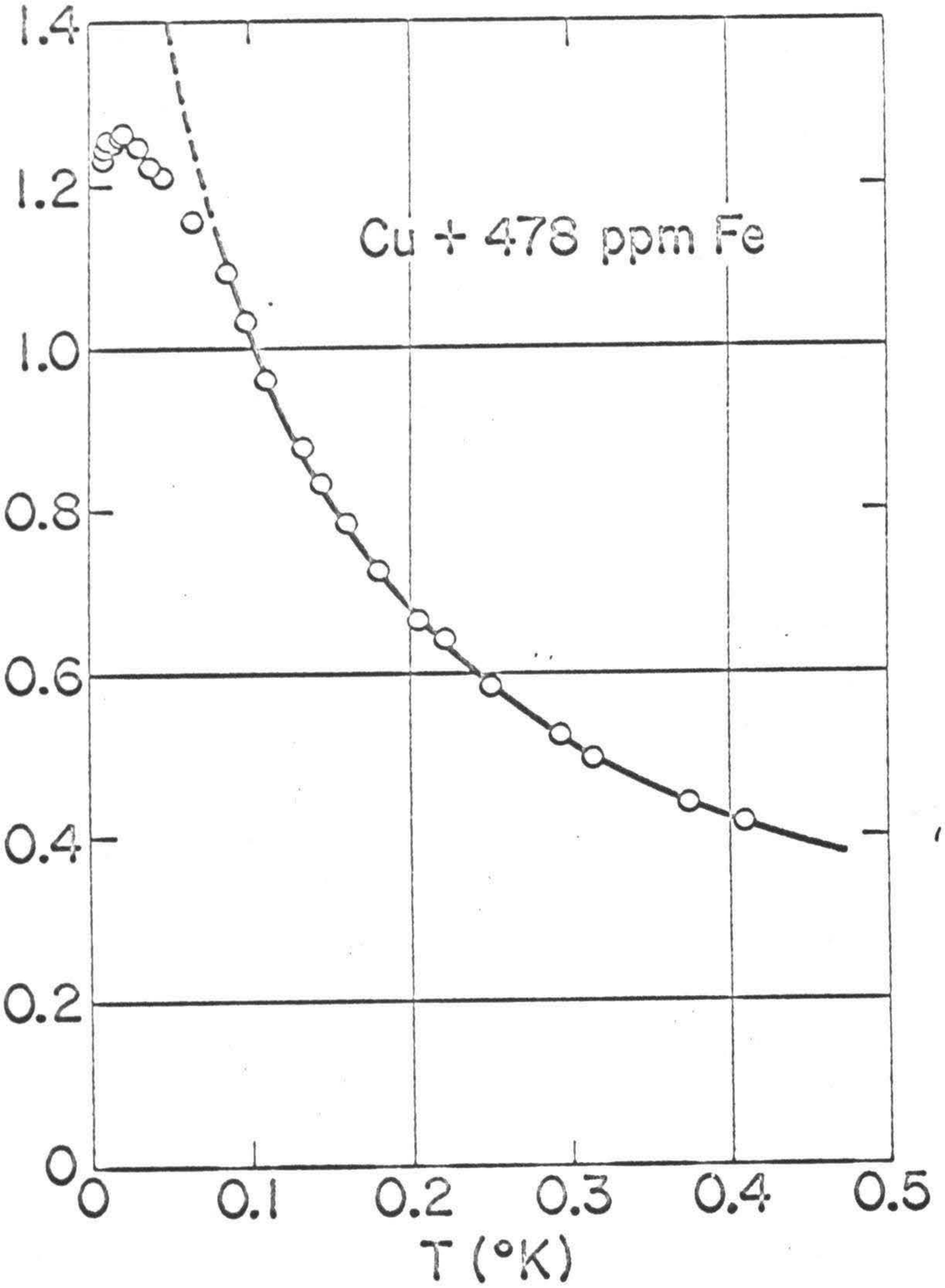
Cu + 478 ppm Fe
σ (10⁻⁴ emu/g)
T (°K)
0
0.2
0.4
0.6
0.8
1.0
1.2
1.4
0.1
0.2
0.3
0.4
0.5

with the parameter values: $\chi_o = 6.6 \times 10^{-9}$ emu/g, $cp^2 = 0.88$ μ_B^2 per alloy atom, and $\theta = -0.08°K$ (rmsd = 0.52×10^{-6} emu/g). The low temperature data themselves show a maximum in the magnetization at approximately 0.02°K.

4. Cu-Ni-Fe (∿1000 ppm Fe; 10, 20, 30 at. % Ni).

The magnetization data for quenched Cu-Ni-Fe alloys containing ∿100 to ∿1000 ppm Fe are listed in Tables 20 through 27. The magnetization data for the deformed alloys are listed in Tables 28 through 33.

a. Quenched alloys.

The data for each alloy were analyzed by least squares fitting of Eq. 13. To simplify the fitting procedure the following assumptions were made for the quenched alloys:

(1) The total concentration of Fe atoms in all clusters is equal to the nominal concentration (z) of Fe in the alloy, i.e.,

$$c_1 + 2c_2 + 3c_3 = z \tag{16}$$

Although samples from some of the Cu-Ni-Fe alloys were analyzed (Table 4) for Fe content, the reliability of these analyses is not known. It would have been desirable to make z a variable parameter in the least squares fitting of Eq. 13 and to assume that the actual Fe concentration of the alloy is that value of z for which the best rmsd value and the least systematic

deviation is obtained. However, such a process would have been very laborious and time consuming.

(2) Since all these alloys were quenched from high temperature, i.e., from 1050°C, it is assumed that they are in a state of thermal equilibrium at some temperature.

The thermal equilibrium may not necessarily correspond to that at 1050°C. In fact Mozer et al.[23] have pointed out that practically no cooling rate can quench the local atomic arrangements in a Cu-Ni alloy at ∿1000°C and that, on the other hand, any reasonable cooling rate (such as the one used here, i.e., approximately 100°C/sec.) will prevent changes below 500°C. Therefore the thermal equilibrium may be expected to represent some temperature between ∿500°C and 1050°C. That in fact the thermal equilibrium at some elevated temperature is quite well retained on quenching to room temperature is indicated by the observation that the magnetization data for the quenched specimen of the $Cu_{0.8}Ni_{0.2}$ alloy with 1000 ppm Fe were reproducible after quenching a second time from the same temperature.

In an alloy which has retained a state of thermal equilibrium, the concentrations of atomic clusters (in the present case c_1 and c_2, the concentrations of clusters with one, and with two Fe atoms, respectively) can be estimated from a single parameter $_{Fe\text{-}Fe}\alpha_1$ defined by the following relation:

$$z_1 = (1 - z)_{Fe\text{-}Fe}\alpha_1 + z \qquad (17)$$

where z_1 is the average concentration of Fe in the nearest neighbor shells of all Fe atoms. When the thermal equilibrium corresponds to a situation where the Fe atoms are distributed randomly in the alloy, the value of $_{Fe\text{-}Fe}\alpha_1$, often referred to as the short-range-order parameter, is zero. A positive value of $_{Fe\text{-}Fe}\alpha_1$ expresses a clustering tendency of the Fe atoms.

For a given value of z, the ratio of the concentrations of isolated Fe atoms and of Fe pairs may be calculated in the following manner. The probabilities p_0 and p_1 for an Fe atom A to have zero (n = 0), or one (n = 1), Fe nearest neighbor are calculated from

$$p_n = \frac{12!}{(12-n)!\ n!} \cdot z_1^{\,n} (1 - z_1)^{12-n} \tag{18}$$

with n = 0 or n = 1, respectively. The concentration of isolated Fe atoms is,

$$c_1 = zp_0 = z(1 - z_1)^{12} \tag{19}$$

The probability that an Fe atom (say A) has one, and only one, Fe atom (say B) in its nearest neighbor shell is,

$$p_1 = 12z_1(1 - z_1)^{11} \tag{20}$$

The Fe atom B, in its turn, has twelve nearest neighbor sites; the Fe atom A is occupying one of these sites, and of the remaining eleven, four are nearest neighbor sites of the Fe atom A as well. In calculating p_1, it has already been insured that there is no Fe atom at any of these four common sites. Now, if

there is an Fe atom, at any of the seven other nearest neighbor sites of the atom B, then a triplet or larger cluster configuration would result; if there is no Fe atom at any of these seven sites then an isolated Fe-Fe doublet, i.e., Fe-pair is formed. Therefore the probability of a given Fe atom being part of an isolated doublet. i.e., the fraction of Fe atoms in doublets, is

$$p_{Fe\text{-}Fe} = 12z_1(1-z_1)^{11}\ (1-z_1)^{7} = 12z_1\ (1-z_1)^{18} \qquad (21)$$

The concentrations of such Fe pairs is

$$c_2 = 1/2\ z_1\ p_{Fe\text{-}Fe} = 6zz_1\ (1-z_1)^{18} \qquad (22)$$

The fraction of Fe atoms in Fe triplets and in clusters involving larger number of Fe atoms is then equal to $(z - c_1 - 2c_2)$. Since the quantity $(z - c_1 - 2c_2)$ was found to be very small when compared to c_1 or $2c_2$, even for an alloy containing 1000 ppm Fe ($z = 1000 \times 10^{-6}$), it is reasonable to assume that it is very nearly equal to the fraction of Fe atoms in triplets, i.e., that the fraction of Fe atoms in clusters involving more than three Fe atoms, is negligible. Then the concentration of Fe-triplets is

$$c_3 = (z - c_1 - 2c_2)/3 \qquad (23)$$

Thus using Eqs. 19, 22, and 23 one can obtain, for a given value of $_{Fe\text{-}Fe}\alpha_1$ the values of c_1, c_2, and c_3.

The data for the following quenched alloys: 1000 ppm Fe in $Cu_{0.9}Ni_{0.1}$, 500 ppm Fe in $Cu_{0.9}Ni_{0.1}$, 1000 ppm Fe in $Cu_{0.8}Ni_{0.2}$

and 500 ppm Fe in $Cu_{0.8}Ni_{0.2}$ were analyzed by least squares fitting of Eq. 13 where c_1, c_2, and c_3 were varied simultaneously by varying a single parameter: $\alpha_{1\,Fe\text{-}Fe}$.

For the quenched $Cu_{0.9}Ni_{0.1}$ and $Cu_{0.8}Ni_{0.2}$ alloys containing 100 ppm Fe, the concentration c_3 was extremely small, so that $c_1 + c_2 \simeq z$ and fits of Eq. 11 with two Brillouin terms were found to be very satisfactory. Here again c_1 and c_2 were simultaneously varied by varying a single parameter $\alpha_{1\,Fe\text{-}Fe}$ and keeping the total Fe concentration constant.

The parameter values obtained for the quenched $Cu_{0.9}Ni_{0.1}$ and $Cu_{0.8}Ni_{0.2}$ alloys, each containing 100, or 500, or 1000 ppm Fe, are presented in Tables 37 and 38, and the fits are illustrated in Figures 36 through 43.

The method of analysis for the quenched $Cu_{0.7}Ni_{0.3}$ alloy with 100 ppm Fe was the same as above, but the magnetization of the binary alloy $Cu_{0.7}Ni_{0.3}$, to which the Fe was added, was first subtracted from the total measured magnetization of the ternary alloy.

$$\Delta\sigma_{Fe} = \sigma \text{ (for } Cu_{0.7}Ni_{0.3} + 100 \text{ ppm Fe)} - \sigma \text{ (for } Cu_{0.7}Ni_{0.3}) \quad (24)$$

This procedure was followed in view of the fact that in $Cu_{0.7}Ni_{0.3}$ itself there are present small Ni-rich magnetic clusters with an average cluster moment of $\mu \simeq 2.76\ \mu_B$. The term $\Delta\sigma_{Fe}$ represents the change in magnetization due to the

Table 37. Parameters from least squares fitting of Eq. 11 or Eq. 13 to magnetization data for quenched $Cu_{0.9}Ni_{0.1}$ alloys containing Fe.

Fe Content (ppm)	100	500	1000
Temp. range (°K)	1.34 to 300	1.51 to 300	2.02 to 300
μ_1 (μ_B)	2.70	2.98	2.96
μ_2 (μ_B)	5.41	5.51	5.76
μ_3 (μ_B)		8.17	10.10
c_1 (ppm)	92.5	375.9	694.1
c_2 (ppm)	3.7	45.9	104.0
c_3 (ppm)		10.7	32.6
θ_1 (°K)	- 0.83	- 2.15	- 4.05
θ_2 (°K)	+ 0.85	- 0.15	0
θ_3 (°K)		+ 0.55	0
χ_o (10^{-6} emu/g)	0.166	0.172	0.165
Fe-$Fe^{\alpha}1$	0.007	0.023	0.029
c_2/c_1	0.041	0.122	0.150
rmsd (10^{-3} emu/g)	0.145	0.237	0.558
rmsd (%)*	0.94	0.38	0.48

*The rmsd value as expressed in percents of the highest value of magnetization used in the fitting.

Table 38. Parameters from least squares fitting of Eq. 11 or Eq. 13 to magnetization data for quenched $Cu_{0.8}Ni_{0.2}$ alloys containing Fe.

Fe Content (ppm)	100	500	1000
Temp. range (°K)	2.84 to ∿300	2.66 to ∿300	1.5 to ∿300
μ_1 (μ_B)	3.76	3.52	3.89
μ_2 (μ_B)	8.35	8.53	6.46
μ_3 (μ_B)		15.25	14.85
c_1 (ppm)	95.9	414.6	711.4
c_2 (ppm)	2.0	35.1	100.7
c_3 (ppm)		5.1	29.0
θ_1 (°K)	- 0.26	- 0.08	- 2.05
θ_2 (°K)	+ 1.00	- 0.77	+ 0.46
θ_3 (°K)		- 2.70	- 0.18
χ_o (10^{-6} emu/g)	0.491	0.506	0.402
Fe-$Fe^{\alpha}1$	0.0035	0.015	0.027
c_2/c_1	0.021	0.085	0.141
rmsd (10^{-3} emu/g)	0.149	0.230	0.947
rmsd (%)*	0.67	0.25	0.48

*The rmsd value as expressed in percents of the highest value of the magnetization used in the fitting.

Figure 36. χ vs. T for quenched $Cu_{0.9}Ni_{0.1}$ alloys containing various amounts of Fe. The solid curves were calculated using parameter values listed in Table 37.

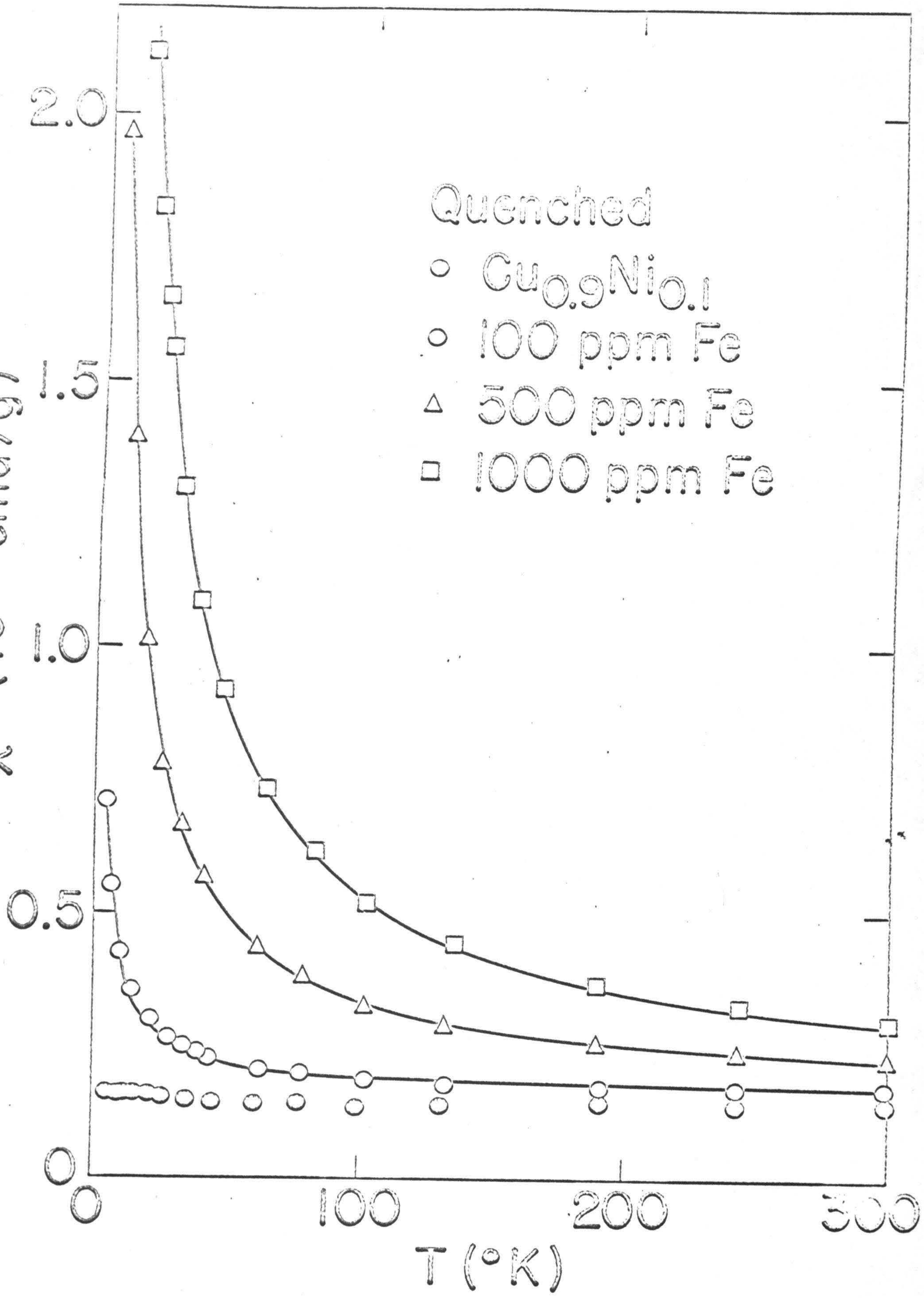
Quenched
○ $Cu_{0.9}Ni_{0.1}$
○ 100 ppm Fe
△ 500 ppm Fe
□ 1000 ppm Fe
χ (10^{-6} emu/g)
2.0
1.5
1.0
0.5
0
0
100
200
300
T (°K)

Figure 37. Magnetization vs. field for quenched $Cu_{0.9}Ni_{0.1}$ with 100 ppm Fe. The empty and filled circles represent measured data (Table 20). The solid curves were calculated using parameter values in Table 37.

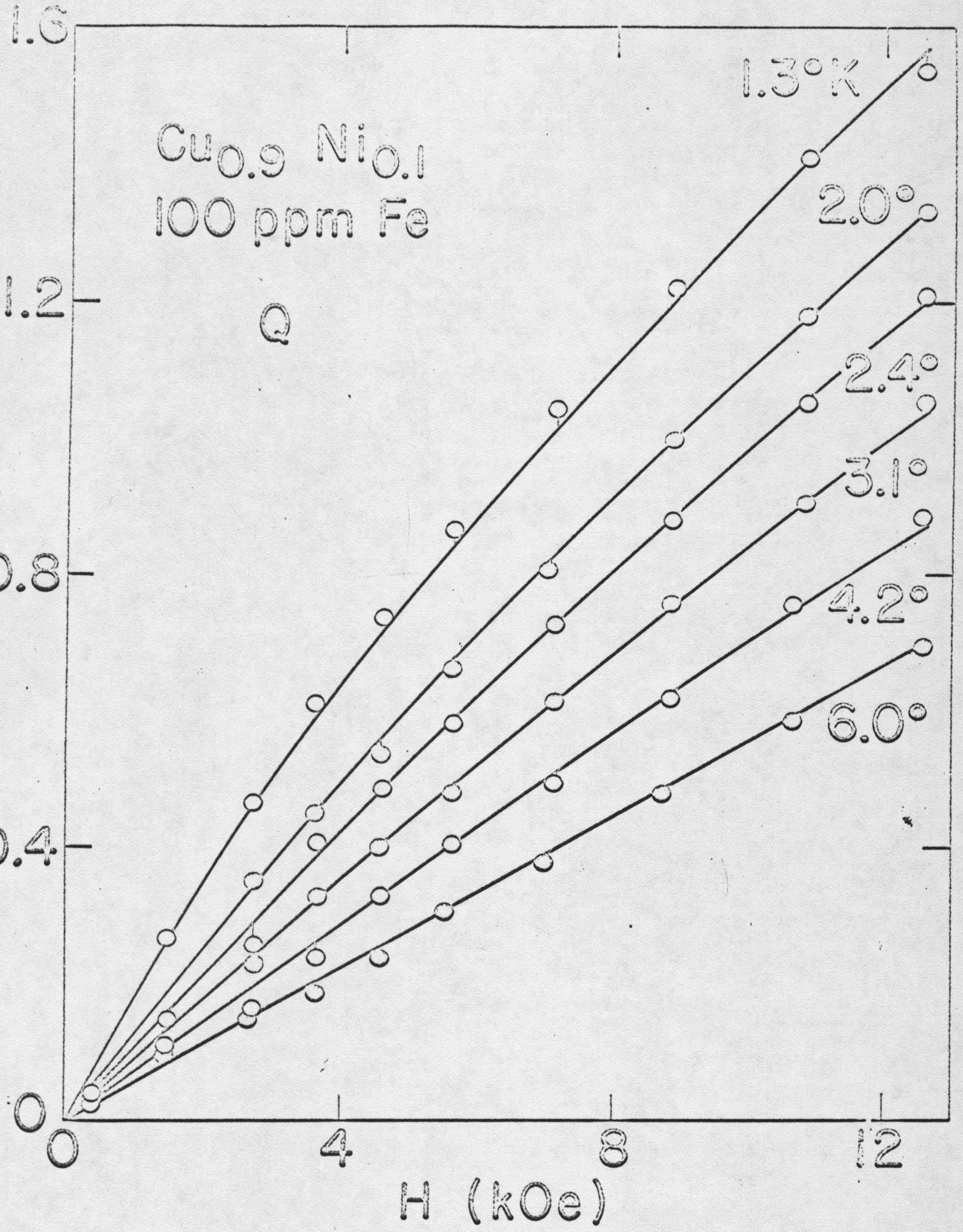
$Cu_{0.9}$ $Ni_{0.1}$
100 ppm Fe
Q
1.3°K
2.0°
2.4°
3.1°
4.2°
6.0°
σ (10⁻² emu/g)
1.6
1.2
0.8
0.4
0
0
4
8
12
H (kOe)

Figure 38. Magnetization vs. field for quenched $Cu_{0.9}Ni_{0.1}$ with 500 ppm Fe. The empty and filled circles represent measured data (Table 21). The solid curves were calculated using parameter values listed in Table 37.

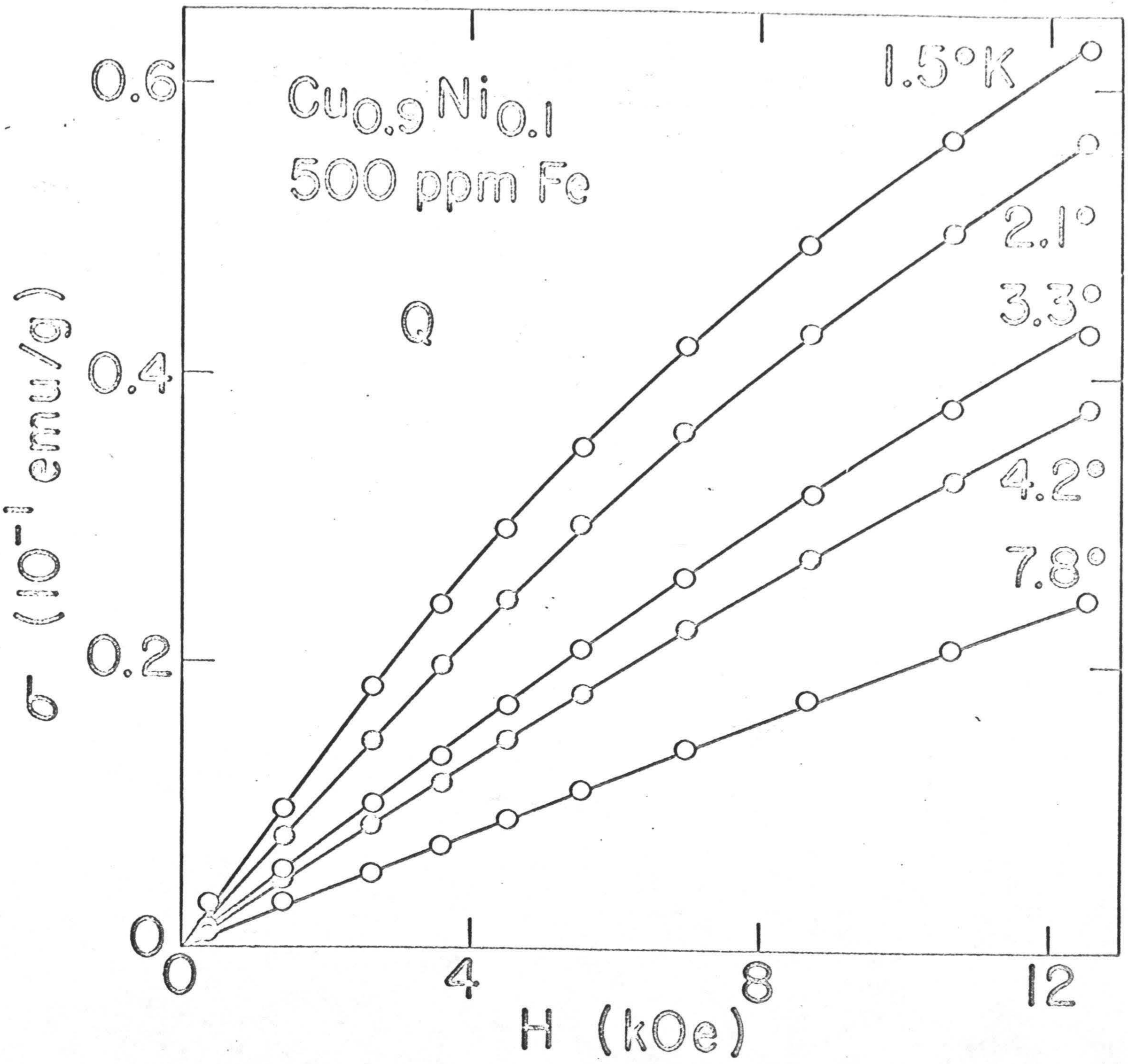
$Cu_{0.9}Ni_{0.1}$
500 ppm Fe
Q
1.5°K
2.1°
3.3°
4.2°
7.8°
0.6
0.4
0.2
0
0
4
8
12
H (kOe)
σ (10⁻¹ emu/g)

Figure 39. Magnetization vs. field for quenched $Cu_{0.9}Ni_{0.1}$ with 1000 ppm Fe. The empty and filled circles represent measured data (Table 22). The dashed curve and the solid curves were calculated using parameter values (Table 37) obtained by least squares fitting of Eq. 13 to experimental data in the temperature range of 2.0° to ~300°K.

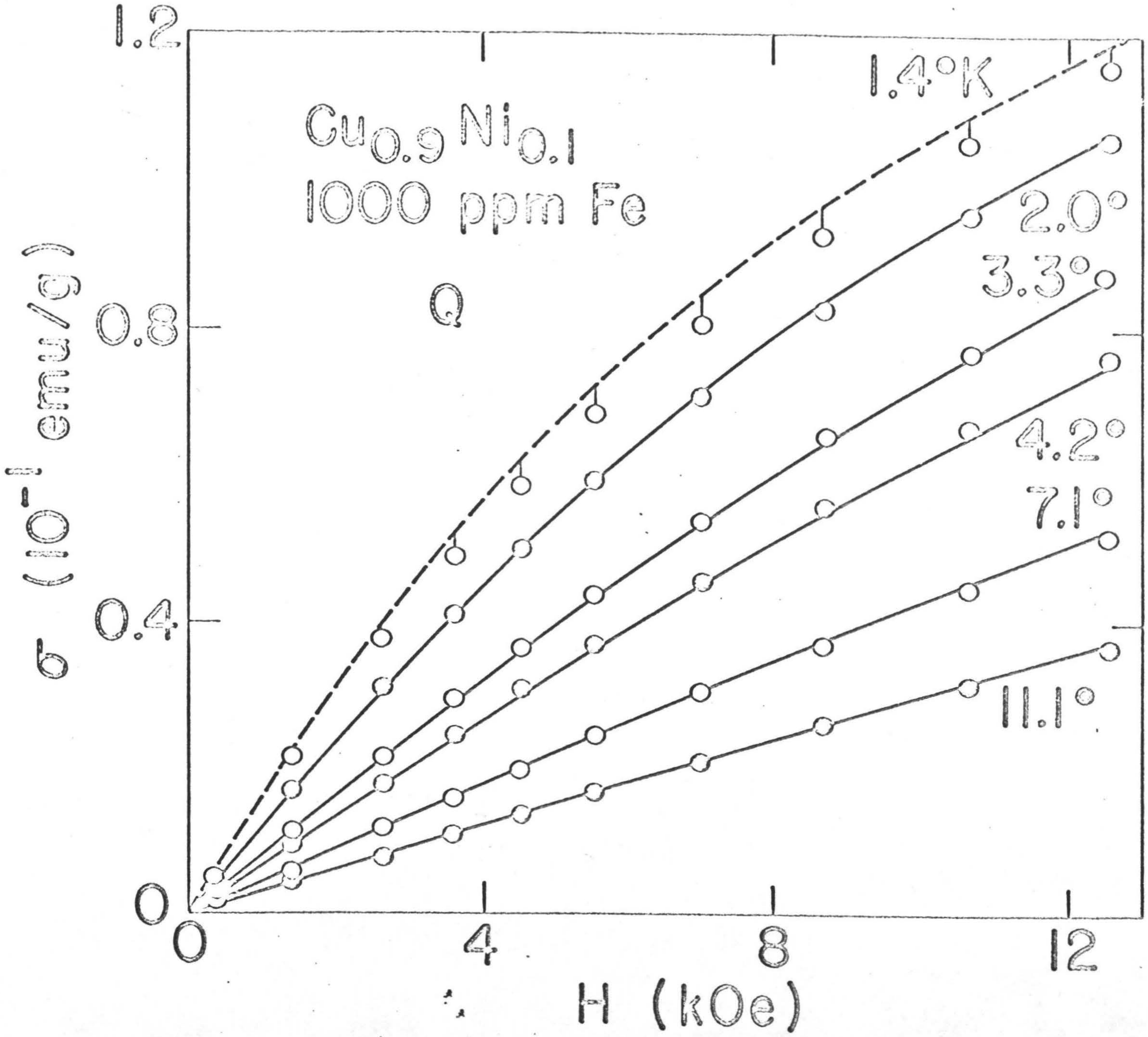
$Cu_{0.9}Ni_{0.1}$
1000 ppm Fe
Q
1.4°K
2.0°
3.3°
4.2°
7.1°
11.1°
1.2
0.8
0.4
0
0
4
8
12
σ (10⁻¹ emu/g)
H (kOe)

Figure 40. χ vs. T for quenched $Cu_{0.8}Ni_{0.2}$ alloys containing various amounts of Fe. The solid curves were calculated using parameter values listed in Table 38.

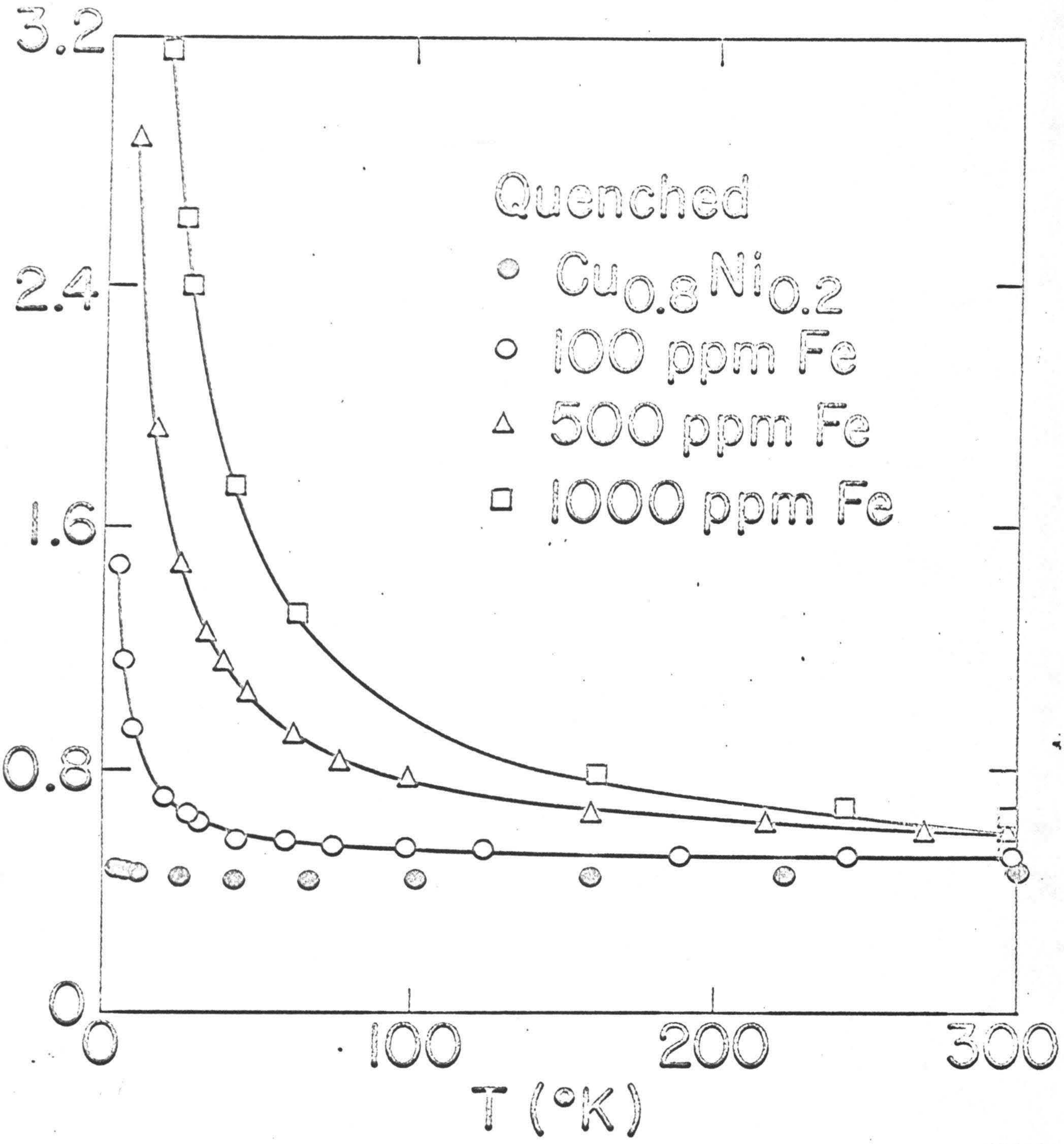
Quenched
$Cu_{0.8}Ni_{0.2}$
100 ppm Fe
500 ppm Fe
1000 ppm Fe
χ (10⁻⁶ emu/g)
3.2
2.4
1.6
0.8
0
0
100
200
300
T (°K)

Figure 41. Magnetization vs. field for quenched $Cu_{0.8}Ni_{0.2}$ with 100 ppm Fe. The empty and filled circles represent experimental data (Table 23). The dashed curve and the solid curves were calculated using parameter values (Table 38) obtained by least squares fitting of Eq. 11 to experimental data in the temperature range of 2.8° to ∿300°K.

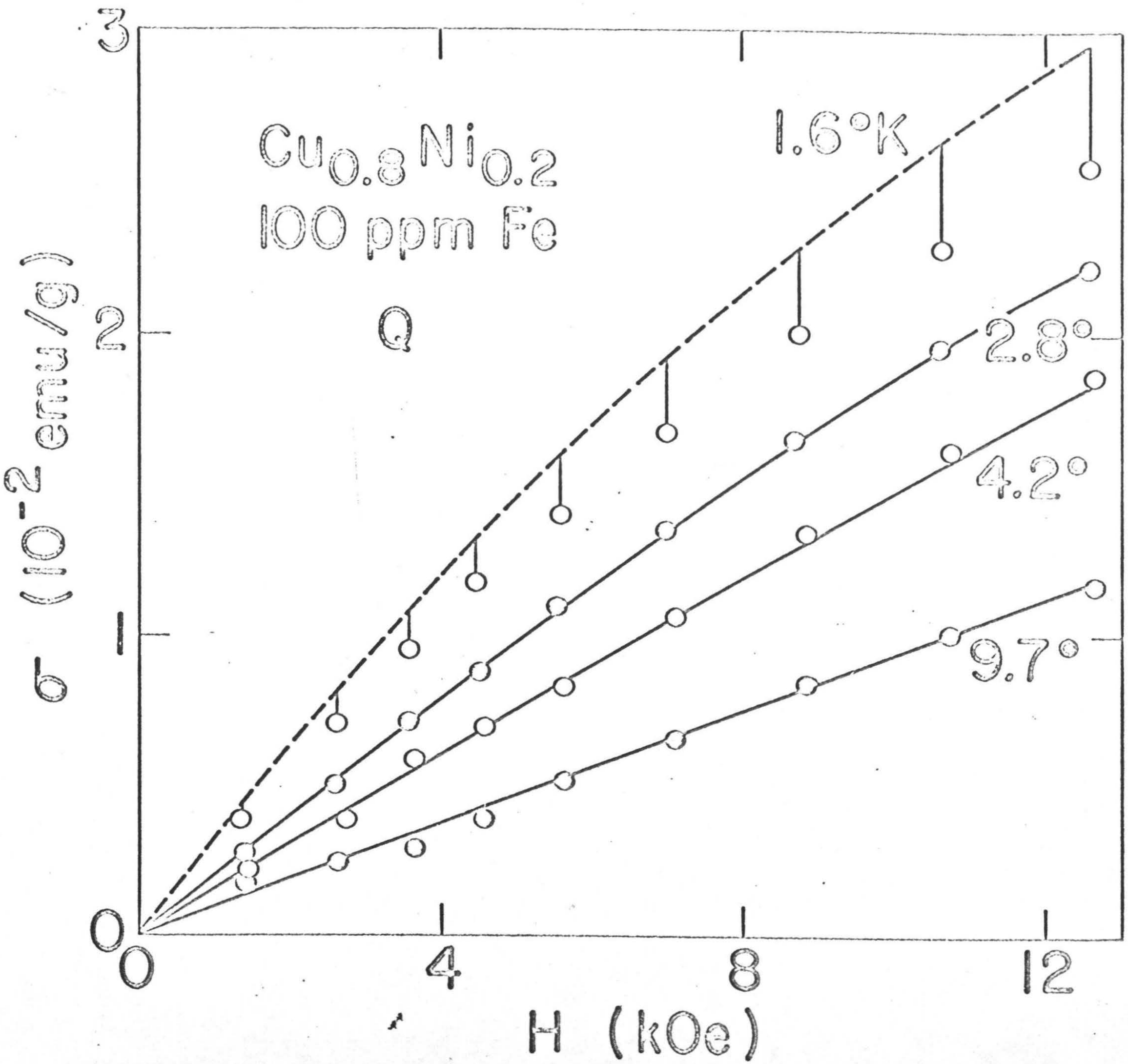
$Cu_{0.8}Ni_{0.2}$
100 ppm Fe
Q
1.6°K
2.8°
4.2°
9.7°
σ (10⁻² emu/g)
H (kOe)
0
1
2
3
0
4
8
12

Figure 42. Magnetization vs. field for quenched $Cu_{0.8}Ni_{0.2}$ with 500 ppm Fe. The empty and filled circles represent measured data (Table 25). The solid curves were calculated using parameter values listed in Table 38.

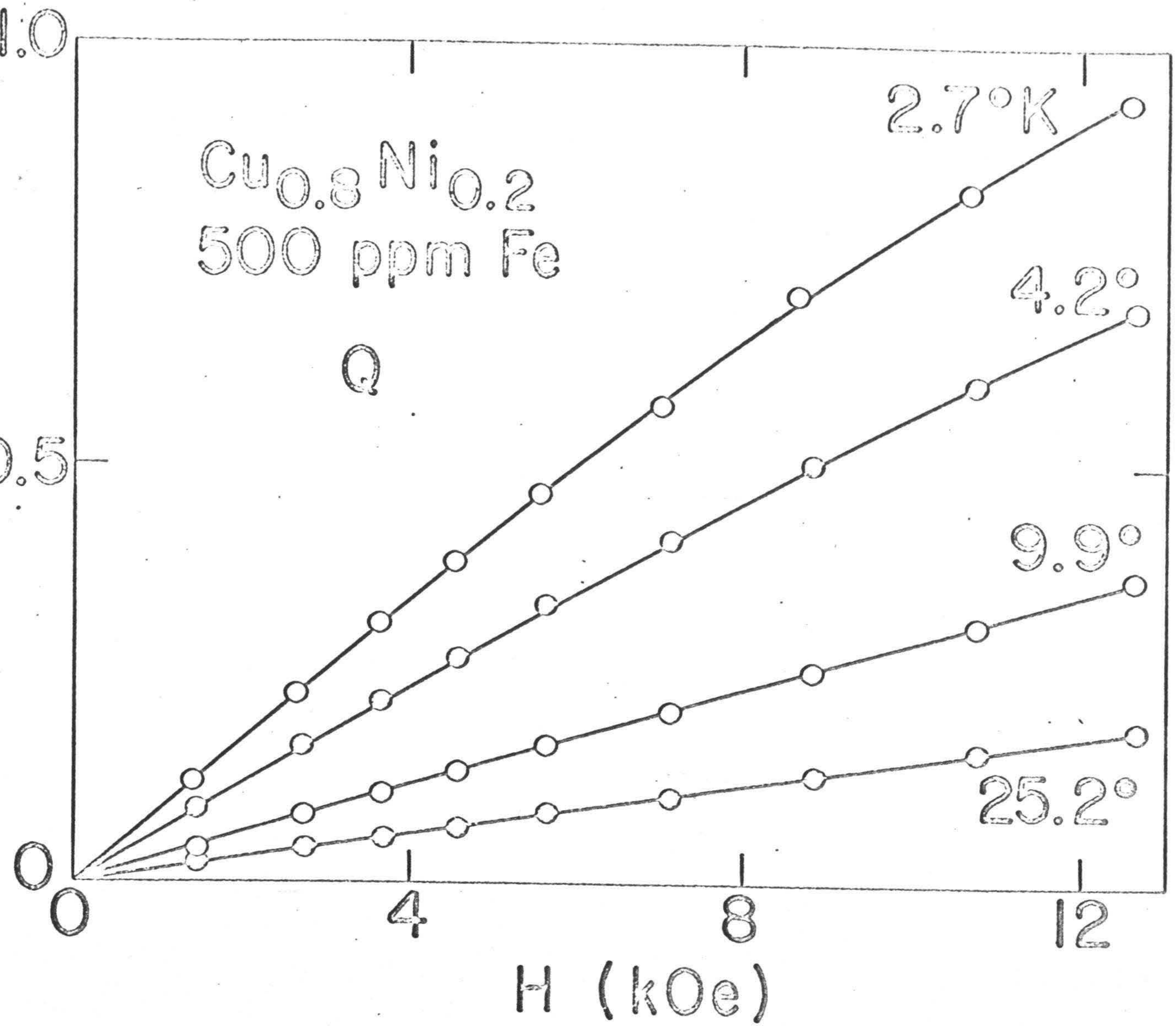
$Cu_{0.8}Ni_{0.2}$
500 ppm Fe
Q
2.7°K
4.2°
9.9°
25.2°
1.0
0.5
0
0
4
8
12
σ (10⁻¹ emu/g)
H (kOe)

Figure 43. Magnetization vs. field for quenched $Cu_{0.8}Ni_{0.2}$ with 1000 ppm Fe. The empty and filled circles represent measured data (Table 26). The solid curves were calculated using parameter values listed in Table 38.

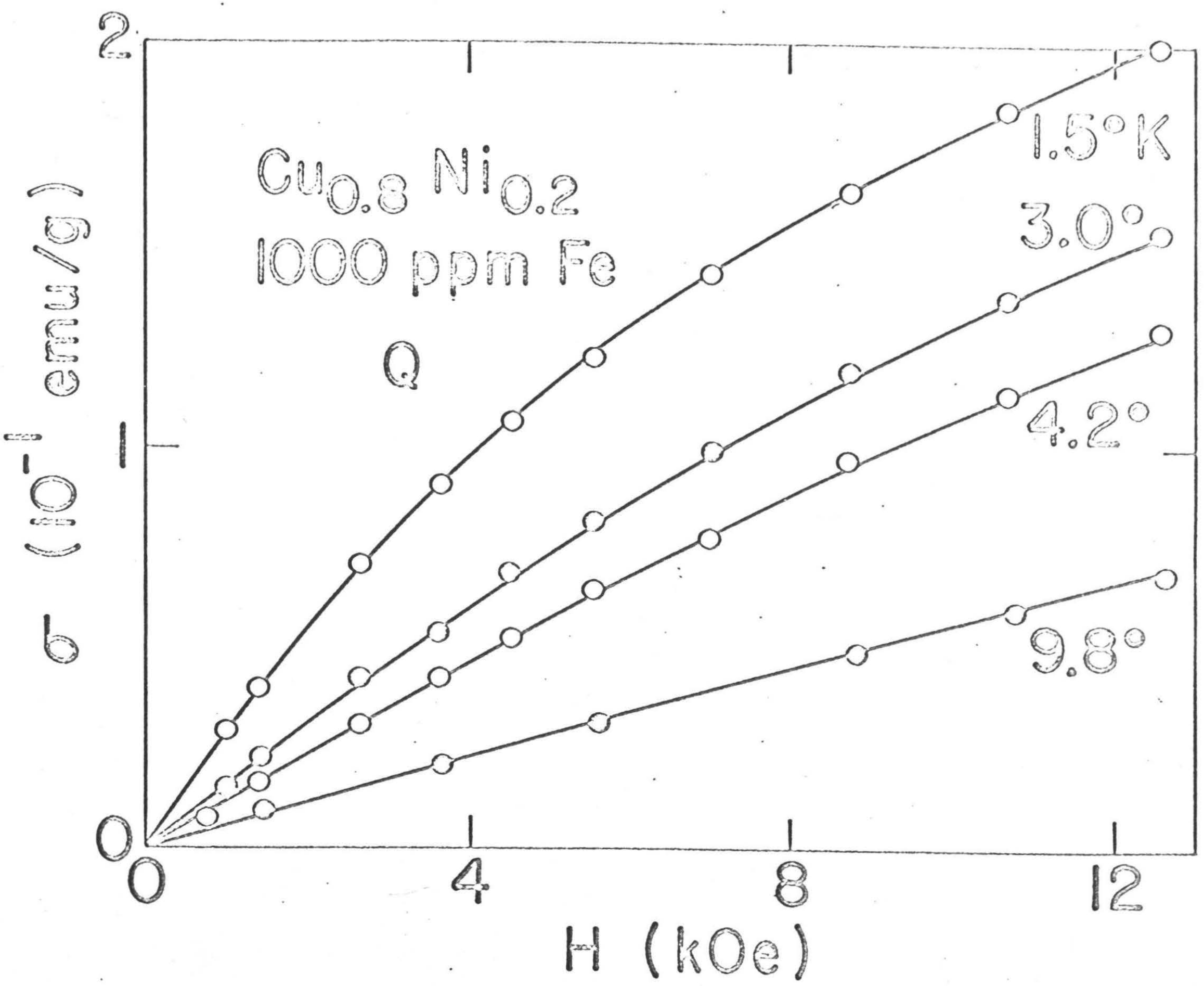
$Cu_{0.8}Ni_{0.2}$
1000 ppm Fe
Q
1.5°K
3.0°
4.2°
9.8°
2
0
0
4
8
12
H (kOe)
σ (10⁻¹ emu/g)

addition of Fe. The parameter values obtained by least squares fitting are given in Table 39; the fit is shown in Fig. 44.

b. Deformed alloys.

The analysis of the data for the deformed alloys was more laborious, since in the deformed state the assumption of thermal equilibrium is not appropriate and the concentrations c_1, c_2, and c_3 can not be derived from a single parameter $_{Fe\text{-}Fe}\alpha_1$ as was done for the quenched alloys. It was therefore necessary to consider two of the concentrations, i.e., c_1 and c_2 as independent, with only the condition $c_1 + 2c_2 + 3c_3 = z$ imposed. The deformed $Cu_{0.9}Ni_{0.1}$ and $Cu_{0.8}Ni_{0.2}$ alloys containing either 500 ppm Fe, or 1000 ppm Fe were analyzed in this way, by least squares fitting Eq. 13. The data for the deformed $Cu_{0.9}Ni_{0.1}$ and $Cu_{0.8}Ni_{0.2}$ alloys containing 100 ppm Fe were analyzed, as those for the corresponding quenched alloys, but fitting Eq. 11 in the manner described above. The results for all these alloys are given in Tables 40 and 41 and the fits are presented in Figures 45 through 52.

The effect of deformation in all cases was to decrease the magnetization, at any temperature and field, as compared with that for the quenched alloy. Table 42 lists the percentage decrease in magnetization at 4.2°K for the different alloys. In Fig. 53 the decrease in the magnetization on deforming the quenched $Cu_{0.8}Ni_{0.2}$ alloys containing 100 and 1000 ppm Fe is well illustrated.

Table 39. Parameters from least squares fitting of Eq. 11 to magnetization of the quenched $Cu_{0.7}Ni_{0.3}$ alloy containing 100 ppm Fe minus the magnetization of $Cu_{0.7}Ni_{0.3}$ without the Fe.

Temp. Range (°K)	4.2 to ∿300
μ_1 (μ_B)	5.20
μ_2 (μ_B)	12.95
c_1	87.6
c_2	6.2
θ_1	+ 0.25
θ_2	-14.1
χ_o (10^{-6} emu/g)	- 0.019
Fe-$Fe^{\alpha}1$	0.013
c_2/c_1	0.071
rmsd (10^{-3} emu/g)	0.179
rmsd (%)*	0.90

*The rmsd as expressed in percents of the highest magnetization value used in the fitting.

Figure 44. $\Delta\sigma_{Fe}$ vs. H at 4.2°K and $\Delta\chi_{Fe}$ vs. T for quenched $Cu_{0.7}Ni_{0.3}$ alloy with 100 ppm Fe. Measured data points: ⊗,O; curves calculated with parameter values from Table 39.

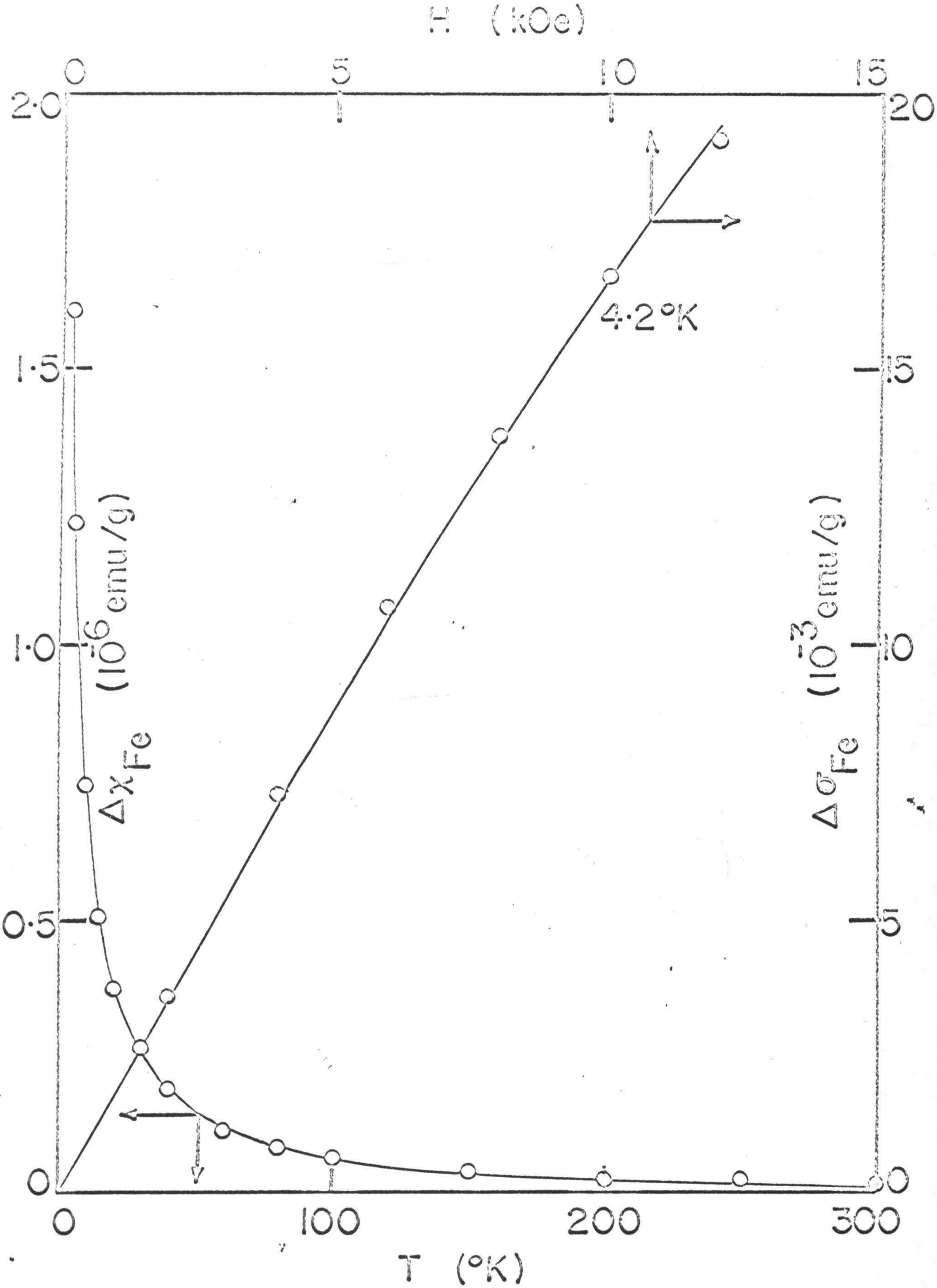
H (kOe)
0
5
10
15
20
4.2°K
$\Delta\sigma_{Fe}$ (10^{-3} emu/g)
$\Delta\chi_{Fe}$ (10^{-6} emu/g)
2.0
1.5
1.0
0.5
0
5
0
T (°K)
0
100
200
300

Table 40. Parameters from least squares fitting of Eq. 11 or Eq. 13 to magnetization data for deformed $Cu_{0.9}Ni_{0.1}$ alloys containing Fe.

Fe Content (ppm)	100	500	1000
Temp. range (°K)	1.44 to ∿300	1.36 to ∿300	2.30 to ∿300
μ_1 (μ_B)	2.50	2.50	2.62
μ_2 (μ_B)	4.38	6.02	5.56
μ_3 (μ_B)		8.10	7.21
c_1 (ppm)	95	394	699
c_2 (ppm	2.5	41	98
c_3 (ppm)		8	35
θ_1 (°K)	- 1.00	- 2.14	- 2.06
θ_2 (°K)	+ 0.84	- 0.11	- 2.08
θ_3 (°K)		- 0.19	+ 1.33
χ_o (10^{-6} emu/g)	0.173	0.180	0.234
c_2/c_1	0.026	0.104	0.140
rmsd (10^{-3} emu/g)	0.094	0.202	0.480
rmsd (%)*	0.73	0.36	0.52

*The rmsd value as expressed in percents of the highest magnetization value used in the fitting.

Table 41. Parameters from least squares fitting of Eq. 11 or Eq. 13 to magnetization data for deformed $Cu_{0.8}Ni_{0.2}$ alloys containing Fe.

Fe Content (ppm)	100	500	1000
Temp. range (°K)	1.44 to ∿300	3.05 to ∿300	1.47 to ∿300
μ_1 (μ_B)	3.75	3.44	3.66
μ_2 (μ_B)	7.37	8.64	6.50
μ_3 (μ_B)		14.22	10.72
c_1	93	420	703
c_2	3.5	31	96
c_3		6	35
θ_1	- 0.96	- 0.36	- 2.31
θ_2	+ 0.55	- 3.04	+ 0.45
θ_3		+ 0.47	+ 0.20
χ_o (10^{-6} emu/g)	0.479	0.480	0.423
c_2/c_1	0.037	0.074	0.136
rmsd (10^{-3} emu/g)	0.253	0.199	0.969
rmsd (%)*	0.98	0.26	0.54

*The rmsd value as expressed in percents of the highest magnetization value used in the fitting.

Figure 45. χ vs. T for deformed $Cu_{0.9}Ni_{0.1}$ alloys containing various amounts of Fe. The solid curves were calculated using parameter values listed in Table 40.

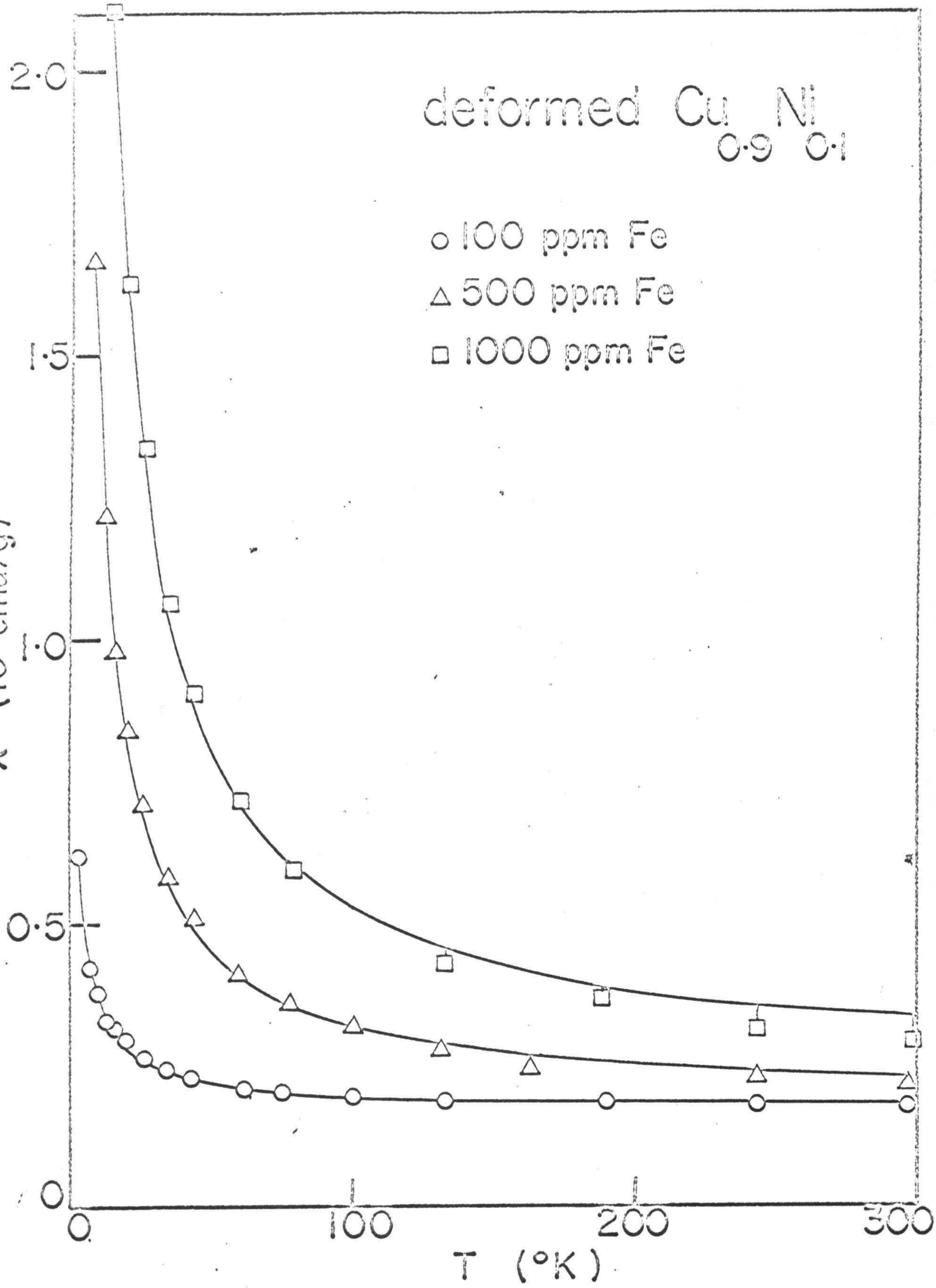
deformed Cu0.9 Ni0.1
o 100 ppm Fe
△ 500 ppm Fe
□ 1000 ppm Fe
χ (10-6 emu/g)
2·0
1·5
1·0
0·5
0
0
100
200
300
T (°K)

Figure 46. Magnetization vs. field for deformed $Cu_{0.9}Ni_{0.1}$ with 100 ppm Fe. The empty and filled circles represent experimental data (Table 28). The solid curves were calculated using parameter values listed in Table 40.

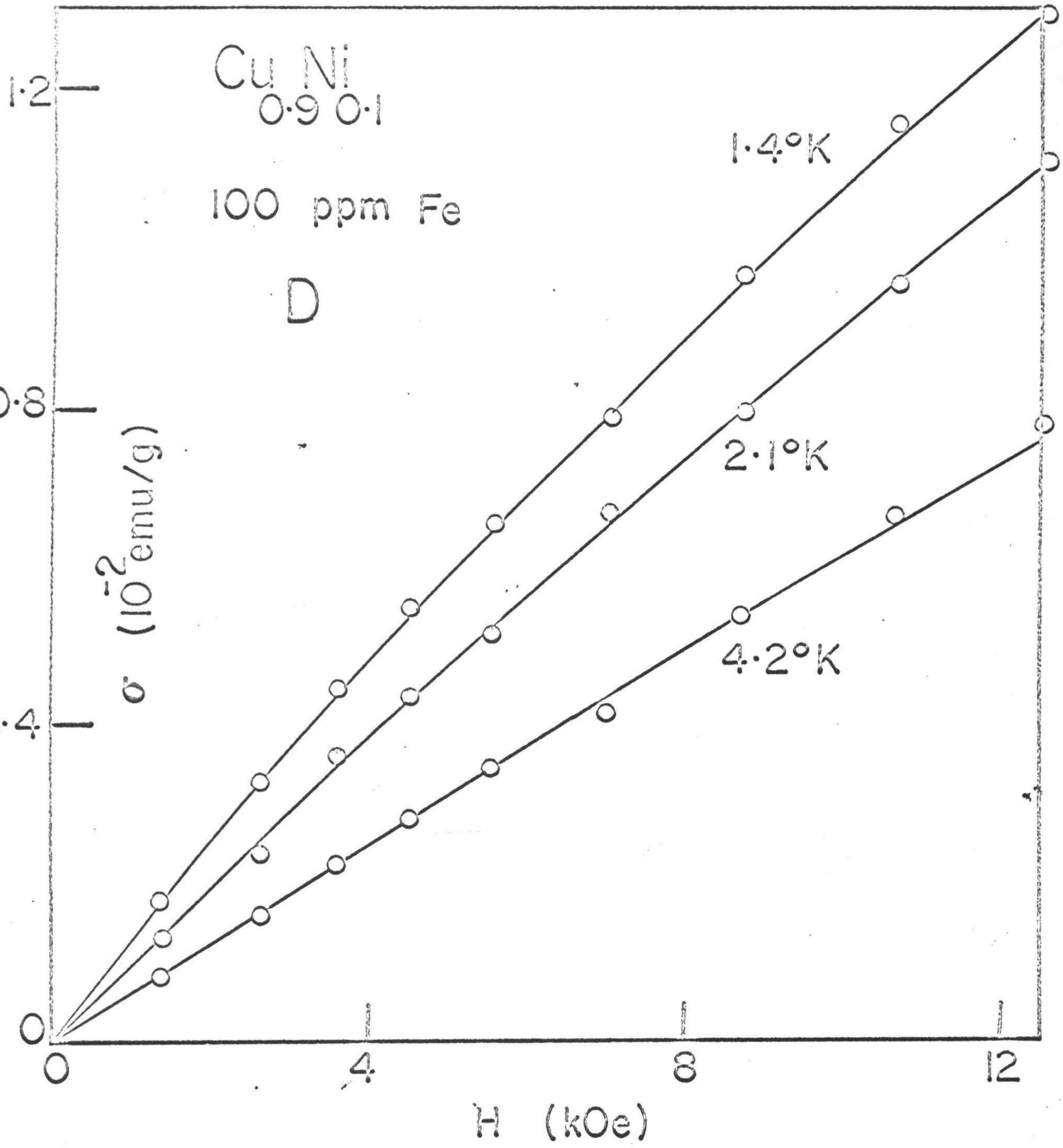
Cu Ni
0·9 0·1
100 ppm Fe
D
1·4°K
2·1°K
4·2°K
σ (10⁻² emu/g)
1·2
0·8
0·4
0
0
4
8
12
H (kOe)

Figure 47. Magnetization vs. field for deformed $Cu_{0.9}Ni_{0.1}$ with 500 ppm Fe. The empty and filled circles represent experimental data (Table 29). The solid curves were calculated using parameter values listed in Table 40.

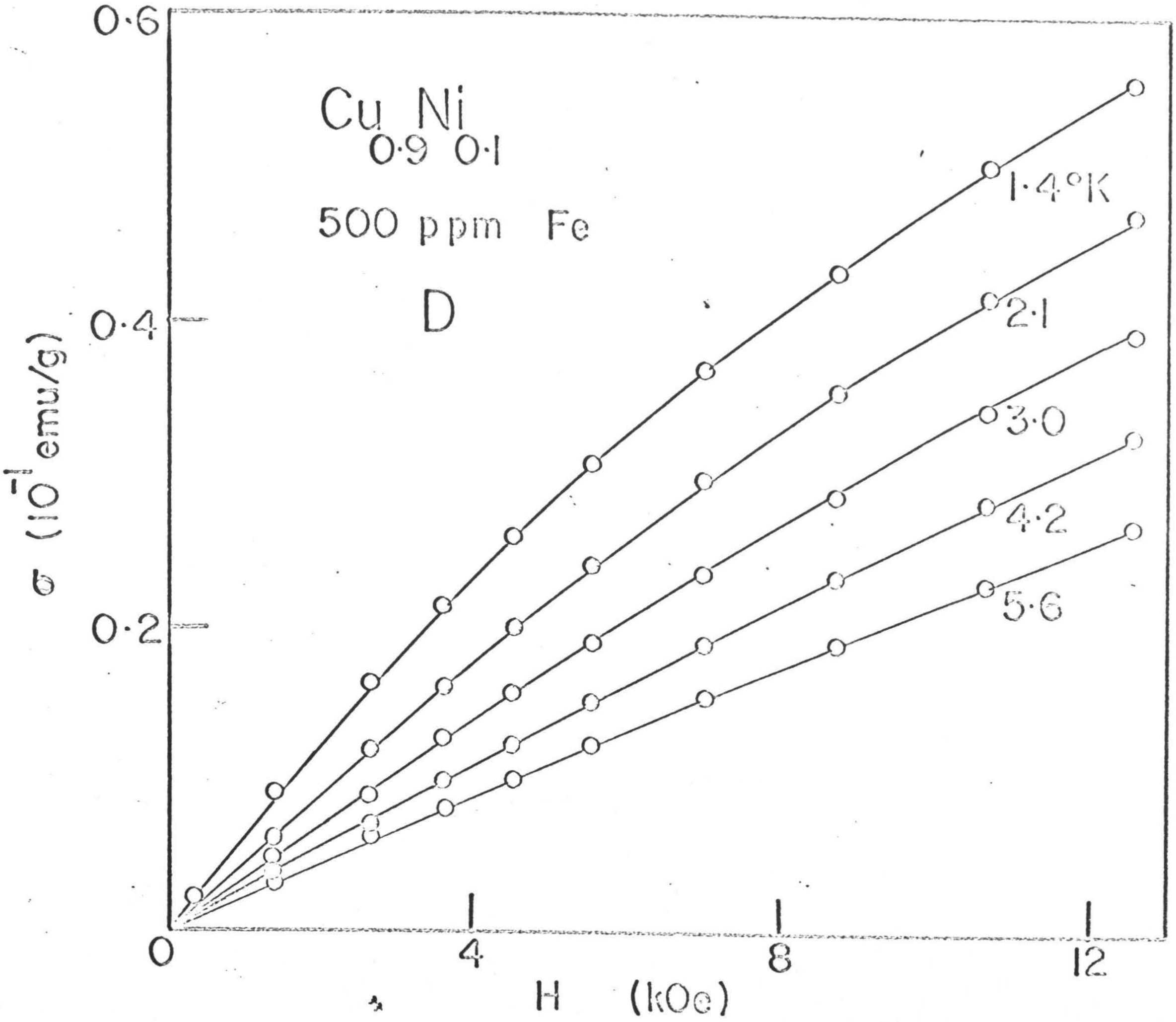
Cu Ni
0·9 0·1
500 ppm Fe
D
1·4°K
2·1
3·0
4·2
5·6
0·6
0·4
0·2
0
4
8
12
H (kOe)
σ (10⁻¹ emu/g)

Figure 48. Magnetization vs. field for deformed $Cu_{0.9}Ni_{0.1}$ with 1000 ppm Fe. The empty and filled circles represent experimental data (Table 30). The dashed curve and the solid curves were calculated using parameter values (Table 40) obtained by least squares fitting of Eq. 13 to experimental data in the temperature range of 2.3° to ∿300°K.

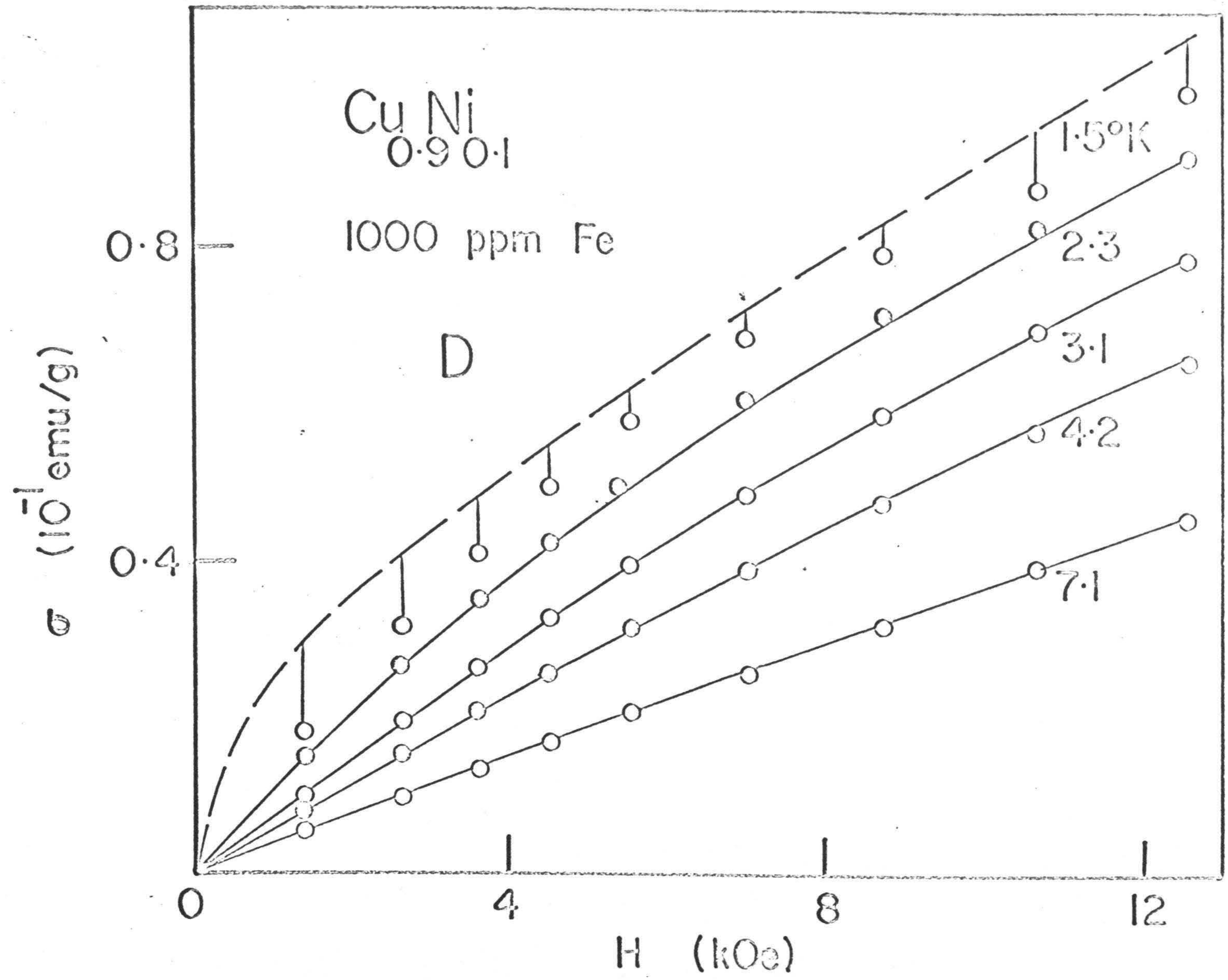
Cu Ni
0·9 0·1
1000 ppm Fe
D
1·5°K
2·3
3·1
4·2
7·1
0·8
0·4
0
4
8
12
σ (10⁻¹ emu/g)
H (kOe)

Figure 49. χ vs. T for deformed $Cu_{0.8}Ni_{0.2}$ alloys containing various amounts of Fe. The solid curves were calculated using parameter values listed in Table 41.

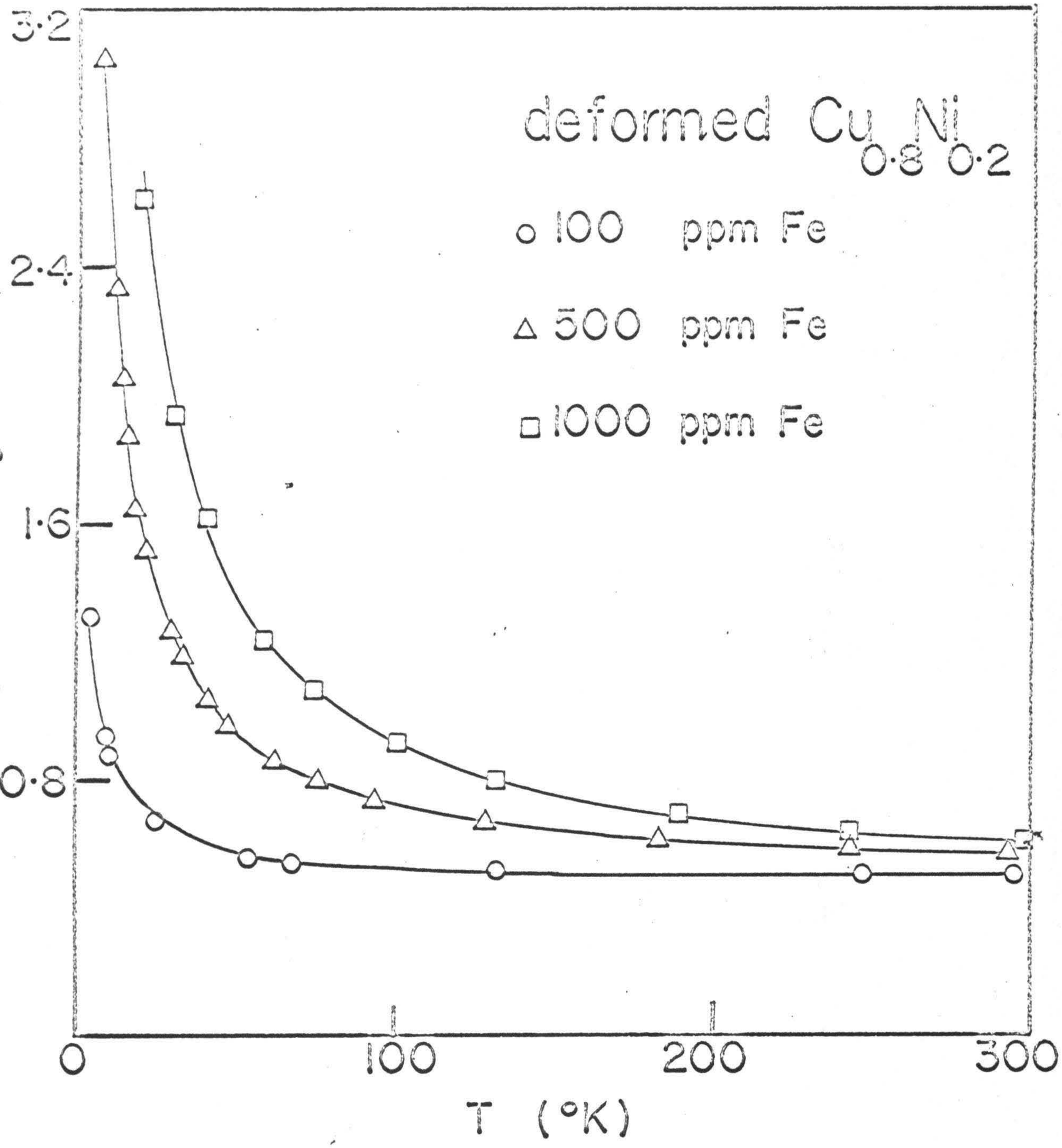
deformed $Cu_{0.8}Ni_{0.2}$
○ 100 ppm Fe
△ 500 ppm Fe
□ 1000 ppm Fe
χ (10^{-6} emu/g)
3·2
2·4
1·6
0·8
0
100
200
300
T (°K)

Figure 50. Magnetization vs. field for deformed $Cu_{0.8}Ni_{0.2}$ with 100 ppm Fe. The empty and filled circles represent experimental data (Table 31). The solid curves were calculated using parameter values listed in Table 41.

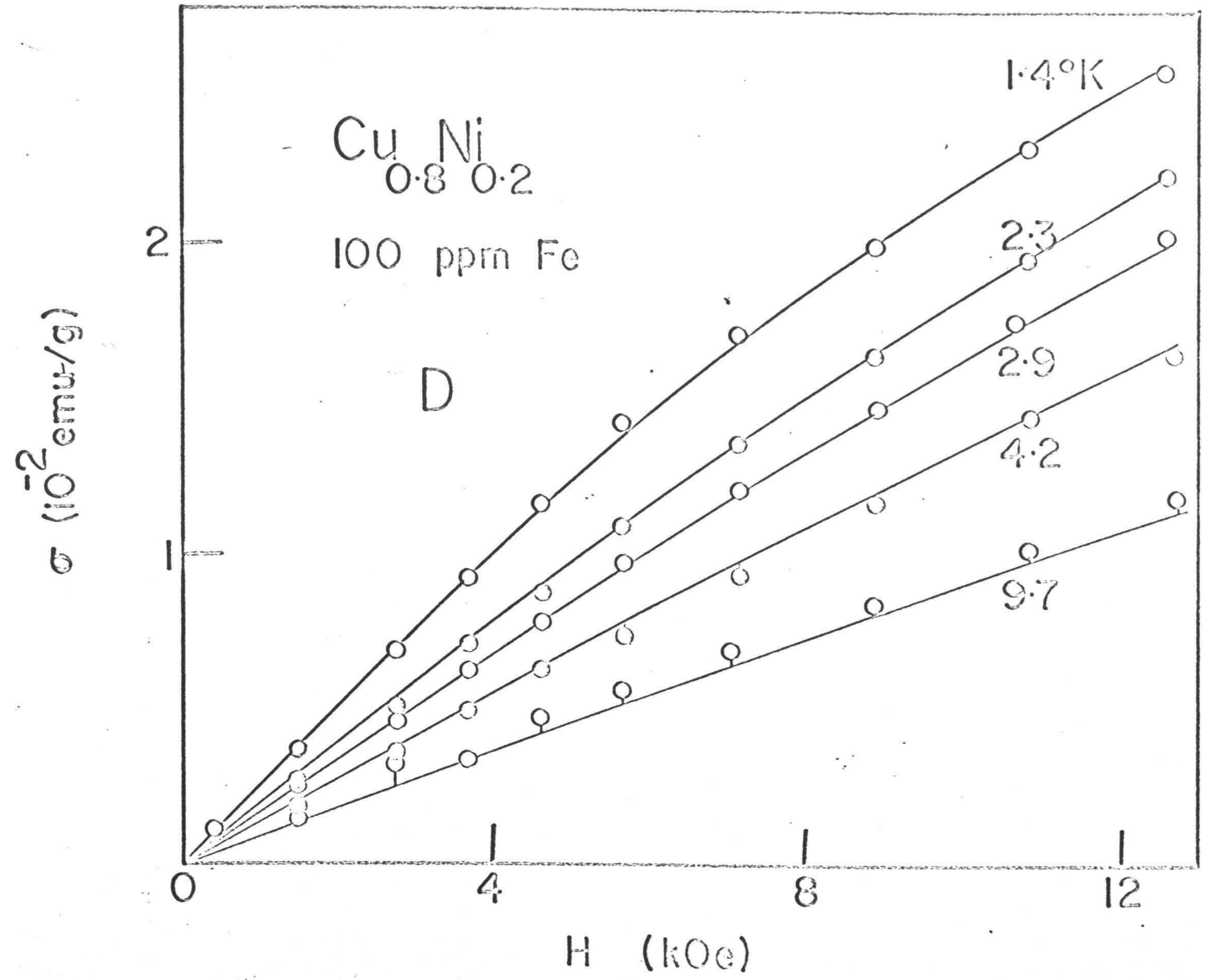
Cu Ni
0·8 0·2
100 ppm Fe
D
1·4°K
2·3
2·9
4·2
9·7
2
1
0
4
8
12
H (kOe)
σ (10⁻² emu/g)

Figure 51. Magnetization vs. field for deformed $Cu_{0.8}Ni_{0.2}$ with 500 ppm Fe. The empty and filled circles represent experimental data (Table 32). The dashed curve and the solid curves were calculated using parameter values (Table 41) obtained by least squares fitting of Eq. 13 to experimental data in the temperature range of 3.1° to ∿300°K.

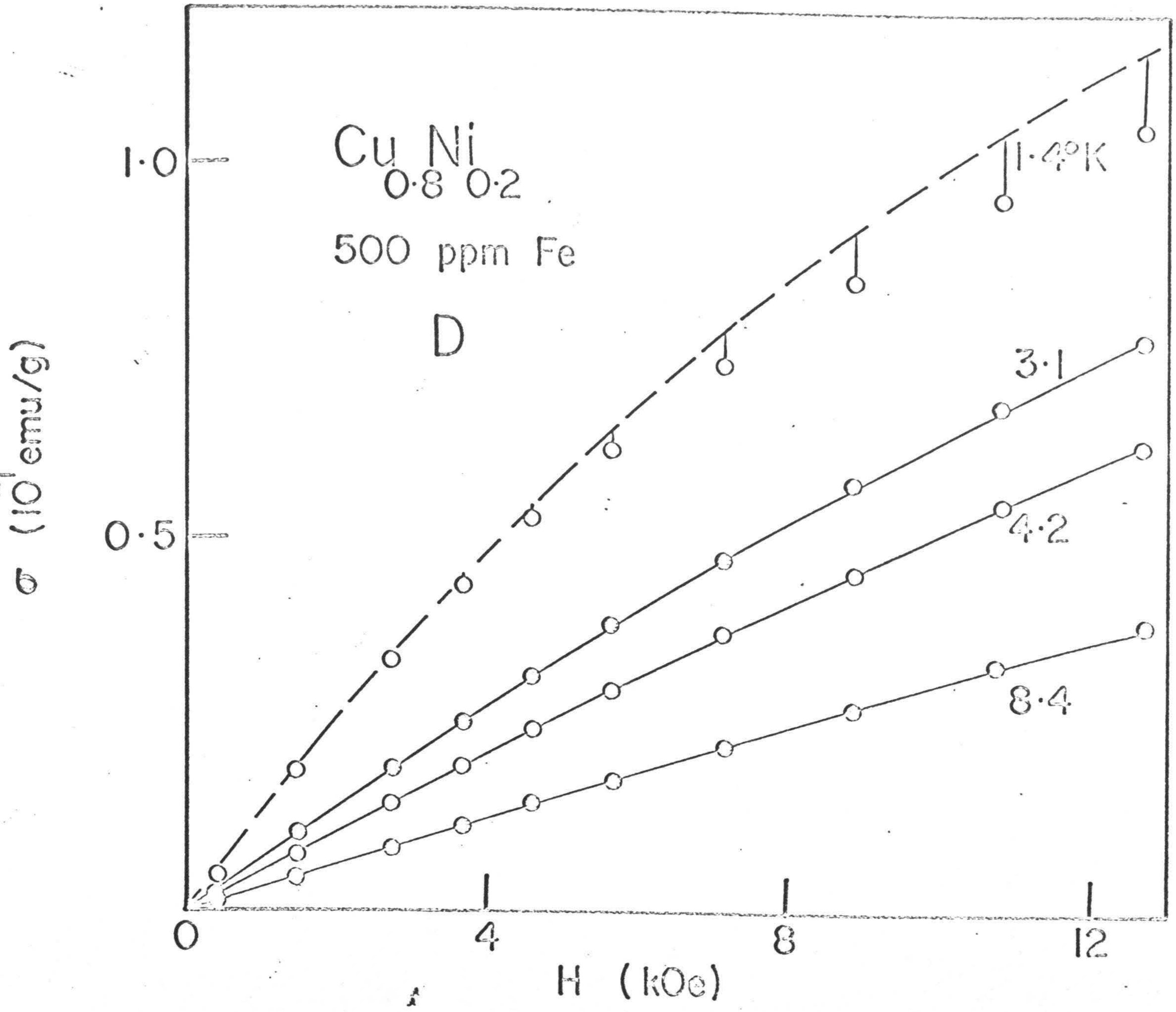
Cu Ni
0·8 0·2
500 ppm Fe
D
1·4°K
3·1
4·2
8·4
1·0
0·5
0
4
8
12
H (kOe)
σ (10⁻¹ emu/g)

Figure 52. Magnetization vs. field for deformed $Cu_{0.8}Ni_{0.2}$ with 1000 ppm Fe. The empty and filled circles represent experimental data (Table 33). The solid curves were calculated using parameter values listed in Table 41.

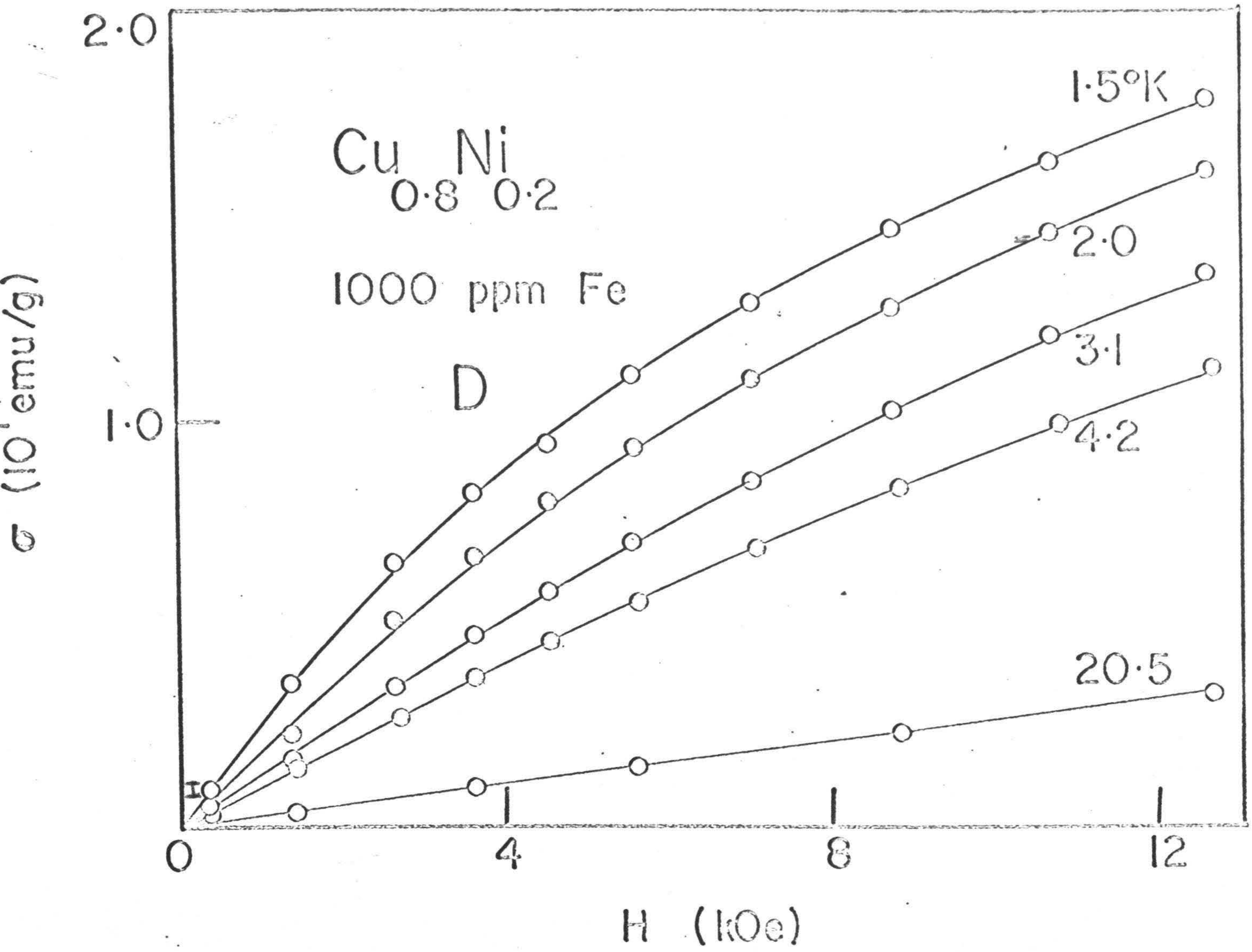
2·0
1·0
Cu Ni
0·8 0·2
1000 ppm Fe
D
1·5°K
2·0
3·1
4·2
20·5
0
4
8
12
H (kOe)
σ (10⁻¹ emu/g)

Table 42. Percentage decrease as a result of plastic deformation, of the magnetization of quenched alloys at 4.2°K in an applied field of ∿12.6 kOe.

Alloy	Magnetization (10^{-3} emu/g)		% Decrease
	Quenched	Deformed	
100 ppm Fe in $Cu_{0.9}Ni_{0.1}$	8.85	7.78	12.1
500 ppm Fe in $Cu_{0.9}Ni_{0.1}$	37.95	32.84	13.5
1000 ppm Fe in $Cu_{0.9}Ni_{0.1}$	76.06	65.39	14.0
100 ppm Fe in $Cu_{0.8}Ni_{0.2}$	18.64	16.47	11.6
500 ppm Fe in $Cu_{0.8}Ni_{0.2}$	68.65	62.90	8.4
1000 ppm Fe in $Cu_{0.8}Ni_{0.2}$	129.80	112.74	13.1

Figure 53. Effect of plastic deformation on the magnetization. Magnetization vs. field at 4.2°K for quenched (empty circles, Table 23) and deformed (filled circles, Table 31) $Cu_{0.8}Ni_{0.2}$ with 100 ppm Fe, and quenched (empty circles, Table 26) and deformed (filled circles, Table 33) $Cu_{0.8}Ni_{0.2}$ with 1000 ppm Fe.

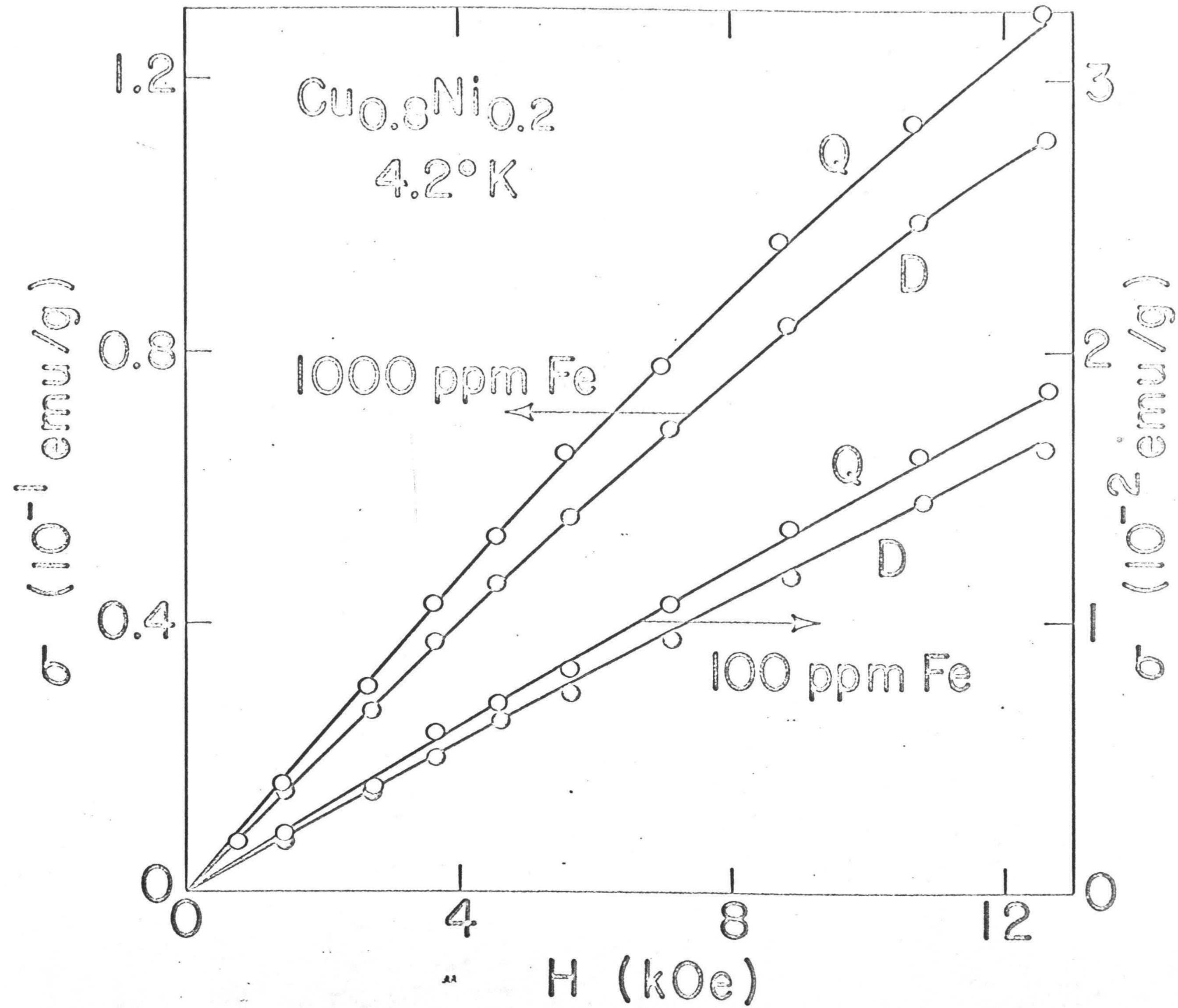
$Cu_{0.8}Ni_{0.2}$
4.2°K
1000 ppm Fe
100 ppm Fe
Q
D
Q
D
1.2
0.8
0.4
0
3
2
1
0
4
8
12
H (kOe)
σ (emu/g)
σ (emu/g)

For some of these alloys, in either the quenched or the deformed state, large systematic deviations were obtained for the data at the lowest temperature (∿1.5°K). In such cases deletion of these data from the fitting resulted is very satisfactory rmsd values and the deviations at higher temperatures could also be minimized. The parameter values in Tables 37 through 41 were obtained from these improved fits. A similar situation was encountered in the analysis of the data for $Cu_{0.6}Ni_{0.4}$. It is not unreasonable to assume that the interaction effects are large at T ≃ 1.5°K, so that the analysis in terms of Brillouin functions is not appropriate.

The accuracy with which the parameter values listed in Tables 37 through 41 were determined may be estimated to: ±5% for χ_o and μ_1, c_1, θ_1; ±10% for μ_2, c_2, θ_2; and ±20% for μ_3, c_3, θ_3.

V. DISCUSSION

A. Cu-Fe

The results of our analysis of the magnetization data for the Cu-Fe alloy with 108 ppm Fe[6] show (Table 36) that the magnetization of this alloy can be well described, in the temperature range of 1.3° to 32.5°K, in terms of isolated Fe, Fe pair, Fe triplet and Fe quadrupulet moments. The value of $\mu_1 = 2.44\ \mu_B$ is very similar to the value of $2.54\ \mu_B$ reported by Tholence and Tournier;[6] it is also in excellent agreement with the results of Franz and Sellmyer,[21] who estimated $\mu = 2.4 \pm 0.4\ \mu_B$, from Curie-Weiss analysis of initial susceptibility data above ∿10°K, for Cu-Fe alloys containing 447 and 842 ppm Fe. The value of $\mu_2 = 4.86\ \mu_B \simeq 2\mu_1$ is not very far from the corresponding value ($\sim 5.4\ \mu_B$) reported by Tholence and Tournier[6] on the basis of the concentration dependence of the magnetization. The principal differences between the earlier[6] and the present interpretation of the data are the presence of dipoles with $\mu_3 \simeq 7.22\ \mu_B$ attributable to groups of three Fe atoms and giant moments of the value of $\mu_4 = 10.17\ \mu_B$, and in the values of θ and c for the single and double Fe dipoles. It is worth noting that the fit is equally good in the entire temperature range (Fig. 32) without any indication of a decrease of μ_1 and μ_2, either by spin compensation or by local spin fluctuations, at temperatures as

low as 1.3°K (i.e., $T < 10^{-1}T_K$ where T_K, the lowest Kondo temperature reported in literature,[24,25] is about 15°K).

The present evaluation of the data of Hirschkoff et al.[9] in the lower temperature range of ∿0.01°K to ∿0.04°K, for a Cu-Fe alloy with 112 ppm Fe indicates the absence here of any appreciable concentration of single Fe dipoles giving rise to a corresponding temperature- and field-dependence of the magnetization expressed by a Brillouin function. Hirschkoff et al.[9] concluded on the basis of the concentration dependence of the magnetization that single Fe dipoles are absent. The least squares fitting of Eq. 13 shows that a Brillouin term corresponding to Fe pair dipoles is absent as well. The large values obtained from these data for μ_1, μ_2, and μ_3 (Table 36) apparently represent averages for a distribution of magnetic clusters, each of which involves more than two Fe moments. Assuming each Fe moment in the clusters to be 2.2 μ_B, the concentration of all Fe atoms participating in dipoles and contributing to the temperature- and field-dependence of the magnetization described by Brillouin functions may be estimated as only about 1.7 ppm, i.e., less than 2% of the total Fe concentration in the alloy.

The question arises here whether the large majority of Fe atoms, which do not contribute to the temperature-dependent magnetization below 0.4°K, may be responsible for the large increase of the temperature independent susceptibility to χ_o = 8.7×10^{-8} emu/g over the corresponding value of $\chi_o = 0.48 \times 10^{-8}$ emu/g for the higher temperature range (Table 36). One

interpretation would be that the isolated Fe moments, present at and above 1.3°K, are fully compensated below 0.4°K. Some authors have suggested[24,25] that the susceptibility at 0°K for a spin compensated Kondo system is $\sim\frac{p^2}{3kT_K}$ where $p^2 = \mu^2_{effective} = \mu(\mu+2)$. Assuming $T_K \sim 15°K$ $_{Kondo}\chi_o \simeq 8 \times 10^{-8}$ emu/g, in good agreement with the value of χ_o in the lower temperature range. However an alternative explanation, not requiring the assumption of spin compensation, is also in good agreement with the data. As seen in Fig. 54 the magnitude of the increase in the field and temperature independent susceptibility, $\Delta\chi_o = 8.2 \times 10^{-8}$ emu/g, agrees quite well with the sum, 8.6×10^{-8} emu/g, of the initial susceptibilities due to the single Fe, the Fe pair and the triple Fe moments, extrapolated to 0.4°K from the higher temperature range. Because of the large negative values of the corresponding θ_1, θ_2 and θ_3 (see Table 36), these initial susceptibilities are practically temperature-independent below 0.4°K. At the low values of the external field used in the measurements,[9] they are nearly independent of the field as well, so that they are incorporated into χ_o in the least squares fitting. Also, extrapolation of the remaining Brillouin term, corresponding to $\mu_4 = 10.17\ \mu_B$, from the higher temperature range to 0.4°K gives a magnetization value in close agreement with the sum of the values at the same temperature of the three Brillouin terms obtained for the lower temperature range. Thus, one may conclude that the present interpretation of the available magnetic data for the copper alloys with approximately 110 ppm Fe

Figure 54. χ_i vs. T for Cu-Fe with ∿110 ppm Fe:

(1) Total initial susceptibility above 0.4°K as extrapolated from the data below 0.4°K of Hirschkoff et al.[9]

(2) Total χ_i (dashed part is an extrapolation below 1.3°K); data above 1.3°K from Tholence and Tournier.[6]

(3) Temperature independent susceptibility χ_o (dashed part is an extrapolation above 0.4°K) as obtained from analysis of the data below 0.4°K, Hirschkoff et al.[9]

(4) The sum of the initial susceptibilities due to $\mu_1 = 2.44$, $\mu_2 = 4.86$ and $\mu_3 = 7.22$, and $\chi_o = 0.48 \times 10^{-8}$ emu/g, as obtained from the analysis of the data above 1.3°K, Tholence and Tournier[6] (dashed part is an extrapolation below 1.3°K).

(5) Temperature independent susceptibility χ_o (dashed part is an extrapolation below 1.3°K) from analysis of the data above 1.3°K, Tholence and Tournier.[6]

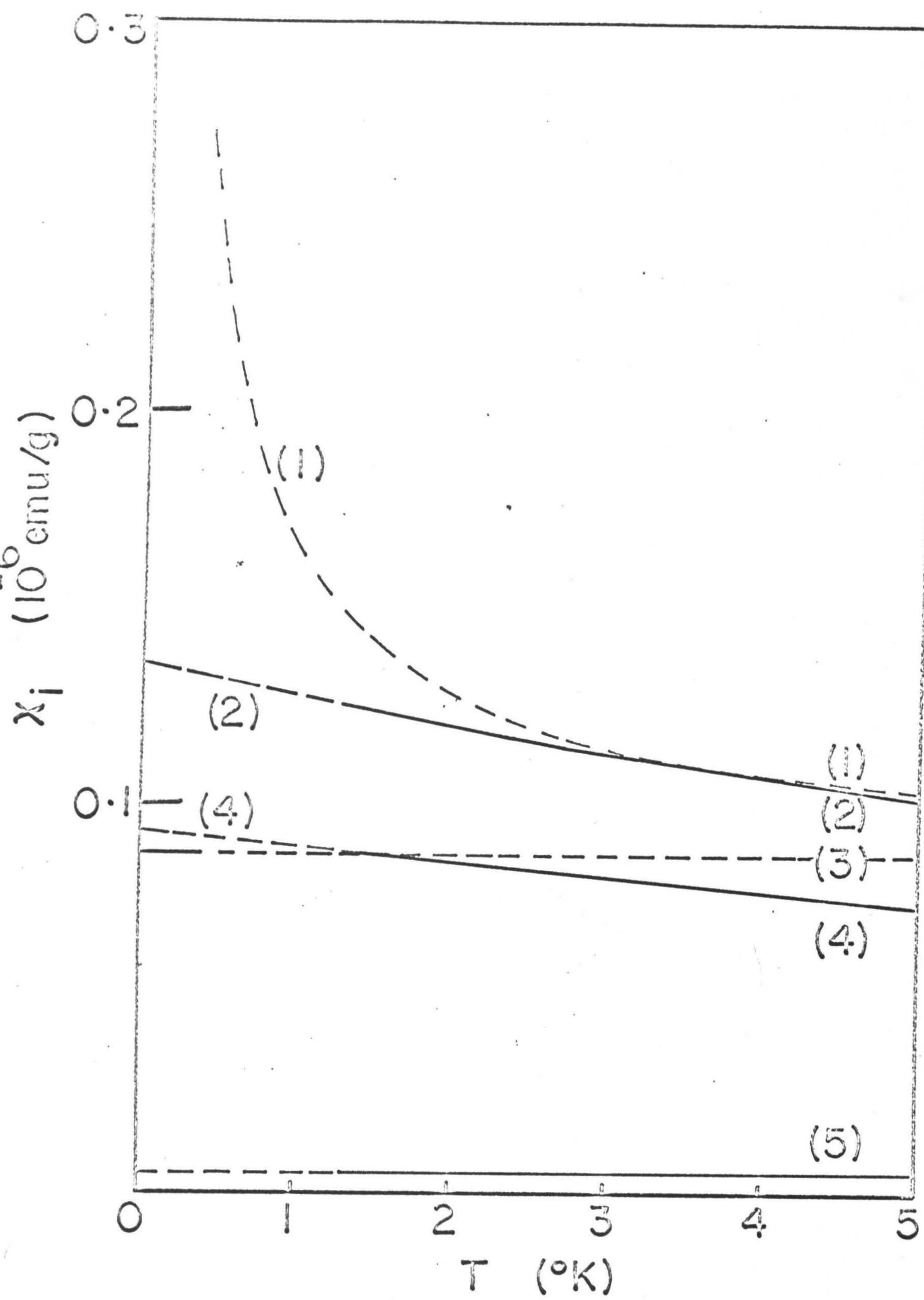
226
0·3
0·2
0·1
χ_i (10^{-6} emu/g)
(1)
(2)
(4)
(1)
(2)
(3)
(4)
(5)
0
1
2
3
4
5
T (°K)

in the two temperature ranges is self consistent and that it does not require the loss of Fe moments by spin compensation or local spin fluctuation, even at temperatures as low as 0.012°K.

It is an interesting question whether the finding of Hirschkoff et al.[9] that the susceptibility in the lower temperature range scales with the second power of the Fe concentration can be reconciled with the absence in the same temperature range of a Brillouin term corresponding to the Fe pair moment of about 4.86 μ_B. According to the interpretation outlined in the preceding paragraph, the dipoles with single Fe and with Fe pair moments are in fact present, but they contribute only to the temperature- and field-independent susceptibility χ_o. Also, if the single Fe moments are compensated by the Kondo mechanism, their contribution to χ_o will be essentially the same. The dependence of the total susceptibility on the Fe concentration represents an average of the concentration dependence of χ_o and of the various Brillouin terms in Eq. 14. This average may approximately correspond to the square of the Fe concentration, provided that χ_o itself is proportional to a lower than second power of the concentration, so that it can compensate the effect on the average of the Brillouin terms, which vary with a higher than second power of the Fe concentration. It is clearly apparent in Fig. 1 of Ref. 9 that the compensation is indeed approximately achieved at 0.4°K. One would not expect it to continue, however, as the temperature is decreased, since the Brillouin terms enter the average with a larger weight at lower temperatures. In fact, Fig. 1 of Ref. 9 shows that the graphs

representing the alloys with different Fe contents diverge. For instance, at T = 0.08°K the susceptibility values would have to be divided by the 1.8th, rather than the 2nd, power of the respective Fe concentrations in order to bring about approximate superposition, analogous to that achieved at 0.4°K through division by the square of the concentration. Thus, the scaling of the susceptibility with the second power of the Fe-concentration, discovered by Hirschkoff et al.,[9] clearly represents the average concentration dependence of the various susceptibility terms at 0.4°K. As pointed out above, such an average presupposes that χ_o scales with a lower than second power of the concentration, i.e., that it comprises an appreciable contribution from either compensated or uncompensated single Fe moments, a contribution essentially linear in Fe-concentration. It may be, therefore concluded that the concentration-dependence of the susceptibility[9] does not contradict the analysis of its field-and-temperature-dependence given in the present work.

On the basis of their neutron magnetic scattering studies with a Cu-Fe alloy, Stassis and Shull[26] recently concluded that at 4.2°K there is absence of any large contribution to the total magnetization by field-induced polarization in the compensating conduction electron cloud. Window[7] concluded, through his Mössbauer effect study of the saturation hyperfine field at isolated Fe nuclei in Cu-Fe alloys, that even at temperatures as low as 1.4°K all the susceptibility can be accounted for by the localized Fe moments, with no contribution from the compensating spin cloud. In view of these findings, and of the results of Tholence

and Tournier,[6] based on the concentration dependence, it appears at present that neither spin compensation nor local spin fluctuations make any noticeable contribution to the magnetization at low temperatures. The present analysis of the field-and temperature-dependence of the magnetization values measured by Tholence and Tournier[6] for 108 ppm Fe in Cu, confirms that the single moments remain unchanged at least to 1.3°K.

In order to explain the high concentration of magnetically interacting pairs of Fe moments for a random alloy, it has been suggested[6] that the Fe atoms participating in a pair moment may not necessarily be nearest neighbors of one another, but that a long range magnetic coupling may be provided between them by the RKKY mechanism. On the other hand, more recent Mössbauer work[7,8] indicates the presence in dilute Cu-Fe alloys (with Fe contents as low as ∿200 ppm[8]) of relatively large concentrations of Fe nearest neighbor pairs and of larger aggregates. It is therefore more plausible to assume that the Fe pair moments and the larger magnetic clusters revealed by the present analysis are associated with nearest neighbor Fe atoms.[27] For more concentrated Cu-Fe alloys (0.2 to 1.71 at. %) Svensson[28] had in fact concluded, from results of magnetic susceptibility measurements, that atomic clustering is present in quenched alloys and that on cold working there is a change in the magnetic structure from clusters to a statistical dispersion of Fe atoms. The ratio of the concentration of Fe-pair moments and of single-Fe moments derived in the present analysis (Table 36) from the

108 ppm Fe alloy data of Tholence and Tournier[6] requires a nearest-neighbor short range order parameter $_{Fe\text{-}Fe}\alpha_1$ of ∿0.017.

A maximum in the magnetization (Fig. 35) at approximately 0.02°K is observed in the 10 Oe data of Hirschkoff et al.[9] for a Cu-Fe alloy with 478 ppm Fe. A similar maximum is found at a lower temperature in their[9] data for the alloy with 380 ppm Fe; for the alloys with still lower Fe contents (e.g., 112 ppm Fe, Fig. 34) a clear-cut maximum is not indicated within the temperature range of the measurements. Such a maximum was found, in the present investigation, for the quenched $Cu_{0.99}Fe_{0.01}$ alloy at approximately 4.3°K (Fig. 29). At lower temperatures the magnetization values measured after cooling the specimen in a magnetic field are higher than those obtained after the specimen was cooled in zero field. Such thermomagnetic history effects, found in mictomagnetic alloys have been interpreted[29, 30] in terms of an interaction of magnetic clusters with the frozen spin-glass matrix in which they are dispersed. In the case of the $Cu_{0.99}Fe_{0.01}$ alloy the pronounced curvature in the σ vs. H graphs at low temperatures (Fig. 26) indicates the presence of large magnetic clusters. The freezing of the spin orientations at low temperatures in Cu-Fe alloys has been concluded from the occurrence of hyperfine splitting in the Mössbauer spectrum.[7,10,11] By interpolation from the Mössbauer ordering temperatures the freezing of the spin-glass matrix in the quenched $Cu_{0.99}Fe_{0.01}$ alloy may be estimated to take place at 8 ± 1°K. That the maximum in the magnetization in Fig. 29 does not correspond to a

Néel temperature is shown by the fact that it does not coincide with the Mössbauer ordering temperature. The quenched $Cu_{0.99}Fe_{0.01}$ alloy has a remanence temperature of 2.8° ± 1.4°K. Franz and Sellmyer[27] observed remanence below 3.5°K for a Cu + 0.6% Fe alloy. That long range antiferromagnetic order is in fact absent from the frozen spin system in Cu-Fe alloys is strongly suggested by the close analogy of their magnetic properties, including the occurrence of remanence, with those of the mictomagnetic Cu-Mn alloys. In the latter the absence of long range antiferromagnetism has been demonstrated by neutron diffraction.[31]

The occurrence of a magnetization maximum suggests that Cu-Fe alloys containing as low an Fe level as 380 ppm may be mictomagnetic.

B. Cu-Ni-Fe

As seen in Figures 36, 40, and 44, Fe additions in amounts of 100 to 1000 ppm increase very much the temperature dependent susceptibility of $Cu_{0.9}Ni_{0.1}$, $Cu_{0.8}Ni_{0.2}$ and $Cu_{0.7}Ni_{0.3}$ alloys. Analysis of the data for the quenched alloys (Tables 37, 38, and 39) indicate that the magnetization of most of these alloys can be well described in a very wide temperature range (~2.5° to 250°K, i.e., over two decades) in terms of magnetic clusters of three average sizes: μ_1, μ_2, and μ_3. Figure 55 shows that at a given Ni concentration, the μ_1 (and μ_2) values for different Fe contents agree very well. As a function of the Ni concentration μ_1 increases from 2.44 μ_B in pure Cu to 5.2 μ_B in

Figure 55. μ_1 and μ_2 for quenched Cu-Ni-Fe alloys as a function of Fe and Ni contents. The μ_1 and μ_2 values for 100 ppm Fe in $Cu_{0.7}Ni_{0.3}$ may involve some error due to the clustering tendency in this alloy of the Ni atoms, giving rise to magnetic dipoles.[1]

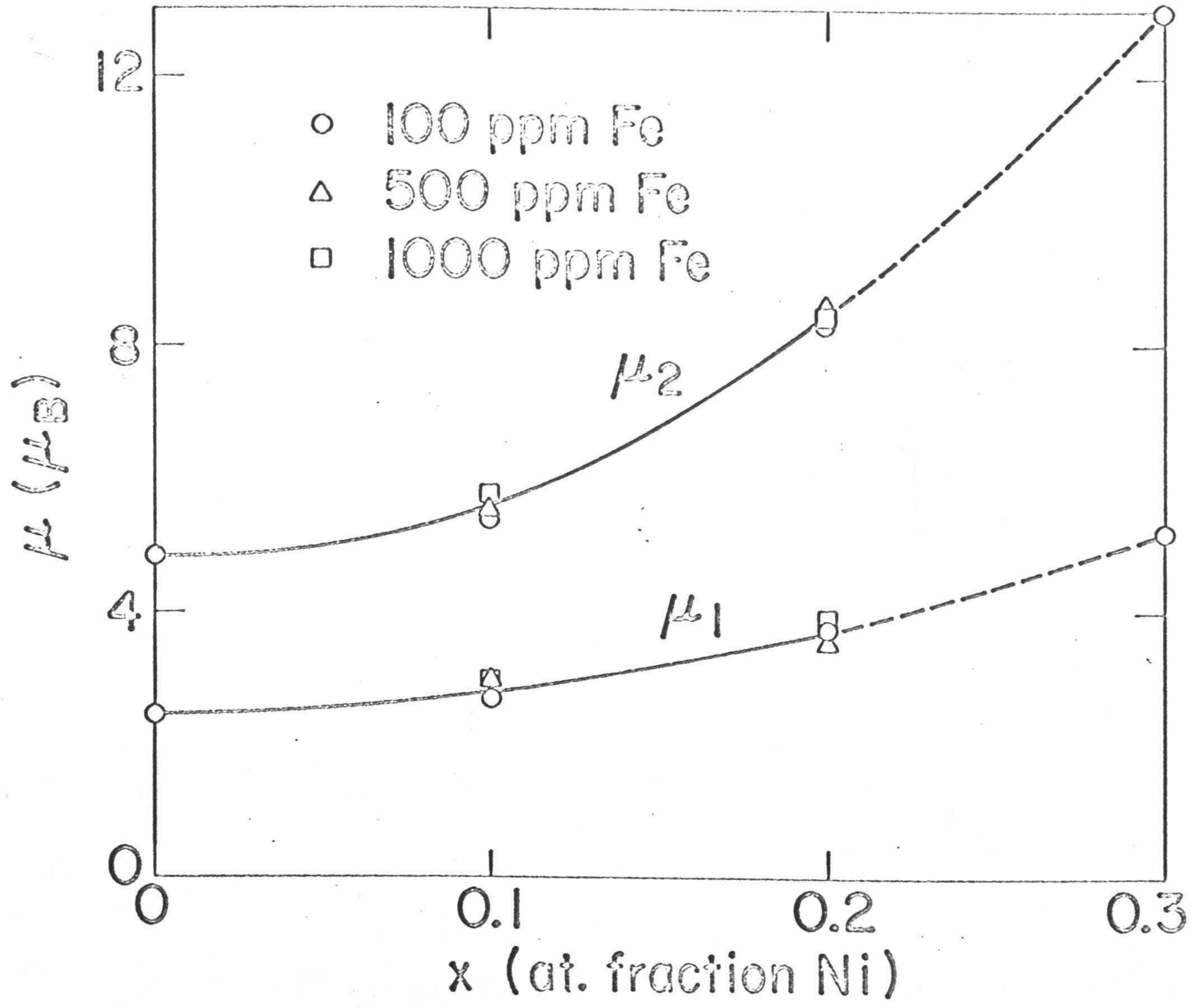
12
8
4
0
0
0.1
0.2
0.3
μ (μB)
x (at. fraction Ni)
100 ppm Fe
500 ppm Fe
1000 ppm Fe
μ2
μ1

$Cu_{0.7}Ni_{0.3}$ (Fig. 55); the corresponding increase in μ_2 is from 4.86 μ_B to 12 μ_B. In view of the fact that in $Cu_{0.7}Ni_{0.3}$ the nickel atoms themselves tend to form magnetic clusters,[1] the values of μ_1 and μ_2 for $Cu_{0.7}Ni_{0.3}$ as shown in Fig. 53 may be slightly in error. The value of μ_1 = 3.76 μ_B for the quenched $Cu_{0.7}Ni_{0.3}$ alloy with 100 ppm Fe is exactly the same as indicated in a preliminary report[2] for a quenched alloy of the same composition, on the basis of high field magnetization data at 4.2°K and of susceptibility data between 4.2°K and 300°K. The increase of μ_1 with the Ni content is qualitatively consistent with the results of Bennett et al.[3] for single Fe clusters. It is seen in Tables 37, 38, and 39 that for all alloys the ratio μ_2/μ_1 roughly corresponds to ∿2 irrespective of the Fe and Ni concentrations. One may then conclude that μ_1 and μ_2 are indeed the moments associated with single Fe and Fe pair clusters. The value of μ_3 does not always correspond to ∿3μ_1 (Tables 37, 38, and 39) and it may represent an average moment for all clusters containing three or more Fe atoms.

It may be noted in Tables 37, 38, and 39 that for each quenched alloy the best fit to the data is obtained when the ratio of the concentration of the single Fe moment to the concentration of Fe pair moments is such as to correspond to a finite positive value of $_{Fe\text{-}Fe}\alpha_1$ suggesting that the Fe atoms in these alloys tend to cluster. On the other hand Bennett et al.[4] proposed that the concentrations of the single Fe and Fe pair moments can be explained, on the basis of a random alloy

model, in which two Fe moments may be coupled via nearest neighbor Ni moments. In order to compare this model with experimental results the concentration of isolated Fe and Fe pair moments may be calculated on the basis of the model in the following manner. Figure 56 shows the atomic sites near an Fe atom at the origin (Site O) in a f.c.c. structure. According to the model of Bennett et al.[4] the moment on the Fe atom at site O can be magnetically coupled, for example, to another Fe moment at site 9, provided that sites 1 and 4 are occupied by Ni atoms, which in the model are assumed to have 0.6 μ_B each. The types of couplings by nearest neighbor sequences that are allowed are: Fe-Fe, Fe-Ni-Fe and Fe-Ni-Ni-Fe. This rules out the possibility of magnetic coupling when the second Fe atom is at site 8, or at 9b which is another type of 9^{th}-nearest neighbor, or at any site more distant than the 9^{th}-nearest neighbor, since in all these cases more than two intermediate Ni atoms would be required for "connection" by a nearest neighbor sequence. Table 43 lists the spatial co-ordinates of one site in each shell up to the 9th-nearest, and the number S_i of crystallographically equivalent sites on shell i, where i varies from 1 to 9. The total number of sites which can be connected to site O, under the assumptions made, is 146. Also listed in Table 43 are the probabilities of connection for Fe atoms at the various sites, through at least one path of two or less nearest neighbor Ni atoms, as a function of the Ni concentration x. For a given value of i, that is for the second Fe atom in any one of the S_i equivalent sites, on

Figure 56. Some atomic sites in an f.c.c. structure.

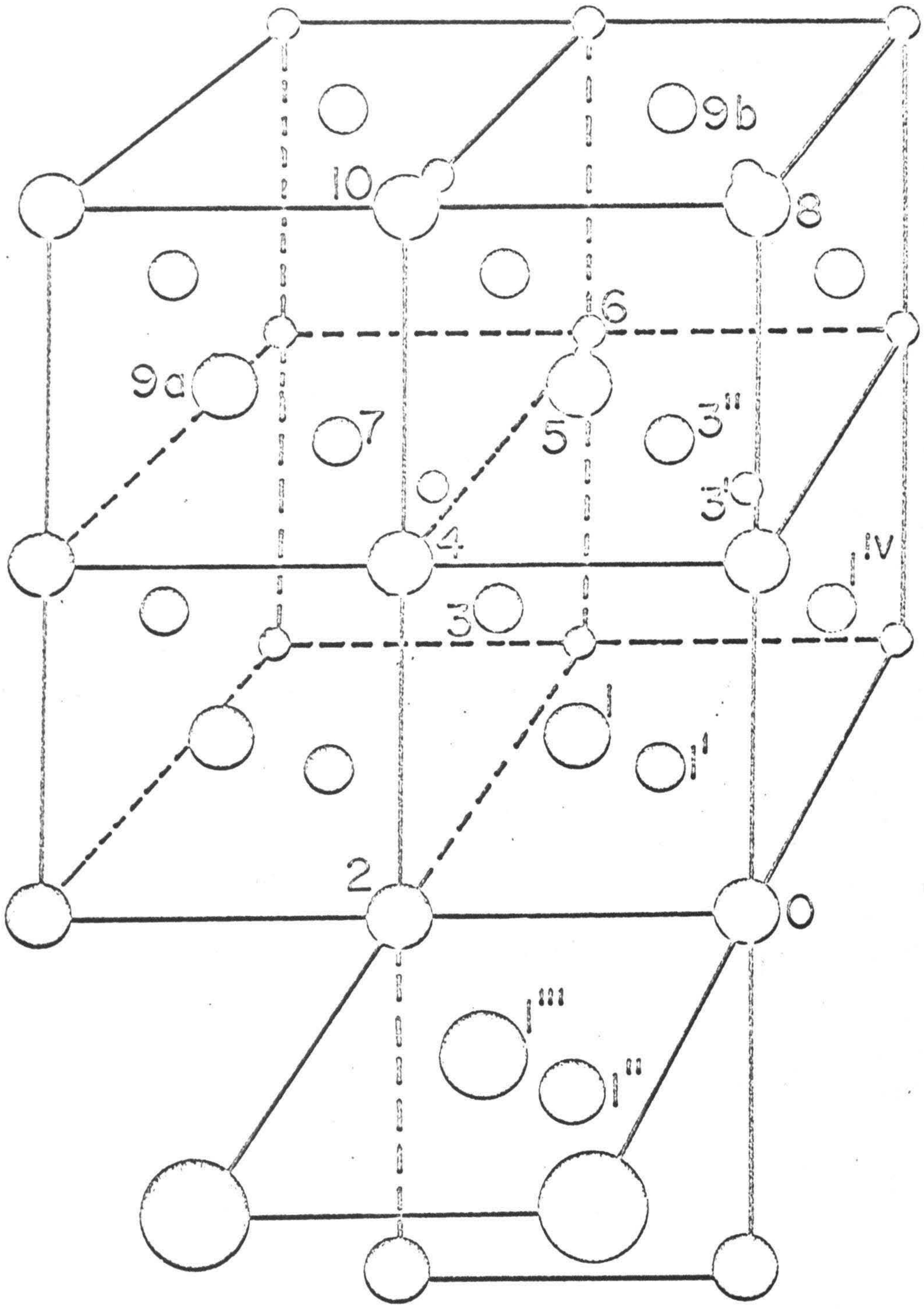
9b
10
8
6
9a
7
5
3''
3'
4
IV
3
1''
2
0
1'''
1''

Table 43. Connection probabilities for random alloy.

Shell No.	Location of atoms	No. of atoms in shell i	Probability of connection through at least one path of two or less nearest neighbor Ni atoms
i		S_i	P_i
1	$<\frac{1}{2},\frac{1}{2},0>$	12	1
2	<1,0,0>	6	$1-(1-x)^4$
3	$<1,\frac{1}{2},\frac{1}{2}>$	24	$1-(1-x)^2[1-x\{1-(1-x)^2\}]^2$
4	<1,1,0>	12	$1-(1-x)(1-x^2)^4$
5	$<1\frac{1}{2},\frac{1}{2},0>$	24	$6x^8-24x^7+35x^6-24x^5+15x^4-16x^3+9x^2$
6	<1,1,1>	8	$-2x^6+6x^5-3x^4-6x^3+6x^2$
7	$<1\frac{1}{2},1,\frac{1}{2}>$	48	$3x^2-2x^3$
8	<2,0,0>	6	0
9a	$<1\frac{1}{2},1\frac{1}{2},0>$	12	x^2
9b	$<2,\frac{1}{2},\frac{1}{2}>$	24	0

Note: Total number of connectable sites: 146.

shell i of the first one, the connection probability P_i is the same. This rule, of course, breaks down for i = 9, i.e., for the 9^{th} nearest neighbor shell where we have two types of sites: 9a and 9b. The manner in which the probabilities P_i were derived may be illustrated by means of a few examples.

(1) The second Fe atom is at site 1: In this case, since the two Fe atoms are nearest neighbors of each other, they are coupled regardless of the Ni concentration and the probability of connection, P_1, is equal to 1.

(2) The second Fe atom is at site 2: Here the coupling can occur provided there is a Ni atom in site 1 or in any of the three alternative connecting sites (1', 1'', 1'''). The probability of finding a Ni atom at a given site is x, and that of a Cu atom is (1-x-z) where z is the Fe concentration. Since z is very small (1000 ppm or 0.001 at the maximum) compared to x (0.100 at the minimum), one may write the probability of finding a Cu atom at a given site as (1-x). The probability that all four connecting sites under consideration are simultaneously occupied by Cu atoms is $(1-x)^4$; the probability that not all of the four sites are occupied by Cu atoms, i.e., the probability that at least one of the four sites is occupied by a Ni atom is given by $1-(1-x)^4$. This is the probability, P_2, of an Fe atom in the second nearest shell being coupled to the Fe atom at the origin via a Ni intermediary.

(3) The second Fe atom is at site 3: In this case, the coupling may be achieved through one or two Ni atoms. Referring

to Fig. 56, the first type of coupling can occur only if there is a Ni atom at at least one of the sites 1 or 1'. The probability that both of these sites are occupied by Cu atoms is $(1-x)^2$. The second type of coupling may occur in either of the following two ways: (a) Given a Ni at 1^{IV}, there should be another Ni atom at least at one of the two sites designated by 3' and 3''. The probability of such an event is $1-(1-x)^2$. The probability of connection through at least one path of two Ni atoms is $\{1-(1-x)^2\}$; and $1-x\{1-(1-x)^2\}$ is the probability that both of these alternative paths are being blocked by Cu atoms. (b) Given a Ni atom at 2, there should be a Ni atom at least at one of the sites 1'' or 1'''. The situation is identical with the one just discussed and so is the connection probability. Finally, one obtains the total probability of all the possible single Ni or double Ni paths being blocked by Cu atoms as equal to $(1-x)^2$ $[1-x\{1-(1-x)^2\}]^2$. Then the probability, P_3, of the Fe atom at site 3 being connected to the one at site 0, through at least one path of two or less nearest neighbor Ni atoms is $1-(1-x)^2$ $[1-x\{1-(1-x)^2\}]^2$. The connection probabilities P_4, and P_{9a} for Fe-sites in shells $\underline{i}$ = 4, and 9a were derived in a similar fashion.

In the determination of the connection probability P_1, or P_2, or P_3 above (or P_4, or P_{9a}), the connecting paths in each case were independent of one another, i.e., each possible connecting path involved Ni sites not involved in any of the other possible connecting paths. Because of the independence of the

paths the calculation was fairly simple. The same results can also be obtained by a more direct but laborious approach by calculating first the probability of each possible arrangement of copper and nickel atoms at the connecting sites, then discarding those configurations which are identical, and finally adding up the probabilities of only those not-identical configurations which provide a "connecting path" through one or two Ni atoms. In the calculation of the connection probabilities P_5, P_6 and P_7 such an approach had to be followed, since in these cases the different possible connecting paths are interlinked. Thus, to connect an Fe atom at a site marked 7 (i.e., i = 7, Fig. 56) to the Fe atom at site O, it is necessary to have Ni atoms (a) at sites 1' and 3; or (b) at sites 1 and 3, or (c) at sites 1 and 4. Clearly paths (a), (b) and (c) are not independent of one another.

Given an Fe atom A at site O, the average number of Fe atoms in its i-shell is zS_i, and the probability of finding an Fe atom at a given site in the i^{th} shell, that is connected to the Fe atom at site O, is zP_i. Then the probability, P_A that, if an Fe atom is located at site O, it is not connected to another Fe atom at any site in shells i = 1 through 9 is given by

$$P_A = \prod_{i=1}^{9} (1-zP_i)^{S_i} \qquad (25a)$$

From Eq. 25a, the concentration of isolated single-Fe clusters is

$$c_1 = z \prod_{i=1}^{9} (1-zP_i)^{Si} \qquad (25)$$

In calculating the concentration of Fe-pair clusters, one has to be careful not to count pairs which are parts of triplets or of larger configurations. The probability that an Fe atom A is connected to another Fe atom B located at any one of the S_i sites in its i-shell, but is not connected to any other Fe atom in any of the remaining (S_i-1) sites on its i-shell, or in any site on its shells $\underline{j}$ = 1 through 9 $(j \neq i)$, is

$$z\, P_i S_i (1-zP_i)^{S_i-1} \prod_{\substack{j=1 \\ j\neq i}}^{9} (1-zP_j)^{S_j}. \qquad (26a)$$

In calculating ${}_iP_{AB}$, the probability of a given Fe atom A being part of a doublet, with another Fe atom B in its i-shell, one also has to ensure that the Fe atom B, in its turn, is connected only to one Fe atom, namely A, which is in the i^{th} shell of B. Then ${}_iP_{AB}$ is

$${}_iP_{AB} = \left[zP_i S_i (1-zP_i)^{S_i-1} \prod_{\substack{j=1 \\ j\neq i}}^{9} (1-zP_j)^{S_j} \right] \cdot$$

$$\left[(1-zP_i)^{(S_i-1)-{}_iS_i} \prod_{\substack{k=1 \\ k\neq i}}^{9} (1-zP_k)^{S_k-{}_iS_k} \right] \qquad (26)$$

where S_k is the co-ordination number of the k^{th} shell of B and ${}_iS_k$ is the number of sites on the k^{th} shell of B that are located also on any of the 1^{st} through 9^{th} shell of A. The Fe

atom B has a total of 146 connectable sites; the atom A is occupying one of these. Of the remaining 145 sites there are $\sum_{k=1}^{9} {}_iS_k$ sites which are among the 145 sites connectable to A. In the first factor in Eq. 26 the condition that none of these common connectable sites have an Fe atom is incorporated. Hence, in the second factor in Eq. 26 these sites were excluded from consideration. Equation 26 can be rewritten as follows:

$$ {}_iP_{AB} = \left[z \prod_{i=1}^{9} (1-zP_i)^{S_i} \right] \left[\frac{P_i S_i}{(1-zP_i)^2} \prod_{k=1}^{9} (1-zP_k)^{S_k - {}_iS_k} \right] $$

$$ = \left[z \prod_{j=1}^{9} (1-zP_j)^{S_j} \right] \left[\frac{P_i S_i}{(1-zP_i)^2} \prod_{k=1}^{9} (1-zP_k)^{S_k - {}_iS_k} \right] \qquad (27) $$

It may be noted that only the second factor in Eq. 27 depends on the value of i. Now, summing over all nine shells, the fraction of Fe atoms in doublets is:

$$ P_{Fe-Fe} = \sum_{i=1}^{9} {}_iP_{AB} = \left[z \prod_{j=1}^{9} (1-zP_j)^{S_j} \right] \cdot $$

$$ \sum_{i=1}^{9} \left[\frac{P_i S_i}{(1-zP_i)^2} \prod_{k=1}^{9} (1-zP_k)^{S_k - {}_iS_k} \right] \qquad (28) $$

The concentration of Fe-pair clusters is

$$c_2 = \frac{1}{2} z \left[z \prod_{j=1}^{9} (1-zP_j)^{S_j} \right] \sum_{i=1}^{9} \left[\frac{P_i S_i}{(1-zP_i)^2} \prod_{k=1}^{9} (1-zP_k)^{S_k - {}_iS_k} \right] \quad (29)$$

The ratio of the concentrations of Fe-pair clusters to single-Fe clusters, from Eq. 29 and Eq. 25, is then:

$$\frac{c_2}{c_1} = \frac{1}{2} z \sum_{i=1}^{9} \left[\frac{P_i S_i}{(1-zP_i)^2} \prod_{k=1}^{9} (1-zP_k)^{S_k - {}_iS_k} \right] \quad (30)$$

With the help of a computer program (Appendix B) the numbers ${}_iS_k$ were determined for k = 1 through 9 for each value of i = 1 through 9. These numbers are listed in Table 44. The ratio c_2/c_1 was computed from Eq. 30 with the aid of another program (Appendix C) for different values of the Fe concentration, z, and of the Ni concentration, x. Figure 57(a) shows the calculated values of c_2/c_1 as compared with the experimental values derived from the analysis of magnetization data (Tables 36 through 41). As described in the section on Data Analysis, the c_2 and c_1 values for quenched alloys were estimated assuming that the ratio c_2/c_1 is a function of a single parameter ${}_{Fe\text{-}Fe}\alpha_1$ expressing the clustering tendency of Fe atoms. The c_2 and c_1 values for deformed alloys were derived without making the above assumption; i.e., c_1 and c_2 were set to be independent of each other. For both quenched and deformed alloys the experimental c_2/c_1 ratios are much higher than the values calculated from Eq. 30, i.e., on the basis of the random alloy model of Bennett et al.[4] The c_2/c_1 ratios for the quenched alloys are systematically

Table 44. The number ${}_iS_k$ of sites on the k^{th} shell of atom B, which are shared with the 1^{st} through 9^{th} shells of atom A.

i \ k	1	2	3	4	5	6	7	8	9	9a	$\sum_k {}_iS_k$
1	11	6	24	12	22	6	32	4	5	10	132
2	12	5	24	8	20	4	24	1	4	12	114
3	12	6	18	9	14	5	22	3	5	10	104
4	12	4	18	6	12	2	24	2	5	10	95
5	11	5	14	6	10	4	20	2	4	6	82
6	9	3	15	3	12	3	18	3	3	9	78
7	8	3	11	6	10	3	15	2	3	7	68
8	8	1	12	4	8	4	16	0	4	4	61
9	5	2	10	5	8	2	12	2	4	8	58
9a	5	3	10	5	6	3	14	1	4	5	56

Figure 57. Experimental and calculated (on the basis of random alloy model) values of c_2/c_1.

(a) The values of c_2/c_1 estimated in the present work for quenched (Q) and deformed (D) alloys as a function of Fe and Ni content (x = 0.1, 0.2, 0.3) as compared to values calculated using Eq. 30 (BSW).

(b) c_2/c_1 values estimated in the present work for quenched alloys with ~100 ppm Fe cross plotted from Fig. 57(a), as compared to values calculated using Eq. 30 (BSW).

Note: The experimental value of c_2/c_1 for 100 ppm Fe in $Cu_{0.7}Ni_{0.3}$ may involve some error due to the clustering tendency in this alloy of the Ni atoms, giving rise to magnetic dipoles.[1]

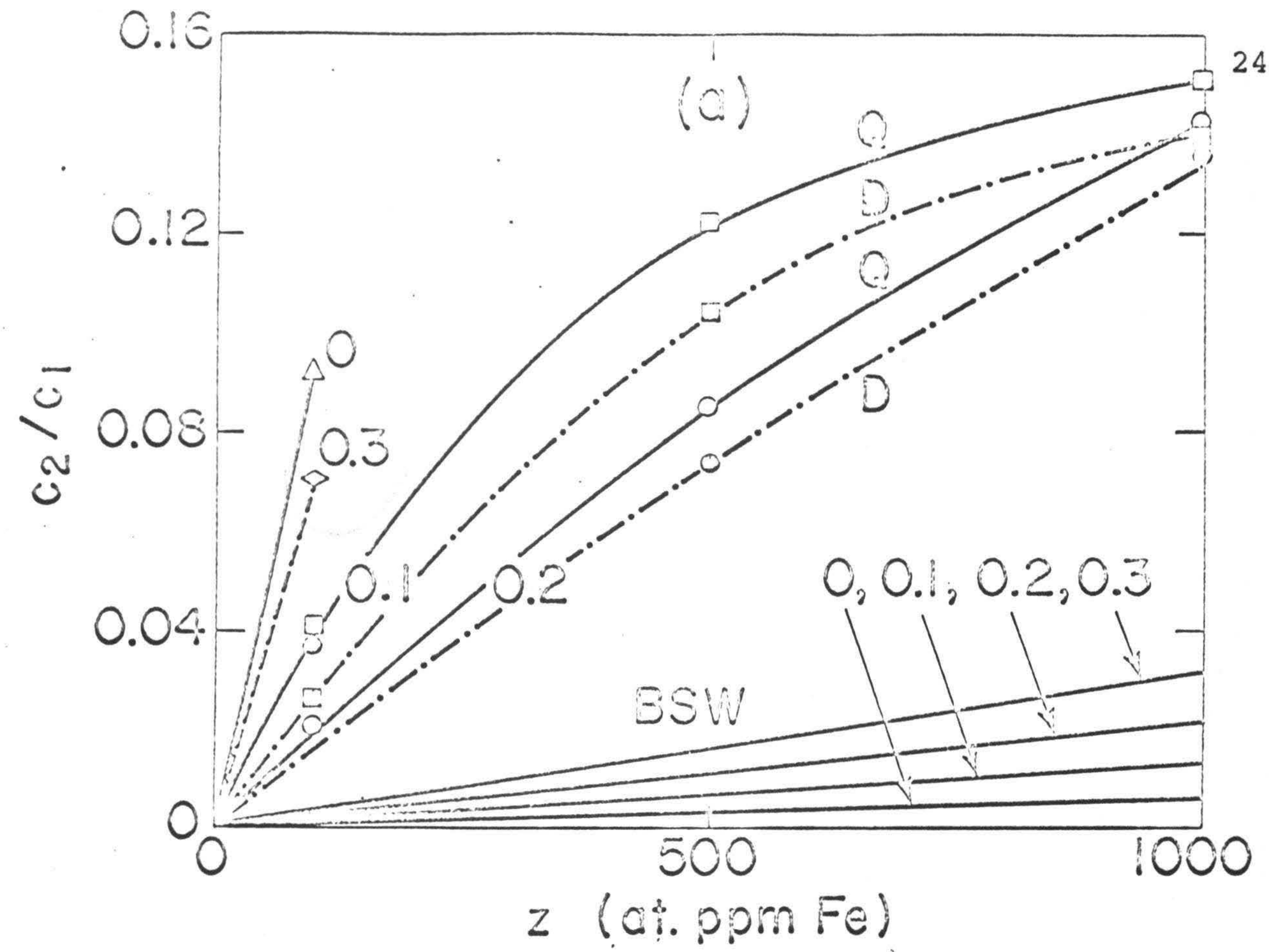
(a)
0.16
0.12
0.08
0.04
0
c_2/c_1
Q
D
Q
D
0
0.3
0.1
0.2
0, 0.1, 0.2, 0.3
BSW
0
500
1000
z (at. ppm Fe)

(b)
0.08
0.04
0
0.004
0.002
c_2/c_1
Q
BSW
0
0.1
0.2
0.3
x (at. fraction Ni)

higher than the corresponding ratios for deformed alloys, suggesting that quenched alloys have more clustering than deformed alloys, although the latter are certainly not random either.

The connection probabilities and hence the Fe pair concentration and thus the ratio c_2/c_1 can be increased by assuming that, while the Fe atoms are randomly distributed, there is a tendency for the Ni atoms to cluster around the Fe atoms, i.e., x_1, the effective Ni concentration in the nearest neighbor shell of all Fe atoms is higher than x, the overall Ni concentration in the alloy. Figure 58 shows that the assumption of the highest possible value of x_1, namely 1, is not sufficient to bring about agreement of the calculated c_2/c_1 values with those experimentally evaluated for the quenched $Cu_{0.9}Ni_{0.1}$ and $Cu_{0.8}Ni_{0.2}$ alloys containing 1000 ppm Fe. This is also true for all the other alloys containing 100 or 500 ppm Fe.

An interesting feature of the random alloy model of Bennett et al.[4] is that it predicts that, for a given Fe concentration, the c_2/c_1 ratio should increase with the Ni concentration. In Fig. 57(b) one finds that for an Fe concentration of about 100 ppm the c_2/c_1 ratio for quenched alloys, as estimated from experimental data, decreases with increasing Ni content up to 20 at. % Ni. The increase in the estimated value of c_2/c_1 between 20 at. % Ni and 30 At. % Ni may not be real; the situation is complicated by the presence of Ni-rich magnetic clusters.[1] In any case, at least up to 20 at. % Ni the dependence of the c_2/c_1 ratio on the Ni concentration as predicted by the random

Figure 58. c_2/c_1 vs. x_1. The assumption of a value of x_1 (the effective Ni concentration in the nearest neighbor shells of all Fe atoms) even as high as 1 is seen not to be sufficient to give high enough c_2/c_1 ratios from calculations based on Eq. 30 to be comparable to the experimentally evaluated values for quenched $Cu_{0.8}Ni_{0.2}$ and $Cu_{0.9}Ni_{0.1}$ alloys containing 1000 ppm Fe.

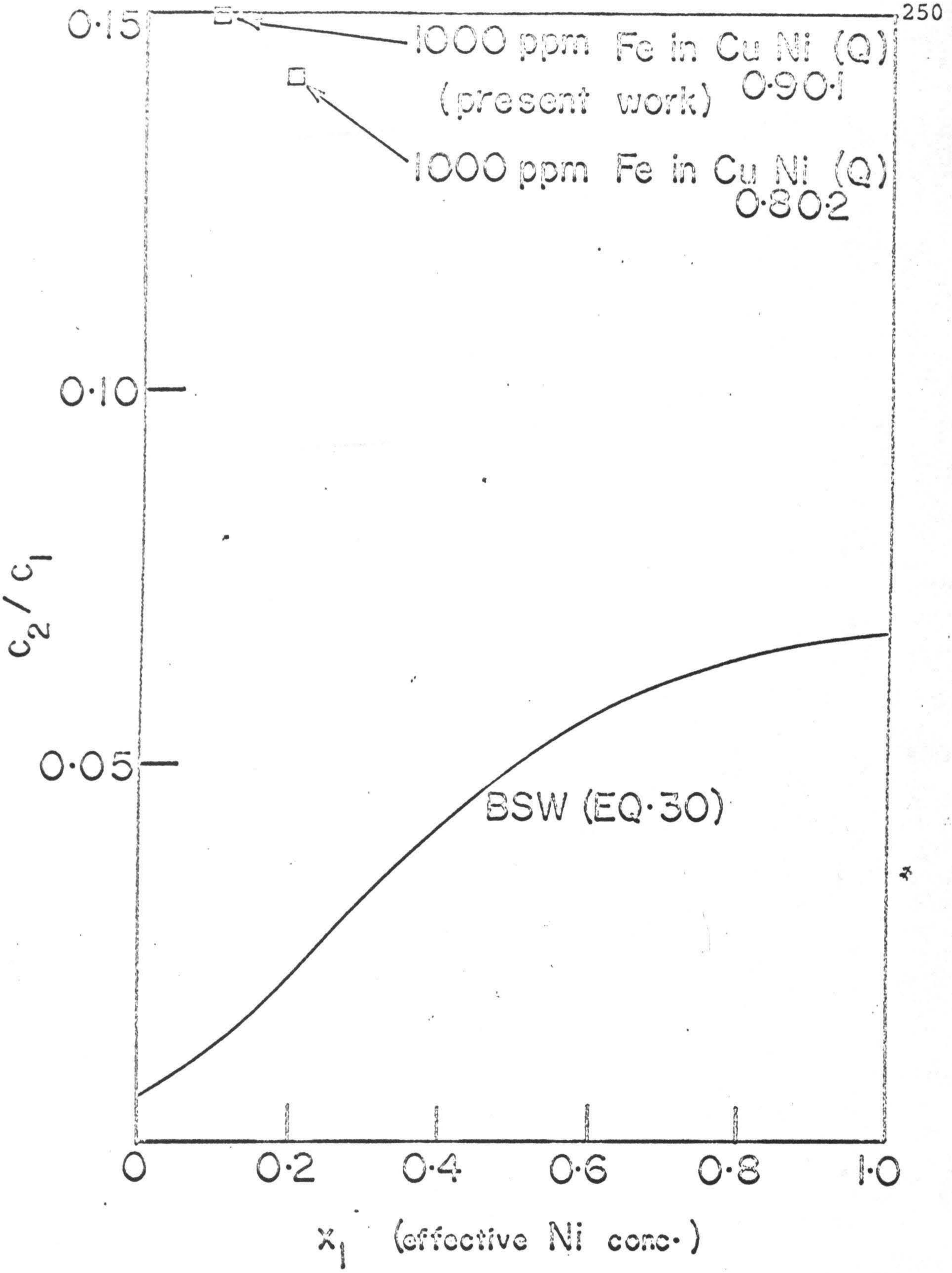
0·15
0·10
0·05
c_2 / c_1
1000 ppm Fe in Cu Ni (Q) 0·901
(present work)
1000 ppm Fe in Cu Ni (Q) 0·802
BSW (EQ·30)
250
0
0·2
0·4
0·6
0·8
1·0
x_1 (effective Ni conc·)

alloy model of Bennett et al.[4] is the opposite of that obtained from the analysis of the experimental data.

One may conclude that in quenched Cu-Ni-Fe alloys there is a tendency for the Fe atoms to cluster. The c_2/c_1 ratios are then well represented by the $_{Fe\text{-}Fe}\alpha_1$ values listed in Tables 37, 38, and 39. It has already been pointed out that for Cu-Fe alloys there is Mössbauer spectroscopic evidence, based on the interpretation of isomer shift and line shape data,[7,8] that Fe atoms tend to form Fe-Fe pairs or larger atomic clusters with nearest neighbor Fe atoms. Window et al.[5] have concluded from isomer shift and quadrupole splitting in the Mössbauer spectra of dilute ^{57}Fe in copper-rich Cu-Ni alloys, that here, too, the Fe atoms have a tendency to cluster. The results of the present investigation are consistent with the finding of Window et al.[5] The values of the short range order parameter $_{Fe\text{-}Fe}\alpha_1$, as evaluated in the present work as a function of Fe and Ni contents, are shown in Fig. 59(a). $_{Fe\text{-}Fe}\alpha_1$ increases with the Fe concentration but decreases with the Ni concentration, at least up to 20 at. % Ni. We define a parameter D by the following equation:

$$D = \frac{z_1}{z} \tag{31}$$

D represents the degree of nonrandomness of the Fe atoms and expresses the increase in the Fe concentration in the nearest neighbor shells of all Fe atoms, over the overall Fe content of the alloy. For a truly random solution $z_1 = z$ and $D = 1$. As seen in Fig. 59(b), for a given Ni concentration D decreases

Figure 59. $Fe\text{-}Fe^{\alpha}{}_1$ and D vs. z.

(a) $Fe\text{-}Fe^{\alpha}{}_1$ for quenched alloys as a function of Fe and Ni content ($x = 0$, 0.1, 0.2, 0.3) from magnetic data.

(b) D for quenched alloys as a function of Fe and Ni content, evaluated from magnetic data.

Note: The $Fe\text{-}Fe^{\alpha}{}_1$ and D values for 100 ppm Fe in $Cu_{0.7}Ni_{0.3}$ may involve some error due to the clustering tendency in this alloy of Ni atoms, giving rise to magnetic dipoles.[1]

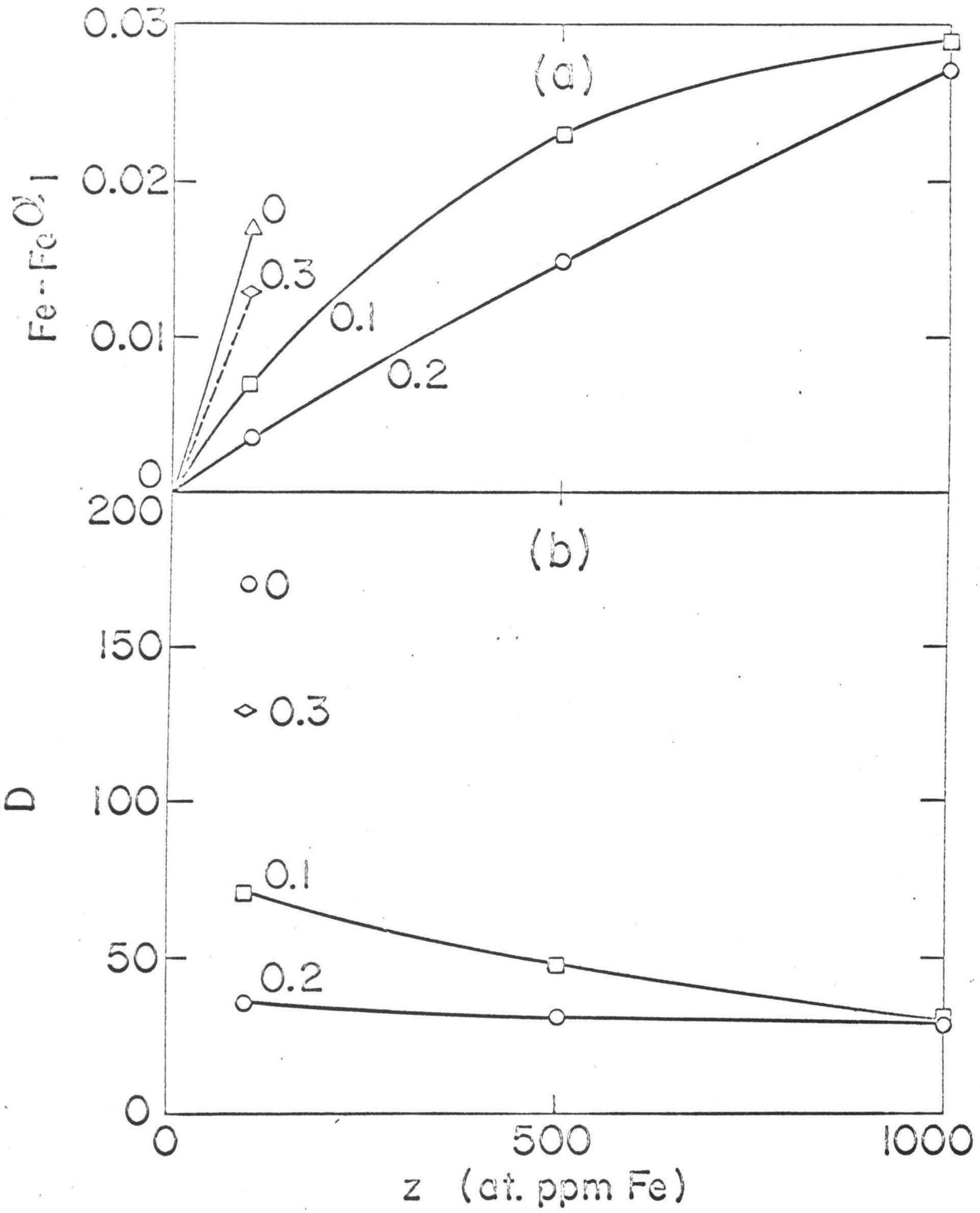
0.03
0.02
0.01
0
Fe - Fe'
(a)
0
0.3
0.1
0.2
200
150
100
50
0
(b)
0
0.3
0.1
0.2
0
500
1000
z (at. ppm Fe)

with increasing Fe content, i.e., the alloys approach randomness. Thus the most dilute solid solutions of Fe in copper-rich Cu-Ni alloys are the most nonrandom as far as the distribution of the Fe atoms is concerned. This very interesting feature has also been observed in deformed Cu-Fe alloys by Campbell et al.[8]

It has already been shown that for quenched alloys the average value of μ_1, the single-Fe cluster moment, increases (Fig. 55) from 2.44 μ_B in pure Cu to 5.2 μ_B in $Cu_{0.7}Ni_{0.3}$. Fe is known to have a moment of 3.1 μ_B in pure Ni.[32] Hence on a weighted average basis the moment on an Fe atom may be expected to change from 2.44 μ_B in Cu to $\sim$2.61 μ_B in $Cu_{0.7}Ni_{0.3}$. Clearly the μ_1 values can not be interpreted as the moment of Fe alone. A simple interpretation would be that those Ni atoms which are nearest neighbors to an Fe atom, have moments and that the moment on the Fe atom and the adjacent Ni moments are aligned with one another, forming a magnetic cluster.[3,2] Two interesting questions that follow are: (a) How much does each Ni contribute to the cluster moment? (b) How many nearest neighbor Ni atoms are there on the average around each Fe? Making a simple assumption that the moment μ_o on a Ni atom nearest neighbor to an Fe atom is independent of the number of Ni atoms in its own (i.e., of the Ni atom in question) nearest and second nearest neighbor shells, the cluster moment μ_1 can be expressed in the following way:

$$\mu_1(x) = \mu_{Fe}\ (x_1) + 12\ \mu_o\ x_1 \qquad (32)$$

where $\mu_{Fe}(x_1)$ is the moment on the Fe atom, which depends upon the concentration x_1 of Ni atoms in its nearest neighbor shell. On a weighted average basis,

$$\mu_{Fe}(x_1) = 2.44 + (3.1 - 2.44)x_1 \tag{33}$$

If one assumes further that x_1 is a simple function of x, the overall Ni concentration in the alloy, i.e.,

$$x_1 = x(1+ax^n) \tag{34}$$

then Eq. 32 can be rewritten as:

$$\mu_1(x) = 2.44 + (0.66 + 12\,\mu_o)(1+ax^n) \tag{35}$$

The parameter values μ_o, a, and n were estimated by fitting Eq. 35 to the μ_1 values for quenched alloys (Fig. 55). The parameter values obtained are: $\mu_o = 0.225\ \mu_B$, a = 11.52, and n = 1.57. The Fe-Ni nearest neighbor short range order parameter $_{Fe\text{-}Ni}\alpha_1$ may then be estimated from the relation:

$$x_1 = x + (1 - x)\ {}_{Fe\text{-}Ni}\alpha_1 \tag{36}$$

The values of $_{Fe\text{-}Ni}\alpha_1$ for different alloys are listed in Table 45 and shown in Fig. 60. The results indicate that $_{Fe\text{-}Ni}\alpha_1$ increases with the Ni content. For the 10 and 20 at. % Ni alloys the $_{Fe\text{-}Ni}\alpha_1$ values as a function of the Fe content show some scatter which is however seen to be random and not systematic. The positive average value of $_{Fe\text{-}Ni}\alpha_1$ for a given Ni content suggests clustering of Ni around Fe, consistent with the

Table 45. Results for quenched alloys for the effective concentration, x_1, of Ni atoms in the nearest neighbor shells of isolated Fe atoms, and the Fe-Ni short range order parameter $_{Fe\text{-}Ni}\alpha_1$. See Figure 59.

x (at. fraction Ni)	z (at. ppm Fe)	x_1 (at. fraction Ni)	$_{Fe\text{-}Ni}\alpha_1$
0.1	100	0.077	-0.025
0.1	500	0.161	0.067
0.1	1000	0.155	0.061
0.2	100	0.393	0.241
0.2	500	0.321	0.152
0.2	1000	0.431	0.289
0.3	100	0.821	0.745

Figure 60. $Fe\text{-}Ni\alpha_1$ as a function of Fe and Ni content (see Table 45) for quenched alloys. The value of $Fe\text{-}Ni\alpha_1$ for 100 ppm Fe in $Cu_{0.7}Ni_{0.3}$ may involve some error due to the clustering tendency in this alloy of the Ni atoms, giving rise to magnetic dipoles.[1]

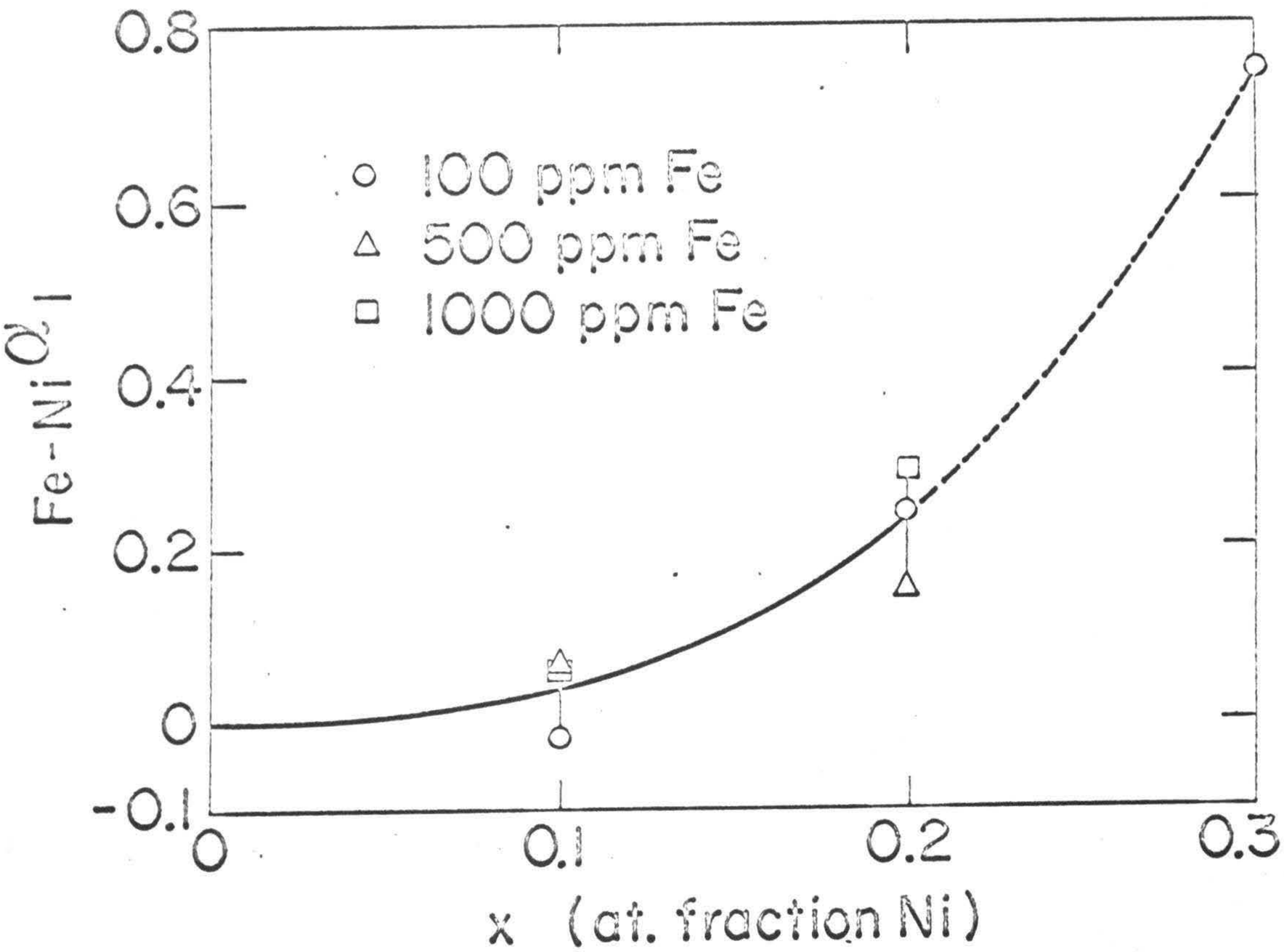
0.8
0.6
0.4
0.2
0
-0.1
0
0.1
0.2
0.3
Fe-Ni α_1
100 ppm Fe
500 ppm Fe
1000 ppm Fe
x (at. fraction Ni)

conclusions of Window et al.[5] Clearly the random alloy model of Bennett et al.[4] is inappropriate for quenched Cu-Ni-Fe alloys.

The effect of deformation is to decrease the magnetization (e.g., Fig. 53). In Table 42 it is seen that the magnitude of the percent decrease in the magnetization, at 4.2°K in an applied field of ∿12.6 kOe, does not vary systematically with the composition. One of the principal reasons is that in the present work no attempt was made to deform the various specimens to exactly the same degree. In any case, as seen in Fig. 57 deformation of quenched alloys tends to partially randomize the Fe-Fe clustering, as evidenced by the systematic decrease in the c_2/c_1 ratios. Another semiquantitative observation that may be made with respect to the effect of deformation is that the μ_1 values systematically decrease (Tables 37 through 41), suggesting a partial randomization of the Fe-Ni clustering as well. Both results are consistent with the conclusions of Window et al.[5] Window et al.[5] also concluded that even in heavily rolled samples there remained some degree of Fe-Ni clustering. Thus, it is difficult to obtain a truly random Cu-Ni-Fe alloy. The results of Bennett et al.[4] indicated that the single Fe cluster moment μ_1 for a $Cu_{0.79}Ni_{0.21}$ alloy is the same (∿ 4.2 μ_B) in both quenched and deformed (cold rolled to ∿10% of the original thickness, i.e., ∿90% reduction of area) conditions. This is inconsistent with the results of the present work and with those of Window et al.[5] Bennett et al.[4] found that for 0.5% Fe in $Cu_{0.79}Ni_{0.21}$ the c_2/c_1 ratio decreased

by ∿50% on deformation. This need not be inconsistent with the smaller change in the c_2/c_1 ratios (Fig. 57) obtained in the present work, since (a) the Fe concentration used by Bennett et al.[4] was five times higher than the maximum in the present investigation and it is expected that there were present in the quenched alloy larger clusters, containing more than three or four Fe atoms, which would have been easier to break up, and (b) the amount of deformation given to the specimens was much higher. It should be noted that the large change in the c_2/c_1 ratio observed by Bennett et al.[4] would be very difficult to explain on the basis of their own random alloy model.[4]

Window et al.[5] concluded, from the hyperfine splitting in the Mössbauer spectra that $(Cu_{0.9}Ni_{0.1})_{0.99}Fe_{0.01}$ and $(Cu_{0.8}Ni_{0.2})_{0.99}Fe_{0.01}$ alloys are magnetically ordered at 1.4°K; the ordering temperature lies between 3 and 4.2°K in the as rolled state, and increases to above 4.2°K for annealed specimens. Bennett et al.[11] claimed that the above two alloys are ferromagnetically ordered with ordering temperatures of 6.2°K and 5.8°K respectively. Results of the present investigation indicate a remanence temperature T_r of ∿2.1°K (Fig. 24) for quenched $(Cu_{0.9}Ni_{0.1})_{0.99}Fe_{0.01}$, much lower than the Mössbauer ordering temperature.[11] Another result of the present work that is important in evaluating the above conclusions is that below 4.2°K the magnetization vs. temperature graph (Fig. 30) shows thermomagnetic history effects. Thus the quenched $(Cu_{0.9}Ni_{0.1})_{0.99}Fe_{0.01}$ alloy is evidently mictomagnetic. The quenched $(Cu_{0.8}Ni_{0.2})_{0.99}Fe_{0.01}$ alloy shows no remanence

(Fig. 25) even at 1.57°K, a temperature quite low compared to the reported Mössbauer ordering temperature.[11] This suggests that the $(Cu_{0.8}Ni_{0.2})_{0.99}Fe_{0.01}$ alloy is also mictomagnetic. Though no thermomagnetic history effect was observed for this alloy in a 1000 Oe field (Fig. 31) it may be expected that such effects would be observable at a lower applied field,[13] and, particularly, at temperatures lower than 1.57°K.

C. Cu-Ni

For the quenched $Cu_{0.7}Ni_{0.3}$ alloy the value of the average permanent moment $\bar{\mu} = 0.00036\ \mu_B$ agrees well with the results of Cornut et al.[33]

For $Cu_{0.6}Ni_{0.4}$, the magnetization values and susceptibilities below 160°K are higher in the aged than in the as-quenched condition (Figs. 17 through 20). Analogous increases in the magnetization as a result of aging have previously been reported.[16,34] Comparing the parameter values for the $Cu_{0.6}Ni_{0.4}$ alloy (Table 35) in the as-quenched and the aged condition, one notes that the most important change on aging is the increase in the average moment of the large magnetic clusters from ∿23 to 29 μ_B. The average moment of the small magnetic clusters does not change perceptibly on aging. Robbins et al.[16] pointed out that in Cu-Ni alloys Ni-rich atomic clusters give rise to magnetic clusters which are responsible for the observed superparamagnetism,[35,36] the low temperature specific heat anomaly,[37,16] and the changes in the magnetization upon low

temperature aging and plastic deformation.[16] Low temperature aging allows the atomic (and, hence, of the magnetic) clusters to grow in size. The present results for $Cu_{0.6}Ni_{0.4}$ are totally consistent with such an interpretation. The considerable increase of the average moment of the large clusters on aging implies a substantial increase in the short range order parameter $_{Ni\text{-}Ni}\alpha_1$. There is no reason to assume that in 3 days the short range order parameter has already attained its equilibrium value on aging at 300° C. It is even possible that in true equilibrium at 300° C the alloy $Cu_{0.6}Ni_{0.4}$ would consist of two phases.

Although the physical significance of the bimodal distribution of cluster moments in the $Cu_{0.6}Ni_{0.4}$ alloy is as yet not clearly understood, it seems quite possible that it is related to a higher degree of atomic clustering at grain boundaries than within the grains, because the grain boundary diffusion rate is higher. This explanation is consistent with the observation that aging at 300° C increases the larger moments much more than the smaller ones. The proposed explanation could be tested by magnetic measurements with a single crystal specimen of the same alloy.

For the quenched $Cu_{0.6}Ni_{0.4}$ alloy the average moment value of $\sim 5.3\ \mu_B$ for the small clusters is smaller and that of $\sim 23\ \mu_B$ for the large clusters is larger than the average moment of about 10 μ_B reported by Hicks et al.[38] from neutron scattering study of weakly ferromagnetic Cu-Ni alloys (46 to 50 at. % Ni) and by Kouvel and Comly[22] on the basis of magnetization

measurements for paramagnetic Cu-Ni alloys containing 32 to 44 at. % Ni. (For quenched $Cu_{0.6}Ni_{0.4}$ a single moment Brillouin analysis of the magnetization data yields an average moment of $\sim$17 μ_B, substantially higher than $\sim$10 μ_B.) The method of analysis used by Kouvel and Comly[22] precluded the possibility of noticing a bimodal moment distribution. The present results for a $Cu_{0.7}Ni_{0.3}$ alloy show that the average moment per cluster in the quenched state is about $\sim$2.8 μ_B. These results suggest that the interpretation of their bulk magnetization data by Kouvel and Comly[22] in terms of an average cluster moment, that remains constant at about $\sim$10 μ_B from 32 to 44 at. % Ni may be incorrect. Cornut et al.[33] also concluded that the giant moments in Cu-Ni alloys are concentration dependent. Earlier magnetization results of Van Elst et al.[35] indicated a large moment of $\sim$60 μ_B for a $Cu_{0.6}Ni_{0.4}$ alloy. However this alloy, as evidenced by the appearance of remanence in the liquid helium temperature range, may have contained a considerable level of Fe impurity (spectroscopic analysis of a specimen of their $Cu_{0.7}Ni_{0.3}$ alloy, kindly made available to us by Prof. Van Den Berg, indicated an Fe level of $\sim$121 ppm). The more recent magnetization results of Acker and Huguenin[34] for $Cu_{0.6}Ni_{0.4}$ have been interpreted in terms of magnetic clusters with average sizes of $\sim$8 μ_B and $\sim$40 μ_B. Qualitatively the present results may be considered to be in agreement with theirs, particularly since the magnetization data used by Acker and Huguenin[34] were limited to a relatively narrow temperature range.

In Fig. 61 the values of χ_o, the temperature- and field-independent susceptibility, are shown as a function of the Ni concentration. There is good agreement with the results of Pugh et al.[36] χ_o may be interpreted as the band susceptibility of the matrix. From Fig. 60 it is seen that χ_o increases monotonically with increasing Ni content. Conversely the magnitude of χ_o is a very good index of the Ni content of the matrix. However, when the Ni concentration is greater than ∿20 at. %, Ni-rich clusters are formed, so that the Ni content of the matrix is lower that the average Ni content of the alloy as a whole. Thus the value of $\chi_o = 1.61 \times 10^{-6}$ emu/g (Table 35[b]) for quenched $Cu_{0.6}Ni_{0.4}$ represents a matrix with less than 40 at. % Ni, and the decrease in the value of χ_o to 1.15×10^{-6} emu/g on aging (Table 35[b]) suggests a further reduction in the Ni content of the matrix due to the increase in the size and the concentration of the Ni-rich clusters. In a simplified picture, the decrease in χ_o on aging directly corresponds to the increase in the average moment per atom from $\bar{\mu} = 0.0097\ \mu_B$ in the quenched condition to $0.0115\ \mu_B$ in the aged condition. If one assumes that the average moment $\bar{\mu}_{Ni}$ per Ni atom in a cluster is the same for both the quenched and the aged specimen of $Cu_{0.6}Ni_{0.4}$, then

$$\bar{\mu}_{Ni} = \frac{0.0097}{0.4 - x_q} = \frac{0.0115}{0.4 - x_a} \qquad (37)$$

where x_q represents the Ni concentration in the matrix of quenched $Cu_{0.6}Ni_{0.4}$, and x_a represents that of the aged alloy.

Figure 61. χ_o vs. at. fraction Ni. Open circles: present data for quenched alloys; filled circle: present result for an aged $Cu_{0.6}Ni_{0.4}$ alloy; triangles: Pugh et al.;[36] squares: Kouvel and Comly.[22] The dashed line represents suggested variation of χ_o as a function of the Ni content of the matrix.

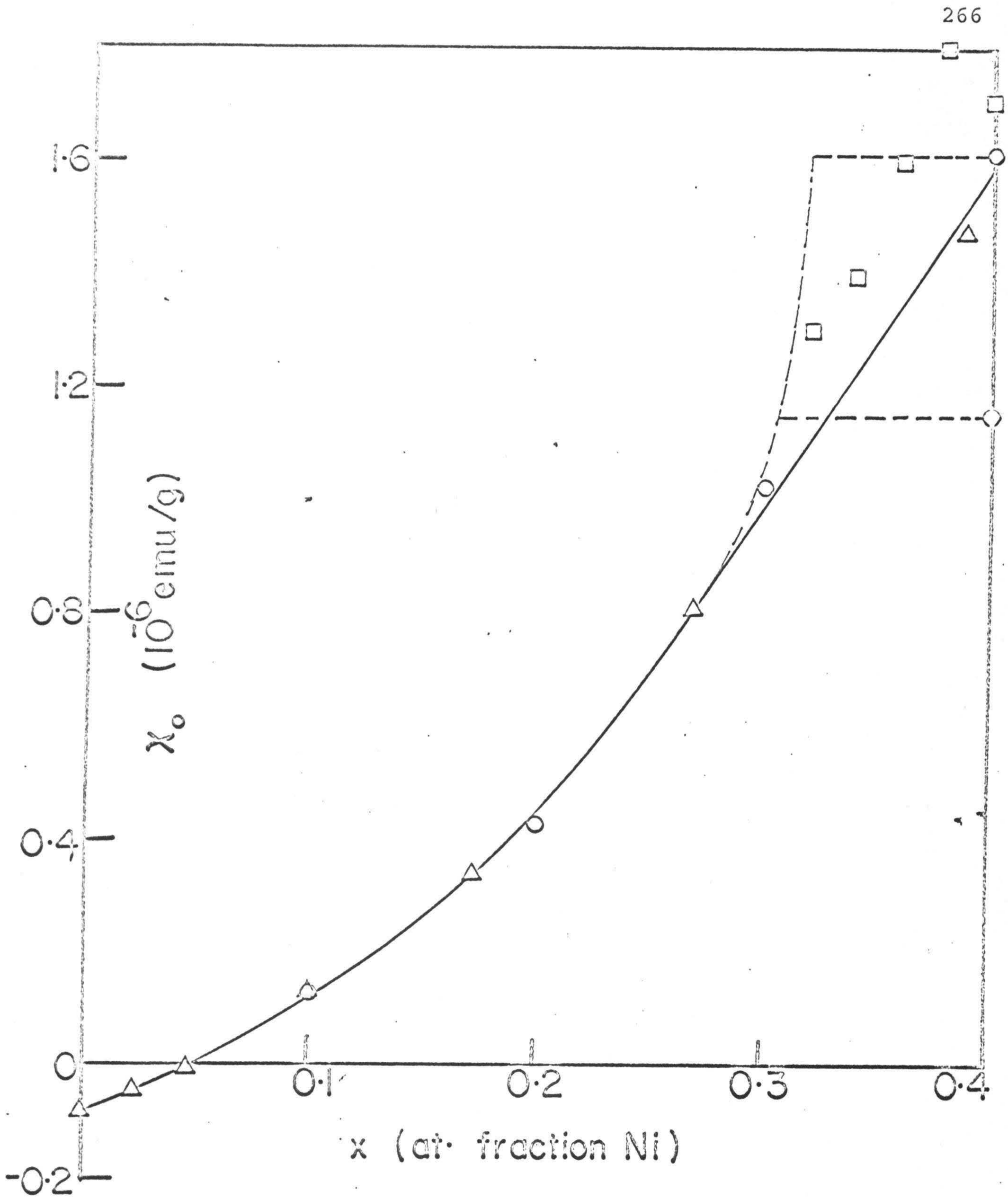
266
·6
·2
0·8
χ_o (10^{-6} emu/g)
0·4
0
0·1
0·2
0·3
0·4
-0·2
x (at· fraction Ni)

There are many possible solutions of Eq. 37. However, to obtain a physically meaningful solution, one may assume (a) $\bar{\mu}_{Ni}$ is less than 0.6 μ_B, the moment on a Ni atom in pure Ni, (b) x_a is greater than 0.3 since χ_o for the $Cu_{0.7}Ni_{0.3}$ alloy, where only a small fraction of the Ni atoms may be in clusters, is lower than that for aged $Cu_{0.6}Ni_{0.4}$, and (c) the x_q and x_a values must be such that when plotted against the experimental χ_o values, the points should lie on a reasonable extrapolation of the χ_o vs. x curve (Fig. 61) for lower Ni concentrations. These conditions are satisfied for a choice of $x_q = 0.32$ and $x_a = 0.305$. The dashed curve in Fig. 61 then represents χ_o versus Ni concentration in the matrix.

One may assume that the temperature- and field-independent susceptibility is

$$\chi_o = \chi_p + \chi_v + \chi_L + \chi_c \tag{38}$$

where χ_p and χ_v are the Pauli (spin) and Van Vleck (orbital) components of the paramagnetic susceptibility and χ_L and χ_c represent the Landau (spin) and ion-core diamagnetic susceptibilities. The value of χ_p (in emu/g) can be calculated from the electronic specific heat co-efficient γ (in 10^{-4}cal/mole-°K^2),

$$\chi_p = \frac{3\mu_B^2\gamma\beta}{\pi^2 k^2 M(1+\lambda)} \tag{39}$$

where $\beta = 4.184 \times 10^3$ ergs/cal, and $(1+\lambda)$ is the electron-phonon enhancement factor for the electronic specific heat. Assuming the electron-phonon enhancement factor to be equal to 1, χ_p was

computed for copper-rich Cu-Ni alloys from the corresponding γ values reported in the literature[39] and is presented in Fig. 62(a). For pure Cu the measured value of χ_o is -0.088×10^{-6} emu/g[36] and the value of χ_p (calculated from γ) is 0.151×10^{-6} emu/g. Assuming $\chi_v \simeq 0$ and $\lambda = 0$, the total diamagnetic susceptibility, i.e., $(\chi_L + \chi_c)$ for pure Cu is -0.239×10^{-6} emu/g. If one further assumes that the diagmagnetic component does not change with the addition of Ni to Cu,[36] χ_p for Cu-Ni alloys can also be estimated from the experimentally determined χ_o values, using Eq. 38. The χ_p values so obtained from the susceptibility data are seen in Fig. 62(a) to be systematically higher than the corresponding values obtained from specific heat results. The Stoner enhancement (S) of the susceptibility[40] for Cu-Ni alloys was estimated from the relation:

$$S = \frac{\chi_p(\text{from susceptibility data})}{\chi_p(\text{from specific heat data})} \qquad (40)$$

The Stoner enhancement factor is presented in Fig. 62(b) as a function of the Ni concentration and is seen to increase with the Ni content. One may postulate that for Ni concentrations higher than 15 at. % the γ values (and the χ_p values derived from them) might have been increased due to a magnetic contribution[41] due to the interaction of the magnetic moment on some Ni atoms[1,2] with a very weak ambient field as described by Marshall for dilute alloys.[42] One may assume that, under such conditions a linear extrapolation of the χ_p values (from specific heat data) from below 15 at. % Ni to higher concentrations

Figure 62. χ_p and S vs. at. fraction Ni.

(a) The Pauli susceptibility χ_p, as calculated from the electronic specific heat coefficient γ [39] (1), and as estimated from the susceptibility data (2). The dashed line (1') is a linear extrapolation to higher Ni concentrations of the χ_p values at and below ∿0.1 at. fraction Ni.

(b) The stoner enhancement factor S; as calculated from curves (1) and (2) in Fig. 62(a).

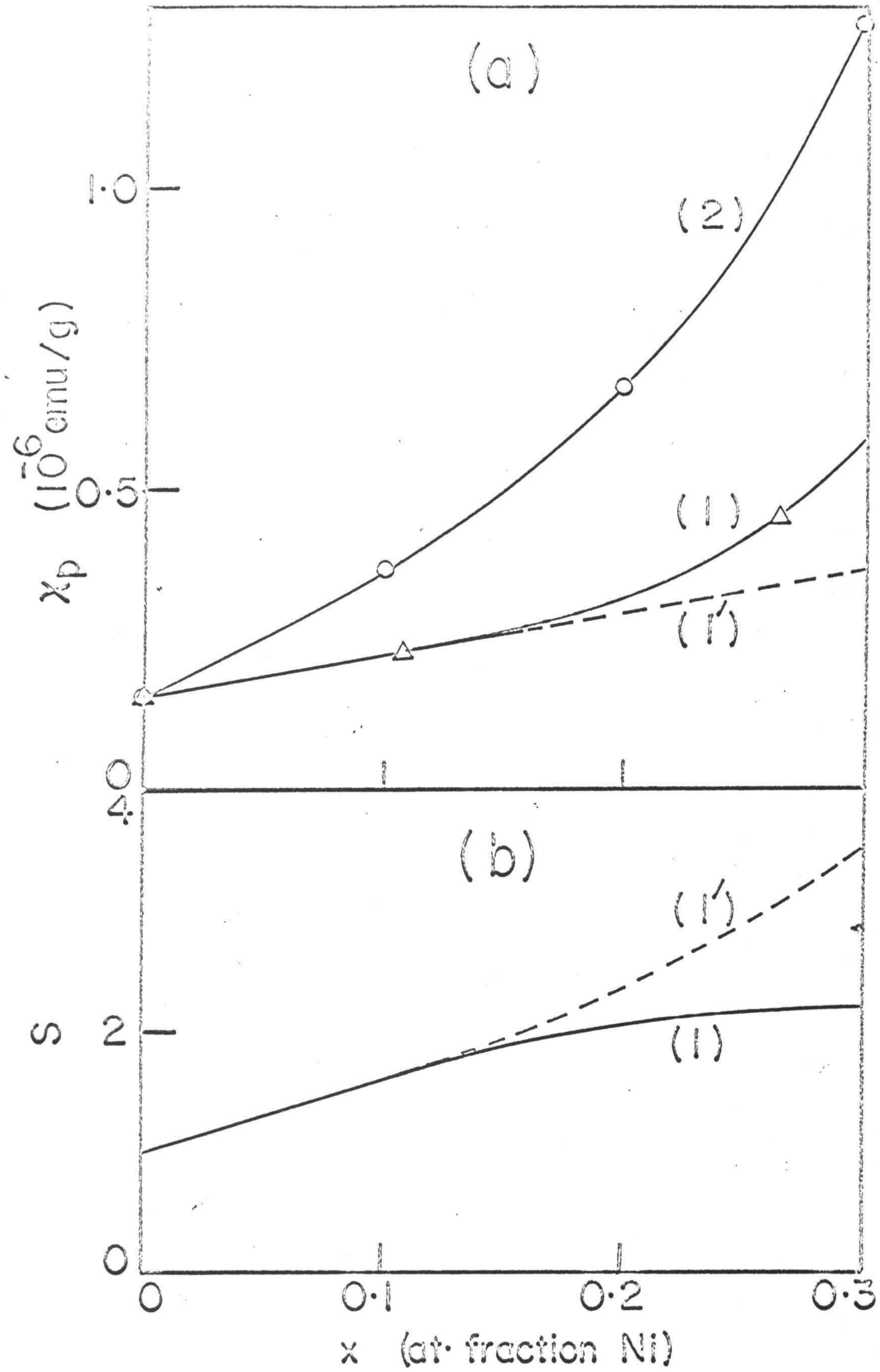
270
(a)
1·0
0·5
0
χ_p (10^{-6} emu/g)
(2)
(1)
(1′)
(b)
(1′)
(1)
S
2
0
0
0·1
0·2
0·3
x (at· fraction Ni)

(line (1') in Fig. 62[a]) may represent more accurately the variation of χ_p with the Ni content than the χ_p calculated directly from the measured γ values (Line [1] in Fig. 62[a]). The corresponding higher rate of increase of the Stoner enhancement factor than the rate of addition of Ni to Cu is shown in Fig. 62(b) by line (1').

For Cu-Ni alloys the average permanent moment $\bar{\mu}$ per alloy atom can be estimated from the model of Robbins et al.[16] in which the moment $\mu_{n,m}$ on a Ni atom is a function of the number n of the nearest, and number m of the second-nearest Ni neighbors:

$$\bar{\mu}(x) = x \sum_{n,m} P_{n,m}\, \mu_{n,m} \qquad (41)$$

where $P_{n,m}$ is the probability a for a given Ni atom to have n Ni nearest neighbors and m second-nearest neighbors. If $y_1 = x + {}_{\text{Ni-Ni}}\alpha_1(1-x)$ and $y_2 = x + {}_{\text{Ni-Ni}}\alpha_2(1-x)$ represent the effective concentration of Ni in the nearest and second-nearest neighbor shells of all Ni atoms in the alloy, then from the usual binomial distribution theorem,

$$P_{n,m} = \frac{12!6!}{(12-n)!(6-m)!n!m!}\, y_1^n (1-y_1)^{12-n}\, y_2^m\, (1-y_2)^{6-m} \qquad (42)$$

12 and 6 being the co-ordination numbers of the nearest and second-nearest neighbor shell of a given site in an fcc lattice. Assuming ${}_{\text{Ni-Ni}}\alpha_1 = 0.121$ and ${}_{\text{Ni-Ni}}\alpha_2 = 0$, the short range order parameters obtained for a furnace cooled $Cu_{0.525}Ni_{0.475}$ alloy by Mozer, Keating and Moss,[23] the average

permanent moment per alloy atom for quenched $Cu_{0.6}Ni_{0.4}$ may be calculated to be $\bar{\mu}' = 0.0129\ \mu_B$; this calculation overestimates the experimental value by about 33%. The model of Robbins et al. is also inaccurate in the weakly ferromagnetic composition range, i.e., around 50 at. % (Fig. 1, Reference 16); for Ni concentrations lower than 50 at. % Ni the model predicts larger $\bar{\mu}$ values than experimentally observed, thus indicating that perhaps smaller (than 0.121) $_{Ni\text{-}Ni}\alpha_1$ values should be assumed for these alloys.

On the basis of the model of Perrier et al.[43] for Cu-Ni alloys of nearly equiatomic composition, which makes the assumption that the quenched alloys are atomically random and that Ni atoms with 8 or more nearest neighbors have a moment of 0.6 μ_B (moment of Ni in pure nickel), while the Ni atoms with fewer Ni nearest neighbors have zero moment, the average moment per alloy atom calculated for quenched $Cu_{0.6}Ni_{0.4}$ is $\bar{\mu}'' = 0.0145\ \mu_B$; this calculation overestimates the average moment by nearly 50%. In fact as may be seen in Fig. 63(b) the model of Perrier et al.[43] predicts, for all alloys containing more than 55 at. % Ni, much larger $\bar{\mu}$ values than those measured. This indicates that much too large moment values (i.e., 0.6 μ_B) were assigned to the Ni atoms with 8, 9, 10 and 11 Ni nearest-neighbors. The assumption of Perrier et al.[43] that quenched Cu-Ni alloys are atomically random is also questionable in view of the recent neutron diffuse scattering work of Aldred et al.[44] who obtained, for a $Cu_{0.5}Ni_{0.5}$ alloy quenched from 1000° C, a value of 0.106

Figure 63. $\text{Ni-Ni}^{\alpha}{}_1$ and $\bar{\mu}$ vs. at. % Cu.

(a) $\text{Ni-Ni}^{\alpha}{}_1$ as a function of the Ni content: Δ, Mozer et al.;[23] □, Cable et al.;[45] O, Aldred et al.;[44] ⊗, Dekhtyar et al.[46] The solid curve drawn shows the assumed variation of the short range order parameter.

(b) $\bar{\mu}$ as a function of Ni content: O and ⊗, present work; Δ, Ahern et al.;[47] □, Perrier et al.[43] The dashed curve represents calculated values based on the model of Perrier et al.[43] The full curve represents calculated values from a modified moment assignment scheme (Fig. 64) and assuming $\text{Ni-Ni}^{\alpha}{}_1$ varies as shown in Fig. 63(a).

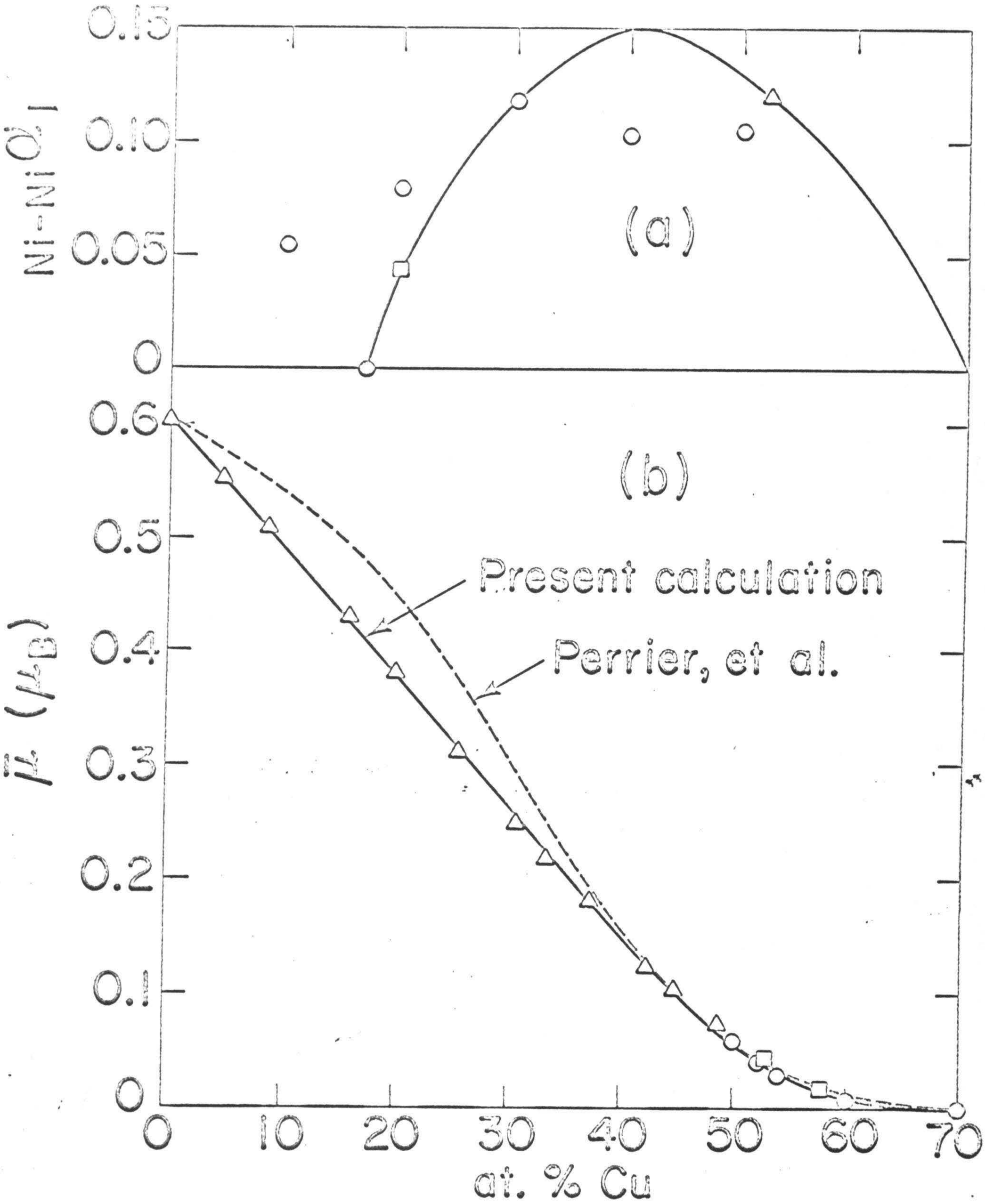
0.15
0.10
0.05
0
Ni-Ni Q_1
(a)
0.6
0.5
0.4
0.3
0.2
0.1
0
μ (μ_B)
(b)
Present calculation
Perrier, et al.
0
10
20
30
40
50
60
70
at. % Cu

for $_{Ni\text{-}Ni}\alpha_1$, in fair agreement with the very accurate results of Mozer et al.[23] for a near equi-atomic furnace cooled alloy. The values of the atomic short range order parameter for a number of Cu-Ni alloys, quenched from ∿1000° C, as obtained by Aldred et al.[44] and by Cable et al.,[45] are shown in Fig. 63(a). Dekhtyar and Chudakov[46] did not find any effect of plastic deformation on the magnetization of a $Cu_{0.83}Ni_{0.17}$ alloy; one may assume that this is an indication of the absence of Ni-rich atomic clusters, i.e., $_{Ni\text{-}Ni}\alpha_1 = 0$.

A revised moment assignment scheme was constructed for Cu-Ni alloys along the lines of the model of Robbins et al.[16] The short range order parameter was assumed to vary with the Ni concentration in the manner shown in Fig. 63(a), taking into full consideration the results of Dekhtyar and Chudakov[46] and the accurate values of $_{Ni\text{-}Ni}\alpha_1$ determined by Mozer et al.[23] and Cable et al.[45] With the $\mu_{n,m}$ values listed in Table 46 and presented in Fig. 64, good agreement was obtained in the entire ferromagnetic composition range between experimental and calculated values of $\bar{\mu}$, the average moment per alloy atom. As seen in Fig. 63(b) the fit is equally good also for superparamagnetic ($Cu_{0.6}Ni_{0.4}$ and $Cu_{0.7}Ni_{0.3}$) alloys.

In a recent paper Garland and Gonis[48] pointed out that one may obtain a good fit to the experimental average moment ($\bar{\mu}$) by using either second nearest neighbor effects[16] or by using cooperative effects in which case the moment on a Ni atom would depend not only on the number of nearest neighbor Ni atoms, but

Table 46. Moment assignments, $\mu_{n,m}$ in μ_B, in Cu-Ni allovs for Ni atoms with n nearest and m second nearest neighbor Ni atoms.

m \ n	6-0	7	8	9	10	11	12
0	0	0	0	0	0	0.556	0.606
1	0	0	0	0	0.400	0.556	0.606
2	0	0	0	0.325	0.512	0.556	0.606
3	0	0	0.250	0.468	0.512	0.556	0.606
4	0	0.05	0.424	0.468	0.512	0.556	0.606
5	0	0.05	0.424	0.468	0.512	0.556	0.606
6	0	0.05	0.424	0.468	0.512	0.556	0.606

Figure 64. A modified moment assignment scheme for Cu-Ni alloys. $\mu_{n,m}$ is the moment on a Ni atom with n nearest and m second nearest neighbor Ni atoms. This is slightly different from the moment assignment scheme of Robbins et al.[16]

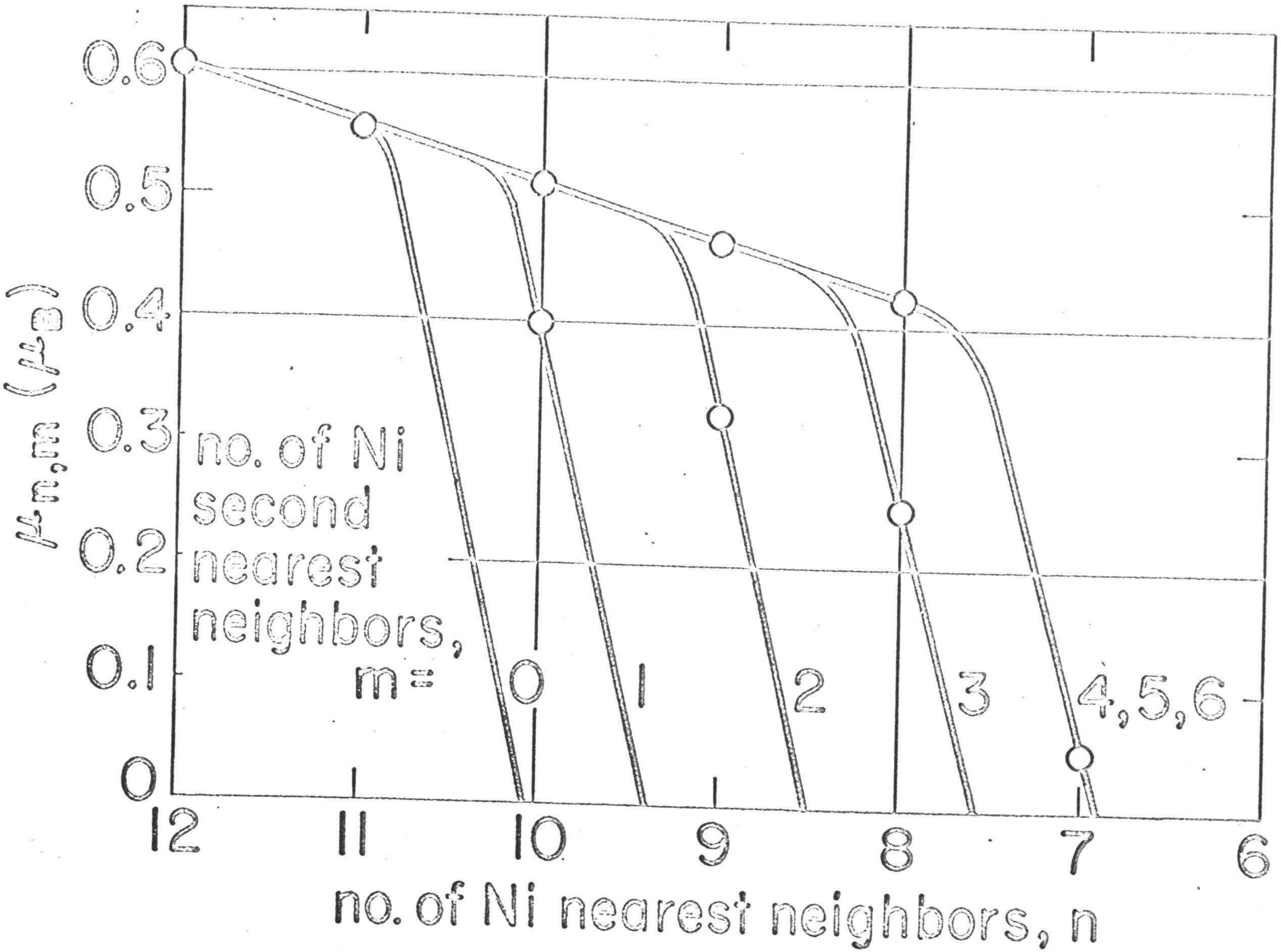
0.6
0.5
0.4
0.3
0.2
0.1
0
$\mu_{n,m}$ (μ_B)
no. of Ni second nearest neighbors, m =
0
1
2
3
4, 5, 6
12
11
10
9
8
7
6
no. of Ni nearest neighbors, n

also on the moment carried by each of these nearest neighbor Ni atoms.[22] Garland and Gonis[48] contend that no purely chemical model can yield a magnetic moment per cluster that is independent of the Ni composition.[22] However, as has been shown in the present work the magnetic moment per cluster does in fact depend on the Ni composition. Garland and Gonis[48] have claimed that the model of Robbins et al. predicts: (a) magnetic clusters of smaller spatial extent than that observed by Hicks et al.,[38] (b) a concentration of magnetic clusters in the superparamagnetic regime much greater than that found by Kouvel et al.,[22] and (c) a much too rapid decrease of the magnetic cluster size with increasing copper concentration, e.g., for $Cu_{0.7}Ni_{0.3}$ a magnetic moment per cluster that is substantially smaller than 3 μ_B.[1] So far no numerically workable model for Cu-Ni alloys has been put forth, which takes into account the co-operative effects. The model of Robbins et al.[16] at least has the virtue that it fits very well all the available information on the average moment per alloy atom over a wide composition range. It should also be pointed out that in their model,[16] since the moment $\mu_{n,m}$ on a Ni atom depends upon the number m of second nearest neighbor Ni atoms, which in turn influence the moment on the n nearest neighbor Ni atoms, co-operative effects of the type suggested by Kouvel and Comly[22] and Garland and Gonis[48] are at least partially accounted for.

VI. SUMMARY

The magnetization of quenched $Cu_{0.9}Ni_{0.1}$ and $Cu_{0.8}Ni_{0.2}$ alloys containing 100 to 1000 ppm Fe can be quantitatively accounted for in terms of magnetic clusters associated with 1, 2, and 3 or more Fe atoms. The ratio of the concentration of the Fe pair clusters to that of single Fe clusters is at all Ni and Fe concentrations much higher than the corresponding ratio calculated on the basis of a random alloy model which assumes long range interaction between Fe moments. Hence Fe - Fe clusters have to be postulated. The nearest-neighbor short range order parameter, corresponding to experimental concentration ratios, increases with the Fe concentration but decreases with the Ni concentration. The dipole moment connected with the single Fe clusters is larger than that expected for Fe alone, and increases with the Ni content. These findings can be accounted for if a contribution to the cluster moment from nearest neighbor Ni atoms is assumed.

The temperature dependence of the magnetic susceptibility of the iron-free binary $Cu_{0.9}Ni_{0.1}$ and $Cu_{0.8}Ni_{0.2}$ alloys is very small, indicating the absence of a measurable concentration of magnetic moments. The magnetization of the $Cu_{0.7}Ni_{0.3}$ alloy can be interpreted in terms of a low but measurable concentration of small nickel-rich magnetic dipoles. For $Cu_{0.6}Ni_{0.4}$ a bimodal distribution of magnetic clusters seems to be appropriate. The

average magnetic moment of ferromagnetic and superparamagnetic Cu-Ni alloys can be described in terms of a local atomic environment model making use of published short range order parameter values.

Analysis of the available magnetic data for Cu-Fe alloys with ∿110 ppm Fe indicates the presence of giant moments in addition to single Fe and Fe pair moments. Down to 1.3°K the results exclude any measurable loss of Fe moments as a result of spin compensation or local spin fluctuation, which might be expected in view of published Kondo temperatures.

The ratio of the concentration of the Fe pair moments to that of the single Fe moments suggests clustering of Fe atoms. Each of the copper alloys containing 380 and 478 ppm Fe, and 1% Fe has a maximum in the magnetization and the temperature of the maximum increases with the Fe content. The $Cu_{0.99}Fe_{0.01}$ alloy is shown to be mictomagnetic.

REFERENCES

1. S. Mishra, H. Claus, and P. A. Beck, Phys. Letters, 31A, 493 (1970).

2. S. Mishra, P. A. Beck, and S. Foner, J. Phys. Chem. of Solids, 32, 1779 (1971).

3. L. H. Bennett, J. T. Swartzendruber, and R. E. Watson, Phys. Rev. Letters, 23, 1171 (1969).

4. L. H. Bennett, L. J. Swartzendruber, and R. E. Watson, J. Appl. Phys., 42, 1547 (1971).

5. B. Window, C. E. Johnson, and G. Longworth, J. Phys. C: Metal Phys., Suppl. No. 2, S218 (1970).

6. J. L. Tholence and R. Tournier, Phys. Rev. Letters, 25, 867 (1970).

7. B. Window, J. Phys. C: Metal Phys., Suppl. No. 3, S323 (1970).

8. S. J. Campbell, P. E. Clark, and P. R. Liddell, J. Phys. F., Metal Phys., 2, L114 (1972).

9. E. C. Hirschkoff, M. R. Shanabarger, O. G. Symco, and J. C. Wheatley, J. Low Temp. Phys., 5, 545 (1971).

10. V. Gonser, R. W. Grant, C. J. Meechan, A. H. Muir, Jr., and H. Weidersich, J. Appl. Phys., 36, 2124 (1965).

11. L. H. Bennett, L. J. Swartzendruber, and R. E. Watson, AIP Conf. Proc. No. 5, Part 2 (1971).

12. E. E. Barton, Ph.D. Thesis, University of Illinois (1969).

13. R. D. Shull, M. S. Thesis, University of Illinois (1973).

14. C. G. Robbins, S. Mishra, and D. J. Chakrabarti, Magnetic Calibration of 1971.

15. R. W. Tustison, M. S. Thesis, University of Illinois (1972).

16. C. G. Robbins, H. Claus, and P. A. Beck; Phys. Rev. Letters, 22, 1307 (1969).

17. R. L. Falge, Jr., and L. J. Swartzendruber, To be published in Phys. Letters.

18. E. J. Hayes and P. A. Beck, Met. Trans., 1, 3267 (1970).

19. H. Okamoto and P. A. Beck, Montashefte für Chemie, 103, 907 (1972).

20. M. D. Daybell and W. A. Steyert, Phys. Rev. Lett., 20, 195 (1968).

21. J. M. Franz and D. J. Sellmyer, To be published.

22. J. S. Kouvel and J. B. Comly, Phys. Rev. Letters, 24, 598 (1970).

23. B. Mozer, D. T. Keating, and S. C. Moss, Phys. Rev., 175, 868 (1968).

24. M. D. Daybell and W. A. Steyert, Rev. of Mod. Phys., 40, 380 (1968).

25. J. E. Van Dam and G. J. Van den Berg, Phys. Stat. Sol., 3(a), 11 (1970).

26. C. Stassis and C. G. Shull, Phys. Rev. B, 5, 1040 (1973).

27. J. M. Franz and D. J. Sellmyer, AIP Conf. Proc. No. 5, 1150 (1972).

28. K. Svensson, Proc. 10^{th} Int. Conf. on Low Temp. Phys., 267 (Moscow, 1966).

29. Paul A. Beck, Met. Trans., 2, 2015 (1971).

30. Paul A. Beck, J. Less-Common Met., 28, 193 (1972).

31. P. Wells and J. H. Smith, J. Phys. F., Metal Phys. 1, 763 (1971).

32. C. G. Shull and M. K. Wilkinson, Phys. Rev., 97, 304 (1955).

33. B. Cornut, J. P. Perrier, B. Tissier, and R. Tournier, Intl. Conf. on Magnetism and Magnetic Matl. (Grenoble, 1970).

34. F. Acker and R. Huguenin, Phys. Letters, 38A, 343 (1972).

35. H. C. Van Elst, B. Lubach, and G. J. Van Den Berg, Physica, 28, 1297 (1962).

36. E. W. Pugh and F. M. Ryan, Phys. Rev., 111, 1038 (1958).

37. K. Schroder, J. Appl. Phys., 32, 880 (1961).

38. T. J. Hicks, B. Rainford, J. S. Kouvel, and G. G. Low, Phys. Rev. Letters, 22, 531 (1969).

39. G. L. Guthrie, S. A. Friedberg, and J. E. Goldman, Phys. Rev., 113, 45 (1959).

40. E. C. Stoner, Acta Met., 2, 259 (1954).

41. C. G. Robbins, H. Claus, and P. A. Beck, J. Appl. Phys., 40, 2269 (1969).

42. W. Marshall, Phys. Rev. 118, 1519 (1960).

43. J. P. Perrier, B. Tissier, and R. Tournier, Phys. Rev. Lett., 24, 313 (1970).

44. T. A. Aldred, B. D. Rainford, T. J. Hicks, and J. S. Kouvel, Phys. Rev., 7B, 218 (1973).

45. J. W. Cable, E. O. Wollan, and H. R. Child, Phys. Rev. Letters, 22, 1256 (1969).

46. I. Ya. Dekhtyar and A. F. Chudakov, Ukrainskii Fizicheskii Zhurnal, 12, 812 (1967).

47. S. A. Ahern, M. J. C. Martin, and W. A. Sucksmith, Proc. Roy. Soc. of Lond., 248A, 145 (1958).

48. J. W. Garland and A. Gonis in "Magnetism in Alloys," Ed: J. T. Waber and Paul A. Beck, TMS, AIME (1972).

APPENDIX A

SIGMA-5 COMPUTER PROGRAM FOR FITTING OF EQ. 9 (OR 11, 13, OR 14) TO MAGNETIZATION DATA

This program makes use of a variational method where the parameters are varied successively till a best fit, characterized by a minimum rmsd is obtained.

Program Steps

Steps 65 through 100, and 195 through 960.

Input Parameters

K is the total number of data points.

K1 is the number by which the mean square deviation should be divided (K1 > K if some of the data points were weighted preferentially).

K2 is the number of that data point starting from which all the data points (i.e., from K2 to K) are weighted.

K3 is the weighting constant.

K4 is the dividing factor for the data, in case the data points were premultiplied by a constant factor for convenience.

K5 is the number up to which (from 1 to K4) the data points are to be eliminated from the final stages of the fitting.

K6 is the number after which (K6 to K) the data points are to be eliminated from the final stages of the fitting.

K7 and K8 represent the numbers between which (i.e., K7 to K8) the data points are to be eliminated from the final stages of the fitting.

G is the average gram-atomic weight of the alloy.

N1, N2, and N3 are the starting values of the cluster moments μ_1, μ_2, and μ_3 respectively, in Bohr magnetons.

C1, C2, and C3 are the starting values of the cluster concentrations c_1, c_2, and c_3 respectively, in atomic fraction.

S1, S2, and S3 are the starting values of the interaction temperatures θ_1, θ_2, and θ_3 respectively, in °K.

X1 is the temperature and field independent susceptibility χ_o (in emu/g).

$X = \Delta\chi_o$ (emu/g)

$Z_1 = \Delta\theta_1$ (°K)

$Z_2 = \Delta\theta_2$ (°K)

$Z_3 = \Delta\theta_3$ (°K)

R_1 is the factor for varying the moment.

R_2 is the factor for varying the concentration.

Input Data

The data are stored in steps 101 through 194. The magnetization M is in emu/g, the field H in Oersteds, and the temperature T in °K (e.g., step 101).

Print Out

rmsd

χ_o

c_1 μ_1 θ_1

c_2 μ_2 θ_2

c_3 μ_3 θ_3

Additional Operations

(a) To Print out data only,

Step 212 GOTO 900

(b) To Print out data and rmsd and deviations for a given set of parameters,

Step 212 GOTO 800

Step 337 PRINT T(I),H(I),M(I),M,D

```
1K1=45
2K2=45
3K3=1
4K4=10
5K5=1
6K6=45
7K7=1
8K8=1
9K=45
10G=42.845
11N1=.3015
12N2=.8566834
13N3=4.5108
20Z7=.5
21C1=5.72076E-4
22C2=1.00122E-4
23C3=1.947E-5
31S1=-1.75
32S2=-1.6
33S3=-.2
40X=1E-9
41X1=1.6E-7
51Z1=.01
52Z2=.01
53Z3=.01
61R1=1.002
62R2=1.002
63Z3=.01
 65PRINT"-----------------------------------------
70PRINT
71PRINT"DEFØRMED 1000 PPM IRØN IN 20%NICKEL-80%CØPPEF
72PRINT"---------------------------"
73PRINT"TRIPLE MØMENT FIT"
74PRINT
75PRINT"FØLLØWING ARE STARTING PARAMETERS"
80PRINT
81PRINTZ7
82PRINT
84PRINTG,K,K1,K2,K3
85PRINTK4,K5,K6,K7,K8
86PRINT
87PRINTC1,N1,S1
88PRINTC2,N2,S2
89PRINTC3,N3,S3
90PRINTX1,X
91PRINTZ1,Z2,Z3
92PRINTR1,R2
93PRINT
101M(1)=.17829,H(1)=12582,T(1)=1.47
195PRINT"CALCULATIØN BEGINS"
196FØRI=1TØKSTEP1
197M(I)=M(I)/K4
```

```
190PRINT
200F=0
210A1,B1,P1,Q1,U1=N1,V1=C1,W1=S1
220U2=N2,V2=C2,W2=S2,U3=N3,V3=C3,W3=S3
230DIMN(3),C(3),S(3),X(1)
240M1=S1,M2=S2,M3=Z3
250L=0
260PRINT
270DIMX(100),M(100),T(100)
210X(1)=X1
211A,B,P,Q,A1,B1,P1,Q1=0
215N(1)=N1,C(1)=C1,S(1)=S1
220N(2)=N2,C(2)=C2,S(2)=S2
225N(3)=N3,C(3)=C3,S(3)=S3
230GOSUB700
235L=L+1
236PRINTL,F
237PRINTA1;B1;P1;Q1
254PRINT
255IFF=0THEN260
256IFY5<(Y7+Y7*1E-3)THEN350
260IFL=1THEN270
265GOTO274
270Y6=Y7,U1=N1,V1=C1,W1=S1,H1=Z1
271N1=N2,C1=C2,S1=S2,Z1=Z2
272N2=U1,C2=V1,S2=W1,Z2=H1
273GOTO210
274IFY6<(Y7+Y7*1E-6)THEN351
276Y6=Y7,U1=N1,V1=C1,W1=S1
277U2=N2,V2=C2,W2=S2,H1=Z1,H2=Z2
279N1=N2,C1=C2,S1=S2,Z1=Z2
280N2=U1,C2=V1,S2=W1,Z2=H1
285GOTO210
300Y=0
305FORI=K5TOK6STEP1
306GOTO950
310M=X(1)*H(I)
311FORJ=1TO3STEP1
312IF(T(I)-S(J))=0THEN363
316M1=2*6.72E-5*H(I)/(T(I)-S(J))
317IFM1<0THEN361
318M2=M1*(N(J)+1)
319IFM2<100THEN322
320M2=N(J)+1
321GOTO323
322M2=(N(J)+1)*(EXP(M2)+1)/(EXP(M2)-1)
323IFM1<170THEN326
324M3=1
325GOTO327
326M3=(EXP(M1)+1)/(EXP(M1)-1)
327E(J)=5581*C(J)*(M2-M3)/G
328M=M+E(J)
```

```
3[illegible]
3[illegible]=N*R(I)
340D=D+2
345IF N=K8GOTO345
346D=D+10
348GOTO345
349Y=Y+D
350NEXTI
355M=Y/11
359Y=SQR(Y)
360GOTO365
361PRINT"T(I)-S(J) NEGATIVE"
362STOP
363PRINT"T(I)-S(J)=0"
364STOP
365RETURN
400C(1)=C1
401GOSUB300
402Y1=Y
403A=0
405C(1)=C1*R2
410A=A+1
411IFA=20THEN480
412IFA>A1THEN414
413GOTO415
414A1=A
415GOSUB300
420IFY1<(Y+Y*1E-3)THEN435
425Y1=Y:C1=C(1)
430GOTO405
435IFA=1THEN450
440GOTO475
450C(1)=C1/R2
451A=A+1
452IFA=20THEN480
453IFA<A1THEN455
454A1=A
455GOSUB300
460IFY1<(Y+Y*1E-3)THEN475
465Y1=Y:C1=C(1)
470GOTO450
475RETURN
480PRINTA;D;P;Q
486PRINT"INCREASE R2"
487GOTO850
500GOSUB400
505Y9=Y1:C9=C1
510D=0
515N(1)=N1*R1
520D=D+1
521IFD=40THEN590
522IFD>B1THEN524
523GOTO525
```

```
[illegible]
525GOSUB400
530IFY9<(Y1+Y1*1E-3)THEN545
535Y9=Y1,C9=C1,N1=N(1)
540GOTO515
545IFB=1THEN554
550GOTO580
554C1=C9
555N(1)=N1/R1
556B=B+1
557IFB=40THEN590
558IFB<B1THEN560
559B1=B
560GOSUB400
565IFY9<(Y1+Y1*1E-3)THEN580
570Y9=Y1,C9=C1,N1=N(1)
575GOTO555
580N(1)=N1,C1=C9
585RETURN
590PRINTA;B;P;Q
596PRINT"INCREASE R1"
597GOTO850
600GOSUB800
605Y8=Y9,C8=C9,N8=N1
610P=0
615S(1)=S1+Z1
620P=P+1
621IFP=10THEN690
622IFP>P1THEN624
623GØTØ625
624P1=P
625GØSUB500
630IFY8<(Y9+Y9*1E-3)THEN645
635Y8=Y9,C8=C9,N8=N1,S1=S(1)
640GØTØ615
645IFP=1THEN654
650GØTØ680
654C1=C8,N(1)=N8
655S(1)=S1-Z1
656P=P+1
657IFP=10THEN690
658IFP<P1THEN660
659P1=P
660GØSUB800
665IFY8<(Y9+Y9*1E-3)THEN680
670Y8=Y9,C8=C9,N8=N1,S1=S(1)
675GØTØ655
680S(1)=S1,C1=C8,N(1)=N8,N1=N8
685RETURN
690PRINTA;B;P;Q
695PRINT"INCREASE Z1"
696GØTØ850
700GØSUB600
```

```
705Y7=Y8,C7=C8,N7=N8,S7=S1
710Q=0
715X(1)=X1+X
716PRINT"X1CHANGED",Y7,X1
717PRINTC7,N7,S7
718PRINTC8,N8,S8
719PRINTC9,N9,S9
720Q=Q+1
721IFQ=10THEN790
722IFQ>Q1THEN724
723GØTØ725
724Q1=Q
725GØSUB600
730IFY7<(Y8+Y8*1E-3)THEN745
735Y7=Y8,C7=C8,N7=N8,S7=S1,X1=X(1)
740GØTØ715
745IFQ=1THEN754
750GØTØ760
754C1=C7,N(1)=N7,S(1)=S7
755X(1)=X1-X
756PRINT"X1CHANGEDDØWN",Y7,X1
757PRINTC7,N7,S7
758PRINTC8,N8,S8
759PRINTC9,N9,S9
760Q=Q+1
761IFQ=10THEN790
762IFQ<Q1THEN764
763Q1=Q
764GOSUB600
765IFY7<(Y8+Y8*1E-3)THEN780
770Y7=Y8,C7=C8,N7=N8,S7=S1,X1=X(1)
775GØTØ755
780C1=C7,N(1)=N7,S(1)=S7,N1=N7,X(1)=X1,S1=S7
785RETURN
790PRINTA;B;P;Q
791PRINT"INCREASE X1"
792GØTØ850
800N(1)=U1,C(1)=V1,S(1)=W1
805N(2)=U2,C(2)=V2,S(2)=W2
806N(3)=U3,C(3)=V3,S(3)=W3
810GØSUB300
815PRINT
820PRINTY
821PRINTX1
822PRINTC1,N1,S1
823PRINTC2,N2,S2
824PRINTC3,N3,S3
825STØP
830END
850STØP
851IFF=0THEN860
855IFY5<(Y6+Y6*1E-3)THEN865
860Y5=Y6
```

```
3 3 3 X 3 = X 1 , Y 3 = Y 1 , Z 3 = Z 1
3 7 0 X 1 = U 3 , Y 1 = V 3 , Z 1 = W 3 , Z 1 = K 3
3 7 3 P = P + 1
3 8 0 G O T O 3 2 0 1
3 8 5 S T O P
9 0 0 F O R I = 1 T O K S T E P 1
9 0 5 P R I N T I , X ( I ) , Y ( I ) , Z ( I )
9 1 0 N E X T I
9 1 5 S T O P
9 5 0 I F I < = K 7 T H E N 3 1 0
9 5 5 I F I > = K 8 T H E N 3 1 0
9 6 0 G O T O 3 3 5 0
>
```

APPENDIX B

SIGMA-5 COMPUTER PROGRAM FOR THE DETERMINATION OF $_iS_k$

$_iS_k$ is the number of sites in an f.c.c. structure which are common to the k^{th} shell of an atom B, that is in the i^{th} shell of an atom A, and the shells 1 through 9 of the atom A.

The program is divided into two main parts: the K Program (steps 95 to 600) and the J Program (steps 649 to 1315). In the J program all the lattice points in the K shell of atom B are generated successively; as each point is generated, the K Program is used to generate all the lattice points in shells 1 through 9 of atom A and a comparison is made to determine if there is an overlap.

The position of the atom B with respect to atom A is represented by a translation vector I. The lattice sites in the k shell of atom B are generated by first generating the lattice sites in the k-shell of A and then applying to each of these sites a lattice translation with the vector I.

The lattice sites in a given shell of atom A are generated by finding out all the crystallographically equivalent sites, in space, of a single site (whose spatial coordinates are known) in that shell.

Input

Step 690 U(=i)

Step 700 G(=k)

Print Out

I i k $_{i}S_{k}$

```
1PRINT
2PRINT
3PRINT
81I(1),J(1),K(1)=515150
82I(2),J(2),K(2)=525050
83I(3),J(3),K(3)=525151
84I(4),J(4),K(4)=525250
85I(5),J(5),K(5)=535150
86I(6),J(6),K(6)=525252
87I(7),J(7),K(7)=535251
88I(8),J(8),K(8)=545050
89I(9),J(9),K(9)=535350
90I(10),J(10),K(10)=545151
94GØTØ649
95PRINT"KPRØGRAM"
100REMKPRØGRAM
160FØRL=1TØ10STEP1
170K=K(L)
180W=0
181DIMN(4,6)
185MATN=ZER(4,6)
190GØSUB200
191GØTØ300
200P=1
205Q=1
206GØSUB2500
210IFK1=N(P,Q)THEN285
215IFN(P,Q)=0THEN250
220P=P+1
225IFP<5THEN210
230P=P-4,Q=Q+1
235IFQ<7THEN210
240GØTØ270
250N(P,Q)=K1
270IFK1=JTHEN280
275GØTØ285
280N=N+1
285RETURN
300K=K-500000
310GØSUB200
320K=K-5000
330GØSUB200
340K=K-50
350GØSUB200
360K=K+5000
370GØSUB200
380K=K+500000
390GØSUB200
400K=K-5000
410GØSUB200
420K=K+50
430GØSUB200
440K=K+5000
```

```
445GØSUB450
446GØTØ480
450E1=K/100
455F1=INT(E1)
460G1=E1-F1
465H1=INT(G1*10↑6+.1)
470K=H1+F1
475RETURN
480W=W+1
490IFW/3-INT(W/3)=0THEN510
500GØTØ190
510GØSUB520
511GØTØ570
520A2=K/100
525B2=INT(A2)
530C2=A2-B2
535C2=C2*100
540B2=B2/100
545D2=INT(B2)
550B2=B2-D2
560K=INT(B2*10↑6+D2*100+C2+.1)
565RETURN
570IFW=>6THEN580
575GØTØ190
580REMMICALCULATIØN
590NEXTL
600RETURN
649N=0
650V1=0
690U=10
700FØRG=1TØ10STEP1
710DIMM(4,6)
720MATM=ZER(4,6)
730T=0
735Y=J(G)
736GØSUB2000
740GØSUB750
741GØTØ830
750R=1
755S=1
756Y5=INT(Y5+.1)
760IFY5=M(R,S)THEN805
765IFM(R,S)=0THEN795
770R=R+1
775IFR<5THEN760
780R=R-4,S=(S+1)
785IFS<7THEN760
790GØTØ800
795M(R,S)=Y5
800GØTØ810
805Y1=Y5
810RETURN
830IFY1=Y5THEN1005
```

```
835GØSUB840
836GØTØ1000
840U1=I(U)
841Y7=Y5
842GØSUB845
843GØTØ900
845Y2=Y7/100
850Y3,Y7=INT(Y2)
855Y4=Y2-Y3
860IFY4>=.5THEN892
865U2=U1/100
870U3,U1=INT(U2+.1)
875U4=U2-U3
880U5=U4-.5
885IFU5-Y4>0THEN894
890U6=ABS(U5-Y4)
891GØTØ895
892GØSUB910
893GØTØ895
894GØSUB945
895RETURN
900GØTØ960
901PRINT"WE ARE ADDING I VECTØR"
910Y5=Y4-.5
915U2=U1/100
920U3,U1=INT(U2+.1)
925U4=U2-U3
930U6=Y5*U4
940RETURN
945U6=.5+U5-Y4
950RETURN
960U7=(U6)*100
965GØSUB845
970U7=U7+(U6)*10↑4
975GØSUB845
980J=INT(U7+U6*10↑6+.1)
981GØSUB1500
990RETURN
1000GØSUB 100
1005Y=Y-500000
1007GØSUB2000
1010GØSUB750
1015IFY1=Y5THEN1030
1020GØSUB840
1025GØSUB100
1030Y=Y-5000
1032GØSUB2000
1035GØSUB750
1040IFY1=Y5THEN1055
1045GØSUB840
1050GØSUB100
1055Y=Y-50
1057GØSUB2000
```

```
1060GØSUB750
1065IFY1=Y5THEN1080
1070GØSUB840
1075GØSUB100
1080Y=Y+5000
1082GØSUB2000
1085GØSUB750
1090IFY1=Y5THEN1105
1095GØSUB840
1100GØSUB100
1105Y=Y+500000
1106GØSUB2000
1110GØSUB750
1115IFY1=Y5THEN1130
1120GØSUB840
1125GØSUB100
1130Y=Y-5000
1131GØSUB2000
1135GØSUB750
1140IFY1=Y5THEN1155
1145GØSUB840
1150GØSUB100
1155Y=Y+50
1156GØSUB2000
1160GØSUB750
1165IFY1=Y5THEN1180
1170GØSUB840
1175GØSUB100
1180Y=Y+5000
1185GØSUB1190
1186GØTØ1220
1190E5=Y/100
1195F5=INT(E5)
1200G5=E5-F5
1202G5=G5*100
1204G5=INT(G5+.2)
1206H5=G5*10↑4
1210Y=H5+F5
1215RETURN
1220T=T+1
1225IFT/3-INT(T/3)=0THEN1235
1230GØTØ736
1235GØSUB1240
1236GØTØ1285
1240A7=Y/100
1245B7=INT(A7)
1250C7=A7-B7
1255D7=(C7)*100
1260E7=(B7)/100
1265F7=INT(E7)
1270G7=E7-F7
1275Y=G7*10↑6+(F7)*100+D7
1280RETURN
```

```
1285IFT>=6THEN1295
1290GØTØ736
1295M1=N-V1
1296PRINTI(U),U,G,M1
1297V1=N
1299PRINT
1300NEXTG
1304PRINT
1305PRINT"TØTAL N FØR ALL J",I(U),U,N
1315END
1500J=INT(J+.1)
1501A9=J/100
1505B9=INT(A9)
1510C9=A9-B9
1515D9=C9*100
1520IFD9=0THEN1560
1525E9=B9/100
1530F9=INT(E9+.1)
1535G9=E9-F9
1540H9=G9*100
1545IFF9=0THEN1570
1550IFH9=0THEN1580
1555GØTØ1585
1560D9=D9+50
1565GØTØ1525
1570F9=F9+50
1575GØTØ1550
1580H9=H9+50
1585J=INT(F9*10000+H9*100+D9+.1)
1590RETURN
2000Y=INT(Y+.1)
2001A9=Y/100
2005B9=INT(A9)
2010C9=A9-B9
2015D9=C9*100
2020IFD9=0THEN2060
2025E9=B9/100
2030F9=INT(E9)
2035G9=E9-F9
2040H9=INT(G9*100+.1)
2045IFF9=0THEN2070
2050IFH9=0THEN2080
2055GØTØ2085
2060D9=D9+50
2065GØTØ2025
2070F9=F9+50
2075GØTØ2050
2080H9=H9+50
2085Y5=F9*10000+H9*100+D9
2090RETURN
2500K=INT(K+.1)
2501A9=K/100
2505B9=INT(A9)
```

```
2510C9=A9-B9
2515D9=C9*100
2520IFD9=0THEN2560
2525E9=B9/100
2530F9=INT(E9)
2535G9=E9-F9
2540H9=INT(G9*100+.1)
2545IFF9=0THEN2570
2550IFH9=0THEN2580
2555GOTO2585
2560D9=D9+50
2565GOTO2525
2570F9=F9+50
2575GOTO2550
2580H9=H9+50
2585K1=INT(F9*10000+H9*100+D9+.1)
2590RETURN
>
```

APPENDIX C

SIGMA-5 COMPUTER PROGRAM FOR CALCULATING THE RATIO c_2/c_1 ON THE BASIS OF THE RANDOM ALLOY MODEL,[4] FROM EQ. 30

Input

Step 1 x(= Ni concentration in at. fraction)

Step 2 z(= Fe concentration in at. fraction)

Print Out

x z

c_1 c_2

c_2/c_1 % Fe atoms in pairs

$(z-c_1-2c_2)$

```
1X=.2
2Z=1000E-6
5PRINT
6PRINT
10DIMS(8,8)
11S(1,1)=11
12S(1,2)=6
13S(1,3)=24
14S(1,4)=12
15S(1,5)=22
16S(1,6)=6
17S(1,7)=32
18S(1,8)=5
21S(2,1)=12
22S(2,2)=5
23S(2,3)=24
24S(2,4)=8
25S(2,5)=20
26S(2,6)=4
27S(2,7)=24
28S(2,8)=4
31S(3,1)=12
32S(3,2)=6
33S(3,3)=18
34S(3,4)=9
35S(3,5)=14
36S(3,6)=5
37S(3,7)=22
38S(3,8)=5
41S(4,1)=12
42S(4,2)=4
43S(4,3)=18
44S(4,4)=6
45S(4,5)=12
46S(4,6)=2
47S(4,7)=24
48S(4,8)=5
51S(5,1)=11
52S(5,2)=5
53S(5,3)=14
54S(5,4)=6
55S(5,5)=10
56S(5,6)=4
57S(5,7)=20
58S(5,8)=4
61S(6,1)=9
62S(6,2)=3
63S(6,3)=15
64S(6,4)=3
65S(6,5)=12
66S(6,6)=3
67S(6,7)=18
```

```
68S(6,8)=3
71S(7,1)=8
72S(7,2)=3
73S(7,3)=11
74S(7,4)=6
75S(7,5)=10
76S(7,6)=3
77S(7,7)=15
78S(7,8)=3
81S(8,1)=5
82S(8,2)=2
83S(8,3)=10
84S(8,4)=5
85S(8,5)=8
86S(8,6)=2
87S(8,7)=12
88S(8,8)=4
100DIMR(8)
101R(1)=12
102R(2)=6
103R(3)=24
104R(4)=12
105R(5)=24
106R(6)=8
107R(7)=48
108R(8)=12
110A=1-X
111B=1-X*X
112C=1-A*A
113D=1-X*C
114E=1-X*(1-A*A*A)
115F=1-X*(1-A*A*A*A)
121P(1)=1
122P(2)=1-A↑4
123P(3)=1-(A*A*D*D)
124P(4)=1-A*B↑4
125P(5)=6*X↑8-24*X↑7+35*X↑6-24*X↑5+15*X↑4-16*X↑3+9*X↑2
126P(6)=-2*X↑6+6*X↑5-3*X↑4-6*X↑3+6*X↑2
127P(7)=3*X↑2-2*X↑3
128P(8)=X*X
300Y1=Z
305FØRJ=1TØ8STEP1
310Y2=(1-Z*P(J))↑R(J)
315Y1=Y1*Y2
320NEXTJ
325C1=Y1
330Y3=.5*Z*C1
400Y6=0
405FØRI=1TØ8STEP1
410Y4=(P(I)*R(I))/((1-Z*P(I))↑2)
415FØRK=1TØ8STEP1
420Y5=(1-Z*P(K))↑(R(K)-S(I,K))
425Y4=Y4*Y5
```

```
430NEXTK
435Y6=Y4*Y6
440NEXTI
445C2=Y3*Y6
450PRINTX,Z
455PRINTC1,C2
456PRINTC2/C1,(100*2*C2)/Z
457PRINT(Z-C1-2*C2)
460PRINT
465STØP
470ENDPRØGRAM
```

VITA

Sanak Mishra was born on December 18, 1945 in Berhampur, India to Harihar and Indumati Misra. He graduated from the Queen of the Missions High School, Berhampur in 1961. On the basis of his performance he was awarded a gold medal by the State Board of Education, and also a Government of India National Merit Scholarship which he held until August, 1968. He entered the Utkal University in 1961 and received the Bachelor of Science Honours degree in Physics in 1965. The same year he joined the Indian Institute of Science, Bangalore, and in 1965 obtained the Bachelor of Engineering degree in Metallurgy. In September, 1968 he began graduate work at the Department of Metallurgy, University of Illinois and received his M.S. degree in August, 1970. The title of his master's thesis was: Paramagnetism in Copper-Rich Copper Nickel Solid Solutions, Effect of Small Iron Additions. In September, 1970 he began studies toward a Ph.D. degree. He is the author of two publications.